Manipulating kinetochore function with synthetic physical interactions

Guðjón Ólafsson

University College London
and
The Francis Crick Institute
PhD Supervisor: Peter Thorpe

A thesis submitted for the degree of
Doctor of Philosophy
University College London

October 2017

Declaration

I Guðjón Ólafsson confirm that the work presented in this thesis is my own. Where information has been derived from other sources, I confirm that this has been indicated in the thesis.

Signature: Date: 08/01/2018

Abstract

The kinetochore is a large protein complex that assembles on centromeres. It enables accurate chromosome segregation by attaching chromosomes to the mitotic spindle via microtubules and by recruiting regulators that control mitosis. Many of these regulators modify kinetochore components by post-translational modifications such as phosphorylation and ubiquitination. For example, when kinetochores fail to attach to microtubules, the kinase Mps1 phosphorylates the kinetochore to activate the spindle assembly checkpoint (SAC).

The abundance of chromosomal instability mutants suggests that numerous kinetochore regulators remain to be identified and the mechanisms of some known regulators are poorly characterised. The kinetochore is highly conserved from yeast to humans and many important discoveries of kinetochore function have been made using *Saccharomyces cerevisiae*. In order to identify kinetochore regulators in budding yeast, I have used the Synthetic Physical Interaction (SPI) technology to separately associate each member of the yeast proteome with a kinetochore protein. In addition, I have recruited several hundred proteins involved in chromosome segregation and post-translational modifications individually to kinetochore proteins representing each of the major kinetochore subcomplexes. I then associated each candidate regulator separately with most of the kinetochore proteins to spatially map their function. This method identifies candidate kinetochore regulators such as chromatin remodelling complexes, phosphatases and kinases; some of which are novel. In this thesis, I focus on three regulators; first, the Cdc14 phosphatase, second, components of the SAC and lastly the Polo-like kinase. These studies reveal kinetochore proteins sensitive to specific regulators and that their action is spatially restricted within the large kinetochore structure.

Acknowledgement

First of all, I would like to thank my supervisor Peter Thorpe for giving me the opportunity to work on this fascinating topic, his endless support and patience, as well as scientific advice, motivation, inspiring conversations, stimulating ideas and friendship.

I would also like to thank past and present members of the Mitotic Control lab, Eva, Elena, Erika, Sonia, Eleanor, Mathilde, Dorine, Lisa, Wenjun, Rowan and Alex, for their support and the fun we have had over the years. Likewise, I am grateful for the support and advice from my thesis committee, James Turner, Martin Singleton and Markus Ralser.

I also thank Andrew Jones and Bram Snijders for their help with phosphoproteomics, as well as Meghna Kataria, Sandra Touati, Silke Hauf, John Diffley and Frank Uhlmann for technical and scientific advice. I also thank Munira Basrai and Mishra Prashant for ongoing collaboration and scientific input.

I would like to give special thanks to my wife Henný, for her understanding and emotional support, as well as for believing in me. Ég elska þig svo mikið!

Finally, I am very grateful for the encouragement and support from my mom, and family and friends back home from Iceland and all over the world, and for their visits to London, which has meant a lot to me.

I want to dedicate my thesis to my dad, who gave me my first microscope and encouraged my passion for nature and science since I was a boy.

Table of Contents

Table of figures

List of tables

Abbreviations

Δ	deletion (of an ORF, C terminus or N terminus)
Φ	hydrophobic residue
5-FOA	5-Fluoroorotic Acid
AID	auxin-inducible degradation/degron
APC/C	anaphase promoting complex/cyclosome
Arg	arginine (R)
Asn	asparagine (N)
Asp	aspartic acid (D)
BiM	diploid bimater assay
˚C	degree Celsius
CCAN	constitutive centromere-associated network
CDE(s)	centromere DNA element(s)
CDK	cyclin-dependent kinase
CEN	centromere
CF	chromosome fragment
C.I.	confidence intervals
CIN	chromosome instability
CFP	cyan fluorescent protein
CLASP	CLIP-associated protein
Clb	cyclin type B
CLIK	Cutoff Linked to Interaction Knowledge tool
CMK	chloromethylketone
CPC	chromosomal passenger complex
CTF	chromosome transmission fidelity
DIC	differential interference contrast
DMSO	dimethyl sulfoxide
DNA	deoxyribonucleic acid
DUB	deubiquitinase
E. coli	*Escherichia coli*
FACT complex	facilitates chromatin transcription complex
FDR	false discovery rate
FEAR	Cdc fourteen early anaphase release
G1	gap 1
G2	gap 2

GAL	galactose
GBP	GFP-binding protein
GFP	green fluorescent protein
Gln	glutamine (Q)
Glu	glutamic acid (E)
GO	gene ontology
GOI	gene of interest
HDAC	histone deacetylase complex
His	histidine (H)
HYG	hygromycin B
HU	hydroxyurea
INO80 complex	inositol requiring chromatin remodelling complex
KAN	kanamycin
kanMX	kanamycin resistant cassette
kb	kilobase pair
kd	kinase-dead mutant
LB	Luria-Bertani broth
LECA	last eukaryotic common ancestor
LED	light-emitting diode
Leu	leucine (L)
LGR	log growth ratio
MAP(s)	microtubule-associated protein(s)
MAT	mating type locus
*MAT***a**	yeast mating type a
MATα	yeast mating type alpha
MCC	mitotic checkpoint complex
MEN	mitotic exit network
MTOC	microtubule-organising centre
NAT	nourseothricin (cloNAT)
NS or n.s.	not statistically significant
OD_{600}	optical density at 600nm
ORF	open reading frame
PBD	polo box domain
PCR	polymerase chain reaction
pd	phosphatase-dead mutant

PEG	polyethylene glycol
POI	protein of interest
PP1	protein phosphatase 1
PP2A	protein phosphatase 2A
PTM	post-translational modification
RENT complex	regulator of nucleolar silencing and telophase complex
RFP	red fluorescent protein
RSC complex	remodelling the structure of chromatin complex
SAC	spindle assembly checkpoint
SAGA complex	Spt-Ada-Gcn5-acetyltransferase complex
S. cerevisiae	*Saccharomyces cerevisiae*
SC	synthetic complete
SD	synthetic deficient
Ser	serine (S)
SGD	*Saccharomyces* Genome Database
SILAC	stable isotope labelling by amino acids in cell culture
SPA	selective ploidy ablation
SPB(s)	spindle pole body(ies)
SPI(s)	synthetic physical interaction(s)
SPO	sporulation media
SPOC	spindle position checkpoint
STD	standard deviation
STUbL	SUMO-targeted ubiquitin ligase
SUMO	small ubiquitin-like modifier
SWI/SNF complex	SWItch/Sucrose Non-Fermentable complex
TCA	trichloroacetic acid
TE	Tris-EDTA
Thr	threonine (T)
Tris	Tris (hydroxymethyl) aminomethane
Turq2	mTurqoise2 fluorescent protein
UDS	universal donor strain
YFP	yellow fluorescent protein
YPD	yeast extract peptone dextrose
WT	wild type

Chapter 1. Introduction

Successful cell division requires that the correct number of chromosomes are segregated into each daughter cell. Defects in this process result in genomic instability and aneuploidy – a situation when daughter cells inherit an abnormal number of chromosomes. Aneuploidy is a hallmark of cancer cells and in human germ cells causes specific birth defects, such as Down syndrome (Hassold & Hunt, 2001; Bharadwaj & Yu, 2004; Yuen *et al.*, 2005; Pfau & Amon, 2012). Therefore, it is important to understand how chromosomes are accurately segregated and to elucidate the quality control mechanisms of chromosome segregation.

The kinetochore, a large protein complex located on centromeres, is a key structural and regulatory entity coordinating chromosome segregation in eukaryotic cells. It links chromosomes to microtubules emanating from spindle pole bodies (SPB; the yeast centrosomes or microtubule-organising centre, MTOC) (Figure 1.1). Its dynamic structure is made up of around 70 different proteins organised into multiple subcomplexes, most of which are highly conserved from budding yeast to humans (Westermann *et al.*, 2007; Biggins, 2013; Hooff *et al.*, 2017). One of the main differences between the kinetochores of these two organisms is that the budding yeast kinetochore assembles on a point centromere defined by a specific ~125 base pair DNA sequence and attaches to a single microtubule, whereas humans have regional centromeres that span up to several megabases of degenerate alpha-satellite DNA and each kinetochore attaches to approximately 30 microtubules.

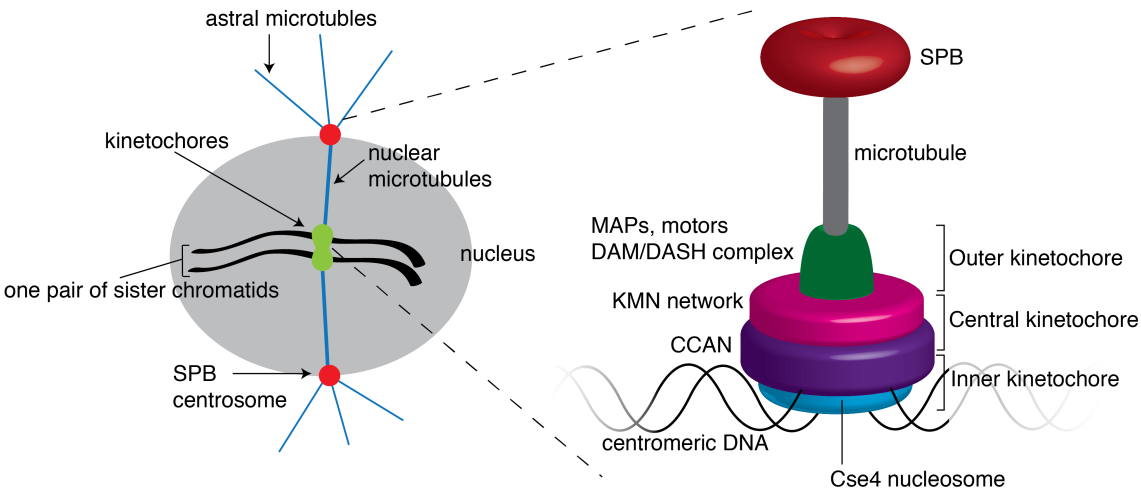

Figure 1.1 The mitotic spindle in budding yeast

A schematic depicting the organisation of the mitotic spindle in budding yeast and showing a simplified layout of the kinetochore. Budding yeast undergoes closed mitosis where the nuclear envelope stays intact throughout mitosis. The spindle pole body (SPB) is the centrosome or microtubule-organising centre (MTOC) in budding yeast and emanates astral and nuclear microtubules. The 16 kinetochores cluster together into one kinetochore focus in budding yeast and a single kinetochore binds a single microtubule. The kinetochore consists of three layers, inner, central and outer kinetochore. The constitutive centromere-associated network (CCAN) at the inner kinetochore binds centromeric DNA or the Cse4 nucleosome. The DAM1/DASH complex, microtubule-associated proteins (MAPs), motor proteins, and some components of the KMN network interact with microtubules. The central kinetochore links together the inner and outer kinetochore.

The relative simplicity of the yeast kinetochore and its conservation with mammals are two key reasons why *Saccharomyces cerevisiae* (budding yeast) is used as a model organism in studying chromosome segregation. In this introduction, I discuss chromosome segregation in budding yeast, as well as introduce mitotic spindle and kinetochore organisation and regulation, and finally describe the aims of my project.

1.1 Brief overview of the budding yeast cell cycle

Our understanding of the cell cycle and how it is controlled by cyclin-dependent kinase (CDK), largely depends on seminal studies performed in the 1970's and 80's by Hartwell and Nurse, in both budding and fission yeast (Hartwell *et al.*, 1970, 1974; Nurse, 1975; Beach *et al.*, 1982; Lee & Nurse, 1987; Russell & Nurse, 1987; Hartwell & Weinert, 1989). As the name suggests, budding yeast divide by budding. It has two haploid mating types (*MAT***a** and *MAT*α) with 16 chromosomes and can also grow as a diploid. The eukaryotic cell cycle, a sequence of events that leads to replication of DNA and its segregation into two daughter cells, is generally divided into two functional stages; S-phase and M-phase, respectively, which are separated by two preparatory gap stages, G1- and G2-phases (Figure 1.2). After a previous cell cycle, the cell enters a G1-phase and takes up nutrients and grows in preparation for S-phase events, such as bud emergence, spindle pole body (SPB) duplication and DNA replication. As soon as the unbudded G1 cell has reached a critical threshold for appropriate size and cyclin-dependent kinase (CDK; Cdc28 in budding yeast) activity, the cell commits to enter the cell cycle through a regulatory point called START, which is the transition into S-phase. DNA replication during S-phase is a highly regulated process to ensure the genetic material has been duplicated accurately before cell division. After DNA replication, the newly formed sister chromatids are held together by the cohesin

complex. In budding yeast the G2-phase is practically absent and partially overlaps with S- and M-phase. In G2-phase the SPBs mature and separate in preparation for mitosis. The SPB is integrated into the nuclear envelope, which does not break down during mitosis (closed mitosis) in budding yeast as it does in most metazoans.

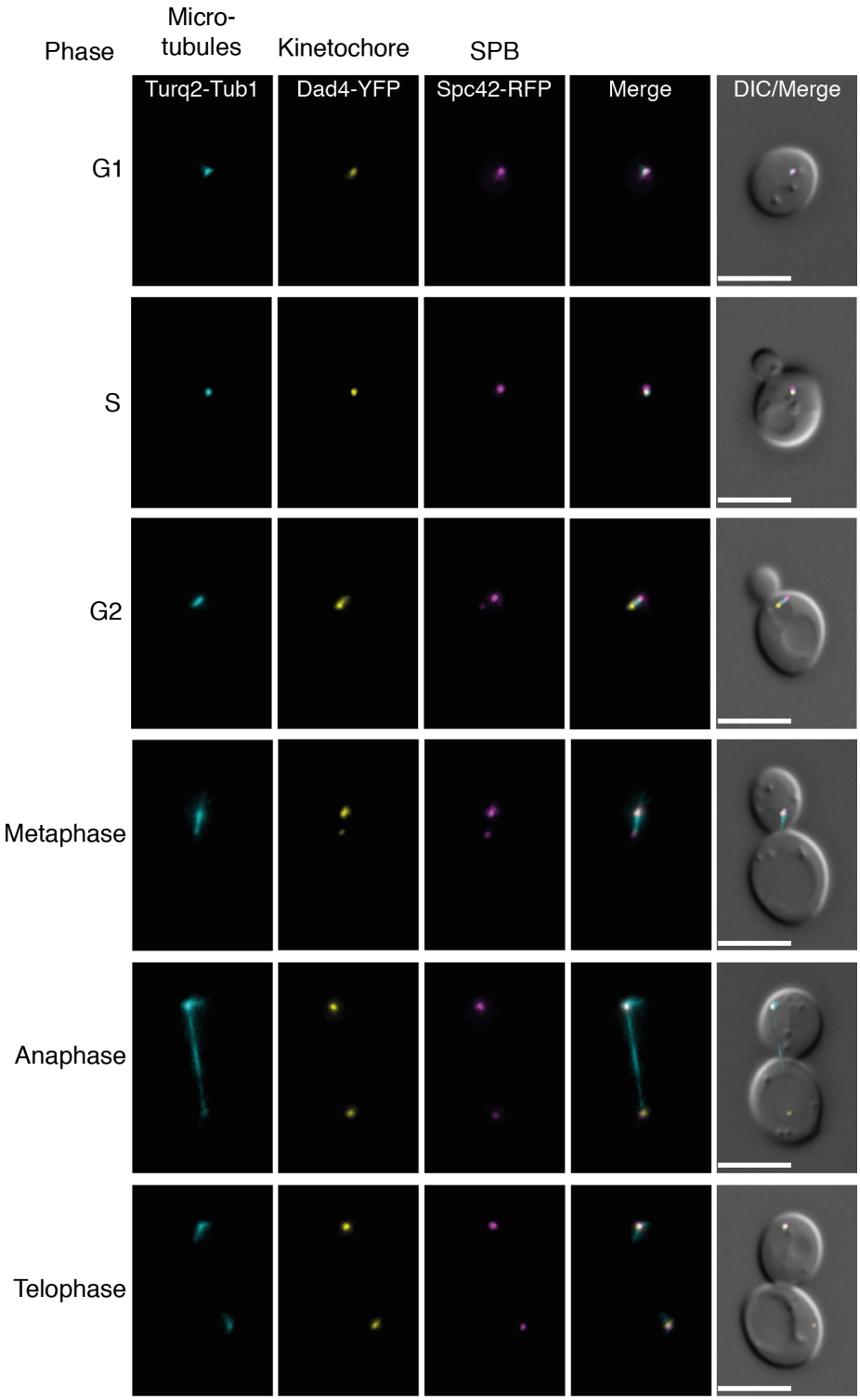

Figure 1.2 Budding yeast cell cycle

Fluorescence microscopy images of cells at different stages of the cell cycle. The 16 kinetochores (Dad4-YFP) in a haploid cell form a single focus in G1- and S-phase and two foci in mitosis. The spindle pole bodies (SPB) (Spc42-RFP) which emanate microtubules (Turquoise-Tub1) and together with kinetochores form the mitotic spindle. Scale bars are 5μm.

Before committing to mitotic entry, the cell has to satisfy several checkpoints. First, the DNA damage checkpoint stops the cell cycle in the events of DNA damage which has to be repaired before the duplicated DNA is separated (Elledge, 1996). Second, the DNA replication checkpoint monitors the status of replication and ensures that the cell does not prematurely enter mitosis without completing DNA replication. Third, the morphogenesis checkpoint monitors the state of bud emergence and ensures that the cell does not attempt mitosis before it buds (Keaton & Lew, 2006; Howell & Lew, 2012). Without going into details of the molecular pathways of these checkpoints, the key regulators of many of the steps are the CDK/cyclins and their activators and inhibitors. For example, the morphogenesis checkpoint prolongs G2-phase by delaying degradation of the CDK inhibitor Swe1 kinase (WEE1 homolog in budding yeast), which binds to and inhibits Clb-CDK complexes (Clb-Cdc28) (Keaton & Lew, 2006). Once a bud has formed, Swe1 is shuttled into the bud neck and phosphorylated by Cdc5 polo-like kinase, an essential driver of cell cycle progression, which results in Swe1 degradation (Sakchaisri *et al.*, 2004; Asano *et al.*, 2005). Therefore, mitotic entry can only be initiated once Clb-Cdc28 has accumulated and activated by Mih1 phosphatase (which reverses Swe1-dependent phosphorylation of Cdc28) allowing it to drive mitotic spindle assembly.

Mitosis can be further subdivided into prophase, metaphase, anaphase and telophase. Metaphase and anaphase are the key mitotic steps in budding yeast and are tightly regulated both spatially and temporally to ensure faithful chromosome segregation. In metaphase, the mitotic spindle is organised by microtubules emanating from each spindle pole body attaching them to sister kinetochores which are assembled on centromeres on sister chromatids. A metaphase checkpoint, called the mitotic checkpoint or spindle assembly checkpoint (SAC; described in detail in section 1.3.1.), ensures the cell remains in metaphase until all kinetochores have attached correctly to spindle microtubules – a process called biorientation. Once the mitotic checkpoint has been satisfied the ubiquitin ligase, anaphase-promoting complex or cyclosome (APC/C), is activated which results in degradation of its key targets such as mitotic

cyclins and the separase inhibitor, securin (Pds1). Degradation of securin allows the protease, separase (Esp1) to cleave cohesin complexes that hold sister chromatids together, therefore leading to their separation, spindle elongation in anaphase, and eventually spindle disassembly in telophase.

Before mitotic exit and spindle disassembly in telophase, another checkpoint, called the spindle position checkpoint (SPOC) ensures proper chromosome segregation into the dividing daughter cells by orienting the nucleus in the bud neck and by repositioning the mitotic spindle with the two separated SPBs positioned at opposite poles so that one SPB is in the mother cell and the other SPB is in the daughter cell (Piatti *et al.*, 2006; Ibrahim, 2015). Since each SPB is linked to a sister chromatid via microtubules this ensures when they are separated and pulled apart in opposite directions, that the mother and the daughter cell each receive a genomic copy.

In contrast to the requirement of upregulating CDK for mitotic entry, to exit mitosis and progress from telophase to cytokinesis, CDK activity has to be downregulated. The APC/C, with its activators Cdc20 (early mitosis) and Cdh1 (late mitosis), target both cyclins and CDK substrates for degradation , and in addition, mechanisms called the FEAR (Cdc14-early anaphase release) and mitotic exit network (MEN), activate the release of Cdc14 phosphatase from the nucleolus, which reverses CDK activity, mainly through dephosphorylating its targets and activating Cdh1 and Swe1; events which are required for mitotic exit and eventually cytokinesis (Jaspersen *et al.*, 1999; Raspelli *et al.*, 2015; Hatano *et al.*, 2016).

1.2 Kinetochore architecture in budding yeast

Throughout the cell cycle, budding yeast kinetochores are connected to SPBs via microtubules, except for a brief period during DNA replication (Kitamura *et al.*, 2007). The centromeric DNA is replicated early in S-phase to allow enough time to re-establish attachment. As mentioned earlier, the kinetochore is composed of different subcomplexes (many present in multiple copies) organised into three layers - inner, central, and outer kinetochore - ranging from the DNA to the spindle microtubules (Figure 1.3 and Table 1.1). The inner kinetochore subcomplexes, often referred to as the CCAN (constitutive centromere-associated network), directly bind to centromeric DNA that is wrapped around a specialised nucleosome that contains the histone H3 variant CENP-A (Cse4 in budding yeast). The term CCAN comes from mammalian

kinetochores, where these proteins remain attached to the centromere throughout the cell cycle and contrasts with outer kinetochore proteins, which only assemble at kinetochores during mitosis. In budding yeast, all kinetochore components remain at centromeres throughout the cell cycle. The outer kinetochore subcomplexes interact with and bind microtubules. Other crucial subcomplexes form the central kinetochore, which mainly serves to link the inner and outer kinetochore, however these subcomplexes also synergistically increase the interaction of the outer kinetochore with microtubules (Cheeseman *et al.*, 2006; Hua *et al.*, 2011), and serve as docking sites for regulatory proteins (Westermann *et al.*, 2007; Liu *et al.*, 2010; Natsume *et al.*, 2013). Even though the subunits of each subcomplex are mostly known, the overall architecture and how these subcomplexes interact to assemble a kinetochore is still somewhat elusive. The 16 kinetochores (one per chromosome) in a haploid budding yeast cell cluster together to form a single focus as seen by fluorescence microscopy, and two foci when the sister kinetochores are segregated in a mitotic cell (Figure 1.2).

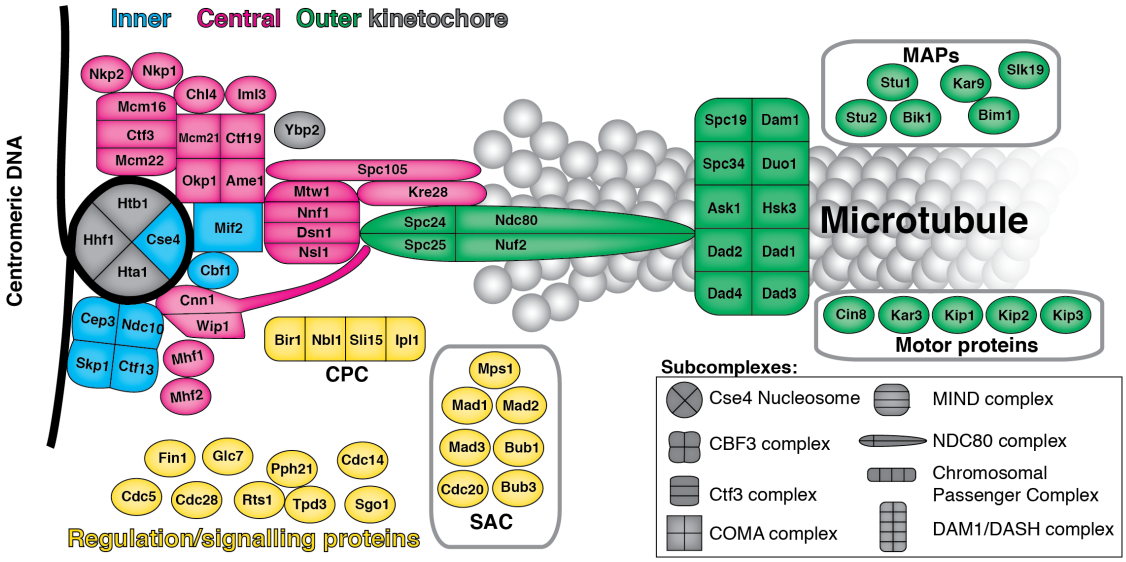

Figure 1.3 The budding yeast kinetochore

A schematic of the budding yeast kinetochore showing a rough layout of the kinetochore subcomplexes. Inner kinetochore subunits, which bind centromeric DNA and the Cse4 nucleosome are coloured blue. Central subunits that link together the inner and outer kinetochore are coloured pink. Outer subunits that associate with microtubules are shown in green. Note that microtubule-associated proteins (MAPs) and motors are not considered structural components of the kinetochore. Many subcomplexes are present in multiple copies per kinetochore, but the schematic shows only one copy of each protein and subcomplex. Typically, the outer subcomplexes are present in more copies than inner kinetochore subcomplexes, for example, the ten-subunit DAM1/DASH complex is present in approximately 16 copies per kinetochore

and forms a ring around the microtubule (see main text for more details). Regulatory and signalling proteins, such as spindle assembly checkpoint (SAC) and chromosome passenger complex (CPC) are shown in yellow (see Table 1.1 for kinetochore homologs in humans and *S. pombe*).

1.2.1 The centromere and the inner kinetochore

The budding yeast centromere consists of three regions called centromere-determining elements (CDEI, II and III), and defines the location of kinetochore assembly. The specialised histone H3 subunit Cse4 associates with the central CDEII centromeric region, and together with Cbf1 homodimer and CBF3 complex (composed of Skp1, Ndc10, Cep3 and Ctf13), bind CDEI and III respectively. These components interact and form the inner kinetochore, onto which other kinetochore subcomplexes assemble. All the components of the CBF3 complex are essential and assemble with the aid of chaperone Hsp90 and co-chaperone Sgt1 (Kitagawa *et al.*, 1999; Stemmann *et al.*, 2002; Bansal *et al.*, 2004). The histone chaperone Scm3 (HJURP in human cells) is necessary for the binding of Cse4 with Ndc10, and is also important for the recruitment of these proteins (Camahort *et al.*, 2007; Mizuguchi *et al.*, 2007; Stoler *et al.*, 2007). Cse4 recruitment to the centromere also depends on the CBF3 complex (Ortiz *et al.*, 1999). Together the CBF3 complex, which is not conserved between yeast and humans, and Cse4 are required for the recruitment of all the central and outer kinetochore proteins in budding yeast. Another important conserved component of this inner kinetochore network is Mif2 (a yeast CENP-C homolog), which forms a homodimer and binds Cse4 and CBF3 complex at the centromere and the COMA and MIND complexes of the central kinetochore, thus linking together the inner and central kinetochore (Cohen *et al.*, 2008; Dimitrova *et al.*, 2016).

1.2.2 The central kinetochore

The kinetochore is often described as a two-layered structure, with inner and outer kinetochore subcomplexes, binding centromeric DNA and microtubules, respectively. However, there are crucial subcomplexes, such as the MIND complex, that do not seem to bind either microtubules or centromeric DNA and/or their key function is to bridge together the inner and outer kinetochore; in addition, these complexes often act as regulatory hubs for signalling at the kinetochore. Therefore, I will regard the kinetochore architecture as a three-layered structure in this introduction. The MIND and the COMA complexes are the two key central complexes that link the inner and outer kinetochore (De Wulf *et al.*, 2003).

The COMA complex, composed of four proteins, the Ame1-Okp1 and the Ctf19-Msm21 heterodimers, is also part of an extended Ctf19 complex, which contains seven additional proteins; subunits of the Ctf3 subcomplex (Ctf3, Mcm16 and Mcm22), Chl4, Iml3, Nkp1 and Nkp2. These proteins are conserved and form the CCAN in most metazoans. These subunits are non-essential proteins in budding yeast, except for Ame1 and Okp1, but all are required for accurate chromosome segregation (Hyland *et al.*, 1999). The Ctf3 subcomplex, and Chl4 and Iml3, sometimes referred to as the Chl4-Iml3 subcomplex, require the Ctf19 protein for proper kinetochore localisation (Pot *et al.*, 2003). The Ame1-Okp1 dimer of the COMA complex is required for recruiting the MIND complex (MIS12 complex in humans) to the kinetochore (Hornung *et al.*, 2014). The C terminus of Ame1-Okp1 dimer associates with Mif2 and the CBF3 complex (and possibly Cse4) at the centromere and the N terminus of Ame1-Okp1 extents towards and binds the MIND complex (Hornung *et al.*, 2014). Thus, together the COMA complex and Mif2 link the MIND complex with the inner kinetochore. Furthermore, the Ctf19 complex is important for loading cohesin onto the pericentromere (Fernius *et al.*, 2013). In addition, the Chl4-Iml1 subcomplex binds Mif2 and participates in chromatid cohesion by recruiting shugoshin (Sgo1) (Hinshaw & Harrison, 2013), which protects cohesin from being cleaved by separase (Esp1).

The MIND complex, composed of two heterodimers Mtw1-Nnf1 and Dsn1-Nsl1, all of which are essential and conserved, is regarded as the main central kinetochore complex, bridging the microtubule-interacting proteins with the centromere-associated proteins. Recently the crystal structure of the MIND/MIS12 complex was solved and revealed a Y-shaped elongated rod-like structure (Dimitrova *et al.*, 2016; Petrovic *et al.*, 2016). The split N-terminal end of the heterotetramer contains double globular heads; one head containing the N-terminal part of the Mtw1-Nnf1 dimer and the other head the N-terminal part of the Dsn1-Nsl1 dimer. The Mw1-Nnf1 N-terminal head interacts with Mif2 and Ame1 and the C terminus of Dsn1 interacts with the NDC80 complex, specifically to the C-terminal part of the Spc24-Spc25 heterodimer (Hornung *et al.*, 2014; Dimitrova *et al.*, 2016). Furthermore, it is suggested that the MIND complex interacts with the C terminus of the SPC105 complex (De Wulf *et al.*, 2003). Therefore, the MIND complex is a crucial connector of three complexes at the centre of the kinetochore, connecting COMA, NDC80 and SPC105 complexes.

The SPC105 complex (KNL1 complex in humans), which also contains Kre28 (ZWINT1 in humans), is an elongated complex that anchors to the MIND complex (De Wulf *et al.*, 2003; Maskell *et al.*, 2010). Even though the N terminus of Spc105 is most likely not bound to any structural component of the kinetochore, it has been shown to have a low affinity to plus-ends of microtubules (Pagliuca *et al.*, 2009). However, it is not required for establishing microtubule attachment; nonetheless it is likely required for kinetochore recruitment of specific microtubule-associated proteins (Bim1, Bik1 and Slk19) and motors (Cin8 and Kar3) (Pagliuca *et al.*, 2009). Perhaps the most important role of the SPC105 complex is in mediating the activation of the spindle assembly checkpoint (described in section 1.3.1. below).

There is an alternative connection between the inner and outer kinetochore; through the elongated Cnn1 protein (CENP-T in humans), whose C terminus (and binding partners Wip1, Mhf1 and Mhf2), either directly binds centromeric DNA or to centromeric proteins, and the N terminus is thought to compete against Dsn1 for binding the Spc24-Spc25 dimer of the NDC80 complex. This competitive binding is suggested to prevent both MIND and SPC105 complex association with the NDC80 complex (Bock *et al.*, 2012; Mechtler *et al.*, 2012; Malvezzi *et al.*, 2013; Thapa *et al.*, 2015). The nature of this competitive binding is unclear, but Cnn1 activity peaks in anaphase and is regulated by Cdc28, Mps1 and Ipl1 (Aurora B in humans) kinases (Bock *et al.*, 2012; Malvezzi *et al.*, 2013; Thapa *et al.*, 2015). Recently, it was shown that the Cnn1 and Ctf3 complexes closely interact and that Cnn1 kinetochore localisation required Ctf3; thereby suggesting that Cnn1, Wip1, Ctf3, Mcm16 and Mcm22 form a separate kinetochore subcomplex that serves to connect the centromere with an extra NDC80 complex in addition to Mif2, the COMA and the MIND complexes (Pekgöz Altunkaya *et al.*, 2016). Similarly, it was shown recently, that CENP-T in human cells can recruit two additional NDC80 complexes and an additional MIS12 complex, thus recruiting three NDC80 complexes in addition to the CENP-C:MIS12 connection which recruits a single NDC80 complex (Huis *et al.*, 2016).

1.2.3 The outer kinetochore and microtubule binding proteins

The SPC105, MIND and NDC80 complexes (KNL1, MIS12 and NDC80 in humans) together form the so-called KMN network which is often referred to as the outer kinetochore. This network is highly conserved between yeast and human, and is crucial

for microtubule binding, regulation of microtubule attachment and mitotic checkpoint activation.

The NDC80 complex is an elongated rod-like complex that is composed of four essential proteins, the Spc24-Spc25 and Ndc80-Nuf2 heterodimers that connect end-to-end and each dimer contains a globular domain at opposite ends (Valverde *et al.*, 2016). The globular domain at the Spc24-Spc25 end interacts with the MIND complex, as mentioned above, and the N-terminal globular regions of the Ndc80-Nuf2 dimer contain calponin-homology domains which bind microtubules along with the N-terminal tail of Ndc80 (Alushin *et al.*, 2012). A “loop” region about halfway between the N-terminal globular domain and the C terminus of Ndc80 associates with the DAM1/DASH complex (Maiolica *et al.*, 2007; Maure *et al.*, 2011). However more recently, it was suggested that the interactions between the NDC80 and DAM1/DASH complexes were more extensive (Kim *et al.*, 2017).

The ten-subunit DAM1/DASH complex is crucial for a proper kinetochore-microtubule attachment in budding yeast, but it is not conserved in humans (Table 1.1). The SKA complex is proposed to be the functional homolog of the DAM1/DASH complex in human cells (Welburn *et al.*, 2009; Chan *et al.*, 2012*b*; van Hooff *et al.*, 2017). The DAM1/DASH complex forms a ring around microtubules *in vitro* and it is thought that about 16 copies of the complex are needed to form a ring around a single microtubule (Miranda *et al.*, 2005; Westermann *et al.*, 2005; Joglekar *et al.*, 2006; Grishchuk *et al.*, 2008; Gonen *et al.*, 2012). Recently, it was reported that a single NDC80 complex could bind two DAM1/DASH complex rings; with the C terminus of Ndc80 interacting with one ring and central and N-terminal regions interacting with a second ring (Kim *et al.*, 2017). The ability of the DAM1/DASH complex to track the dynamically growing and shrinking plus end of microtubules enables it to couple depolymerisation with chromosome movement, thus ensuring chromosome segregation (Asbury *et al.*, 2006; Westermann *et al.*, 2006).

The outer kinetochore also contains a number of accessory proteins, namely microtubule-associated proteins (MAPs), such as Stu1, Stu2, Bim1, Bik1 and Slk19, and motor proteins, Kip1, Kip3, Cin8 and Kar3. Some MAPs and motor proteins associate with both cytoplasmic (astral) and nuclear microtubules and control their dynamics. Other MAPs associate specifically with the nuclear microtubules and

kinetochore subunits involved in microtubule attachment, but are not considered as structural components of the kinetochore (Biggins, 2013). Instead, they transiently interact with the outer kinetochore and are often required for the regulation of kinetochore-microtubule attachment during specific times or conditions. Furthermore, MAPs and kinesin motors often contain microtubule polymerase or depolymerase activity and have been shown to control microtubule dynamics at the kinetochore (Blake-Hodek *et al.*, 2010; Reber & Hyman, 2015). The MAPs and kinesin motors are also important for mitotic spindle alignment, kinetochore clustering, and sliding along microtubules, and to resolve lateral kinetochore-microtubule attachments in early mitosis and direct laterally attached kinetochores towards the microtubule plus ends (Tytell & Sorger, 2006; Tanaka *et al.*, 2007; Wargacki *et al.*, 2010; Gandhi *et al.*, 2011; Richmond *et al.*, 2013; Shrestha & Draviam, 2013). In addition, both MAPs and motors are required for crosslinking microtubules of the mitotic spindle and are important for controlling spindle elongation during anaphase (Gardner *et al.*, 2008; Rizk *et al.*, 2014; Maiato *et al.*, 2017 and references therein). The precise molecular mechanisms of these MAPs and motors at the kinetochore are not fully understood, but evidence for some of their functional roles have been accumulating in recent years. For example, Stu2 (a member of XMAP215 protein family and homolog of human ch-TOG), interacts with the NDC80 complex and stabilises microtubule attachment when microtubule tips are assembling and kinetochores are under tension, but destabilises attachment when kinetochores are not under tension and the tips are disassembling (Miller *et al.*, 2016). This activity is thought to retain selectivity upon correct kinetochore-microtubule attachments. Another MAP, Stu1 (budding yeast CLASP1/2 homolog), binds unattached kinetochores in a SPC105 complex-dependent manner, stabilises kinetochore-microtubule attachment in metaphase, and relocalises to the spindle midzone in anaphase to stabilise the spindle (Funk *et al.*, 2014).

Table 1.1 Conservation of kinetochore subunits

		Subcomplex	*S. cerevisae*	Human	*S. pombe*
Inner kinetochore	CCAN	CBF3	Ndc10	-	-
			Ctf13	-	-
			Cep3	-	-
			Skp1	-	-
			Ybp2	-	-
Central kinetochore			Cse4	CENP-A	Cnp1
			Cbf1	CENP-B	Abp1
			Mif2	CENP-C	Cnp3
		COMA	Ctf19	CENP-P	Fta2
			Okp1	CENP-Q	Fta7
			Mcm21	CENP-O	Mal2
			Ame1	CENP-U/PBIP1	Mis17
		Ctf3	Mcm16	CENP H	Fta3
			Ctf3	CENP-I	Mis6
			Mcm22	CENP-K	Sim4
			Nkp1	-	Fta4
			Nkp2	-	Cnl2
		Chl4-Iml3	Chl4	CENP-N	Mis15
			Iml3	CENP-L	Fta1
		CNN1	Cnn1	CENP-T	Cnp20
			Wip1	CENP-W	New1
			Mhf1	CENP-S	Mhf1
			Mhf2	CENP-X	Mhf2
	KMN	MIND	Mtw1	MIS12	Mis12
			Dsn1	DSN1	Mis13
			Nnf1	NNF1	Nnf1
			Nsl1	NSL1	Mis14
		SPC105	Spc105	KNL1/Blinkin	Spc7
			Kre28	ZWINT-1	Sos7
		NDC80	Ndc80	Hec1	Ndc80
			Spc24	SPC24	Spc24
			Spc25	SPC25	Spc25
			Nuf2	NUF2	Nuf2
Outer kinetochore		DAM1/DASH	Dam1	Ska1*	Dam1
			Duo1	Ska2*	Duo1
			Spc19	Ska3*	Spc19
			Spc34	-	Spc34
			Ask1	-	Ask1
			Dad1	-	Dad1
			Dad2	-	Dad2
			Dad3	-	Dad3
			Dad4	-	Dad4
			Hsk3	-	Hsk3
		MAPs	Stu1	CLASP1/2	Peg1
			Stu2	XMAP215	Dis1/Alp14
			Slk19	-	-
			Bim1	EB1	Mal3
			Bik1	CLIP-170	Tip1
		Motor proteins	Kar3	KIFC1	Pkl1
			Cin8	KIF11	Cut7
			Kip2	KIF22	Tea2
			Kip3	KIF18	Klp6
			Kar9	-	-
Regulation		CPC	Sli15	INCENP	Pic1
			Bir1	Survivin	Cut7
			Nbl1	Borealin	Mug118
			Ipl1	Aurora B	Ark1
		SAC	Mps1	Mps1/TTK	Mph1
			Mad1	Mad1	Mad1
			Mad2	Mad2	Mad2
			Bub1	Bub1	Bub1
			Mad3	BubR1	Mad3
			Cdc20	Cdc20	Slp1
			Cdc28	CDK1	Cdc2
			Fin1	-	-
			Glc7	PP1'	Dis2
			Sds22	PP1'	Sds22
			Pph21	PP2A'	Ppa1
			Pph22	PP2A'	Ppa2
			Rts1	B56	Par2
			Tpd3	PP2A'	Paa1
			Cdc55	B55	Pab1
			Cdc14	CDC14	Clp1
			Sgo1	SGO1	Sgo1
			Cdc5	PLK1	Plo1

1.3 Mitotic and spindle regulation via the kinetochore

1.3.1 The spindle assembly checkpoint

During cell division, eukaryotic cells ensure that the replicated genetic material is accurately divided between the two daughter cells. This requires that kinetochores on every sister chromatid correctly attach to the mitotic spindle. When even a single kinetochore is unattached the cell activates a checkpoint referred to as the mitotic checkpoint or spindle assembly checkpoint (SAC) (Rieder *et al.*, 1995). This evolutionary conserved checkpoint ensures the cell remains in metaphase until sister kinetochores have achieved correct attachment to microtubules emanating from opposite spindle poles (biorientation). Defects during this process can cause chromosome missegregation or aneuploidy, which is frequently found in cancer cells. SAC genes are commonly misregulated in cancer cells (Kops *et al.*, 2005); however, it is debated whether aberrant SAC, and indeed aneuploidy, is a driver of - or a consequence of cancer.

Two studies published in Cell in 1991 formed the basis of our understanding of the mitotic checkpoint (Hoyt *et al.*, 1991; Li & Murray, 1991). These studies, performed in budding yeast, identified the key components of the checkpoint (except for Mps1) and showed that cells with mutations in these genes were inviable when the mitotic spindle was compromised by treatment with microtubule poison. These studies confirmed prevalent ideas, that cells use a surveillance mechanism to regulate chromosome segregation, which had remained for decades. Subsequent studies, elucidated the mechanism of the SAC and determined that the signal produced by the checkpoint to pause the cell cycle was generated at the kinetochore (Musacchio & Salmon, 2007; Joglekar & P., 2016 and references therein).

The SAC operates via a signalling cascade of sequential recruitment of checkpoint proteins (Figure 1.4). An unattached kinetochore recruits a complex of Bub3 and Bub1 kinase through the phosphorylation of MELT motifs on Spc105 (KNL1 in humans), a member of KMN network (KNL1, MIND and NDC80 subcomplexes). These MELT motif repeats are phosphorylated by Mps1 kinase, the key upstream regulator of the SAC (Hardwick *et al.*, 1996; Saurin *et al.*, 2011; Shepperd *et al.*, 2012; Primorac *et al.*, 2013; London & Biggins, 2014). This in turn leads to the recruitment of other checkpoint proteins Mad1 and Mad2, which together form a platform that is able to rapidly convert

free inactive open-Mad2 (O-Mad2) to active closed-Mad2 (C-Mad2) (De Antoni *et al.*, 2005; Moyle *et al.*, 2014). C-Mad2 along with Mad3 (BubR1 in humans) and Bub3 forms the mitotic checkpoint complex (MCC), which functions to inhibit Cdc20 and thereby prevents it from activating the E3 ubiquitin ligase known as the anaphase-promoting complex or cyclosome (APC/C) (Hardwick *et al.*, 2000; Sudakin *et al.*, 2001; Herzog *et al.*, 2009; Lau & Murray, 2012). Inactive APC/C is unable to ubiquitylate securin (Pds1) and mitotic cyclins, thus preventing their destruction by the proteasome. Thus, stabilised securin binds separase (Esp1) and prevents it from cleaving cohesin; hence this, along with high level of CDK activity, maintain cells in metaphase (Ciosk *et al.*, 1998; Uhlmann *et al.*, 2000; Musacchio & Salmon, 2007 and references therein).

As mentioned above, the SAC is also activated when chromosomes are misattached to the spindle and kinetochores not under tension. The Aurora B kinase (Ipl1 in budding yeast), the catalytic member of the chromosomal passenger complex (CPC), destabilises incorrect microtubule attachments by phosphorylating sites on the NDC80 and DAM1/DASH outer kinetochore subcomplexes (Biggins & Murray, 2001; Ruchaud *et al.*, 2007; Carmena *et al.*, 2012*b*). This Aurora B/Ipl1-dependent destabilisation of microtubule-kinetochore attachment creates unattached kinetochores, thereby activating SAC (Pinsky *et al.*, 2006). However, the CPC has also been proposed to be more directly involved in the SAC. For example, artificial tethering of Mps1 to Mis12 (Mtw1 homolog in budding yeast) was shown to rescue SAC deficiency of Aurora B inhibition in human cells, suggesting a role for CPC in recruiting Mps1 to unattached kinetochores (Saurin *et al.*, 2011). In addition, there is evidence to show that Aurora B has a role in SAC signal maintenance, after recruitment of checkpoint proteins (Maldonado & Kapoor, 2011*a*).

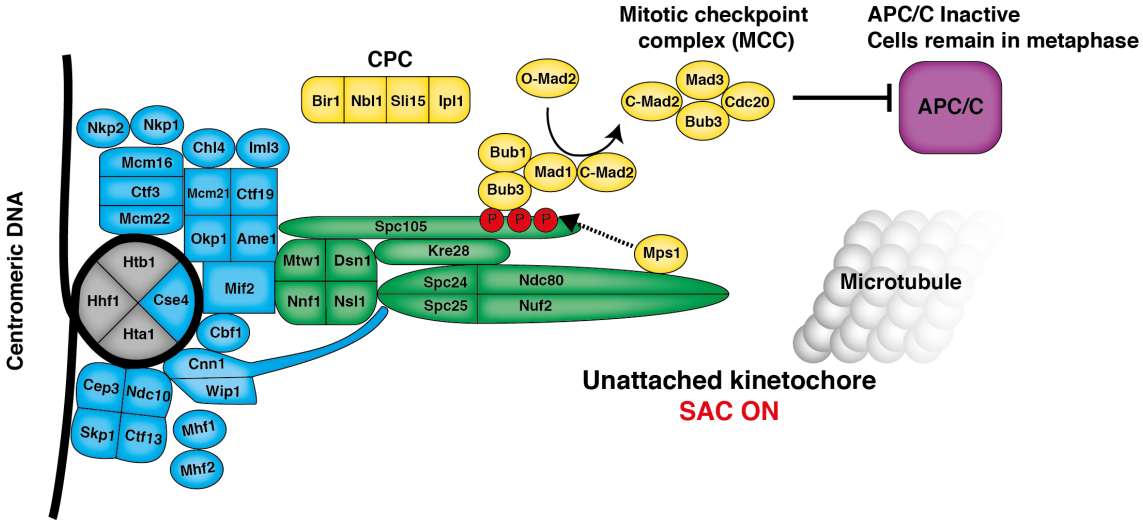

Figure 1.4 Schematic of the spindle assembly checkpoint (SAC)

A schematic showing the locations of the kinetochore subcomplexes and recruitment of SAC components. Subunits of the inner kinetochore and constitutive centromere-associated network (CCAN) are shown in blue, the KMN network subunits are shown in green, and chromosomal passenger complex (CPC) and SAC components in yellow. The red dots on Spc105 refer to the MELT repeats which are phosphorylated by Mps1 kinase to recruit the Bub1-Bub3 complex which in turn recruits the Mad1-Mad2 complex and results in the formation of the mitotic checkpoint complex (MCC) which inhibits Cdc20-dependent activation of the anaphase-promoting complex (APC) (see details in the main text).

Conversely to the phosphorylation events at the kinetochore required during SAC activation, dephosphorylation by counteracting phosphatases is needed for SAC silencing and maintenance of microtubule attachments, when all kinetochores have achieved bipolar attachment to the spindle (De Wulf *et al.*, 2009; Maldonado & Kapoor, 2011*b*; Rosenberg *et al.*, 2011). Protein phosphatase 1 (PP1; Glc7 in budding yeast) and protein phosphatase 2A (PP2A; Pph21/22 in budding yeast) antagonise Mps1 and Aurora B kinase activity on attached kinetochores to facilitate the silencing of the SAC (Pinsky *et al.*, 2009; Liu *et al.*, 2010; Rosenberg *et al.*, 2011; London *et al.*, 2012; Funabiki & Wynne, 2014; Zhang *et al.*, 2014; Espert *et al.*, 2014). The N-terminal SSILK and RVSF motifs of KNL1 are binding sites for PP1, which are inhibited by Aurora B phosphorylation. When kinetochores are correctly attached to microtubules and under tension, the recruitment of PP2A to the kinetochore, via phosphorylation of BUBR1, leads to dephosphorylation of these KNL1 N-terminal sites, subsequently creating a docking site for PP1 recruitment, which reverses Mps1 phosphorylation of the KNL1 MELT motifs, thereby silencing the SAC (Nijenhuis *et al.*, 2014).

It has been shown that forced recruitment of Glc7 to Spc105 did not prematurely silence the SAC, which suggests that PP1 is necessary but not sufficient for SAC silencing in budding yeast (Rosenberg *et al.*, 2011). As alternative (or parallel) mechanisms for SAC silencing other models have been proposed; either suggesting that microtubule binding to kinetochores competes against SAC protein recruitment and results in removal of Mps1 from kinetochores (DeLuca *et al.*, 2003; Jelluma *et al.*, 2010; Espeut *et al.*, 2012; Hiruma *et al.*, 2015; Ji *et al.*, 2015), or kinetochore-microtubule end-on attachment physically prevents Mps1 from accessing the MELT motifs on KNL1/Spc105. Consistent with the latter model, the DAM1/DASH complex has been suggested to act as a barrier between Mps1 (which probably binds to the N terminus of Ndc80) and Spc105 on attached kinetochores in budding yeast (Aravamudhan *et al.*, 2015; Joglekar & Aravamudhan, 2016).

A similar model is proposed for downregulating the CPC activity at the outer kinetochore for anaphase transition (Tanaka *et al.*, 2002; Maresca & Salmon, 2010; Lampson & Cheeseman, 2011). When kinetochores are attached and under tension it is suggested that this creates either an internal kinetochore stretch or increases the distance between sister kinetochores, thus pulling the outer kinetochore complexes away from the centromere, allowing Ipl1-substrates (such as Ndc80 and Dam1) to sufficiently escape a central zone of CPC activity at the outer kinetochore. The CPC, an elongated complex, is recruited at the inner kinetochore or between sister kinetochores (inner centromere) (van der Waal *et al.*, 2012; Carmena *et al.*, 2012 and references therein). Furthermore, Cdc14 dephosphorylation of Sli15, a CPC subunit, relocalises CPC from the centromere to the spindle midzone in anaphase for spindle elongation (Pereira & Schiebel, 2003; Mirchenko & Uhlmann, 2010), which could also contribute to reduced CPC activity at the kinetochore-microtubule attachment sites, for anaphase progression.

1.3.2 Post-translational regulation of kinetochore proteins

Many kinases and phosphatases plus a number of other signalling proteins with different post-translational modification (PTM) activity, such as methylation, acetylation, sumoylation and ubiquitylation, have been shown to be important for kinetochore function and chromosome segregation (Li *et al.*, 2006; Montpetit *et al.*, 2006; Choy *et al.*, 2011; Latham *et al.*, 2011; Akiyoshi *et al.*, 2013*b*; Au *et al.*, 2013). Some kinetochore proteins are regulated by several PTMs, for example, Dsn1, a subunit of

the MIND complex, is targeted by CDK/Cdc28, Aurora B/Ipl1 kinase, and by phosphatase Cdc14 (Akiyoshi & Biggins, 2010). Ipl1 phosphorylation of Dsn1 is required for MIND complex kinetochore recruitment and stabilisation of Dsn1, but after dephosphorylation of these Ipl1 sites, it is ubiquitylated by Mub1/Ubr2 and degraded by the proteasome. However, Dsn1 can be stabilised if a key CDK site on the protein is phosphorylated in the absence of Ipl1-phosphorylation (Akiyoshi *et al.*, 2013*b*). In addition, Ipl1 phosphorylation of Dsn1 increases the interaction between the inner and outer kinetochore, by phosphorylating sites on the N-terminal arm of Dsn1 which relieves its auto-inhibitory activity of Mif2 and Ame1 binding to the MIND complex (Dimitrova *et al.*, 2016).

Another example of multiple regulatory modifications on a kinetochore protein is the tight regulation of the centromeric histone variant Cse4. Mislocalisation of Cse4 outside the centromere results in genomic instability, hence its regulation is important for accurate chromosome segregation. Cse4 is regulated by Psh1, an E3 ubiquitin ligase, which prevents excessive Cse4 chromosome loading by targeting it for proteosomal degradation (Hewawasam *et al.*, 2010; Ranjitkar *et al.*, 2010). Furthermore, phosphorylation of Psh1 by casein kinase 2 (CK2; Cka2 in budding yeast) was shown to regulate the Cse4-Psh1 association (Hewawasam *et al.*, 2014). Additionally, chromatin remodelling complexes, such as SWI/SNF, FACT and INO80 have been shown to have a role in maintaining Cse4 at the centromere (Gkikopoulos *et al.*, 2011; Deyter & Biggins, 2014; Hildebrand *et al.*, 2016). Moreover, Cse4 sumoylation by E3 ligases, Siz1 and Siz2, and ubiquitylation by the SUMO-targeted ubiquitin ligase (STUbL), Slx5, contribute significantly to preventing Cse4 mislocalisation (Ohkuni *et al.*, 2016). Cse4 is protected from Psh1-dependent degradation by Pat1, a Topoisomerase II-associated protein (Mishra *et al.*, 2013, 2015), and Ubp8, a component of the SAGA-DUB (deubiquitin) complex (Canzonetta *et al.*, 2015). Interestingly, deletion of *PSH1*, which increases Cse4 levels, also increases Mif2 and COMA complex proteins at the kinetochore, but not MIND, NDC80 and DAM1/DASH complex proteins. However, if *UBR2* is also deleted, MIND complex subunits and Spc105 (not NDC80 and DAM1/DASH complex subunits) proteins do increase, supporting the notion of tight and distinct regulation of different kinetochore proteins and their recruitment to kinetochores (Herrero & Thorpe, 2016). Concurrently, it has been reported that methylation of Cse4 is required for kinetochore recruitment of subunits of the Ctf19 and MIND complexes, but not Cse4 itself (Samel *et al.*, 2012). In

addition, Cse4 is also phosphorylated by Ipl1, likely to destabilise aberrant kinetochores and ensure correct chromosome segregation (Boeckmann *et al.*, 2013).

Taken together, it is clear that kinetochore proteins can be regulated by multiple post-translational modifications by different regulatory proteins. Furthermore, the same kinetochore regulator can have different roles depending on its location at the centromere-kinetochore-microtubule axis. For example, the Aurora B/Ipl1 kinase along with its CPC, is one such regulator, whose function at the inner kinetochore seems to stabilise interactions and promote kinetochore assembly, in contrast to its outer kinetochore activity in destabilising microtubule attachment. Therefore, the spatial and temporal control of kinetochore regulators during the cell cycle is crucial for maintaining high-fidelity chromosome segregation.

1.4 Project aims

Methods using artificial tethering of two proteins such as direct fusion of two individual open reading frames (ORFs) have been extensively used to study the effects of forced recruitment of proteins. For example, fusing cyclin-B (cdc13) with CDK (cdc2) in fission yeast is sufficient to drive cell-cycle progression (Coudreuse & Nurse, 2010) and fusing Mad2 to either Mad3 or Cdc20 activates the SAC in budding yeast (Lau & Murray, 2012), and similarly, Mad1 fused to Mis12 (ortholog of Mtw1 in budding yeast) has been shown to activate the SAC in human cells (Maldonado & Kapoor, 2011*a*). In addition, many important findings of kinetochore regulation have been discovered by artificial tethering experiments. For example, when Polo-like kinase (Plk1) was tethered to proteins in different subcompartments at the human kinetochore, it revealed several functional roles for Plk1 at the kinetochore (Lera *et al.*, 2016). Recently, an optogenetic system was developed to artificially recruit SAC and motor proteins to human kinetochores (Zhang *et al.*, 2017*b*). These kinds of experiments emphasise the insight gained from artificially recruiting SAC and other signalling components to the kinetochore. A number of alternative methods for artificial association of two proteins have also been used successfully (Sharma *et al.*, 2003; Devit *et al.*, 2005; Banaszynski *et al.*, 2006; Haruki *et al.*, 2008; Levskaya *et al.*, 2009; Kennedy *et al.*, 2010; Yang *et al.*, 2013; Natsume *et al.*, 2013; Wang *et al.*, 2016).

In the lab, we have developed a proteome-wide protein-protein association system which allows us to create forced protein interactions in vivo across the whole proteome

in budding yeast (Olafsson & Thorpe, 2015, 2017; Berry *et al.*, 2016). For this system, which we term synthetic physical interactions or SPI, we utilise the GFP-binding protein (GBP) (Rothbauer *et al.*, 2006, 2008) and the GFP collection of strains with most genes tagged with GFP (Huh *et al.*, 2003).

Even though our understanding of kinetochore regulation is increasing, many questions still remain unanswered. Four key aspects of kinetochore regulation need further future investigation:

- What is the underlying molecular basis of cell-cycle dependent kinetochore recruitment of proteins directly involved in microtubule attachment and/or in the SAC?
- What is the mechanistic role of regulators that control assembly and disassembly of kinetochore subcomplexes and/or protein level of kinetochore subunits during the cell cycle?
- Where are the critical phosphorylation and other PTM sites that contribute to recruitment of kinetochore regulators?
- Are there other, currently unknown, regulators of the kinetochore?

The underlying assumption of my project is that the spatial arrangement of regulatory proteins (such as those described above) is critical for normal kinetochore homeostasis and checkpoint function. The key aim of my project is to use the SPI system to identify new regulators of kinetochore function via their position at the kinetochore and characterise their mechanism and to further characterise the role of existing regulators with higher spatial resolution.

Chapter 2. Materials & Methods

2.1 General yeast and bacterial methods

2.1.1 Yeast strains

S. cerevisiae strains used in this project were either W303 (Zou & Rothstein, 1997) or S288C (Brachmann *et al.*, 1998) background. The strains are listed in Table 2.1.

Table 2.1 Yeast strains

Strain	Genotype	Source
W8164-2B	*MATα CEN1-16::Gal-Kl-URA3*	Reid et al. 2011
W6995-6A	*MAT**a** ADE2 bar1::LEU2 trp1-1 LYS2 ura3::3xURA3-tetOx112 TetR-mRFP1(iYGL119W) SPC110-YFP::HIS3 RAD5*	Thorpe et al. 2009
All GFP strains	*MAT**a** his3Δ1 leu2Δ0 met15Δ0 ura3Δ0 XXX-GFP::HIS3*	Huh et al. 2003
BY4741	*MAT**a** his3Δ1 leu2Δ0 met15Δ0 ura3Δ0*	Brachmann et al. 1998
BY4742	*MATα his3Δ1 leu2Δ0 met15Δ0 ura3Δ0*	Brachmann et al. 1998
YAL6B	*MAT**a** his3Δ1 leu2Δ0 met15Δ0 ura3Δ0 arg4Δ::KANMX lys1Δ::KANMX*	Gruhler et al. 2005
PT15-18A	*MAT**a** ADE2 TRP1 lys2Δ leu2-3,112 his3-11 cse4Δ::KANMX CSE4-GFPint::URA3*	Herrero and Thorpe 2016
PT19-C	*MAT**a** HTA1-CFP::NAT*	Olafsson and Thorpe 2015
PT33-34A	*MAT**a** ADE2 leu2-3,112 trp1-1 LYS2 MTW1-YFP RAD5*	Herrero and Thorpe 2016
PT39-30A	*MATα ADE2 TRP1 leu2-3,112 his3-11,15 ura3-1 lys2Δ RAD5 MTW1-CFP*	Eva Herrero
PT54-20D	*MAT**a** TRP1 ura3::3xURA3-tetOx112 TetR-mRFP SMC1-YFP::KANMX HTA1-CFP*	Olafsson and Thorpe 2016
PT63-1D	*MATα ADE2 leu2-3,112 his3-11,15 URA3 LYS2 can1-100 trp1-1 cdc20::prMET3-CDC20::TRP1 MTW1-YFP*	This Study
PT63-12B	*MAT**a** ADE2 leu2-3,112 his3-11,15 URA3 LYS2 can1-100 trp1-1 cdc20::prMET3-CDC20::TRP1 MTW1-YFP*	Eva Herrero
PT72	*MATα ADE2 lyp1Δ::STE3pr-LEU2 trp1-1 LYS2 leu2-3,112 ura3 DYN1 bub3Δ::KAN CSE4-GFP::HIS3*	Olafsson and Thorpe 2015
PT73-7A	*MAT**a** CSE4-CFP::HIS3*	Olafsson and Thorpe 2016
PT95-19C	*MAT**a** ADE2 TRP1 FOB1-CFP*	Olafsson and Thorpe 2015
PT95-35A	*MATα ADE2 trp1-1 leu2-3,112 his3-11,15 FOB1-CFP*	Olafsson and Thorpe 2015
PT129-1A	*MATα ADE2 LYS2 SPC110-CFP::KAN RAD5*	Olafsson and Thorpe 2015

PT142-1C	*MATα ADE2 TRP1 leu2-3,112 his3-11,15 ura3-1 lys2Δ RAD5 ASK1-CFP*	Olafsson and Thorpe 2015
PT147-7C	*MAT**a** TRP1 lys2Δ DAD4-YFP::NAT SPC42-RFP::HYGMX*	Berry et al. 2016
PT149	*MATα/MAT**a** FOB1-CFP CDC5-GFP::HIS3*	Olafsson and Thorpe 2015
PT150	*MATα/MAT**a** FOB1-CFP TOM70-GFP::HIS3*	Olafsson and Thorpe 2015
PT151	*MATα/MAT**a** FOB1-CFP YPR174C-GFP::HIS3*	Olafsson and Thorpe 2015
PT152	*MATα/MAT**a** FOB1-CFP NUP1-GFP::HIS3*	Olafsson and Thorpe 2015
PT153	*MATα/MAT**a** FOB1-CFP CDC14-GFP::HIS3*	Olafsson and Thorpe 2015
PT154	*MATα/MAT**a** MTW1-CFP CDC14-GFP::HIS3*	Olafsson and Thorpe 2015
PT155	*MATα/MAT**a** ASK1-CFP CDC14-GFP::HIS3*	Olafsson and Thorpe 2015
PT156	*MATα/MAT**a** ASK1-CFP CDC5-GFP::HIS3*	Olafsson and Thorpe 2015
PT157	*MATα/MAT**a** ASK1-CFP TOM70-GFP::HIS3*	Olafsson and Thorpe 2015
PT158	*MATα/MAT**a** ASK1-CFP YPR174C-GFP::HIS3*	Olafsson and Thorpe 2015
PT159	*MATα/MAT**a** ASK1-CFP NUP1-GFP::HIS3*	Olafsson and Thorpe 2015
PT209-7A	*MAT**a** ura3::3xURA3-tetOx112 TetR-mRFP(iYGL119W) MTW1-YFP*	Olafsson and Thorpe 2015
PT257	*MAT**a** ADE2 leu2-3,112 his3-11,15 URA3 LYS2 can1-100 trp1-1 cdc20::prMET3-CDC20::TRP1 MTW1-YFP SPC110-CFP::KAN*	This Study
PT262	*MATα ADE2 LYS2 SPC110-CFP::KAN DAD2-YFP::HYGMX RAD5*	This Study
T16	*MATα ADE2 leu2-3,112 TRP1 lys2Δ MTW1-YFP RAD5 mad1Δ::KAN*	Olafsson and Thorpe 2016
T17	*MATα ADE2 leu2-3,112 TRP1 lys2Δ MTW1-YFP RAD5 mad3Δ::KAN*	This Study
T18	*MATα ADE2 leu2-3,112 TRP1 lys2Δ MTW1-YFP RAD5 bub1Δ::KAN*	This Study
T19	*MATα ADE2 leu2-3,112 TRP1 lys2Δ MTW1-YFP RAD5 bub3Δ::KAN*	This Study
T77	*MAT**a** his3Δ1 leu2Δ0 met15Δ0 ura3Δ0 TRP LYS CDC20-GFP::HIS3 mad1Δ::KAN*	Olafsson and Thorpe 2016
T78	*MAT**a** his3Δ1 leu2Δ0 met15Δ0 ura3Δ0 TRP LYS CBF2-GFP::HIS3 mad1Δ::KAN*	Olafsson and Thorpe 2016
T79	*MAT**a** his3Δ1 leu2Δ0 met15Δ0 ura3Δ0 TRP LYS IPL1-GFP::HIS3 mad1Δ::KAN*	Olafsson and Thorpe 2016
T80	*MAT**a** his3Δ1 leu2Δ0 met15Δ0 ura3Δ0 TRP LYS BIR1-GFP::HIS3 mad1Δ::KAN*	Olafsson and Thorpe 2016
T81	*MAT**a** his3Δ1 leu2Δ0 met15Δ0 ura3Δ0 TRP LYS CSE4-GFP::HIS3 mad3Δ::KAN*	This Study

T82	*MAT***a** *his3Δ1 leu2Δ0 met15Δ0 ura3Δ0 TRP LYS CDC20-GFP::HIS3 mad3Δ::KAN*	This Study
T83	*MAT***a** *his3Δ1 leu2Δ0 met15Δ0 ura3Δ0 TRP LYS CBF2-GFP::HIS3 mad3Δ::KAN*	This Study
T84	*MAT***a** *his3Δ1 leu2Δ0 met15Δ0 ura3Δ0 TRP LYS IPL1-GFP::HIS3 mad3Δ::KAN*	This Study
T85	*MAT***a** *his3Δ1 leu2Δ0 met15Δ0 ura3Δ0 TRP LYS BIR1-GFP::HIS3 mad3Δ::KAN*	This Study
T87	*MAT***a** *his3Δ1 leu2Δ0 met15Δ0 ura3Δ0 TRP LYS CDC20-GFP::HIS3 bub3Δ::KAN*	This Study
T88	*MAT***a** *his3Δ1 leu2Δ0 met15Δ0 ura3Δ0 TRP LYS CBF2-GFP::HIS3 bub3Δ::KAN*	This Study
T89	*MAT***a** *his3Δ1 leu2Δ0 met15Δ0 ura3Δ0 TRP LYS IPL1-GFP::HIS3 bub3Δ::KAN*	This Study
T90	*MAT***a** *his3Δ1 leu2Δ0 met15Δ0 ura3Δ0 TRP LYS BIR1-GFP::HIS3 bub3Δ::KAN*	This Study
T221	*MAT***a** *his3Δ1 leu2Δ0 met15Δ0 ura3Δ0 TRP LYS BIR1-GFP::HIS3 bub1Δ::KAN*	This Study
T222	*MAT***a** *his3Δ1 leu2Δ0 met15Δ0 ura3Δ0 TRP LYS CBF2-GFP::HIS3 bub1Δ::KAN*	This Study
T223	*MAT***a** *his3Δ1 leu2Δ0 met15Δ0 ura3Δ0 TRP LYS CDC20-GFP::HIS3 bub1Δ::KAN*	This Study
T224	*MAT***a** *his3Δ1 leu2Δ0 met15Δ0 ura3Δ0 TRP LYS IPL1-GFP::HIS3 bub1Δ::KAN*	This Study
T226	*MAT***a** *his3Δ1 leu2Δ0 met15Δ0 ura3Δ0 TRP LYS CBF2-GFP::HIS3 mad2Δ::KAN*	This Study
T227	*MAT***a** *his3Δ1 leu2Δ0 met15Δ0 ura3Δ0 TRP LYS CDC20-GFP::HIS3 mad2Δ::KAN*	This Study
T228	*MAT***a** *his3Δ1 leu2Δ0 met15Δ0 ura3Δ0 TRP LYS IPL1-GFP::HIS3 mad2Δ::KAN*	This Study
T229	*MAT***a** *ADE2 leu2-3,112 his3-11,15 ura3-1 TRP1 lys2Δ RAD5 CSE4-GFP::HIS3*	This Study
T306	*MAT***a** *his3Δ1 leu2Δ0 met15Δ0 ura3Δ0 CBF2-GFP::HIS3 ubr2Δ::NATMX*	Olafsson and Thorpe 2015
T307	*MAT***a** *his3Δ1 leu2Δ0 met15Δ0 ura3Δ0 BIR1-GFP::HIS3 ubr2Δ::NATMX*	Olafsson and Thorpe 2015
T308	*MAT***a** *his3Δ1 leu2Δ0 met15Δ0 ura3Δ0 NUF2-GFP::HIS3 ubr2Δ::NATMX*	Olafsson and Thorpe 2015
T309	*MAT***a** *his3Δ1 leu2Δ0 met15Δ0 ura3Δ0 NSL1-GFP::HIS3 ubr2Δ::NATMX*	Olafsson and Thorpe 2015
T310	*MAT***a** *his3Δ1 leu2Δ0 met15Δ0 ura3Δ0 NNF1-GFP::HIS3 ubr2Δ::NATMX*	Olafsson and Thorpe 2015
T311	*MAT***a** *his3Δ1 leu2Δ0 met15Δ0 ura3Δ0 DAD2-GFP::HIS3 ubr2Δ::NATMX*	Olafsson and Thorpe 2015
T312	*MAT***a** *his3Δ1 leu2Δ0 met15Δ0 ura3Δ0 STU2-GFP::HIS3 ubr2Δ::NATMX*	Olafsson and Thorpe 2015
T317	*MAT***a** *his3Δ1 leu2Δ0 met15Δ0 ura3Δ0 TRP LYS CSE4-GFP::HIS3 ubr2Δ::NATMX*	Olafsson and Thorpe 2015
T373	*MAT***a** *his3Δ1 leu2Δ0 met15Δ0 ura3Δ0 CDC14-GFP::HIS3 DSN1-3xHA::HYGMX*	Olafsson and Thorpe 2015

T374	*MAT***a** *his3Δ1 leu2Δ0 met15Δ0 ura3Δ0 SPC24-GFP::HIS3 DSN1-3xHA::HYGMX*	Olafsson and Thorpe 2015
T376	*MAT***a** *his3Δ1 leu2Δ0 met15Δ0 ura3Δ0 NNF1-GFP::HIS3 DSN1-3xHA::HYGMX*	Olafsson and Thorpe 2015
T414	*MAT***a** *NUF2-GFP::HIS3 mad3Δ::KAN*	Olafsson and Thorpe 2015
T415	*MAT***a** *NNF1-GFP::HIS3 mad3Δ::KAN*	Olafsson and Thorpe 2015
T416	*MAT***a** *MTW1-GFP::HIS3 mad3Δ::KAN*	Olafsson and Thorpe 2015
T417	*MAT***a** *CDC14-GFP::HIS3 mad3Δ::KAN*	Olafsson and Thorpe 2015
T418	*MAT***a** *KRE28-GFP::HIS3 mad3Δ::KAN*	Olafsson and Thorpe 2015
T419	*MAT***a** *NSL1-GFP::HIS3 mad3Δ::KAN*	Olafsson and Thorpe 2015
T420	*MAT***a** *CEP3-GFP::HIS3 mad3Δ::KAN*	Olafsson and Thorpe 2015
T421	*MAT***a** *DAD3-GFP::HIS3 mad3Δ::KAN*	Olafsson and Thorpe 2015
T422	*MAT***a** *BIK1-GFP::HIS3 mad3Δ::KAN*	Olafsson and Thorpe 2015
T423	*MAT***a** *BUB3-GFP::HIS3 mad3Δ::KAN*	Olafsson and Thorpe 2015
T424	*MAT***a** *MIF2-GFP::HIS3 mad3Δ::KAN*	Olafsson and Thorpe 2015
T425	*MAT***a** *CBF1-GFP::HIS3 mad3Δ::KAN*	Olafsson and Thorpe 2015
T426	*MAT***a** *SLI15-GFP::HIS3 mad3Δ::KAN*	Olafsson and Thorpe 2015
T427	*MAT***a** *AME1-GFP::HIS3 mad3Δ::KAN*	Olafsson and Thorpe 2015
T428	*MAT***a** *MCM21-GFP::HIS3 mad3Δ::KAN*	Olafsson and Thorpe 2015
T429	*MAT***a** *CTF19-GFP::HIS3 mad3Δ::KAN*	Olafsson and Thorpe 2015
T430	*MAT***a** *STU2-GFP::HIS3 mad3Δ::KAN*	Olafsson and Thorpe 2015
T431	*MAT***a** *DSN1-GFP::HIS3 mad3Δ::KAN*	Olafsson and Thorpe 2015
T432	*MAT***a** *mtw1Δ::KAN with plasmid pHT10 [MTW1-GBP LEU2]*	Olafsson and Thorpe 2015
T441	*MAT***a** *his3Δ1 leu2Δ0 met15Δ0 ura3Δ0 MTW1-GFP::HIS3 fin1Δ::KANMX*	This Study
T442	*MAT***a** *his3Δ1 leu2Δ0 met15Δ0 ura3Δ0 CTF19-GFP::HIS3 fin1Δ::KANMX*	This Study
T443	*MAT***a** *his3Δ1 leu2Δ0 met15Δ0 ura3Δ0 CEP3-GFP::HIS3 fin1Δ::KANMX*	This Study
T444	*MAT***a** *his3Δ1 leu2Δ0 met15Δ0 ura3Δ0 DAD2-GFP::HIS3 fin1Δ::KANMX*	This Study

T445	*MAT**a** his3Δ1 leu2Δ0 met15Δ0 ura3Δ0 NUF2-GFP::HIS3 fin1Δ::KANMX*	This Study
T446	*MAT**a** his3Δ1 leu2Δ0 met15Δ0 ura3Δ0 NNF1-GFP::HIS3 fin1Δ::KANMX*	This Study
T449	*MATα trp1-1 his3-11,15 leu2-3,112 ura3-1 RAD5 MET17 ADE2 LYS2 CEN1-16::Gal-Kl-URA3 CDC14-GBP::KANMX*	Olafsson and Thorpe 2015
T450	*MAT**a** his3Δ1 leu2Δ0 met15Δ0 ura3Δ0 CDC14-GBP::KANMX*	This Study
T479	*MATα ADE2 leu2-3,112 TRP1 lys2Δ MTW1-YFP RAD5 SPC110-CFP::KANMX*	This Study
T498	*MAT**a** his3Δ1 leu2Δ0 met15Δ0 ura3Δ0 CDC14-GFP::HIS3 fin1Δ::KANMX*	This Study
T501	*MATα ADE2 leu2-3,112 his3-11,15 ura3-1 TRP1 lys2Δ RAD5 ASK1-CFP BIR1-YFP::KANMX*	Olafsson and Thorpe 2016
T527	*MAT**a** his3Δ1 leu2Δ0 met15Δ0 ura3Δ0 CDC5-GBP::KANMX*	This Study
T528	*MAT**a** his3Δ1 leu2Δ0 met15Δ0 ura3Δ0 MPS1-GBP::KANMX*	This Study
T541	*MAT**a** CEP3-GFP::HIS3 mad1Δ::KAN*	This Study
T542	*MAT**a** KRE28-GFP::HIS3 mad1Δ::KAN*	This Study
T543	*MAT**a** NDC80-GFP::HIS3 mad1Δ::KAN*	This Study
T544	*MAT**a** AME1-GFP::HIS3 mad1Δ::KAN*	This Study
T545	*MAT**a** BUB1-GFP::HIS3 mad1Δ::KAN*	This Study
T546	*MAT**a** SPC105-GFP::HIS3 mad1Δ::KAN*	This Study
T548	*MAT**a** his3Δ1 leu2Δ0 met15Δ0 ura3Δ0 CSE4-GFPint::HIS3MX6*	Lisa Berry
T594	*MAT**a** BUB1-GFP::HIS3 mad3Δ::KAN*	This Study
T595	*MAT**a** SPC105-GFP::HIS3 mad3Δ::KAN*	This Study
T596	*MAT**a** NDC80-GFP::HIS3 mad3Δ::KAN*	This Study
T603	*MAT**a** DAD1-GFP::HIS3 mad3Δ::KAN*	This Study
T604	*MAT**a** DAD4-GFP::HIS3 mad3Δ::KAN*	This Study
T605	*MAT**a** BIM1-GFP::HIS3 mad3Δ::KAN*	This Study
T607	*MATα ADE2 leu2-3,112 his3-11,15 URA3 LYS2 can1-100 trp1-1 cdc20::prMET3-CDC20::TRP1 MTW1-YFP Turq2-TUB1::HIS3MX6*	This Study
T608	*MAT**a** MTW1-GFP::HIS3 CDC5-AID::HYGMX*	This Study
T609	*MAT**a** AME1-GFP::HIS3 CDC5-AID::HYGMX*	This Study

T610	*MAT***a** *NDC80-GFP::HIS3 CDC5-AID::HYGMX*	This Study
T611	*MAT***a** *CNM67-GFP::HIS3 CDC5-AID::HYGMX*	This Study
T612	*MAT***a** *his3Δ1 leu2Δ0 met15Δ0 ura3Δ0 CSE4-GFPint::HIS3MX6 mad1Δ::KANMX*	This Study
T616	*MAT***a** *his3Δ1 leu2Δ0 met15Δ0 ura3Δ0 arg4Δ::KANMX lys1Δ::KANMX MTW1-YFP::HIS3MX6*	This Study
T619	*MAT***a** *his3Δ1 leu2Δ0 met15Δ0 ura3Δ0 arg4Δ::KANMX lys1Δ::KANMX MTW1-YFP::HIS3MX6 mad1Δ::NATMX*	This Study
T620	*MAT***a** *ADE2 leu2-3,112 his3-11,15 URA3 LYS2 can1-100 trp1-1 cdc20::prMET3-CDC20::TRP1 MTW1-YFP Turq2-TUB1::HIS3MX6*	This Study
T621	*MAT***a** *ADE2 trp1-1 LYS2 his3-11,15 ura3-1 SPC42-RFP::HYGMX DAD4-YFP::NATMX Turq2-TUB1::HIS3MX6*	This Study
T664	*MATα his3Δ1 leu2Δ0 lys2Δ0 ura3Δ0 CSE4-YFPint::HIS3MX6*	This Study
E433	*MATα his3Δ1 leu2Δ0 lys2Δ0 ura3Δ0 mad1Δ::KANMX*	Winzeler et al. 1999
E434	*MATα his3Δ1 leu2Δ0 lys2Δ0 ura3Δ0 mad2Δ::KANMX*	Winzeler et al. 1999
E435	*MATα his3Δ1 leu2Δ0 lys2Δ0 ura3Δ0 mad3Δ::KANMX*	Winzeler et al. 1999
E436	*MATα his3Δ1 leu2Δ0 lys2Δ0 ura3Δ0 bub1Δ::KANMX*	Winzeler et al. 1999
E437	*MATα his3Δ1 leu2Δ0 lys2Δ0 ura3Δ0 bub3Δ::KANMX*	Winzeler et al. 1999

2.1.2 Yeast growth conditions

Unless stated otherwise yeast cells were grown at 30˚C in either rich (YPD; 1% yeast extract, 2% bacto-peptone and 2% bacto-agar for solid media) or synthetic complete (SC; 109μM adenine sulphate, 95μM L-Arginine sulphate, 95μM L-Histidine HCl, 229μM L-Isoleucine, 457μM L-Leucine, 164μM L-Lysine HCl, 134μM L-Methionine, 303 μM L-Phenylalanine, 98μM L-Tryptophan, 166μM L-Tyrosine,178μM Uracil, 1280μM L-Valine, 5g/L ammonium sulphate, 1.7g/L yeast nitrogen base, and 2.5% difco agar for solid media) media containing 2% glucose as a carbon source. For microscopy, cells were grown in SC media supplemented with 100mg/ml of adenine and grown overnight at 23˚C.

2.1.3 Yeast transformations

Genomic integration transformations of yeast strains were done by high-efficiency lithium acetate (LiOAc) method adapted from (Gietz & Schiestl, 2007). Strains were

grown in appropriate medium (usually YPD) overnight at 30˚C and diluted 100-fold in 50ml of fresh media and grown for ~5 hours or until the cell density reached OD_{600} ≈ 0.5-0.7. Next, the cells were collected by centrifugation at 4000 rpm for 5 min and the pellet washed in 10ml of TE/LiOAc solution (10mM Tris-HCl pH7.5, 1mM EDTA, 100mM LiOAc). After resuspension in 600µl TE/LiOAc, 200ul of the cells were mixed with 150µg of salmon sperm DNA (Sigma-Aldrich), 200-500ng of transforming DNA and 700µl TE/LiOAc solution containing 40% polyethylene glycol (PEG; average molecular weight 3350g/mol). Next, the samples were incubated at 30˚C for 30 min and then heat shocked at 42˚C for 15 min. Approximately 450µl of the sample was plated onto appropriate selection media and incubated at 30˚C for 2-3 days until colonies appeared. Selected colonies were then streaked onto fresh plates with the same selection medium to isolate transformants. In cases of transformation with drug selection, after the heat shock step desciribed above, the cells were collected by centrifugation and resuspended in 1ml YPD and incubated at 30˚C shaking for 2-4 hours to allow for the expression of the drug resistance marker gene. Subsequently the whole sample was plated onto the drug selection medium. Alternatively, after the heat shock step, the whole sample was plated straight onto a YPD plate and incubated overnight at 30˚C and then replica plated onto the drug selection plate.

Yeast transformations with plasmid DNA was performed as above, but with reduced amounts of cells (30µl), salmon sperm DNA (5µl), plasmid DNA (50-100ng) and TE/LiOAc/40%PEG (140µl). ≤50µl of sample was plated onto appropriate selection plates.

For gap repair ligation of plasmids (Rothstein, 1983), the transformation was performed exactly the same, but 50ng of cut plasmid DNA was mixed with 50ng of DNA insert and ~150µl plated onto appropriate solid media.

2.1.4 *E. coli* transformation and plasmid purification

For all bacterial work, I used electro-competent *E.coli* cells, ElectroMAX DH10B (Invitrogen). The *E.coli* cells were incubated at 37˚C in Luria-Bertani broth (LB) (1% bacto-tryptone, 0.5% yeast extract, 1% NaCl pH 7.5 and 1.5% bacto-agar for solid media). For plasmid selection, 0.05-0.1 mg/ml ampicillin (Sigma-Aldrich) was added to the LB media.

E.coli were transformed with plasmids by electroporation. 5-10µl of transforming DNA was mixed with 20µl of 10% glycerol and 10µl of electro-competent *E.coli.* The sample was transferred into a chilled 2mm Gene Pulser cuvette (Bio-Rad) and electroporated using a Gene Pulser Xcell device (Bio-Rad) at 2.5KV, 200Ω and 25µF. Next, the sample was immediately removed from the device and mixed with 1ml of SOC medium (2% bacto-tryptone, 0.5% yeast extract, 10mM NaCl, 2.5mM KCl, 10mM $MgCl_2$, 10mM $MgSO_4$, 20mM glucose) and incubated at 37˚C shaking for 1 hour. Finally, the transformations were plated onto LB ampicillin plates and incubated at 37˚C overnight. To isolate individual transformants a couple of colonies were selected and streaked onto fresh plates.

To purify plasmid DNA from the transformed *E.coli,* a 4ml culture was grown overnight shaking at 37˚C and cells collected by centrifugation at 8000 rpm for 2 min and then GeneJet Plasmid Miniprep Kit (Thermo Scientific) was used according to manufacturer's instructions.

2.1.5 Yeast crosses and tetrad dissections

Haploid *MAT***a** and *MATα* strains auxotrophic for different markers were mated on YPD and incubated at 30˚C for 24 hours. Diploids were selected by replica plating onto appropriate solid medium and incubated at 30˚C for 2 days and further isolated by replica plating onto a double selection and incubated at 30˚C for further 2 days. Single colonies were selected and patched onto sporulation solid media (SPO; 75mg/l of each: adenine sulphate, L-Histidine HCl, Lleucine, L-Lysine HCl, L-Methionine, L-Tryptophan, Uracil, 0.02g/ml potassium acetate, 2.5mg/ml yeast extract, 1mg/ml glucose and 2% bacto-agar) and incubated for at least 3 days at 23˚C, to induce spore formation.

Before spore or tetrad dissections, their presence was confirmed with microscopy by visual inspection of tetrad formations. Then a small amount of cells was picked from the SPO plate and mixed with a 100µl of 5% of glusulase enzyme and incubated at room temperature for ~5 min, to remove the asci walls that holds the spores together. Next, 10-20µl of spores were plated on one side of a YPD plate and allowed to dry and dissections performed by micromanipulation using an MSM300 dissection microscope (Singer Instruments). After the tetrads were dissected and spores separated, the YPD

plate was incubated at 30˚C for 2-3 days and tetrads scored for genotype by replica plating onto appropriate selection plates.

2.1.6 Yeast genomic DNA extraction

To extract DNA from yeast I used the phenol "Smash n'Grab" extraction method (Hoffman & Winston, 1987). First, 1ml from an overnight yeast culture was centrifuged at 5000 rpm for 5 min to collect cells. The pellet was resuspended in 200µl of Smash n'Grab buffer (1% SDS, 2% Triton-X-100, 100mM NaCl, 10mM Tris-HCL pH8, 1mM EDTA) and 200µl of phenol/chloroform (Invitrogen) and 250µl of glass beads (0.4-0.5mm diameter (Sigma-Aldrich)) were added. The sample was then mixed by vortexing for 2 min and cell debris was removed by centrifugation at 4˚C and 13,000 rpm for 10 min. 100µl of the supernatant was transferred to a new Eppendorf and 200µl of phenol/chloroform was added. The vortexing and centrifugation was repeated as before and 50µl of the supernatant was dialysed in TE for ~20 min on nitrocellulose membrane filter discs (0.025µm) (Millipore) and then stored at -20˚C.

A faster phenol-free DNA extraction method (based on (Lõoke *et al.*, 2011) was also used to quickly acquire DNA for applications such as diagnostic PCR. A single colony or 100µl of overnight yeast culture was resuspended in 100µl of 200mM LiOAc/1%SDS solution and incubated at 70˚C for 5 min. 300µl of 96% ethanol was added and the sample mixed by vortexing for 1 min. The sample was then centrifuged at 13,000 rpm for 3 min and the supernatant discarded. Next, the pellet was washed with 70% ethanol and dissolved in 100µl of water. Cell debris was removed by a further 30 sec centrifugation and 0.5-1.0µl of the supernatant was used for PCR.

2.1.7 Serial dilutions spot assay

Yeast cultures were grown overnight at 30˚C and cell density was measured (OD_{600}) and adjusted so that each culture had the same OD_{600}. Ten-fold serial dilutions were performed and 4µl of each were spotted onto appropriate solid media and incubated at 30˚C for 2-3 days.

2.2 Molecular biology

2.2.1 PCR and gel electrophoresis

High-fidelity polymerase chain reactions (PCR) was performed using PfuUltra II fusion, HS DNA polymerase (Agilant Technologies) or Q5-High Fidelity polymerase (New England BioLabs) according to manufacturer's instructions. For diagnostic PCRs, I used DreamTaq Green master mix (Fermentas) following the manufacturer's instructions. PCR reactions were run either in MJ Mini Personal or T100 Thermal Cyclers (Bio-Rad).

Primer design was done by using SeqBuilder (DNAstar) software and all oligonucleotides were acquired from Sigma-Aldrich. A list of the primers used is available upon request.

PCR products (and other DNA fragments) were confirmed by DNA gel electrophoresis. 0.5-1.5% agarose (Invitrogen) gels were made in TEA buffer (40mM Tris, 20mM acetic acid and EDTA). Before casting the gel, 0.1µl/ml of GelRed Nucleic Acid Gel Stain (Biotium) was added for staining DNA. The DNA samples were mixed with 10x loading dye (20% FicoII containing bromophenol blue or orange G dyes) before loading onto the gel and then run at 90V on a mini horizontal submarine Hoefer HE33 unit (Amersham Biosciences). DNA fragment bands were visualised using a BioDoc-It UV imaging system and their size estimated by comparing them with 1kb Gene Ruler DNA ladder (Thermo Scientific).

After the PCR products were confirmed they were purified using a GeneJET PCR purification Kit (Thermo Scientific) following manufacturer's instructions. The DNA concentration was measured by NanoVue Plus spectrophotometer (GE Healthcare). In cases when DNA fragments were extracted from the agarose gel, I used a GeneJET Gel Extraction Kit (Thermo Scientific).

2.2.2 Plasmid construction

Plasmid sequences were designed using SeqBuilder (DNAstar) software and typically made by gap-repair cloning, using a donor plasmid which was cut with an appropriate restriction enzyme(s) and combined with a PCR product or other DNA insert. If a wild-

type gene or gene fusions were used as DNA insert, the genes were amplified with PCR from genomic DNA from a wild-type yeast strain and, when appropriate, assembled further using PCR. In some cases where a more complex genetic construct design or mutant genes were used as DNA inserts, I used commercially synthesised DNA fragments (GeneArt DNA string; Thermofisher Scientific). Then gap repair ligation in yeast was used to combine the cut plasmids with the DNA inserts (see section 2.1.3 for details).

To modify DNA sequence of an existing plasmid, for example to make mutations on a single or few residues, I used QuickChange Lightning Multi Site-Directed Mutagenesis Kit (Agilent Technologies) according to manufacturer's instructions.

All plasmid sequences were validated with Sanger sequencing (GENEWIZ, LLC or Genomics Equipment Park at the Francis Crick Institute). The plasmids used in this project are listed in Table 2.2.

Table 2.2 Plasmids

Plasmid	Genotype (all have *ARS209*, *CEN6 and AMP*)	Source
pWJ1512	*pCUP1 LEU2*	Reid et al. 2011
pHT4	*pCUP1 GBP-RFP LEU2*	Olafsson and Thorpe 2015
pHT10	*pCUP1 MTW1-GBP-RFP LEU2*	Olafsson and Thorpe 2015
pHT11	*pCUP1 SPC42-GBP-RFP LEU2*	This study
pHT36	*pCUP1 MAD2-GBP LEU2*	Olafsson and Thorpe 2016
pHT95	*pGAL1 MAD2-CDC20 LEU2*	This study
pHT98	*pGAL1 CDC20-MAD2 LEU2*	This study
pHT99	*pCUP1 NAT*	Olafsson and Thorpe 2015
pHT101	*pGAL1 MAD2 LEU2*	Olafsson and Thorpe 2016
pHT102	*pGAL1 CDC20 LEU2*	Olafsson and Thorpe 2016
pHT103	*pGAL1 LEU2*	Olafsson and Thorpe 2016
pHT108	*pGAL1 MAD2 HIS3*	Olafsson and Thorpe 2016
pHT109	*pGAL1 BIR1 LEU2*	Olafsson and Thorpe 2016
pHT110	*pGAL1 CSE4 LEU2*	Olafsson and Thorpe 2016
pHT111	*pGAL1 CSE4-GFP LEU2*	This study
pHT112	*pGAL1 IPL1 LEU2*	This study
pHT113	*pGAL1 CBF2 LEU2*	This study
pHT114	*pGAL1 MAD2-BIR1 LEU2*	This study
pHT115	*pGAL1 MAD2-CSE4 LEU2*	Olafsson and Thorpe 2016
pHT116	*pGAL1 MAD2-CSE4-GFP LEU2*	This study
pHT117	*pGAL1 MAD2-IPL1 LEU2*	This study
pHT118	*pGAL1 MAD2-CBF2 LEU2*	This study
pHT119	*pCUP1 MAD2 LEU2*	Olafsson and Thorpe 2016
pHT186	*pGAL1 MAD2-GBP-RFP LEU2*	Olafsson and Thorpe 2016
pHT187	*pGAL1 CSE4-MAD2 LEU2*	Olafsson and Thorpe 2016
pHT199	*pGAL1 GBP LEU2*	Olafsson and Thorpe 2016
pHT205	*pGALS YFP NAT*	Eva Herrero
pHT208	*pCUP1 DAD2*	Berry et al. 2016

pHT234	*pCUP1 DAD2-GBP*	Berry et al. 2016
pHT210	*pCUP1 NUF2*	Olafsson and Thorpe 2015
pHT211	*pCUP1 NUF2-GBP*	Olafsson and Thorpe 2015
pHT296	*pCUP1 MTW1 LEU2*	Olafsson and Thorpe 2015
pHT297	*pCUP1 SPC42 LEU2*	This study
pHT304	*pCUP1 CBK1 LEU2*	This study
pHT305	*pCUP1 CBF1-GBP LEU2*	Olafsson and Thorpe 2015
pHT310	*pCUP1 CBF1 LEU2*	Olafsson and Thorpe 2015
pHT311	*pCUP1 CTF19 LEU2*	Olafsson and Thorpe 2015
pHT312	*pCUP1 CTF19-GBP LEU2*	Olafsson and Thorpe 2015
pHT313	*pCUP1 MIF2 LEU2*	Olafsson and Thorpe 2015
pHT314	*pCUP1 MIF2-GBP LEU2*	Olafsson and Thorpe 2015
pHT317	*pCUP1 CBK1-GBP LEU2*	This study
pHT318	*pCUP1 CNN1 LEU2*	Olafsson and Thorpe 2015
pHT320	*pCUP1 GBP-CNN1 LEU2*	Olafsson and Thorpe 2015
pHT321	*pCUP1 CDC42 LEU2*	This study
pHT322	*pCUP1 GBP-CDC42 LEU2*	This study
pHT335	*pCUP1 SKP1 LEU2*	Olafsson and Thorpe 2015
pHT336	*pCUP1 SKP1-GBP LEU2*	Olafsson and Thorpe 2015
pHT337	*pCUP1 CTF3 LEU2*	Olafsson and Thorpe 2015
pHT338	*pCUP1 CTF3-GBP LEU2*	Olafsson and Thorpe 2015
pHT339	*pCUP1 KRE28 LEU2*	Olafsson and Thorpe 2015
pHT340	*pCUP1 KRE28-GBP LEU2*	Olafsson and Thorpe 2015
pHT341	*pCUP1 CHL4 LEU2*	Olafsson and Thorpe 2015
pHT342	*pCUP1 CHL4-GBP LEU2*	Olafsson and Thorpe 2015
pHT343	*pCUP1 GBP-CBF1 LEU2*	Olafsson and Thorpe 2015
pHT344	*pCUP1 CBF1-4Ala-GBP LEU2*	Olafsson and Thorpe 2015
pHT346	*pCUP1 MAD1 LEU2*	Olafsson and Thorpe 2016
pHT353	*pCUP1 GBP-CDC14 LEU2*	Olafsson and Thorpe 2015
pHT354	*pCUP1 CDC14 LEU2*	Olafsson and Thorpe 2015
pHT355	*pCUP1 GBP-cdc14-C283S LEU2*	Olafsson and Thorpe 2015
pHT356	*pCUP1 GBP-cdc14-C283A LEU2*	Olafsson and Thorpe 2015
pHT357	*pCUP1 MAD1-GBP LEU2*	Olafsson and Thorpe 2016
pHT357	*pCUP1 MAD1-GBP LEU2*	Olafsson and Thorpe 2016
pHT358	*pCUP1 mad1-RLK/AAA-GBP LEU2*	Olafsson and Thorpe 2016
pHT358	*pCUP1 mad1-RLK/AAA-GBP LEU2*	Olafsson and Thorpe 2016
pHT359	*pCUP1 MAD1-4Ala-GBP LEU2*	Olafsson and Thorpe 2016
pHT360	*pCUP1 mad1-RLK/AAA-4Ala-GBP LEU2*	Olafsson and Thorpe 2016
pHT361	*pGALS CDC14 NAT*	This study
pHT362	*pGALS cdc14-C283S NAT*	This study
pHT363	*pGALS MTW1-CDC14 NAT*	This study
pHT364	*pGALS MTW1-cdc14-C283S NAT*	This study
pHT365	*pGALS DSN1-CDC14 NAT*	This study
pHT369	*pCUP1 DSN1 NAT*	Olafsson and Thorpe 2015
pHT378	*pCUP1 dsn1-S69D NAT*	Olafsson and Thorpe 2015
pHT379	*pCUP1 dsn1-S264D NAT*	Olafsson and Thorpe 2015
pHT380	*pCUP1 dsn1-S240,250D NAT*	Olafsson and Thorpe 2015
pHT381	*pCUP1 dsn1-S69,170,240,250,264D NAT*	Olafsson and Thorpe 2015
pHT382	*pCUP1 dsn1-S69,170,264D NAT*	Olafsson and Thorpe 2015
pHT383	*pCUP1 mad2ΔC-GBP LEU2*	Olafsson and Thorpe 2016
pHT398	*pGAL1 NET1 HIS3*	This study
pHT401	*pCUP1 mad1-RIL/AAA-GBP LEU2*	Olafsson and Thorpe 2016
pHT402	*pCUP1 mad1-RIL/AAA-4Ala-GBP LEU2*	Olafsson and Thorpe 2016
pHT403	*pCUP1 mad1-A736T-GBP LEU2*	Olafsson and Thorpe 2016
pHT404	*pCUP1 mad1-A736T-4Ala-GBP LEU2*	Olafsson and Thorpe 2016

pHT406	*pCUP1 mad1-T133A, V188N-GBP LEU2*	Olafsson and Thorpe 2016
pHT407	*pCUP1 mad2-RQ/AA-GBP LEU2*	Olafsson and Thorpe 2016
pHT411	*pCUP1 CDC14-GBP LEU2*	Olafsson and Thorpe 2015
pHT412	*pCUP1 cdc14-C283S-GBP LEU*	Olafsson and Thorpe 2015
pHT425	*pCUP1 CDC5-GBP LEU2*	This study
pHT426	*pCUP1 CDC5 LEU2*	This study
pHT429	*pCUP1 ASK1 NAT*	This study
pHT430	*pCUP1 SPC24 NAT*	This study
pHT431	*pCUP1 CDC14-GBP(no RFP) LEU2*	Olafsson and Thorpe 2015
pHT432	*pCUP1 cdc14-C283S-GBP(no RFP) LEU2*	Olafsson and Thorpe 2015
pHT436	*pCUP1 cdc5-L158G-GBP (cdc5-as1) LEU2*	This study
pHT438	*pCUP1 spc24-T130E NAT*	This study
pHT440	*pCUP1 MPS1-GBP LEU2*	Olafsson and Thorpe 2016
pHT441	*pCUP1 MPS1 LEU2*	Olafsson and Thorpe 2016
pHT442	*pCUP1 cdc5-K110A-GBP LEU2*	This study
pHT444	*pCUP1 cdc5-T242A-GBP LEU2*	This study
pHT450	*pCUP1 mps1-M516G-GBP (mps1-as1) LEU2*	This study
pHT452	*pCUP1 mps1-D580A-GBP LEU2*	Olafsson and Thorpe 2016
pHT466	*pCUP1 RIO1 LEU2*	This study
pHT467	*pCUP1 RIO1-GBP LEU2*	This study
pHT468	*pCUP1 rio1-kd-GBP LEU2*	This study
pHT474	*pCUP1 MPS1-uberlink-GBP LEU2*	This study
pHT475	*pCUP1 mps1-D580A-uberlink-GBP LEU2*	This study
pHT486	*pCUP1 spc105-6A-GFP NAT*	This study
pHT487	*pGALS spc105-6A-YFP NAT*	Olafsson and Thorpe 2016
pHT490	*pADH1-ABF2 pTEF1-GBP-AID-RFP LEU2*	This study
pHT494	*pCUP1 GLC7 NAT*	Olafsson and Thorpe 2016
pHT497	*pCUP1 cdc5ΔC-GBP LEU2*	This study
pHT498	*pCUP1 cdc5ΔC-L158G-GBP LEU2*	This study
pHT499	*pCUP1 cdc5ΔC-K110A-GBP LEU2*	This study
pHT500	*pCUP1 cdc5ΔC-T242A-GBP LEU2*	This study
pHT501	*pADH1-ABF2 pTEF1-ZraI-GBP-AID-RFP LEU2*	This study
pHT502	*pCUP1 cdc5-L158G-WHK/FAM-GBP-RFP LEU2*	This study
pHT503	*pCUP1 cdc5-T242A-WHK/FAM-GBP-RFP LEU2*	This study
pHT504	*pCUP1 cdc5-WHK/FAM-GBP-RFP LEU2*	This study
pHT507	*pADH1-ABF2 pTEF1-CDC5-GBP-AID-RFP LEU2*	This study
pHT511	*pADH1-ABF2 pTEF1-MPS1-GBP-AID-RFP LEU2*	This study
pHT516	*pADH1-ABF2 pTEF1-MTW1-GBP-AID-RFP LEU2*	This study
pHT517	*pCUP1 GBP-AID-RFP LEU2*	This study
pHT523	*pADH1-ABF2 pCUP1-GBP-AID-RFP LEU2*	This study
pHT524	*pADH1-ABF2 pCUP1-MPS1-GBP-AID-RFP LEU2*	This study
pHT525	*pADH1-ABF2 pCUP1-mps1-D580-GBP-AID-RFP LEU2*	This study
pHT526	*pADH1-ABF2 pCUP1-CDC5-GBP-AID-RFP LEU2*	This study
pHT527	*pADH1-ABF2 pCUP1-cdc5-K110A-GBP-AID-RFP LEU2*	This study
pHT528	*pADH1-ABF2 pCUP1-cdc5-T242A-GBP-AID-RFP LEU2*	This study
pHT529	*pGALS MPS1 NAT*	This study
pHT530	*pGALS CDC5 NAT*	This study

pHT531	*pGALS CDC5ΔN (PBD) NAT*	This study
pHT532	*pGALS GLC7 NAT*	This study
pHT533	*pGALS IPL1 NAT*	This study
pHT534	*pGALS FIN1 NAT*	This study
pHT535	*pGALS fin1-5A NAT*	This study
pHT546	*pCUP1 NBP1 LEU2*	This study
pHT547	*pCUP1 NBP1-GBP LEU2*	This study
pHT548	*pCUP1 YPR174C LEU2*	This study
pHT549	*pCUP1 YPR174C-GBP LEU2*	This study
pHT550	*pGAL1 MTW1-CDC5 LEU2*	This study
pHT551	*pGAL1 MTW1-cdc5-K110A LEU2*	This study
pHT556	*pCUP1 nbp1-SS264-265AA-GBP-RFP LEU2*	This study
pHT557	*pGAL1 AME1-CDC5 LEU2*	This study
pHT558	*pGAL1 AME1-cdc5-K110A LEU2*	This study
pHT559	*pGAL1 BIM1-CDC5 LEU2*	This study
pHT560	*pGAL1 BIM1-cdc5-K110A LEU2*	This study
pHT561	*pGAL1 DAD2-CDC5 LEU2*	This study
pHT562	*pGAL1 DAD2-cdc5-K110A LEU2*	This study
pHT563	*pADH1-ABF2 pCUP1-PBD-mGBP-AID-RFP LEU2*	This study
pHT564	*pADH1-ABF2 pCUP1-PBD-WHK/FAM-mGBP-AID-RFP LEU2*	This study
pHT565	*pGAL1 AME1-cdc5ΔC LEU2*	This study
pHT566	*pGAL1 CDC5-AME1 LEU2*	This study
pHT567	*pGAL1 cdc5-K110A-AME1 LEU2*	This study
pHT568	*pGAL1 cdc5ΔC-AME1 LEU2*	This study
pHT569	*pGAL1 cdc5ΔC-K110A-AME1 LEU2*	This study
pHT570	*pGAL1 cdc5ΔC-T242A-AME1 LEU2*	This study
pHT572	*pGAL1 MTW1 LEU2*	This study
pHT573	*pGAL1 CDC5 LEU2*	This study
pHT574	*pGAL1 cdc5-K110A LEU2*	This study
pHT580	*pGAL1 cdc5ΔC-GBP-RFP LEU2*	This study
pHT581	*pGAL1 cdc5ΔC-K110A-GBP-RFP LEU2*	This study
pHT582	*pADH1-AFB2 pGAL1-GBP-RFP LEU2*	This study
pHT583	*pADH1-AFB2 pGAL1-cdc5ΔC-GBP-AID-RFP LEU2*	This study
pHT586	*pCUP1 CDC5-AID-GBP-AID-RFP LEU2*	This study
pHT589	*pGAL1 AME1-cdc5ΔC-K110A LEU2*	This study
pHT597	*pGALS ask1-S216A, S250A NAT*	This study
pHT598	*pGALS dam1-S218A, S221A NAT*	This study
pHT599	*pCUP1 cdc5ΔN-mGBP (PBD) LEU2*	This study
pHT600	*pCUP1 cdc5ΔN-WHK/FAM-mGBP (PBD) LEU2*	This study
pHT601	*pGALS ASK1 NAT*	This study
pHT602	*pGALS DAM1 NAT*	This study
pHT629	*pGAL1 ACM1 NAT*	This study
pHT630	*pGAL1 acm1-S87A,S95A NAT*	This study
pHT631	*pGAL1 acm1-S87D,S95D NAT*	This study
pHT632	*pGAL1 BIM1 NAT*	This study
pHT633	*pGAL1 bim1-7A (S139,148,149,165,166A, T175A, S176A NAT*	This study
pHT634	*pGAL1 bim1-7D (S139,148,149,165,166D, T175D, S176D NAT*	This study
pHT635	*pGAL1 CDH1 NAT*	This study
pHT636	*pGAL1 BIK1 NAT*	This study
pHT637	*pGALS dam1-6A (S20,218,221,257,265,292A) NAT*	This study

2.3 Cell biology and fluorescence microscopy

2.3.1 Fluorescence microscopy

To examine the location of tagged proteins within the cells I used widefield epifluorescence microscopy. Log phase cells were embedded in 0.7% low melting point agarose dissolved in the appropriate growth medium. The depth of agarose between the slide and coverslip was fixed at 6-8μm, slightly larger than the diameter of the average yeast cell, which maintains a consistent distance from the coverslip to the cell nucleus. Cells were imaged with a Zeiss Axioimager Z2 microscope (Carl Zeiss AG, Germany), using a 63x 1.4NA oil immersion lens, illuminated using a Zeiss Colibri LED illumination system (CFP = 445nm, GFP = 470nm, YFP = 505nm, RFP = 590nm). Bright field contrast was enhanced with differential interference contrast (DIC) prisms. The resulting light was captured using a Hamamatsu ORCA ERII CCD camera containing an ER-150 interline CCD sensor with 6.45μm pixels, binned 2x2, or a Hamamatsu Flash 4.0 Lte. camera containing a FL-400 CMOS sensor with 6.5 mm pixels, binned 2x2 (Hamamatsu (Hamamatsu Photonics, Japan). The exposure times were set to ensure that CCD pixels were not saturated. The ORCA ERII 12 bit images have a pixel size of 205 nm in x and y, a z step size of 300 nm, and an effective dynamic range of ~3000 grey levels. The Flash 4.0 16-bit images have a pixel size of 206 nm in x and y, a z step size of 300 nm, and an effective dynamic range of ~30,000 grey levels. Images shown in the figures were prepared using Volocity imaging software (Perkin Elmer Inc., USA).

CFP/GFP overlap – for some of the fluorescence microscopy images (Figure 3.6), I used three colour imaging of the GFP-GBP interaction. This involved using CFP and GFP together. For these experiments, the CFP fluorophore was excited at 445nm and the emission collected between 425 and 460nm, the GFP was excited at 470nm and the emission collected between 440 and 480nm. Consequently, there is significant overlap between these two channels as indicated on Figure 3.6, I used the GBP-RFP signal to distinguish true GFP signal from the CFP bleed-through.

2.3.2 Fluorescence image analysis

A quantitative measurement of Smc1-YFP (cohesin) fluorescence (Figure 4.6 C&D) was measured using a custom script for Volocity software. Cells were counted

manually and n = number of cells from a single experiment. The CFP signal produced from a tagged histone (Hta1-CFP) was used to select 3D regions (volumes) representing the nucleus. The mean YFP intensity (Smc1-YFP) within this volume was measured. To correct for background, an external volume three pixels from the edge of the CFP-defined nucleus was chosen, and the mean YFP intensity in this background region was subtracted from the nuclear signal to produce a background-corrected value for each nucleus measured.

The sister kinetochore distance (Figure 5.18 B) and the SPB-kinetochore distance (Figure 3.18 E) measurements were analysed using a freely-available semi-automatic ImageJ tool, FociQuant, which quantifies kinetochore foci fluorescence in a high-throughput manner and can be adapted to also measure distances between two foci (Ledesma-Fernández & Thorpe, 2015). In brief, the kinetochore foci are detected semi-automatically by first manually selecting the mitotic spindle region in budded cells, which contain separated sister kinetochores, the tool then uses the 'FindMaxima' function in ImageJ to automatically identify the sister kinetochore foci. In these experiments, the number of cells counted typically from a single experiment is indicated as n. The software fits a Gaussian plot to the intensity profile of each kinetochore focus in two dimensions (x and y) to accurately determine their position, allowing the distance between the two foci to be calculated. The FociQuant tool is available for download: https://sourceforge.net/projects/fociquantitation/files/.

2.3.3 Cell cycle and spindle morphology analysis

Yeast cells with fluorescently tagged tubulin (Turq2-Tub1), kinetochore (Dad4-YFP) and SPB (Spc42-RFP) carrying plasmids of interest, for example pGAL1-Cdc5ΔC-Ame1, were assessed using fluorescence microscopy (Figure 5.15). Overnight cultures growing in 2% raffinose 0.1% glucose SC –leu +ade media at 23˚C were resuspended and in fresh media with either 2% glucose or 2% galactose SC –leu +ade and incubated at 23˚C for 4 hours before imaging. The cell-cycle stages were estimated based on bud, spindle and SPB morphology (see Figure 1.2 in the introduction for example of yeast cells at different cell-cycle stages). Unbudded cells with a single kinetochore/SPB focus were categorised as G1-phase cells. Cells with small buds and single kinetochore/SPB focus were considered in S-phase. Cells with small- or medium-sized buds and two SPB foci were categorised as G2-phase cells. Medium- or large-budded cells with two kinetochore/SPB foci close together (≤1.5μm and ≤3μm

respectively) were considered metaphase cells. Cells with the two kinetochore/SPB foci, one in the mother and the other in the daughter and connected by microtubules were classified as anaphase cells. Finally, telophase cells were scored as cells which had divided the kinetochore/SPB foci into the mother and daughter and spindle had disassembled (no microtubules connecting the two foci). The number of cells counted from a single experiment are indicated as n.

The cell cycle status of a yeast strain with fluorescently tagged kinetochore (Mtw1-YFP) and tubulin (Turq2-Tub1) encoding Cdc5-GBP-RFP (or mutants) from a plasmid was analysed in a similar way (Figure 5.17 C, D&E and Figure 5.18 A, C&D). These cells were also analysed after growing in either galactose (expression on) or glucose (expression off) media for four hours. But since these cells did not have a fluorescently-tagged SPB, I could not distinguish between S- and G2-phase cells, hence cells with small-medium buds and a single kinetochore focus or small-budded cells with duplicated kinetochore foci but in very close proximity (<0.5μm) were categorised as S/G2-phase cells. The other cell-cycle phases were classified as before. Cells without RFP foci were discounted and only cells with RFP foci were counted and the number counted is indicated as n.

2.3.4 Large-budded cell analysis

To assess mitotic arrest of cells, overnight cultures of yeast strains with fluorescently-labelled kinetochore proteins and expressing GBP fused to a protein of interest, were collected by centrifugation and imaged using fluorescence microscopy. Cells were counted and large-budded cells that had the segregated sister kinetochores (for example Mtw1-YFP) in the bud neck and a colocalised GBP-RFP and YFP signal at the kinetochore foci were quantified as percentage of total cells. Large-budded cells that did not have a GBP-RFP signal or had undergone anaphase/telophase were excluded from this analysis. The number of cells quantified are indicated as n.

2.4 Synthetic physical interaction assay

2.4.1 Equipment and material used for SPI screening

A detailed description of the synthetic physical interactions method has been recently published (Olafsson & Thorpe, 2017). All plates described in this method are the Singer Plus plates (Singer Instruments Ltd, Somerset, UK), which are designed for use

with the ROTOR robotic pinning platform. The liquid and solid media used was made as described before, except for the 2% galactose SC –leucine (GAL SC –leu) 5-FOA agar plates, which were made by the following protocol. First, 20g Bacto agar was mixed with 500ml of water and melted/sterilised using an autoclave. A 500ml solution was prepared containing 1.7g yeast nitrogen base without amino acids, 5g ammonium sulfate, 41mg –leucine amino acid mix, 30mg uracil and 750mg 5-Fluoro-orotic acid (5-FOA) and 2% (weight by volume) galactose. This solution was allowed to dissolve with stirring for approximately 1 hour at room temperature, then filter sterilized through a 0.22μm filter and placed in a 60°C incubator or water bath. When the autoclaved agar had cooled to 55-60°C, the warmed solution was added slowly and mixed well by gentle stirring and poured after ~5 min.

The ROTOR robotic pinning platform (Singer Instruments Ltd, Somerset, UK) allows 96-, 384- and 1536-arrays of yeast colonies on rectangular agar plates to be copied from plate to plate using sterile pins. It is also simple to convert between 96-, 384- and 1536-arrays. The options for the Singer ROTOR pinning robot settings are quite extensive, for example the pinning pressure, diameter and frequency can be customised. For 1536 colony density format I used the following settings for source and target plates: Pinning; Pin Pressure: 25%, Repeat Pin: 2 times. Dry Mix: Diameter: 0.1 mm, Cycles: 2 rotations. For 384 colony density format I used the following settings for source and target plates: Pinning; Pin Pressure: 10%, Repeat Pin: 2 times. Dry Mix: Diameter: 0.3 mm for source plates and 0.1 mm for target plates, Cycles: 2 rotations. For ‘lawn plates’ I changed The ROTOR robot pinning settings of the ‘Dry Mix: Diameter’ to 1 mm for source plates. This is to ensure that cells are picked up in cases where there might be gaps or uneven cell density on lawn plates, thus pinning with an increased diameter further ensures cells are picked up.

I scanned the plates using a desktop flatbed scanner (Epson V750 Pro, Seiko Epson Corporation, Japan) at 300dpi resolution in transmission mode. The plate lids were removed and the plates were inserted upside down in the scanner. The images were saved in lossless ‘tiff’ format for use with the ScreenMill software.

2.4.2 GFP binding protein (GBP)

There are various peptide sequences derived from camelid antibodies that bind to GFP. The first GBP (also known as a nanobody or chromobody) clone was isolated by Uhlrich Rothbauer, Heinrich Leonhardt and colleagues (Rothbauer *et al.*, 2006, 2008), but more recently a large repertoire of GBPs have been isolated (Fridy *et al.*, 2014). The sequence encoding GBP is sufficiently short (<400 bp) so that it can be introduced at either the 5' or 3' end of open reading frames (ORFs) to create N- or C-terminal tags of GBP target proteins with ease and usually does not perturb their function. I use a plasmid to drive expression of the GBP-tagged target protein.

2.4.3 Plasmids for Synthetic Physical Interactions

In principle, any suitable plasmid could be used to introduce the GBP-tagged target protein into the GFP strains. I have used a single-copy *CEN* plasmid based upon pWJ1512 (Reid *et al.*, 2011) (Figure 2.1). This plasmid (pHT4) contains a *LEU2* marker gene for selection and a *CUP1* promoter to drive expression of the GBP construct. The *CUP1* promoter is active without copper, but its expression can be elevated with added copper (Butt *et al.*, 1984). The strains of the GFP collection are auxotrophic for leucine, uracil and methionine. However, the selective ploidy ablation method (Reid *et al.*, 2011) to transfer plasmids uses selection against URA^{+}; consequently, plasmids encoding *LEU2* or *MET15* could be used in addition to any drug selection markers (such as NAT, Kanamycin, Hygromycin or Nourseothricin). In cases where I have included additional plasmids in the same strain I have used *LEU2* and NAT selection markers (for example see Figure 3.14 and section 3.2.5). In addition to a fusion plasmid (Figure 2.1 C), as standard controls I typically use a GBP plasmid (Figure 2.1 A) and 'Gene of Interest' (GOI) plasmid (Figure 2.1 B) as controls in the SPI screens. The GBP fusions thus contain the sequence that encodes a protein of interest (POI) followed by a flexible linker sequence (normally 8 amino acids; repeats of glycines and serines) and then the GBP sequence. The plasmids are assembled using the previously described gap-repair cloning technique, which combines a linearized plasmid with PCR products or other DNA inserts using in vivo recombination and then validated by Sanger sequencing.

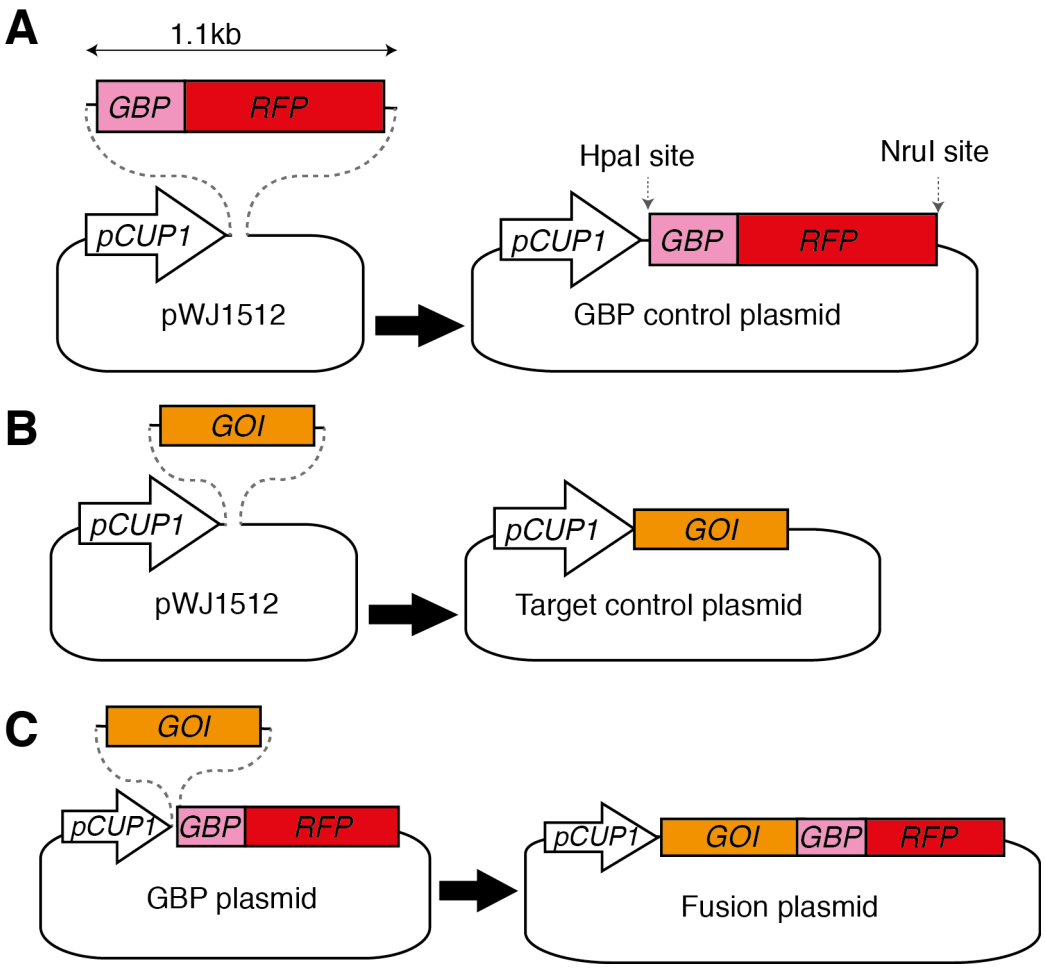

Figure 2.1 Plasmids for the SPI screens

A-C) A cut pWJ1512 plasmid containing a *CUP1* promoter was used as a template and gap-repaired with either a GBP-RFP (A) or gene of interest (GOI) (B) insert. The GBP control plasmid (pHT4) in (A) was cut using the HpaI restriction enzyme and gap-repaired using the GOI insert to create the GBP-fusion plasmids (C).

We estimate, based on linker length and structure of GFP and GBP (Yang *et al.*, 1996; Fisher *et al.*, 1999; Kirchhofer *et al.*, 2010), that the approximate maximum distance between the GFP-tagged protein and the GBP-tagged protein, when GFP and GBP interact, is ≤10nm (Figure 2.2).

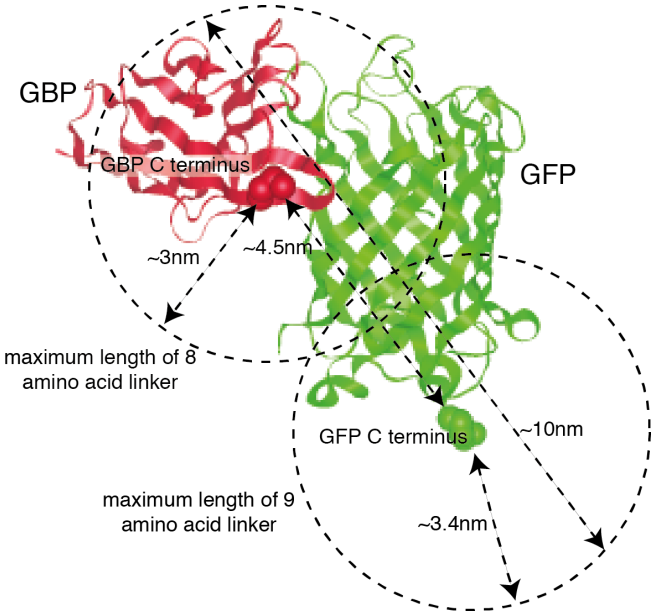

Figure 2.2 Estimation of the distance between the GBP- and GFP-tagged proteins

The interaction of the GBP and GFP structures are shown and are based on published structures of both proteins (see references in text). Based on this interaction and the linker lengths; 8 amino acids at C terminus of GBP (red balls) and 9 amino acids at the GFP C terminus (green balls) we estimate that the approximate maximum distance between the GBP- and GFP-tagged proteins is ~10nm, but could be anywhere within this range since the linkers are flexible.

2.4.4 Yeast strains/GFP collection

The GFP collection of strains is currently distributed by ThermoFisher Scientific (MA, USA) and contains 4159 strains each with an ORF C-terminally tagged with GFP and a downstream *HIS3MX* cassette. All the strains are derivatives of BY4741 (*MAT***a** *his3Δ1 leu2Δ0 met15Δ0 ura3Δ0*) (Huh *et al.*, 2003).

The *MATα* universal donor strain (W8164-2B; referred to as UDS) is available from the Rothstein lab (Reid *et al.*, 2011), *MATα CEN1-16*^{GCS} *can1-100 his3-11,15 leu2-3,112 LYS2 met17 trp1-1 ura3-1 RAD5*, where *CEN1-16*^{GCS} indicates that all the centromeres contain a counter-selectable *Kluveromyces lactis URA3::GAL* promoter cassette (Hill & Bloom, 1989). UDS has conditional centromeres on all the 16 chromosomes so that by selection on specific media (galactose and 5-FOA) all donor chromosomes can be eliminated, reverting the nascent diploid cells back to haploidy (maintaining the GFP-tagged gene). Alternatively, the cells can be kept as diploid cells (by selecting on –his and –leu media) to investigate dominant effects of the SPIs, since these heterozygous diploids have an extra set of chromosomes with an untagged version of the GFP-

tagged gene. UDS can be grown with glucose as a carbon source and is readily transformed with plasmids for the SPI screen.

2.4.5 Selective ploidy ablation (SPA)

The selective ploidy ablation method was developed by the Rothstein lab (Reid *et al.*, 2011). I use the following protocol to transfer plasmids into a collection of GFP strains for the SPI screens (Figure 2.3). Initially, the arrayed GFP strains were copied onto rectangular YPD agar plates using a pinning robot (see section 2.4.1 for robot details). I typically have a copy of the GFP library stored at 4°C on YPD plates, with 384 strains on each plate. Prior to the screen the GFP library copied/re-pinned onto fresh YPD plates at 1536 colonies/plate density, i.e. 4 replicates of each of the 384 GFP strains on each plate for the proteome-wide SPI screens or 16 replicates of 96 GFP strains in the retests or the kinetochore-specific SPI screens. Next, 5-10ml cultures of the UDS strain (W8164-2B) each containing a separate plasmid for the SPI assay (for example GBP alone, kinase alone, kinase-GBP, kinase mutant-GBP) are grown in selective media at 30°C, shaking, overnight. The cells were collected by centrifugation at 5000g for 5 min. Each lawn provides sufficient UDS cells to mate with four arrays of GFP strains, if there are more than four plates of GFP strains then additional lawns will be required. The cell pellets were resuspended in ~400µl of growth media and plated onto YPD plates using 4mm sterile glass beads to spread the cells onto the rectangular agar plates and incubated overnight at 30°C. The GFP strain colonies were pinned onto fresh YPD plates and the lawns were overlaid onto these YPD plates by pinning as previously. These plates were then incubated at 30˚C for 6-7 hours (or overnight) for mating. Next, the colonies were pinned onto GAL SC –leu rectangular solid media and incubated at 30˚C for 24 hours. The colonies were then re-pinned onto GAL SC –leu 5-FOA plates and incubated at 30˚C for further 24-72 hours, depending on colony sizes. Finally, images of the plates were captured by using a desktop scanner (see section 2.4.1 for details).

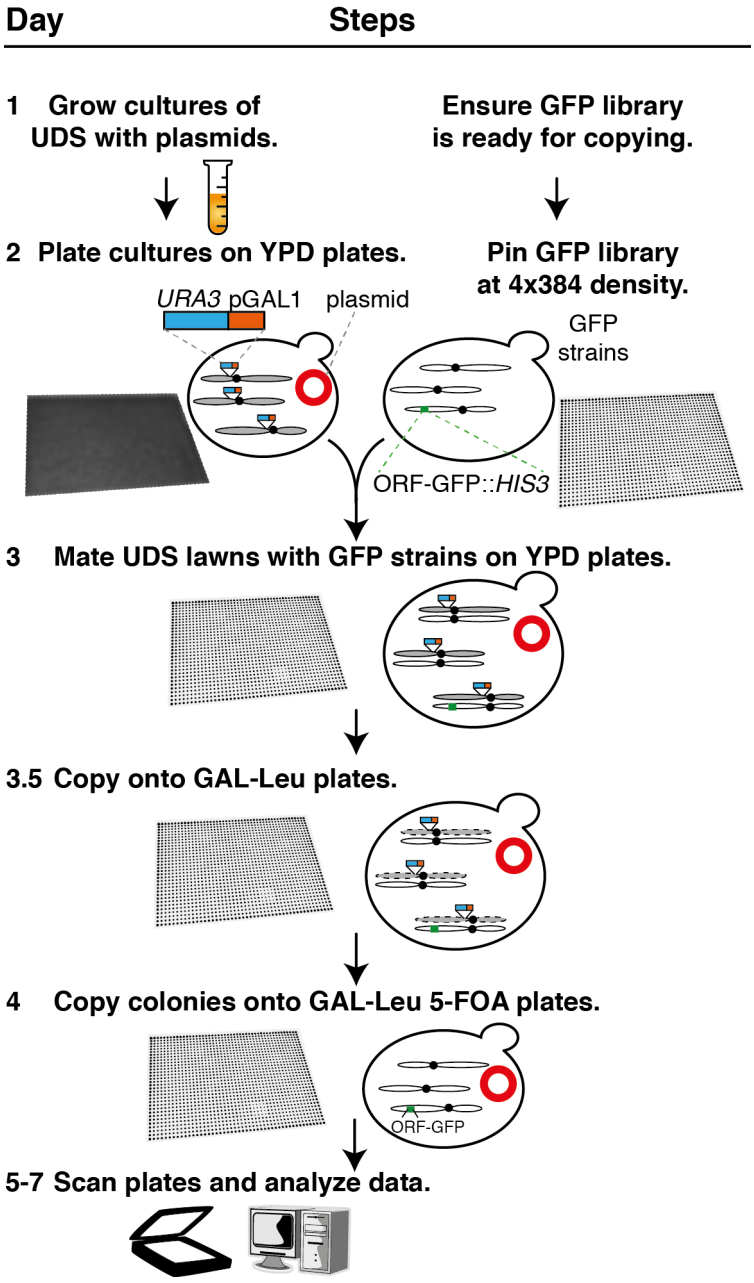

Figure 2.3 Illustrated SPI screen protocol

The individual steps of the selective ploidy ablation (SPA) method used in the SPI screens are illustrated with a daily timeline on the left side (see text for details). The universal donor strain (UDS) is depicted with its conditional centromeres and the plasmid (red circle) being transferred into the GFP library. After the UDS has been transformed with the plasmids the proteome-wide SPI screen can be completed within one week.

Alternatively to, or in parallel with the haploid assay, the cells from the mating step above, can be kept as diploid cells by copying them onto –histidine –leucine media with glucose as a carbon source. A diploid screen will determine dominant effects of the GBP-GFP association, since these diploids have an extra set of chromosomes

encoding an untagged version of the GFP-tagged protein. For a diploid screen, the steps after mating were adjusted. The mated colonies were pinned onto glucose SC –his –leu rectangular agar plates and grown for ~24 hours at 30˚C. Then the colonies were pinned again onto fresh glucose SC –his –leu plates and incubated for further ~24 hours at 30˚C before imaging. The diploid cells in glucose media typically grow faster than haploid cells in galactose and 5-FOA, thus the time needed to grow cells for the diploid assay was reduced compared with the haploid assay.

2.4.6 Quantitative analysis of high-throughput yeast growth

Throughout this work I used colony size as a surrogate for growth. I employed the 'CM engine' (Colony Measurement engine), a freely available ImageJ plugin and part of the ScreenMill suite of software (Dittmar *et al.*, 2010) for quantitative analysis of colony sizes. CM engine analyses images and reports the size of each colony on the plate in pixels, colony circularity and location coordinates. I used the default settings. The output file from the CM engine is a 'Log file', which lists the measurements for each colony. This log file was uploaded to the next part of ScreenMill; the Data Review engine (DR engine), which is available online: http://www.rothsteinlab.com/tools/screen_mill/dr_engine_setup. Here the comparisons between the colonies on the control plates and the experiment plates are performed. For validation of growth defects, plate images were normalised using specific controls (such as a non-GFP strain) on the plate as a reference, rather than the default plate median. For an easy read-out of the data I generated a 'Key file'. The Key file is a list ascribing each position on each plate with a particular query GFP-tagged gene. I ran the DR engine with the default settings.

The resulting data output includes the Log Growth Ratio (LGR) or z-score for each query protein to assess specific interactions that affect growth (Figure 2.4 B). The LGR is the natural log of the average colony size on the controls divided by the average colony size of the experiment. Hence higher LGRs indicate a stronger growth defect.

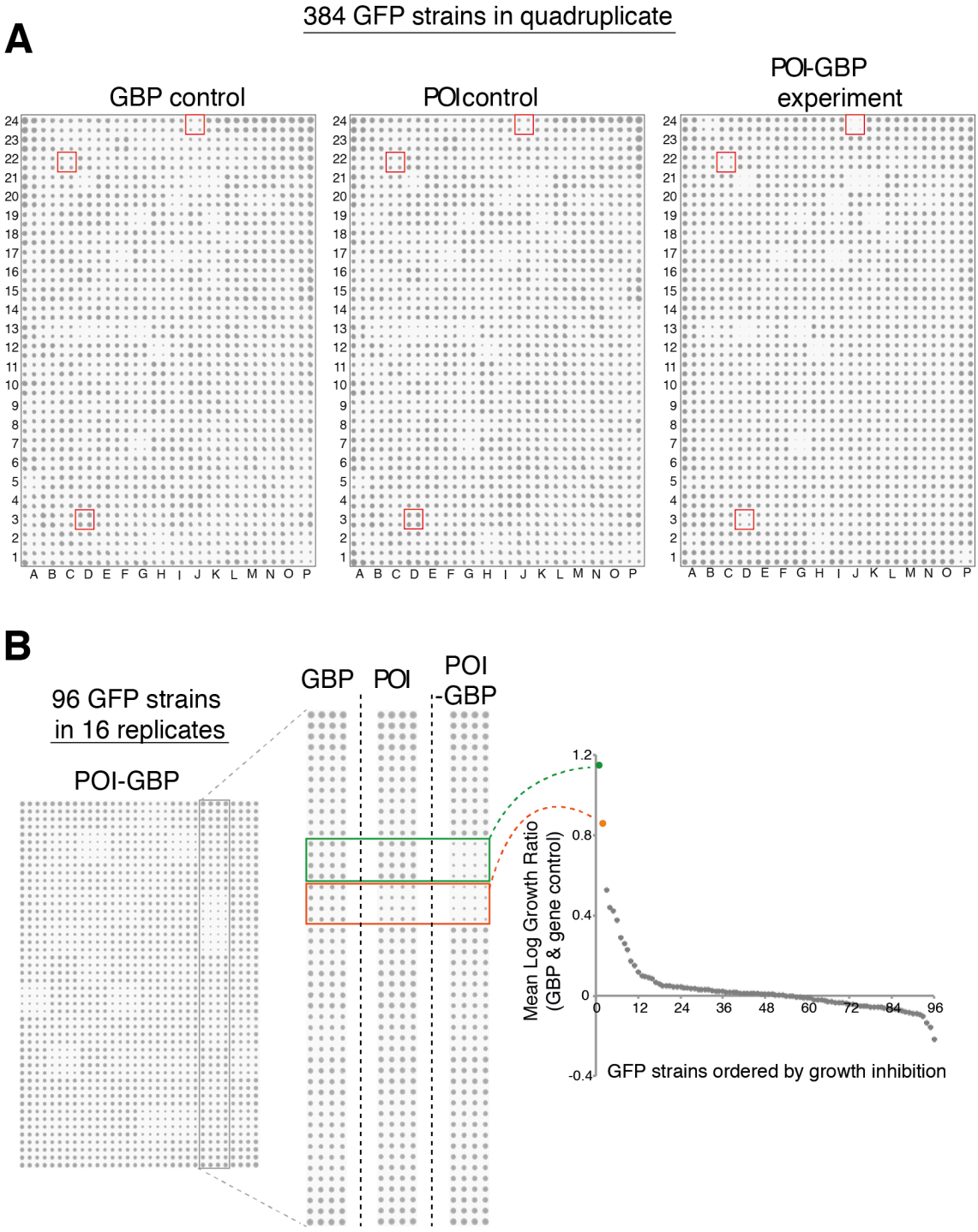

Figure 2.4 Example of SPI data

A) In the proteome-wide SPI screens each plate has an array of 384 GFP strains, each copied in quadruplicate, hence 1536 colonies in total on each plate. On each separate plate the GFP strains contain a different plasmid – the GBP control, the untagged protein of interest (POI) control and the POI-GBP fusion, from left to right. The three highlighted strains (red boxes) show three strains that are affected in the experiment but not controls.
B) In smaller SPI screen, such as the restests or the kinetochore-specific screens, the GFP strains were arrayed on plates so that each had 16 replicates. Two strains that

result in a SPI phenotype are highlighted with rectangles (orange and green). The Mean Log Growth Ratios (LGR) of the two controls versus experiment are then plotted to show the strongest SPIs (the orange and green dots represent the same SPIs indicated with the rectangles and are the strongest SPIs on this plate).

To understand how a specific LGR equates with a growth difference, we calculated the theoretical difference in the number of yeast cells relative to colony size assuming that colonies are hemispheres (Figure 2.5 A). This worked well in practice and showed that a typical LGR of 0.4 equated with ~80% more cells on the control than the experiment (Figure 2.5 B). The formula we derived for converting LGR to the ratio of the number of yeast on control and experiment (RY) is $RY = e^{1.5LGR}$ (Olafsson & Thorpe, 2017).

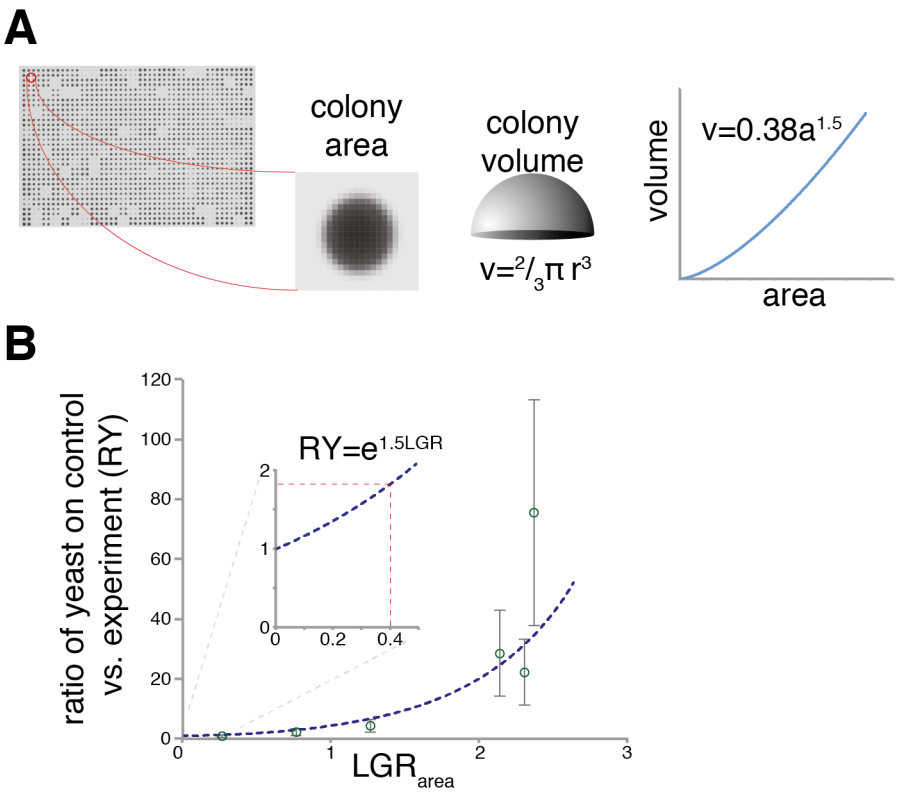

Figure 2.5 Estimation of cell number in a colony

A-B) The assessment of growth relies upon measuring colony area as a surrogate for the number of yeast on the plate. (**A**) We theorised that colonies approximate to hemispheres and consequently the relationship between area (a) and volume (v) is $v=0.38a^{1.5}$. (**B**) We collected and counted the number of cells in colonies to confirm the relationship between the ratio of yeast on control versus experiment (RY) and the LGR and found that broadly our data fit the model. We note that a cut-off of LGR = 0.4, the minimum LGR observable by eye, equates with growth ratio of 1.8, a 45% drop in the number of cells on the experiment versus the control (inset).

Plate based screens often suffer from spatial anomalies, such as colonies growing larger at the top of the plate than the bottom (Collins *et al.*, 2006; Baryshnikova *et al.*,

2010). I used a simple smoothing algorithm to spatially adjust the relative growth rates on plates (Olafsson & Thorpe, 2015). However, the detection of SPIs usually did not significantly change after using the smoothing algorithm, since the z-score or LGR cut-off is quite conservative (Figure 2.6). The PERL script is freely available online: http://www.sourceforge.net/projects/zspatialcorrect/files/spatial1_0.plx/download.

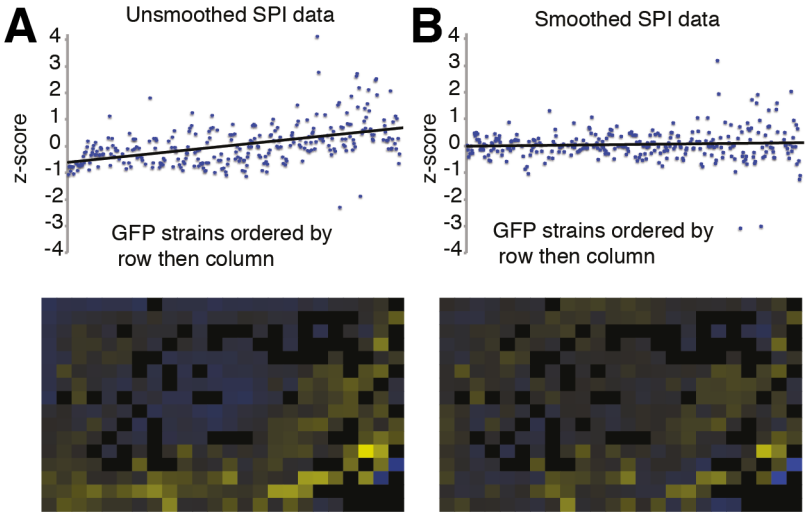

Figure 2.6 Smoothing algorithm to eliminate spatial anomalies on plates

A-B) Spatial defects caused by cells growing differently across a plate is highlighted by plotting the LGR or z-scores by their row and column (**A**); a linear trend line is added to clarify the spatial defect (top panel). The bias is also visualised by a colour-coded map of the plate showing high z-scores in yellow (light) and low z-scores in blue (dark) (bottom panel). A simple smoothing algorithm can correct this defect by normalising scores in each row and column (**B**).

Throughout the thesis I present the SPI data as dot plots of either z-scores or log growth ratios (LGRs) on the y-axis and each GFP strain separated on the x-axis, showing high positive LGRs or z-scores on the left and lower scores on the right (as shown in Figure 2.4 B). Each dot on these graphs represents the ratio between the colony sizes of the control strain (for example a GFP strain containing the GBP control plasmid) versus the colony size of the comparer strain (for example a GFP strain containing the POI-GBP plasmid). The proteome-wide screen data are normally distributed and the ScreenMill software uses the mean and standard deviation and calculates the z-scores from the values accordingly. Since the experiments are done with four or 16 replicates, the average growth ratio is calculated and then this value is converted into z-scores or LGRs. In addition to the dot plots, I also show bar graphs displaying the LGRs on the y-axis and the GFP strains on the x-axis (for example see Figure 4.4 A). These bar graphs use exactly the same data as the dot plots, but the data are presented in a bar graph form for easier comparison between two different

LGRs (for example comparing wild-type and mutant strain). The ScreenMill software does not calculate standard deviations or errors of the four or 16 replicates, hence there are no error bars in these graphs. In cases of different colony sizes within the replicates, the ScreenMill software employs an exclusion algorithm, which compares the value of each replicate to one another. It then determines significant differences based on comparisons of the normalised size of each colony with the median of the replicates and excludes any colony that is 45% greater or less than the median value (Dittmar *et al.*, 2010).

2.5 Chromosomal instability assays

2.5.1 Plasmid loss assay

Strains were transformed with a *CEN* plasmid containing a selectable marker (NAT), in addition to any other indicated *LEU2* plasmids, and grown overnight in 2% glucose SC –leu NAT medium, and then switched to 2% galactose SC –leu for 7 hours to express GAL-controlled genes or gene fusions. For at least eight replicates, ~500–1000 cells with each of the four expression plasmids were then plated out on SC –leu and SC –leu NAT plates. The percentage of plasmid loss was calculated by subtracting the number of colonies growing on the SC –leu NAT to the number of colonies growing on SC –leu. The number of colonies counted are indicated as n.

2.5.2 Chromosome loss assay

Chromosome loss was assessed using the chromosome transmission fidelity (CTF) assay (Spencer *et al.*, 1990; Yuen *et al.*, 2007). In short, the assay utilises a haploid *ade2-101* strain carrying an artificial chromosome fragment (CF) containing *SUP11::URA3.* The expression of *SUP11* suppresses an accumulation of a red pigment caused by the *ade2-101* mutation, thus the cells remain unpigmented if they retain the CF, but upon loss of the CF the cells turn red and the resulting colonies develop red sectors. To assess loss of the CF in cells containing the indicated plasmids (such as *CSE4-MAD2* in Figure 4.6 F) were transferred into a *ade2-101* strain containing the *SUP11* CF and were grown overnight in SC –leu –ura medium, and the cells were collected by centrifugation and washed before dividing them between 2% galactose SC –leu –ura medium to express the fusions, or 2% glucose SC –leu –ura medium to repress expression, for 7 hr. Then a colony colour-sectoring assay was performed by plating out ~1000 cells onto YPD plates and resulting red sectored

colonies were scored as chromosome loss events. The experiment was performed in quadruplicate and less than half-sectored red colonies were excluded. The number of colonies quantified are indicated as n.

2.5.3 Diploid bimater assay (BiM)

A few GFP strains that were detected as SPIs were selected for the bimater assay (Yuen *et al.*, 2007). These SPIs were recreated in heterozygous diploid strains containing a GFP-tagged protein and, unrelated to this assay, a CFP-tagged nucleolar protein, Fob1, by transferring in the indicated plasmids (such as Mtw1-GBP or the GBP control as seen in Figure 3.5). Note that GBP does not bind CFP. Four independent isolates of each heterozygous diploid GFP strain with the Mtw1-GBP and the GBP control plasmids were patched in 1cm^2 squares on SC –leu –his plates, to select for the *GFP-HIS3MX* cassette and the plasmids. These diploid patches and *MAT***a** and *MATα* tester lawns were grown for 2 days at 30˚C and replica plated onto fresh YPD plates and either the *MAT***a** and *MATα* lawns were overlaid and incubated at 30˚C for 24 hours for mating. The mating plates were next replicated onto synthetic deficient (SD) solid media to select for mated products and the colonies/patches were visually inspected for growth after two days of incubation at 30˚C. The bimater phenotype was evaluated by the ability of the diploid strains to mate with the mating tester strains and hence their ability to grow on SD media. The ability of the diploid strain to mate with haploid strains can result from the loss of the *MAT* locus, either by loss of chromosome III, chromosomal rearrangements, mitotic recombination, or gene conversion (Yuen *et al.*, 2007).

2.5.4 Twin spot assay

Strains with a tetracycline operator array, inserted at the *URA3* locus of chromosome V and a tetracycline repressor linked to RFP (*ura3-1::3xURA3-tetOx112 TETR-RFP)*, and a GFP/YFP-tagged gene and the indicated plasmid, such as *MTW1-YFP,* and Cdc14-GBP or cdc14-pd-GBP plasmids, both lacking RFP to prevent interference with the TetR-mFRP signal (for example see Figure 3.12 C), and grown overnight in synthetic media at 23°C. The resulting cells were imaged with fluorescence microscopy and mitotic large-budded cells were assessed for segregated or unsegregated sister chromatids by inspecting the TetR-mFRP foci. The number of cells counted from a single experiment are indicated as n.

2.6 Other methods

2.6.1 Protein extraction

Protein extractions were prepared by using a trichloroacetic acid (TCA) precipitation protocol adapted from (Keogh *et al.*, 2006). In short, cells were grown in appropriate media (YPD or SC –leu) to OD_{600} of ~1.0 and collected by centrifugation and washed with 20% TCA. All further steps were performed on ice with pre-chilled solutions. Pelleted cells were frozen at -80˚C and thawed on ice and resuspended in 250µl 20% TCA and glass bead lysis was performed. The cell suspension was collected without glass beads. 1ml of 5% TCA was added and Bradford protein assay (Bio-Rad) was performed to determine protein content of the samples. Proteins were collected by centrifugation and pellets washed with 750µl 100% ethanol. The protein extract was resuspended in lysis buffer containing protease inhibitors (cOmplete, EDTA-free from Roche) and incubated at 30˚C for 20 minutes with or without Lambda phosphatase according to manufacturer's instructions (New England Biolabs, Inc.). Next, the protein was collected by centrifugation and resuspended in 70µl of 3x Laemmli buffer and 30µl of 1M Tris-HCl pH 9.4. Finally, the samples were boiled at 95˚C for 5 minutes and debris removed by centrifugation and supernatant analysed further.

2.6.2 SDS-PAGE and Western blot analysis

7.5% acrylamide gels containing 50µM Phos-Tag™ and 100µM $MnCl_2$ solution were prepared according to manufacturer's specifications (Koike's group, Hiroshima University). The samples were loaded so that each had same amount of proteins per lane and gels were run at 60V for 1 hour and then 100V for 4 hours and 30 minutes in 1x SDS running buffer. Gels were transferred to PVDF membranes for 1 hour at 100V. Membranes were blocked for 30 minutes using 50% blocking buffer (Li-Cor) and 50% PBS with gentle shaking. Primary mouse anti-HA antibody (Roche) was diluted 1:2000 in blocking buffer with 0.1% Tween and membranes incubated with gentle shaking for 1 hour. Membranes were washed 4 times for 5 minutes with PBST and then secondary goat anti-mouse HRP antibody (Abcam) diluted 1:20,000 in blocking buffer with 0.1% Tween and 0.1% SDS was added and membranes incubated for 1 hour. Finally, membranes were washed as before and ECL reagents (Lumi-Light from Roche) were introduced for 2 minutes for detection and film exposed for 1 minute.

2.6.3 Flow cytometry

The protocol for sample preparation and cell cycle analysis using flow cytometry was adapted from (Haase & Reed, 2002; Rosebrock, 2017). Briefly, after growing cells to log phase (OD_{600} = 0.6) they were fixed for 24 hours in 70% ethanol at -20°C. The cells were collected by and resuspended in 250µl of ribonuclease (RNase) solution (50mM Tris-HCl pH7.5, 100 g/ml RNaseA (Sigma-Aldrich)) and incubated at 37°C for 3 hours. Cells were then washed once with water and resuspended in 500µl of pepsin solution (50mM HCl, 5mg/ml pepsin (Sigma-Aldrich)) and incubated at 37˚C for 1 hour. Next, the cells were collected by centrifugation at 13,000 rpm for 1 min and resuspended in 1ml SYTOX solution (50mM Tris-HCl pH7.5; 1µM SYTOX Green nucleic acid stain (Invitrogen)) and incubated overnight at 4˚C. Finally, before FACS analysis the samples were sonicated for 10 sec using a microtip probe sonicator (Philip Harris Scientific). The cells were analysed in a BD LSR II Flow cytometer. The resulting data were analysed to calculate G1, S and G2/M populations using FlowJo™ 10.3 software (FlowJo, LLC).

2.6.4 Sample preparation for SILAC

I prepared samples for the stable isotope labelling with amino acids in cell culture (SILAC) experiment using an adapted protocol from (Gruhler *et al.*, 2005). First, 5ml culture of the “light” Mtw1-GFP *mad1*Δ strain (T619) containing cdc5-kd-FAM-GBP plasmid (pHT503) was grown in SC –leu 2% glucose overnight or >8 generations. In parallel, 5ml culture of the “heavy” Mtw1-GFP *mad1*Δ strain containing cdc5-kd-GBP plasmid (pHT444) was grown in SC –leu 2% glucose +100 mg/L of “heavy” lysine and arginine + 20 mg/L proline overnight or >8 generations. In addition, a heavy culture with T619 cells containing the cdc5-kd-FAM plasmid and a light culture containing the cdc5-kd-GBP plasmid were prepared in the same way. The cultures were diluted 100-fold into 50ml of fresh media to and grown up OD_{600} = 0.6. Next, samples 1A, 1B, 1C, 1D (Table 2.3) were made by combining 25ml light and 25ml heavy culture in separate 50ml falcon tubes. The cells were collected by centrifugation and resuspended in 20% cold TCA, then washed twice with 10ml of cold acetone (-20˚C). Next, the cells were resuspended in 800µl of beating buffer (8M urea, 50mM ammonium bicarbonate, 5mM EDTA) and 900µl of acid-washed glass beads were added and the cells fractionated by using a cell breaker at 4˚C on fast-prep (5.5 m/s) 2 x 60 sec. Finally, the samples were centrifuged at 13,000 rpm for 15 min and the supernatant collected for further analysis.

The samples with combined heavy and light cultures of T619 cells with the same plasmids (samples 1C and 1D in Table 2.3) were generated to control for any effects other than from the plasmid differences. The protein content was measured by using a Bradford assay kit (Bio-Rad) following the manufacturer's instructions.

The subsequent steps required for SILAC such as, protein cleavage, phospho-peptide enrichment, mass spectroscopy and data filtering were performed by Andrew Jones and Bram Snijders in the Francis Crick Institute Science and Technology Platform for Protein Analysis and Proteomics.

Table 2.3 Samples generated for SILAC

		Heavy	
		[cdc5-kd-GBP] *MTW1-YFP mad1Δ* (pHT444 in T619)	[cdc5-kd-FAM-GBP] *MTW1-YFP mad1Δ* (pHT503 in T619)
Light	[cdc5-kd-GBP] *MTW1-YFP mad1Δ* (pHT444 in T619)	1C	1A
	[cdc5-kd-FAM-GBP] *MTW1-YFP mad1Δ* (pHT503 in T619)	1B	1D

Chapter 3. Results 1: Identification of kinetochore regulators using synthetic physical interactions

3.1 Introduction

The kinetochore acts as a conductor of mitotic progression and accurate chromosome segregation through regulation of spindle dynamics. Many signalling enzymes such as kinases and phosphatases are recruited to the kinetochore at specific times during the cell cycle to regulate kinetochore activity and homeostasis (Trinkle-Mulcahy & Lamond, 2006; Moorhead *et al.*, 2007; De Wulf *et al.*, 2009; Zich & Hardwick, 2010). As described in the introduction many kinetochore proteins are regulated by a number of different post-translational modifications (PTMs), such as phosphorylation, methylation, acetylation and ubiquitylation, which are important for controlling kinetochore function, microtubule attachment, and the correct timing of chromosome segregation. For example, the spindle assembly checkpoint (SAC) functions to prevent aneuploidy via a signalling cascade. In order to temporarily pause the cell cycle to allow correct kinetochore-microtubule attachment, the SAC is activated when microtubules are not connected to kinetochores by recruiting Mps1 kinase, which phosphorylates targets at the kinetochore resulting in recruitment of checkpoint components which activate the SAC to prevent metaphase-anaphase transition (see section 1.3.1 in the introduction for detailed description of the SAC). The kinase activity then has to be reversed by phosphatases to continue the cell cycle. Therefore, the balance between phosphorylation and dephosphorylation at the kinetochore is important for cell-cycle progression and is tightly regulated both spatially and temporally to achieve accurate chromosome segregation.

Experiments using artificial association of two proteins have increased our understanding of biological processes such as the SAC and other signalling pathways. Nevertheless, so far it has not been possible to study forced protein-protein associations systematically across the proteome, and to my knowledge, proteome-wide in vivo forced protein associations have not been used to identify novel regulatory proteins. The aim of this chapter is to identify novel kinetochore regulators using synthetic physical interactions. The data presented in this chapter have been partly published (Olafsson & Thorpe, 2015).

3.2 Results

3.2.1 Proteome-wide Mtw1 SPI screen

In order to identify novel kinetochore regulators, I used the synthetic physical interaction (SPI) methodology (described in detail in section 2.4) to systematically recruit specific proteins to the kinetochore. For the kinetochore SPI screen, I chose the essential central kinetochore component Mtw1 (Mis12 in metazoan), a member of the MIND complex, which is a part of the KMN network (KNL1/SPC105, MIS12/MIND, NDC80), which plays an important role as a regulatory hub for signalling at the kinetochore. The four subunit MIND complex (Mtw1, Nnf1, Nsl1, Dsn1) acts as a linker between the inner constitutive centromere-associated network (CCAN) and the outer kinetochore (NDC80 and DAM1/DASH complexes) which binds microtubules. I engineered a plasmid encoding Mtw1 directly fused to GBP (Mtw1-GBP) under the control of a constitutive promoter (*pCUP1*). This plasmid was then transferred into a library of strains, each of which encodes a different protein tagged with GFP (Huh *et al.*, 2003). Thus, in each resulting strain, Mtw1 is associated with a different cellular protein (Figure 3.1 A). My rationale is that perturbations to mitosis will inhibit growth, consequently I use colony size as a readout for the SPI assays. In addition to Mtw1-GBP, I created two control plasmids containing Mtw1 and GBP alone, to control for ectopic expression of *MTW1* and the binding of GBP to GFP-tagged proteins, respectively. By virtue of the RFP-tag on the GBP I was able to visualise the GBP-GFP association in cells containing GFP-tagged protein and expressing GBP-RFP (Figure 3.1 B).

To confirm that the Mtw1-GBP fusion was functional, I first deleted the endogenous *MTW1* from the genome in a strain containing the Mtw1-GBP plasmid, thus indicating that the expression of Mtw1-GBP can compensate for the loss of the essential *MTW1* gene (data not shown). Second, I confirmed that the Mtw1-GBP fusion protein localises to the kinetochore by introducing the Mtw1-GBP construct into strains containing CFP-tagged proteins, which GBP does not bind, and found that the Mtw1-GBP-RFP signal colocalises with the kinetochore, Cse4-CFP, and is localised as expected in strains containing CFP-tagged SPB and histone (Figure 3.1 C). In addition, I confirmed that the GBP-tagged Mtw1 can successfully recruit various GFP-tagged proteins to the kinetochore (Figure 3.1 D).

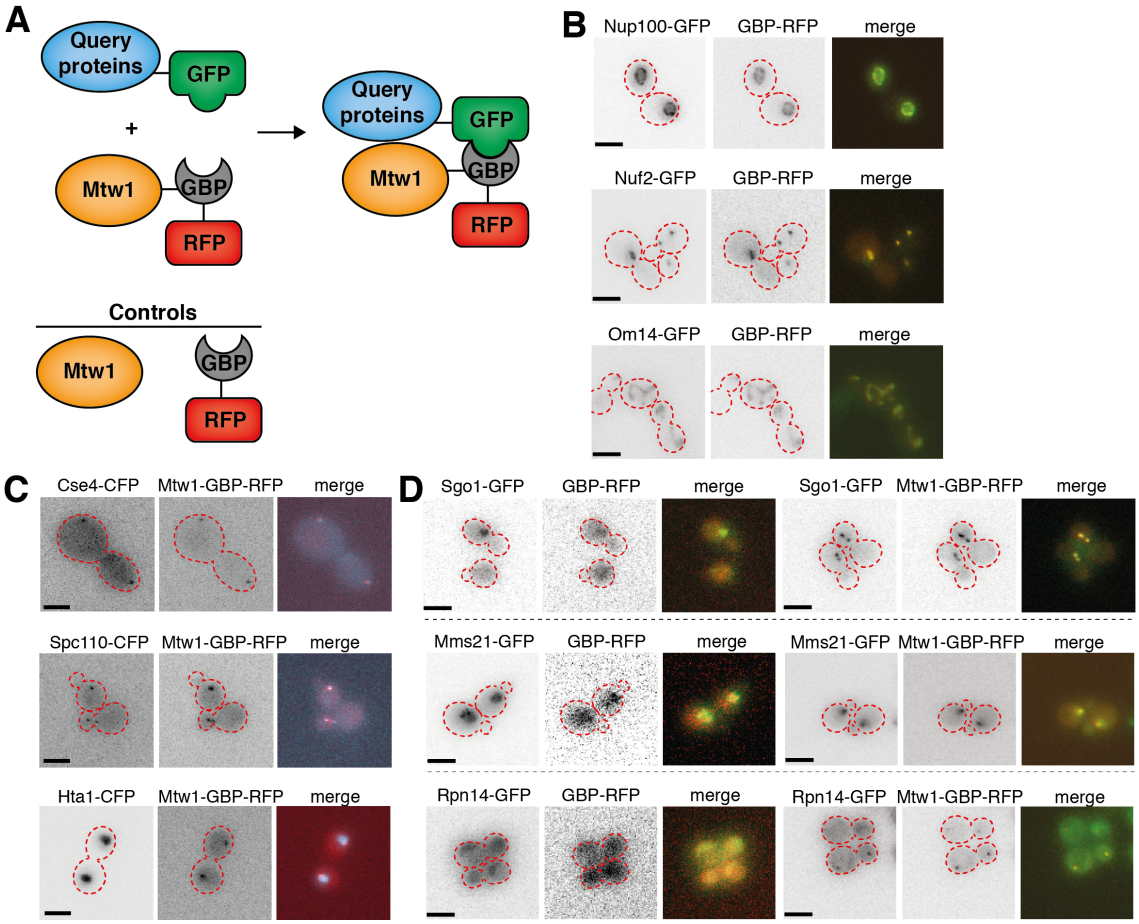

Figure 3.1 Mtw1-GBP successfully recruits GFP-tagged proteins

A) A schematic of the forced association of two proteins when a plasmid encoding Mtw1-GBP fusion is introduced into a strain containing GFP-tagged protein. For the SPI screen, I use two controls: Mtw1 alone to control for its ectopic expression and GBP alone to control for the GBP binding to the GFP protein.
B) The GBP is tagged with RFP and by using fluorescence microscopy it can be seen to colocalise with GFP-tagged proteins, for example with Nup100-GFP at the nuclear pore, Nuf2-GFP at the kinetochore, and Om14-GFP at the mitochondria.
C) The Mtw1-GBP-RFP localises normally to the kinetochore as can be seen in non-GFP strains. Mtw1-GBP-RFP colocalises with Cse4-CFP, localises between SPB foci in a mitotic cell containing Spc110-CFP, and forms kinetochore foci in the nucleus as seen in a cell containing histone tagged with CFP (Hta1-CFP).
D) Cells expressing Mtw1-GBP-RFP can successfully recruit GFP-tagged proteins which are normally diffused in the nucleus (Sgo1-GFP and Mms21-GFP) or cytoplasm (Rpn14-GFP) to the kinetochore. All scale bars are 5μm.

For the Mtw1 proteome-wide SPI screen, I used the selective ploidy ablation (SPA) technique (Reid *et al.*, 2011) to introduce the Mtw1-GBP and the control plasmids into the GFP collection of strains (see section 2.4.5 for details). In brief, the GFP strains are arrayed on agar plates, four colonies per strain, and each of the three plasmids are transferred into a universal donor strain (UDS) which is then mated with the GFP strains using a pinning robot. The resulting diploid strains are subsequently pinned to

different selection (and counter-selection) media, which results in haploid GFP strains containing the controls or Mtw1-GBP plasmids and the relative growth differences between colonies are compared and quantified using an automated colony measurement software (Dittmar *et al.*, 2010)(see section 2.4.6 for details). An example of the raw data is illustrated in Figure 3.2 A and shows an agar plate from the SPI screen containing 1536 colonies, with each GFP strain in quadruplicate. GFP-strains expressing the Mtw1-GBP fusion that produce smaller colonies compared to controls are defined as synthetic physical interactions or SPIs. The Mtw1 and GBP controls produced similar results, thus I use the average of the two controls as a measure of growth effects (Figure 3.2 C). Interestingly, most forced associations with Mtw1 do not inhibit growth (z-score ≅ 0) (Figure 3.2 B). However, relative to the two controls 128 GFP strains produced a SPI growth phenotype when Mtw1-GBP was expressed (z-score >1.5).

It is a concern that the SPI growth phenotype caused by some forced associations of GFP-tagged proteins with a highly localised GBP-tagged structural protein, such as Mtw1, is a result of mislocalisation of an essential protein away from its functional location. In order to investigate how many of these Mtw1 SPIs are a result of mislocalisation of an essential protein, I asked if these SPIs would be suppressed in strains that also contain an untagged version of the GFP-tagged protein. Therefore, I repeated the proteome-wide Mtw1 SPI screen in heterozygoes diploid strains (Figure 3.2 D&E). Consistently, the resulting data shows that 73% (94/128) of the haploid SPIs were suppressed in the diploid assay. Importantly, the data shows that 56 heterozygous diploid GFP strains were affected by the expression of Mtw1-GBP, of which 34 were common with the haploid Mtw1 SPIs (Figure 3.2 E inset). Further in agreement with the idea that mislocalisation of an essential GFP-tagged protein can cause a SPI phenotype in haploid cells, 54% (69/128) of the haploid SPIs were strains with essential GFP-tagged proteins, by contrast the diploid SPIs were 34% (19/56) essential GFP strains, which is a statistically significant difference (Fisher's exact test p-value = $9x10^{-3}$).

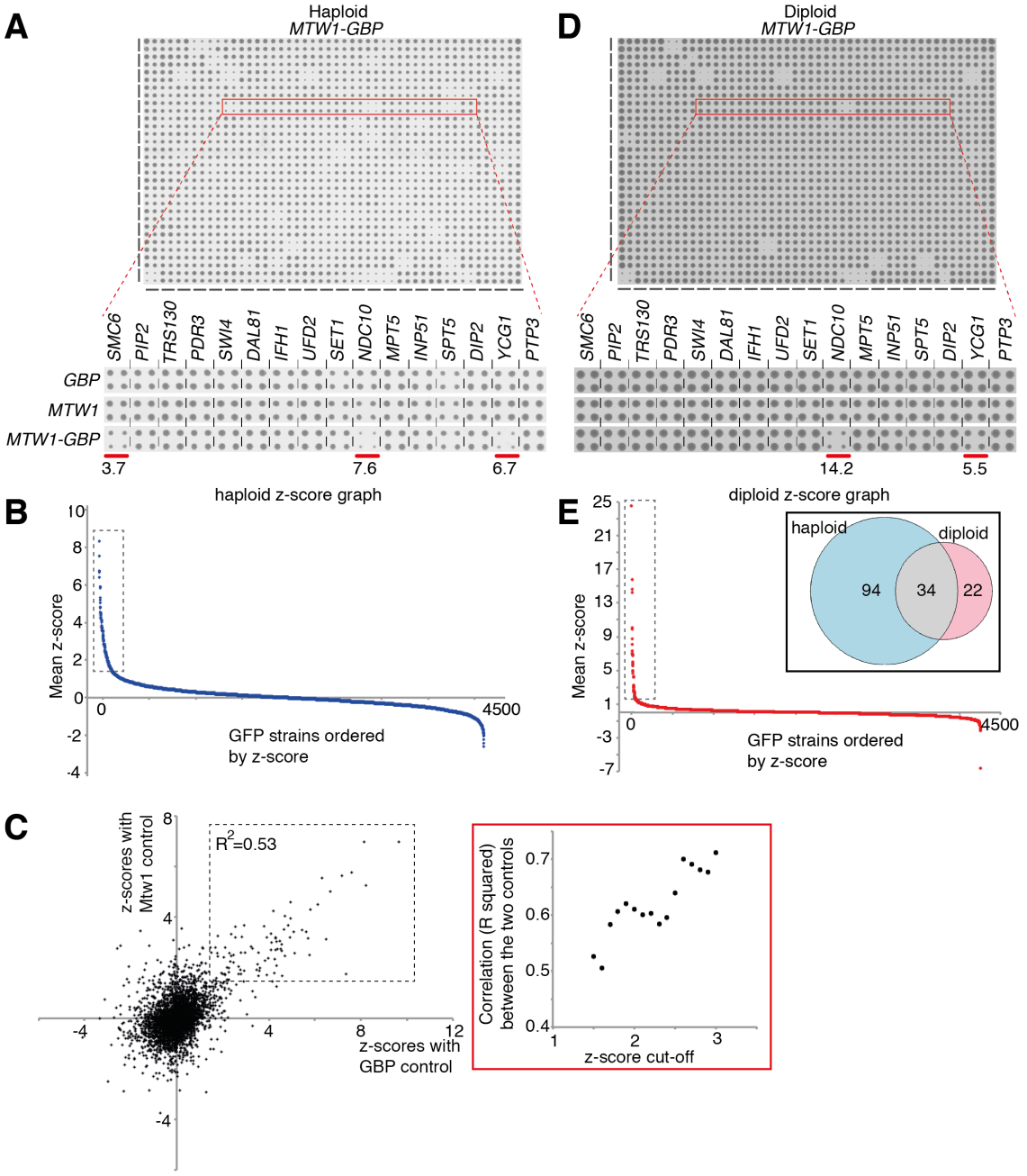

Figure 3.2 Mtw1 proteome-wide SPI screen

A) An example of the haploid SPI data showing four colonies of each GFP strain arrayed on agar plate (1536 colonies per plate) and below are crops from plates with GFP strains containing the three different plasmids. The colony size differences are highlighted with red bars and corresponding z-scores are indicated.
B) The quantification of the SPI data results in z-scores for each forced interaction; high z-score >1.5 indicates greater growth inhibition compared to controls. The z-scores from the haploid Mtw1 SPI screen are plotted in order of growth inhibition of the GFP strains with the most growth restricted strains to the left. The boxed area shows 128 haploid SPIs with z-scores >1.5.
C) The z-scores from the two controls in the Mtw1 SPI screen are plotted on each axis in a scatter graph and correlation of the affected strains is high (squared correlation

coefficient, R^2 = 0.53). The plot in the red box shows the correlation (R^2) between the two controls is higher with increasing z-score.
D) An example of the diploid SPI data (same GFP strains as in figure A). The colony size differences are highlighted with red bars and corresponding z-scores are indicated.
E) The z-scores from the diploid Mtw1 SPI screen are plotted in order of growth inhibition. Diploid SPIs (56) with high z-scores >1.5 are shown inside the boxed area. Inset: The Venn diagram indicates that a majority of the diploid SPIs (34 of 56) are common with those from the haploid SPI screen.

3.2.2 Validation and bioinformatics analysis of Mtw1 SPIs

Next, I asked if the Mtw1 SPIs were enriched for interactions (genetic, physical, etc.) from genomics and proteomics databases. Since, it is known that functionally related genes and proteins are enriched for interactions (Novick *et al.*, 1989; Gavin *et al.*, 2002), I utilised the Cutoff Linked to Interaction Knowledge tool (CLIK) (Dittmar *et al.*, 2013) to plot the interaction density of the haploid and diploid SPI data (Figure 3.3 A&B). The CLIK plots show that approximately the top 100 strongest SPIs in both the haploid and the diploid SPI screens are enriched for interactions, thus suggesting they are likely true positives and perhaps function in common pathways. Nevertheless, a key concern with any genome-wide assay is the level of false positives and negatives produced due to the high-throughput methodology. Hence, to verify the CLIK analysis, I decided to test the false discovery rate (FDR) directly. I retested the strongest SPIs from the haploid and diploid screens at a higher density with 16 replicates per strain (Figure 3.3 C). This high-density retest identified 112 haploid and 79 diploid SPIs. Out of the original 34 SPIs that were common between haploid and diploid proteome-wide screens, only one failed to confirm, and also, the high-density retest confirmed a number of additional SPIs that were just below the threshold of z-score of 1.5 in the original screens. Consequently, 61 Mtw1 SPIs are common between the haploid and diploid sets after high-density retesting. This validation indicates that the SPI method is robust with good correlation between the proteome-wide and the high-density repeated data (Figure 3.3 D&E). Furthermore, the false discovery rate increases as the strength of the phenotype decreases, which is expected for quantitative screens (Figure 3.3 F&G). Moreover, the number of validated SPIs are consistent with that predicted by the CLIK analysis. Finally, I asked if the strength of the SPI phenotype correlated with protein abundance of the GFP-tagged protein, since low-abundance proteins could be more easily disrupted simply based on the stoichiometric interaction with Mtw1-GBP. Surprisingly though, I found no correlation between number of GFP-tagged protein per cell and growth inhibition (Figure 3.3 H&I).

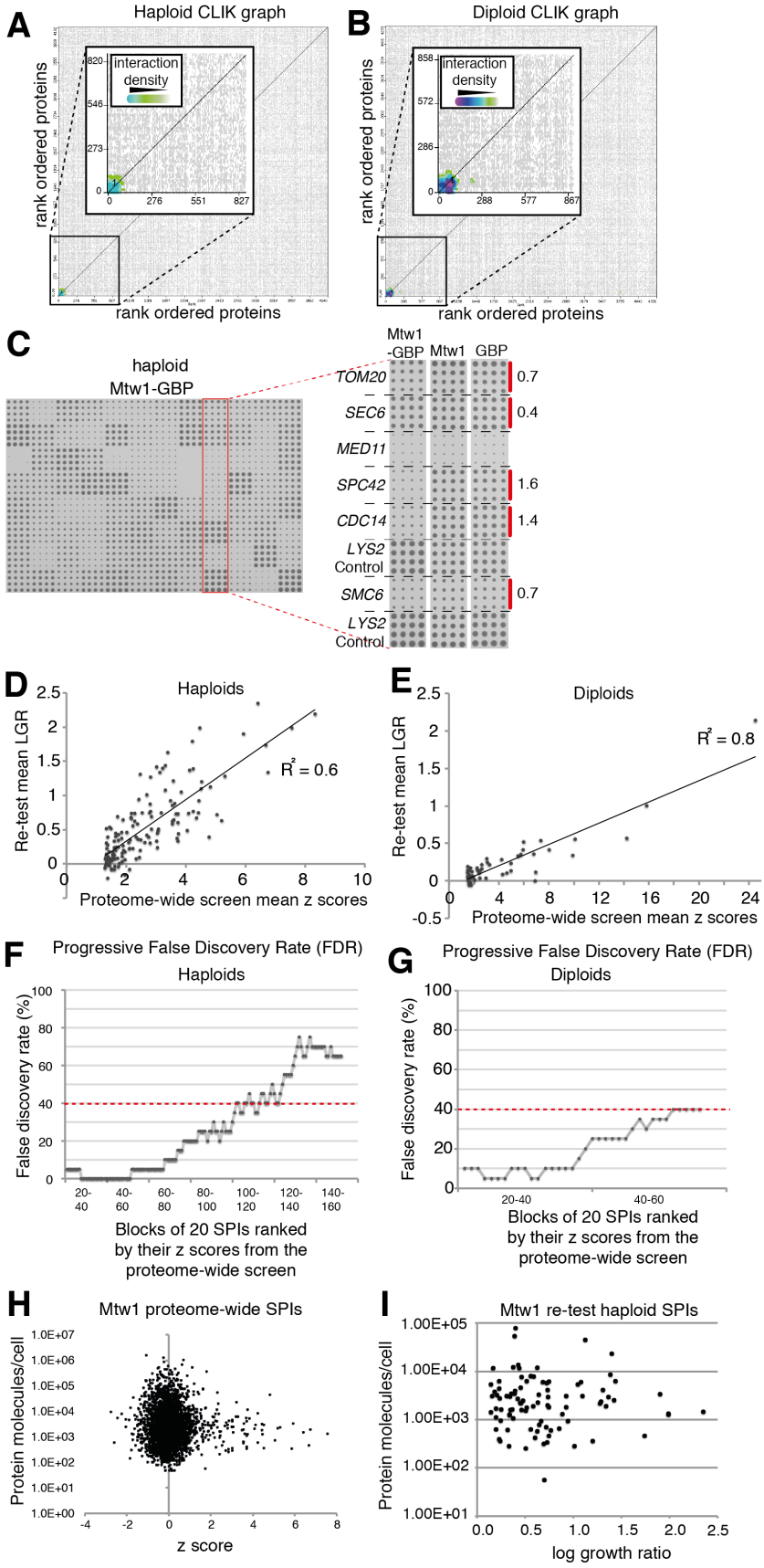

Figure 3.3 Mtw1 SPI screen validation

A) The results of CLIK analysis of the haploid Mtw1 SPI data show that the GFP-tagged proteins in the 100-most growth-restricted strains have a higher than average interaction density. Inset: An enlarged view of the top ~800 proteins.
B) The CLIK analysis for the diploid screen is shown as in A; this also shows that only the top ~100 SPIs show a high interaction density.
C) An example of data from the retest Mtw1 haploid SPI screen. All candidate SPIs were retested using a high-density (16 replicate) format. The data for eight strains is magnified as an inset, showing both strong SPIs (Spc42 and Cdc14) and weaker SPIs (Sec6), highlighted in red, with the log growth ratio (LGR) indicated.
D-E) Both the haploid (D) and diploid (E) retest data (log growth ratios LGR) correlate well with the original proteome-wide data (z-scores); squared correlation coefficient, R^2 = 0.6 and 0.8, respectively.
F-G) The false discovery rate (FDR) was below 40% for 100 strongest SPIs in the haploid retest screen (F) and 60 of the strongest diploid SPIs had also a FDR below 40% in the retest screen.
H-I) The strength of the SPI growth phenotype does not correlate with the amount of protein molecules per cell for the GFP-tagged protein in either the Mtw1 proteome-wide SPI analysis (H) or the retest (I).

Collectively these data show that the SPI methodology is robust and identifies a set of proteins that are enriched for genetic and physical interactions, suggesting that they function together. Thus, I predicted that the Mtw1 SPIs identified would share biological processes and/or function in the same pathways. To test this, I used gene ontology (GO) enrichment analysis of the 61 validated Mtw1 SPIs. The GO analysis revealed a number of significantly enriched categories of molecular functions, biological processes, and cellular components, such as chromosome organisation, nuclear transport, the nuclear pore, histone modification/deacetylation, and condensin complex (Table 3.1). These enrichment categories and a subset of Mtw1 SPIs that were common between haploids and diploids in both the proteome-wide screen and the high-density retest, are illustrated as a heat map network showing also the physical and genetic interactions between the SPIs (Figure 3.4). This SPI network highlights the notion that proteins which cause a growth defect when forcibly associated with Mtw1 share common functions.

Table 3.1 Gene Ontology analysis of Mtw1 SPIs

Process	Gene name
Chromosome organization (6.09×10^{-19})	*CDC5, RFA1, NUP2, SMC2, NUP170, RFA2, DNA2, NUP100, LCD1, PHO23, PDS5, CYC8, NUP157, SIF2, NUP60, HOS4, SNT1, MLP1, MCM21, RXT3,SMC4, ULS1, SET3, HST1, YCG1, SGO1, UME1, CTI6, CSE4, IRR1, BRN1, NUP1*
Function	
Chromatin modification (1.08×10^{-5})	*PHO23, UME1, HOS4, SNT1, RXT3, CTI6, CYC8, SET3, NUP170, HST1, SIF2, LCD1*
Nuclear transport (8.71×10^{-8})	*NUP2, MEX67, NMD3, MLP1, NUP170, NUP188, NMD5, KAP120, NUP100, MSN5 NUP157, NUP60, NUP1*
Component	
Nuclear pore (1.28×10^{-10})	*MEX67, NUP2, MLP1, NUP170, NUP188, NUP60, POM33, NUP157, KAP120, NUP100, NUP1*
Histone deacetylase complex (2.34×10^{-10})	*UME1, PHO23, HOS4, SNT1, RXT3, CTI6, SET3, HST1, SIF2*
Condensin complex (6.73×10^{-7})	*SMC2, SMC4, BRN1, YCG1*

GO enrichment analysis was performed using GOrilla online software available on: http://cbl-gorilla.cs.technion.ac.il/

Since, the aim of the Mtw1 SPI screen is to identify proteins that regulate kinetochore function, the hope is that the assay would detect any proteins when constitutively bound to the kinetochore could misregulate it and thus disrupt mitosis, subsequently causing a growth defect. Accordingly, I first asked if mutants of the genes encoding Mtw1 SPIs identified were involved in chromosomal instability. To this end I used the phenotype enrichment analysis tool, ScreenTroll (Thorpe *et al.*, 2012), and found that the Mtw1 SPIs are indeed enriched for genes in which mutations/deletions give a chromosomal instability (CIN) phenotype and interestingly show synthetic lethality with genes involved in sumoylation (Table 3.2). This indicates that the Mtw1 SPIs are enriched for proteins likely involved in regulation of kinetochore function.

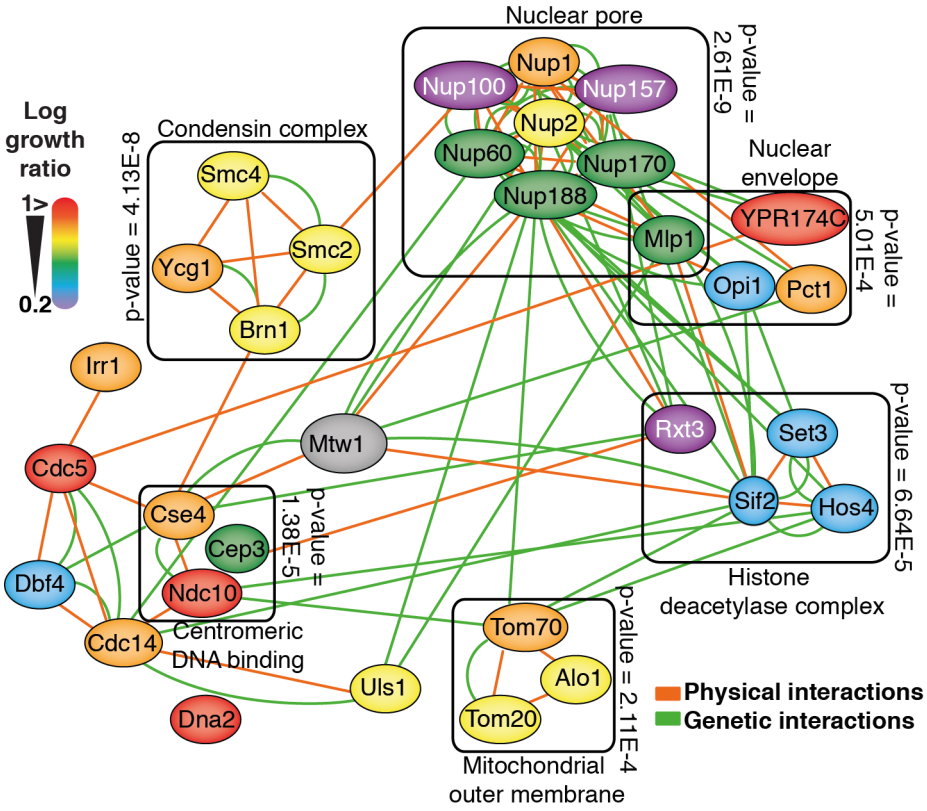

Figure 3.4 Mtw1 SPI network

A subset of the confirmed Mtw1 SPIs (a group of 31 SPIs that were common between haploid and diploids in both the proteome-wide analysis and also the high-density retest) are shown as nodes, colour-coded according to the strength of the SPI (red indicates strong interactions, purple indicates weak interactions). The genetic and physical interactions between these proteins are indicated by green and orange edges, respectively. A selection of the gene ontology enrichment for this set of proteins is indicated by grouping related proteins in boxes with the associated p-value of enrichment.

Table 3.2 Phenotypic enrichment analysis of Mtw1 SPIs

A

#	Screen	ORFs in screen	# common hits	Rank Score*
1	Synthetic lethal/sick with ulp1-333sgg	332	16	2.21E-06
2	Yeast Chromosomal INstability (CIN) essential genes	324	14	3.79E-05
3	Synthetic lethal/sick with ubc9-2	313	13	1.14E-04
4	Tetraploid Sensitive	39	5	1.16E-04
5	Yeast Chromosomal INstability (CIN) genes Master list	723	21	1.26E-04
6	Synthetic lethal/sick with mms21-sp	280	10	0.002
7	Synthetic lethal/sick with ulp2-DAmP	63	4	0.008
8	Enhanced sporulation	102	5	0.009

*The lower the rank score the more significant the representation

B

1. There are 332 ORFs in the Synthetic lethal/sick with ulp1-333sgg screen.Makhnevych *et al.* 2009. Molecular Cell 33; 124-135.
YKR095W (MLP1), YBL097W (BRN1), YHR164C (DNA2), YGR140W (CBF2), YFR031C (SMC2), YML103C (NUP188), YHR170W (NMD3), YDR052C (DBF4), YLR086W (SMC4), YDR318W (MCM21), YDR356W (SPC110), YAR007C (RFA1), YNL097C (PHO23), YAR002W (NUP60), YBR237W (PRP5), YBL079W (NUP170)

2. There are 324 ORFs in the Yeast Chromosomal INstability (CIN) essential genes screen. Stirling et al. 2011. Plos Genetics. 7; e1002057.
YHR164C (DNA2), YGR140W (CBF2), YHR172W (SPC97), YFR028C (CDC14), YDR052C (DBF4), YLR086W (SMC4), YDR356W (SPC110), YAR007C (RFA1), YMR168C (CEP3), YLR409C (UTP21), YKL049C (CSE4), YIL109C (SEC24), YNL312W (RFA2), YIL026C (IRR1)

3. There are 313 ORFs in the Synthetic lethal/sick with ubc9-2 screen. Makhnevych et al. 2009. Molecular Cell 33; 124-135.
YBL097W (BRN1), YHR164C (DNA2), YML103C (NUP188), YHR170W (NMD3), YDR052C (DBF4), YLR086W (SMC4), YDR356W (SPC110), YAR007C (RFA1), YNL097C (PHO23), YAR002W (NUP60), YLR335W (NUP2), YBR237W (PRP5), YBL079W (NUP170)

4. There are 39 ORFs in the Tetraploid Sensitive screen. Storchova et al. 2006. Nature 443; 541-547.
YDR356W (SPC110), YGR140W (CBF2), YOR073W (SGO1), YMR001C (CDC5), YHR172W (SPC97)

5. There are 723 ORFs in the Yeast Chromosomal INstability (CIN) genes Master list screen. Stirling et al. 2011. Plos Genetics. 7; e1002057.
YPL125W (KAP120), YHR164C (DNA2), YGR140W (CBF2), YOR073W (SGO1), YHR172W (SPC97), YFR028C (CDC14), YDR052C (DBF4), YML086C (ALO1), YLR086W (SMC4), YBR112C (CYC8), YDR356W (SPC110), YDR318W (MCM21), YAR007C (RFA1), YMR168C (CEP3), YLR409C (UTP21), YKL049C (CSE4), YIL109C (SEC24), YAR002W (NUP60), YNL312W (RFA2), YBL079W (NUP170), YIL026C (IRR1)

6. There are 280 ORFs in the Synthetic lethal/sick with mms21-sp screen. Makhnevych et al. 2009. Molecular Cell 33; 124-135.
YLR086W (SMC4), YKR095W (MLP1), YBL097W (BRN1), YHR164C (DNA2), YFR031C (SMC2), YAR002W (NUP60), YLR335W (NUP2), YDR052C (DBF4), YBL079W (NUP170), YOR191W (ULS1)

7. There are 63 ORFs in the Synthetic lethal/sick with ulp2-DAmP screen. Makhnevych et al. 2009. Molecular Cell 33; 124-135.
YBL097W (BRN1), YHR164C (DNA2), YIL062C (ARC15), YIR006C (PAN1)

8. There are 102 ORFs in the Enhanced sporulation screen. Deutschbauer et al. 2002. PNAS 99; 15530-15535.
YBR103W (SIF2), YNL097C (PHO23), YKR029C (SET3), YMR307W (GAS1), YHL020C (OPI1)

The output from the Screentroll analysis highlights the overlap between the Mtw1-SPIs and published groups of genes that share a common phenotype. The tool can be downloaded (www.rothsteinlab.com/tools/apps/screenTroll).The most statistically significant overlaps are shown (A) and the specific genes that cause the overlap are listed (B).

3.2.3 Mtw1 SPIs as candidates for kinetochore regulators

Next, I wanted to examine the Mtw1 SPI phenotype in more detail. I predicted that a misregulation at the kinetochore caused by the forced associations would be likely to give a CIN phenotype, I thus used an established assay for assessing CIN in diploid

cells (Yuen *et al.*, 2007). I picked five Mtw1 SPIs (Cdc5, Tom70, Ypr174c, Nup1 and Cdc14) that gave a strong growth phenotype in haploids and were validated in both haploids and diploids. The plasmids encoding the Mtw1-GBP fusion and the GBP control were transferred into diploid strains containing a single GFP allele and their CIN phenotype assessed using the bimater CIN assay (BiM) (Yuen *et al.*, 2007) (see section 2.5.3 for details). In short, heterozygoes GFP diploid strains containing the Mtw1-GBP plasmid and GBP control plasmid, were tested for mating with both haploid *MAT***a** and *MATα* strains and if the diploid strains are able to mate with both mating types it suggests loss of chromosome III, which contains the mating locus *MAT* (see more detailed description in methods). I found that three out of the five Mtw1 SPIs tested, showed a clear CIN phenotype (Cdc5, Tom70 and Ypr174c) (Figure 3.5).

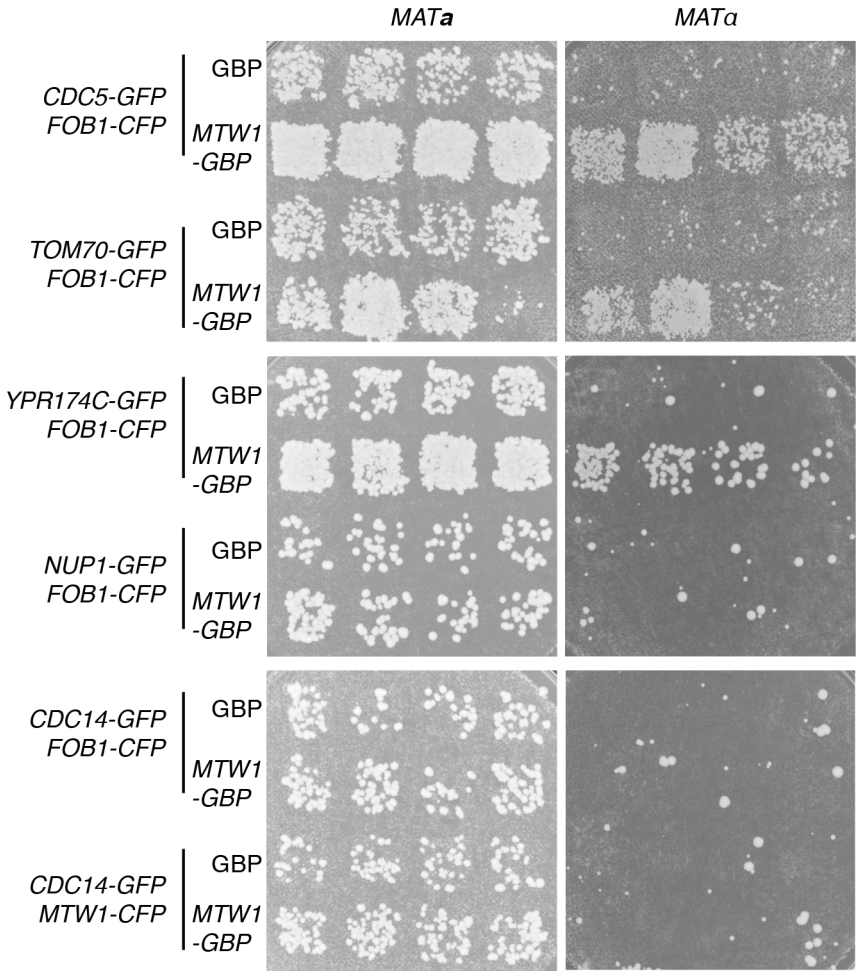

Figure 3.5 Chromosomal instability analysis of Mtw1 SPIs

Chromosome loss of Mtw1 SPIs was assessed using the bimater CIN assay. A selection of SPIs were recreated in diploid cells (heterozygous for the GFP tag). These diploids, which contain either the GBP or Mtw1-GBP plasmids, were patched onto plates and mated with either *MAT***a** or *MATα* strains. I found that the Mtw1-GBP

plasmid causes three GFP strains to have elevated chromosome loss (Tom70, Ypr174c, and Cdc5). In contrast, I found no increased chromosome loss for the Mtw1-Cdc14 SPI. Note that the Fob1-CFP tag is not related to this assay.

As pointed out previously, it is possible that some GFP-tagged proteins are not recruited to the kinetochore in cells expressing the Mtw1-GBP construct, and furthermore it is conceivable that the GFP-tagged protein is able to remove the GBP-tagged kinetochore protein away from the kinetochore. Another possibility is that both the GFP-tagged protein and the GBP-tagged protein are both mislocalised to an ectopic location within the cell which is atypical for both proteins since the GFP-GBP interaction is very strong (Rothbauer *et al.*, 2006) and creates a "tug-of-war" between the two proteins, and finally a fraction of the GFP-tagged protein could be recruited to the location of the GBP-tagged protein and vice versa within the same cell (Berry *et al.*, 2016). It is important to note that the cells expressing Mtw1-GBP plasmid do also contain the untagged endogenous *MTW1* gene. To investigate if these Mtw1 SPI phenotypes are caused by the colocalisation of Mtw1 and the GFP-tagged protein I used fluorescence microscopy imaging. Cells expressing Mtw1-GBP recruited both Cdc5-GFP and Ypr174c-GFP to the kinetochore (Figure 3.6 A&B). In contrast, Mtw1-GBP did not relocalise the nucleoporin Nup1 to the kinetochore, but rather the Mtw1-GBP-RFP signal was mislocalised and colocalised with Nup1-GFP at the nuclear periphery, although without affecting the kinetochore structure itself, since Ask1, an outer kinetochore component tagged with CFP (which GBP does not bind), was not mislocalised away from the kinetochore (Figure 3.6 C). Similarly, Tom70-GFP did not colocalise with Mtw1-GBP-RFP at the kinetochore, however they did colocalise at cytoplasmic regions that are most likely mitochondria, since Tom70 is a mitochondrial translocase, and interestingly strong Mtw1-GBP-RFP and Tom7-GFP signals were colocalised in a polarised manner at the plasma membrane in a dividing cell (Figure 3.6 D). This fluorescence imaging analysis of the Mtw1 SPIs are in agreement with the idea that Mtw1-GBP can recruit GFP-tagged proteins to the kinetochore that are not tightly bound structural components, such as enzymes like Cdc5 kinase. However, membrane-bound proteins such as Nup1 and Tom70 are harder to mislocalise. I cannot rule out that mislocalisation of a fraction of the Mtw1 does not, at least partially, contribute to the SPI phenotype, although many of the SPIs are recapitulated in heterozygous diploid cells, which have two alleles of untagged *MTW1*. This implies that there might be factors other than simply mislocalisation of Mtw1-GBP causing the phenotype in specific cases, such as the Mtw1-Tom70 SPI.

To conclude, these results indicate that using the SPI method to associate a kinetochore protein systematically to each member of the budding yeast proteome can potentially identify proteins involved in regulating kinetochore function. Regulatory proteins that are normally recruited to the kinetochore at specific times during the cell cycle to orchestrate mitosis and/or regulate kinetochore homeostasis are usually involved in post-translational modifications of kinetochore subunits. These kinetochore regulators are often enzymes such as kinases, phosphatases and ubiquitin ligases. Hence, I am interested in proteins that regulate post-translational modifications in the set of SPIs (Figure 3.4). Three out of the 61 Mtw1 SPIs are directly involved in phosphoregulation. First, Dbf4 is the regulatory subunit of the Cdc7 kinase (DDK; Dbf4-dependent kinase in humans). Second, the polo-like kinase Cdc5, which was identified as a high-copy suppressor of *DBF4* mutants (Kitada *et al.*, 1993). Cdc5 has multiple roles during mitosis and Plk1, its human homolog, has reported roles at the kinetochore, which are described in detail in chapter 5. Third, Cdc14 is a mitotic phosphatase that reverses CDK activity to facilitate the cell-cycle progression from anaphase, through telophase and eventually cytokinesis (Stegmeier *et al.*, 2002; Sanchez-Diaz *et al.*, 2012). Finally, other post-translational modification proteins in the set of 61 Mtw1 SPIs include several subunits of both SET3 and RPD3 histone deacetylase (HDAC) complexes, and the SUMO-targeted ubiquitin ligase (STUbL), Uls1. I chose to follow up the conserved Cdc14 phosphatase and investigated further the phenotype caused by its constitutive kinetochore localisation.

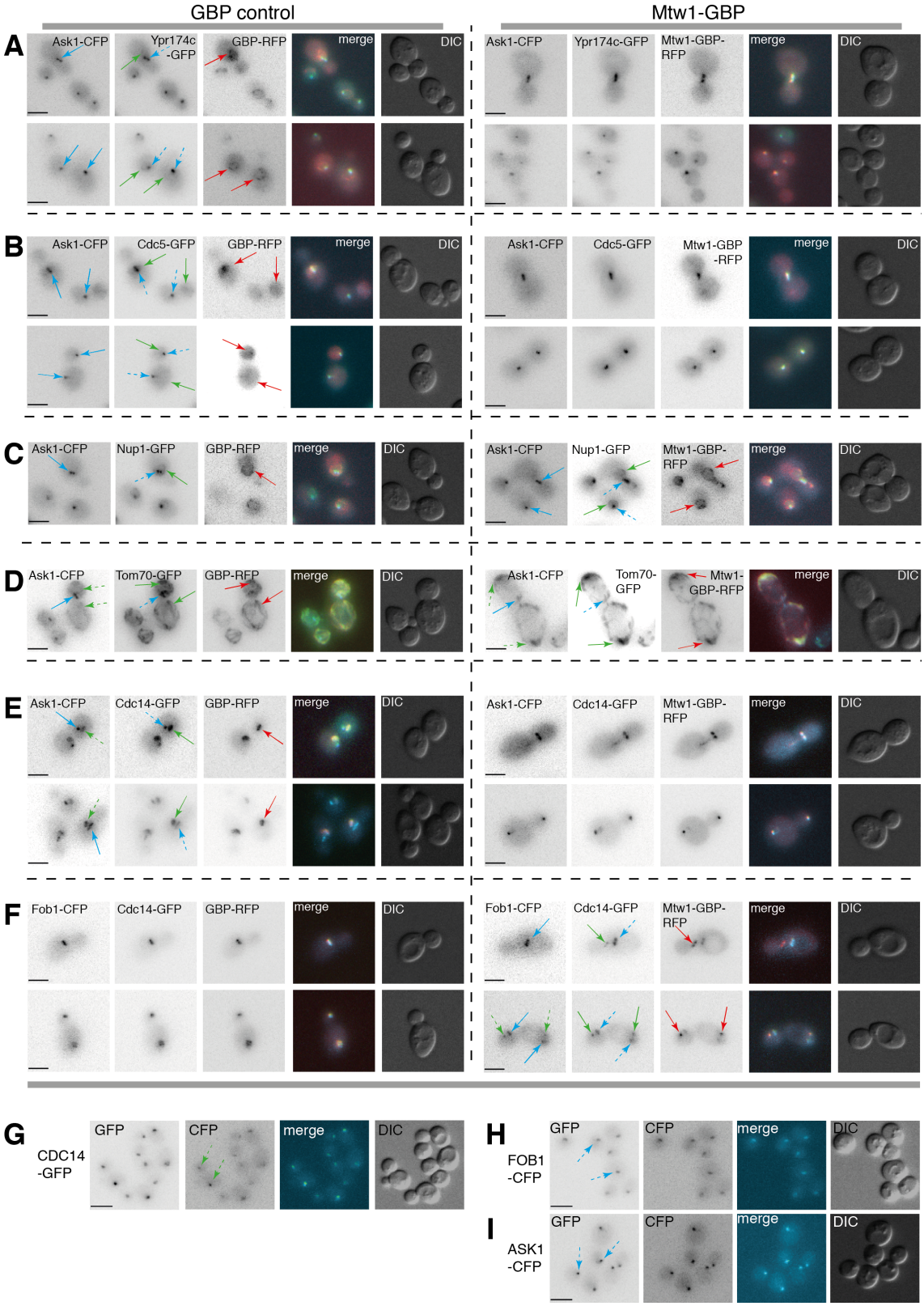

Figure 3.6 Mtw1-GBP localisation in GFP strains

A-E) To ask whether the Mtw1-GBP was sufficient to relocalise GFP proteins to the kinetochore or if the Mtw1-GBP was mislocalised away from the kinetochore, I introduced the GBP-RFP and Mtw1-GBP-RFP plasmids into Ypr174c-GFP (A), Cdc5-

GFP (B), Nup1-GFP (C), Tom70-GFP (D), and Cdc14-GFP (E) strains containing a CFP-tagged outer kinetochore protein Ask1-CFP (GBP does not bind CFP).
F) The GBP-RFP and Mtw1-GBP-RFP plasmids were introduced into a Cdc14-GFP strain containing Fob1-CFP to mark the nucleolus.
In all of these images, because the emission spectra of CFP and GFP overlap (see section 2.3.1 for details) there is significant bleed-through of CFP signal into the GFP images and, to a lesser extent, GFP signal into the CFP images (G-I). Consequently, I have labelled the CFP locations with blue arrows and the GFP locations with green arrows (unless all of the signals overlap). The blue arrows are dashed in the GFP images (and vice versa) to indicate that this is bleed-through of emission. Since, the GBP binds GFP but not CFP, the GFP locations are defined as both a GFP signal and an RFP signal. All scale bars are 5μm.

3.2.4 Cdc14 kinetochore SPIs

Cdc14 phosphatase is essential in budding yeast and is kept in the nucleolus by Net1/Cfi1 during most of the cell cycle. At anaphase onset Cdc14 is transiently released from the nucleolus as a part of the FEAR network (Cdc14 early anaphase release) and is then released fully later on to control the mitotic exit network (MEN) (Visintin *et al.*, 1998; Stegmeier *et al.*, 2002). The key role of Cdc14 is to reverse the action of Cdk, by directly dephosphorylating Cdk substrates and by activating both the Cdk inhibitor Swe1 and APC/C-Cdh1 which is responsible for destruction of cyclins (Jaspersen *et al.*, 1999; Raspelli *et al.*, 2015; Hatano *et al.*, 2016). Moreover, Cdc14 has been shown to have additional roles such as dephosphorylation of Sli15, a regulatory subunit of the Aurora B/Ipl1 kinase, which results in relocalisation of Ipl1 from the kinetochore to the spindle midzone, in a process important for spindle elongation (Pereira & Schiebel, 2003).

Since, Cdc14-GFP was constitutively associated with Mtw1-GBP at the kinetochore and further fluorescence microscopy analysis of the mitotic spindle revealed that some Cdc14-GFP cells expressing Mtw1-GBP had aberrant mitotic phenotype, such as multiple kinetochore foci or lagging kinetochores in anaphase (Figure 3.7 A). I thus wanted investigate this SPI phenotype in more detail. I analysed the cell morphological state of these cells and found that Cdc14-GFP strain expressing Mtw1-GBP had drastically increased proportion of large-budded cells compared to Cdc14-GFP strain expressing GBP alone (Figure 3.7 B), although without leading to CIN phenotype (Figure 3.5).

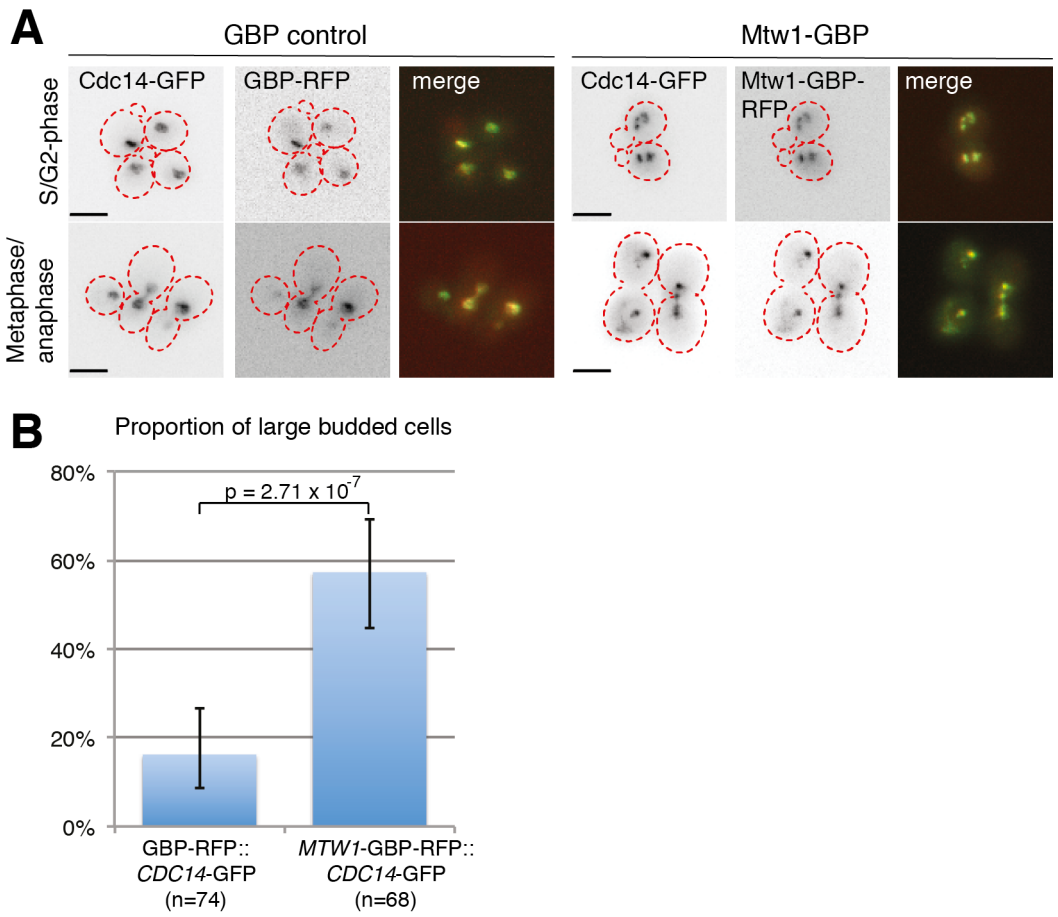

Figure 3.7 Expression of Mtw1-GBP in Cdc14-GFP cells results in mitotic defects

A) The GBP-RFP and Mtw1-GBP-RFP plasmids were introduced into a Cdc14-GFP strain and cells imaged with fluorescence microscopy. The GBP-RFP signal colocalises with Cdc14-GFP at the nucleolus. The Mtw1-GBP-RFP signal forms multiple foci, likely at the nucleolus and the kinetochore. All scale bars are 5μm. **B**) Large-budded cells were quantified and were significantly increased when Mtw1-GBP was expressed compared to GBP control. Error bars are 95% binomial confidence intervals and p-value was calculated using a Fisher's exact test.

It is possible, as noted above, that the expression of GBP-tagged Mtw1 in Cdc14-GFP cells mislocalises the entire kinetochore to the nucleolus or that it disrupts kinetochore assembly by titrating away kinetochore proteins bound to Mtw1-GBP. In addition, I cannot exclude the possibility that the essential activity of Cdc14-GFP is compromised by forcing the Mtw1-GBP association, although this is unlikely since the growth defect remains in heterozygous diploid cells. Therefore, I wanted to explore more closely the localisation of the Mtw1-GBP Cdc14-GFP association in cells using fluorescence microscopy. I labelled individually the nucleolus and kinetochore with a fluorophore that does not bind GBP in a Cdc14-GFP strain, Fob1-CFP and Ask1-CFP, respectively. I then introduced the Mtw1-GBP or GBP control plasmids into these two strains and

found that Cdc14-GFP did relocalise to the kinetochore in the Ask1-CFP strain (Figure 3.6 E), although some Mtw1-GBP-RFP did colocalise with the nucleolus in the Fob1-CFP strain (Figure 3.6 F).

To evaluate the kinetochore-Cdc14 SPI in more detail and to examine where at the kinetochore Cdc14 can produce a SPI phenotype, I decided to make a plasmid with Cdc14 fused to GBP and introduce this into a collection of different GFP-tagged kinetochore strains. I engineered constructs with GBP fused individually to the C- and N-termini of Cdc14 (Cdc14-GBP and GBP-Cdc14, respectively), and in addition to the standard GBP and gene (*CDC14*) only controls, I decided to create plasmids encoding catalytically-inactive mutants of Cdc14 (cdc14-C283A and cdc14-C283S) (Pereira *et al.*, 2002; Bloom *et al.*, 2011) fused to GBP (cdc14-CA-GBP, GBP-cdc14-CA and GBP-cdc14-CS), to control for the phosphatase activity of Cdc14. Before performing the Cdc14 kinetochore-specific SPI screen, I wanted to test if the Cdc14-GBP fusion was functional. First, using fluorescence microscopy I saw that the GBP-tagged Cdc14 (and phosphatase-dead Cdc14) localised normally to the nucleolus (Figure 3.8 A-C). Second, I was able to introduce the *CDC14-GBP-RFP* allele into the endogenous *CDC14* locus in a wild-type strain, without disrupting growth indicating it functions normally within the cell (data not shown). The GBP-tagged Cdc14, wild-type and mutants, were successfully recruited to GFP-tagged kinetochore proteins (Figure 3.8 D-F).

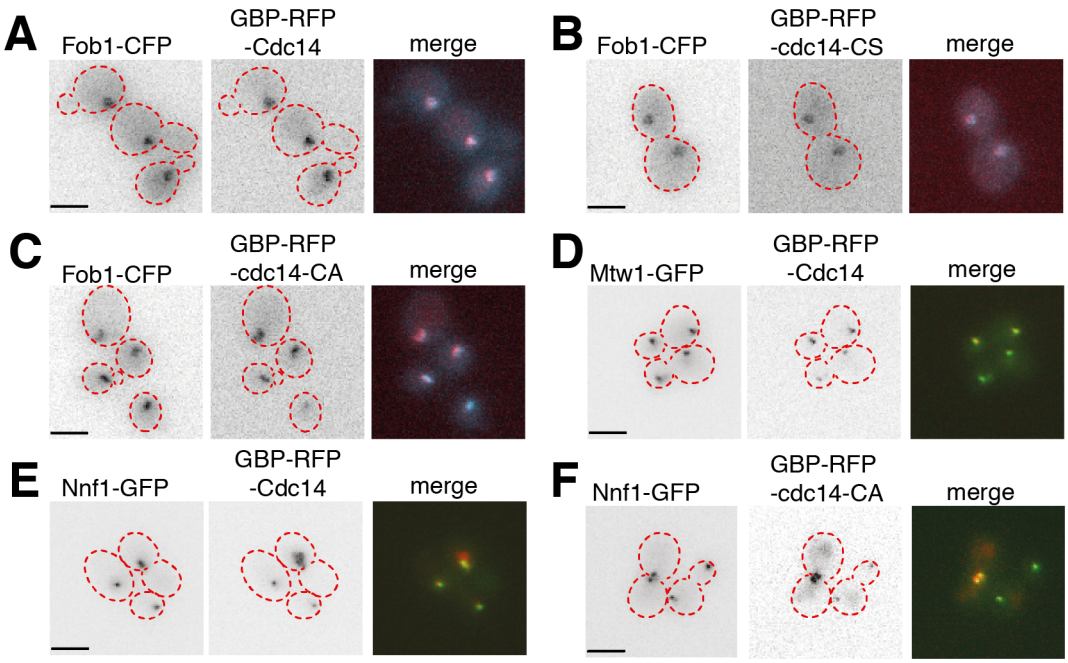

Figure 3.8 Cells with GFP-tagged kinetochore proteins can successfully relocalise GBP-tagged Cdc14 to the kinetochore

A-C) Fluorescence microscopy imaging of cells expressing GBP-RFP-Cdc14 (A) and phosphatase-dead mutants (B&C) shows that they colocalise with Fob1-CFP at the nucleolus.
D-F) Cells containing Mtw1-GFP (D) and Nnf1-GFP (E) can recruit the GBP-tagged Cdc14 to the kinetochore, as well as the phosphatase-dead mutant GBP-RFP-cdc14-CA (F). All scale bars are 5μm.

I transferred the GBP-tagged Cdc14 plasmids and control plasmids listed above separately into a set of 88 kinetochore and kinetochore-related GFP strains using the same method as before but at a higher-density of 16 replicates per strain (Figure 3.9 A&B). I next compared the colony sizes of GFP strains expressing the Cdc14-GBP fusions with both strains expressing the untagged Cdc14 and with strains expressing the catalytic-mutant fusions, which allows me to assess the effect of forced phosphatase activity of Cdc14 at the kinetochore. The C-terminal Cdc14-GBP fusion produced more SPIs than the N-terminal GBP-Cdc14 fusion, although the data correlated well (Figure 3.9 C), and using the untagged Cdc14 as control produced more SPIs compared to the phosphatase-dead mutant controls (Figure 3.9 E&F). The two mutants (GBP-cdc14-CA and GBP-cdc14-CS) gave equivalent results (Figure 3.9 D), hence I will refer to both of them as phosphatase-dead mutants or cdc14-pd for short. Regardless of which wild-type Cdc14-GBP fusion construct is used or which control was compared, I found that MIND complex subunits consistently produced a SPI growth phenotype when forced to associate with active Cdc14 (Figure 3.9 E&F). I also found that forced association of Cdc14 with components of other kinetochore subcomplexes inhibits growth, such as the DAM1/DASH complex (Dad1, Dad2, and Dad3), the CBF3 complex (Ndc10 and Cep3), the COMA complex (Mcm21 and Ctf19), microtubule-associated proteins (MAPs) Bik1 and Stu2, two members of the KMN network (Nuf2 and Kre28), and finally subunit of the chromosomal passenger complex (CPC), Bir1.

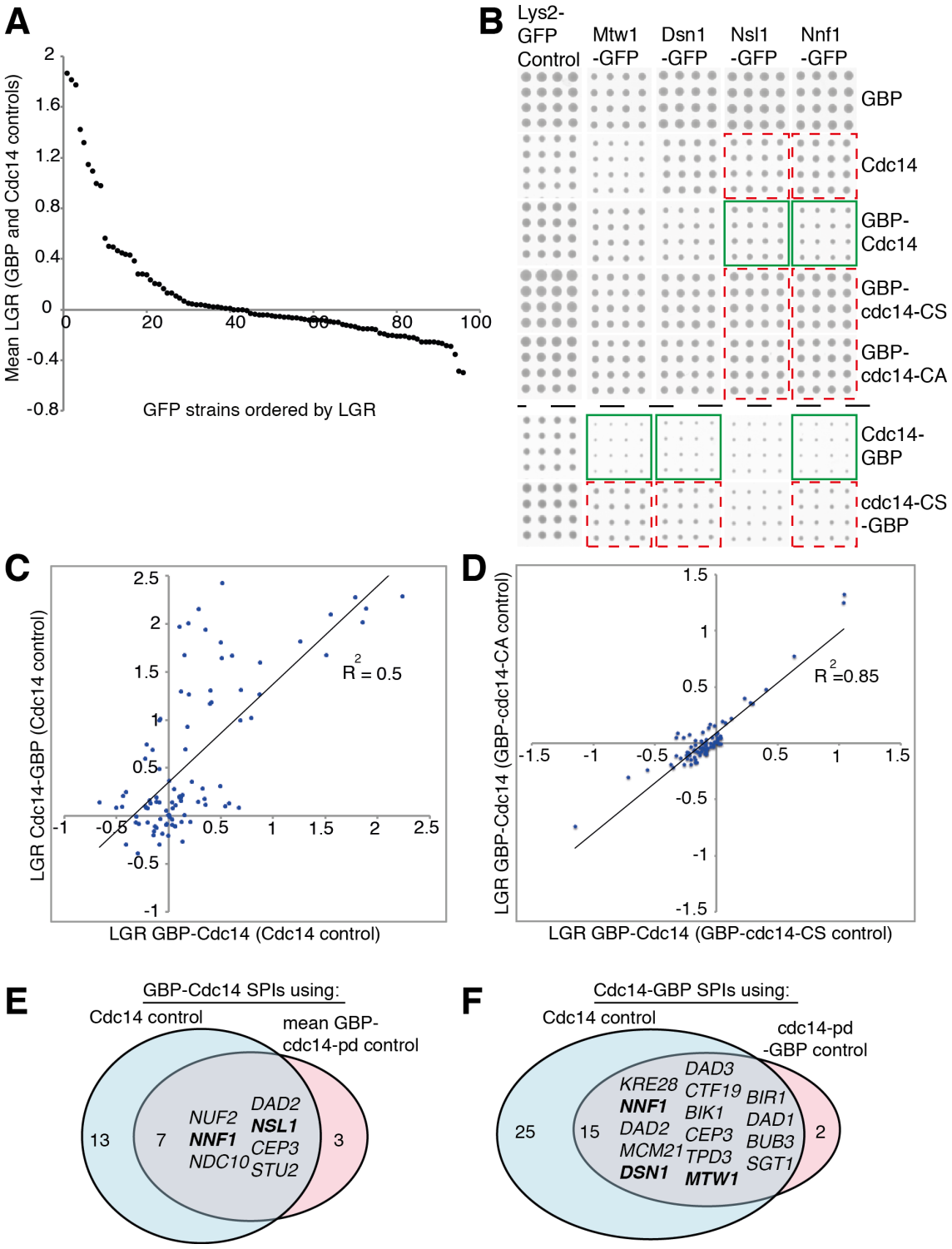

Figure 3.9 Kinetochore-specific Cdc14 SPI screen

A) The average SPI data using the GBP-Cdc14 construct compared with the GBP and Cdc14 controls are plotted in order of the strength of the growth inhibition. I note that some Cdc14 SPIs appear to enhance the normal growth of cells. For example, recruitment of active GBP-Cdc14 to Kip3-GFP and Ndc80-GFP enhances cell growth. However, I find these “growth-enhancing” interactions are rarely consistent between

controls (both Kip3 and Ndc80 are not found when using Cdc14 as a control). Consequently, I have not investigated these interactions further.
B) An example of the SPI data showing colonies of strains with GFP-tagged MIND complex subunits arrayed with 16 replicates per strain, expressing all the different Cdc14 constructs and controls used in the Cdc14 SPI assay. Forced interactions that produced SPIs (LGR > 0.4) using the Cdc14 and mutant controls are highlighted (green for experiment, red for controls).
C) The N-terminal and C-terminal GBP fusions to Cdc14 give well-correlated SPI data (log growth ratios; LGRs); squared correlation coefficient, R^2 = 0.5. Although the strength of the SPIs is increased using the C-terminal Cdc14-GBP fusion (Y-axis).
D) The two catalytically-inactive Cdc14 N-terminal GBP fusions gave equivalent log growth ratios (LGRs) compared with the wild-type GBP-Cdc14; squared correlation coefficient, R^2 = 0.85.
E) The N-terminally GBP-tagged Cdc14 (GBP-Cdc14) compared with Cdc14 control gave SPI phenotypes with 20 GFP strains and compared with the phosphatase-dead mutant control gave 10 SPIs, 7 of which overlap between the two groups.
F) The C-terminally GBP-tagged Cdc14 (Cdc14-GBP) gave 40 SPIs relative to the Cdc14 control and 17 relative to the phosphatase-dead mutant control, of which 15 overlap. Subunits of the MIND complex are highlighted in bold.

In Figure 3.10 the most consistent Cdc14 kinetochore SPIs are mapped onto a schematic of the kinetochore subcomplexes. This Cdc14 kinetochore SPI map is superimposed with known CDK sites and shows that many SPIs overlap with these sites or are in subcomplexes that contain CDK phosphosites.

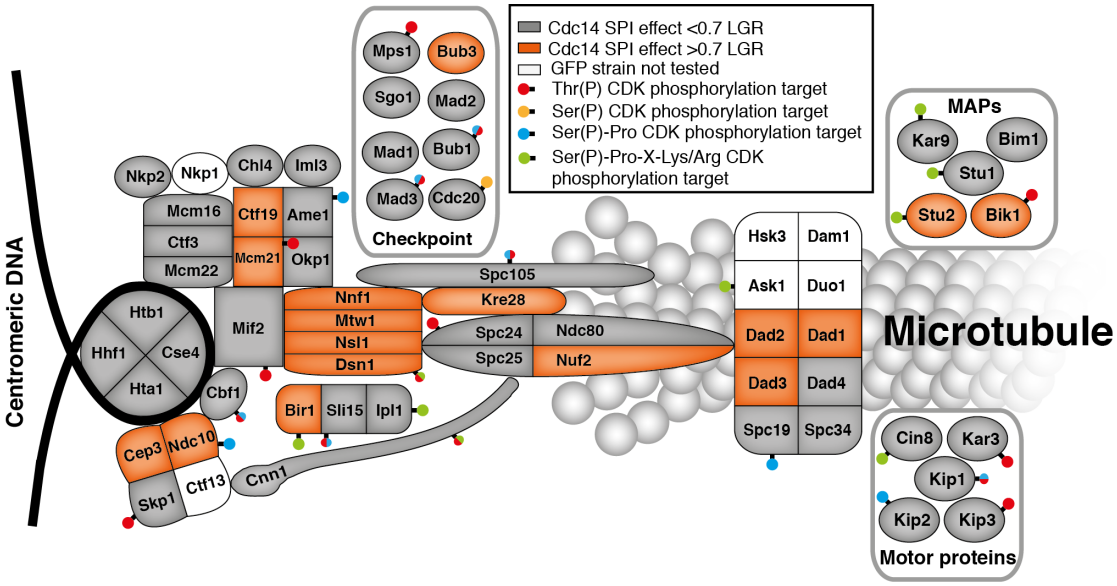

Figure 3.10 Cdc14 kinetochore SPI map

A schematic of the kinetochore with the most consistent Cdc14 SPIs coloured in orange. The SPIs were chosen from the overlaps in Figure 3.9 E&F and the average log growth ratio (LGR) was calculated using the Cdc14 control from both the C- and N-terminally GBP-tagged Cdc14 SPI screens. The known CDK targets are superimposed as “lollipops”.

Next, I asked if stoichiometry of the Cdc14-GBP fusion determines the strength of the growth inhibition in these SPIs. I analysed fluorescence microscopy images of cells containing either endogenous *CDC14-GBP-RFP* or plasmid encoding Cdc14-GBP-RFP (both wild-type and cdc14-pd) and compared the RFP fluorescence intensity. The plasmid-encoded Cdc14-GBP-RFP intensity was ~1.5-fold higher than the endogenously tagged Cdc14 (Figure 3.11 A). In addition, I up-regulated the level of the plasmid-encoded Cdc14-GBP-RFP by using increasing concentrations of copper (Figure 3.11 B) and subsequently, repeated the Cdc14 SPI assay with the GFP kinetochore strains to see if this would influence the SPI phenotype, but this had only minimal effects (Figure 3.11 C-F). I also examined if the strength of the SPI phenotype correlates with protein abundance, but found no correlation (Figure 3.11 G&H).

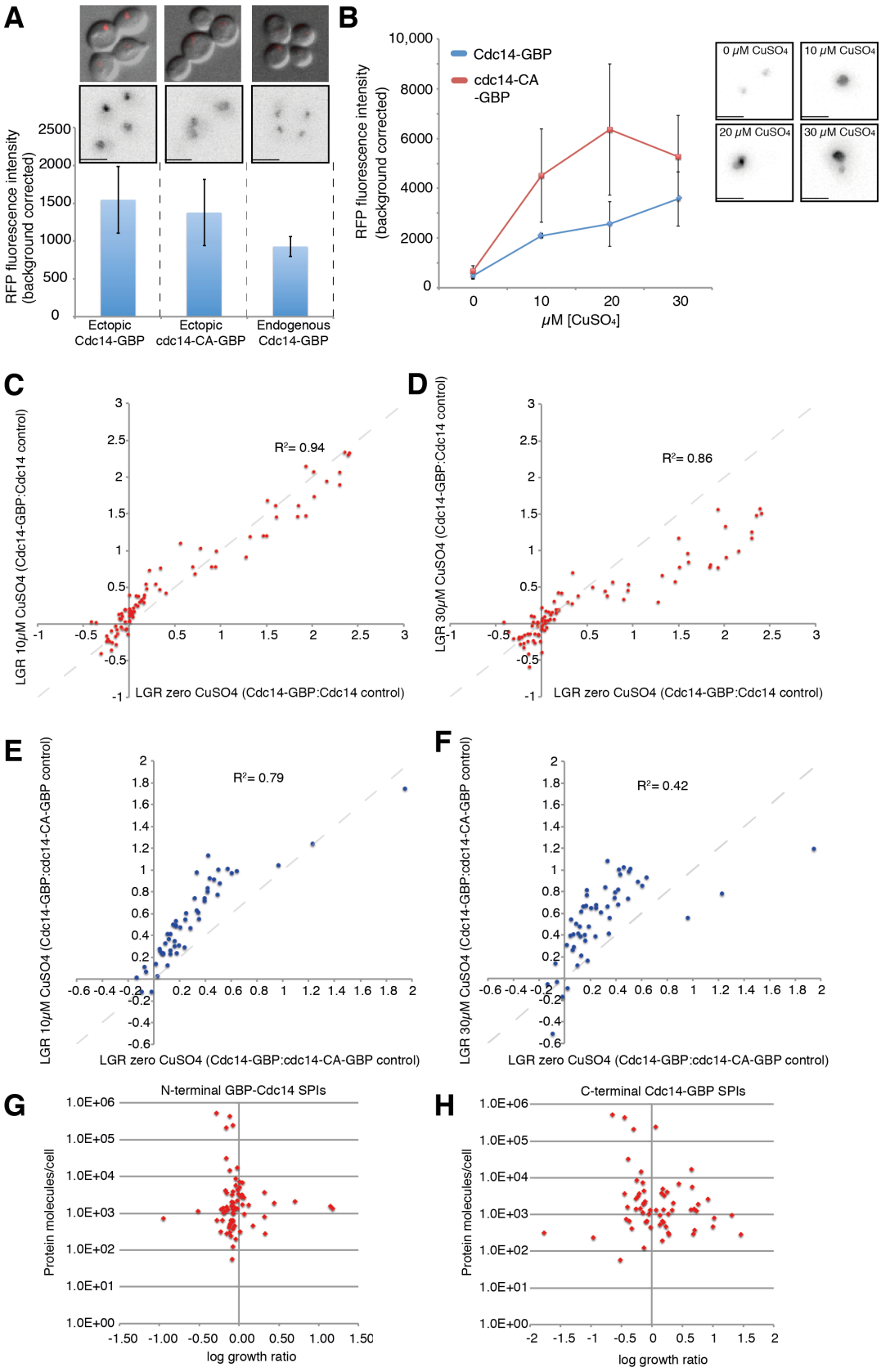

Figure 3.11 Stoichiometry analysis of Cdc14 SPIs

A) RFP fluorescence intensity of endogenously encoded Cdc14-GBP was compared with plasmid-encoded wild-type and mutant Cdc14-GBP without copper ($CuSO_4$) addition. Ectopically expressed Cdc14-GBP (both wild-type and mutant) has ~1.5× higher RFP signal than endogenously expressed Cdc14-GBP; error bars indicate SD of fluorescence intensity. (Scale bars, 5 μm.)
B) Fluorescence intensity of Cdc14-GBP and cdc14-CA-GBP with addition of $CuSO_4$ to drive the expression from the plasmid. The RFP signal increases with higher concentration of copper in both wild-type and mutant strains; error bars indicate SD. (Inset) Examples of wild-type Cdc14-GBP at different concentrations of copper; beyond 30 μM copper overexpression of CDC14 becomes toxic to cells. I note that wild-type Cdc14-GBP levels are lower than mutant, perhaps indicating partial toxicity of overexpression of *CDC14*. (Scale bars, 5 μm.)
C-D) Comparing Cdc14-GBP with Cdc14 control gave equivalent results on the different $CuSO_4$ concentrations (0 μM and 10 μM or 30 μM $CuSO_4$ each correlate well).
E-F) Comparing Cdc14-GBP with the mutant cdc14-CA-GBP control with both 0 μM and 10 μM $CuSO_4$ correlates well, whereas 0 μM and 30 μM CuSO4 correlates to a lesser extent. The weaker correlation of 0 μM with 30 μM may be because of partial toxicity of this level of overexpression of *CDC14.* I note that the strength of the SPI phenotype is slightly increased with increased concentration of copper.
G-H) The strength of the Cdc14 SPI growth phenotype does not correlate with the amount of protein molecules per cell for the GFP- tagged proteins.

Furthermore, I asked if the growth defect caused by the forced Cdc14 kinetochore association was a result of spindle assembly checkpoint (SAC) activation, since the Cdc14-GFP strain expressing Mtw1-GBP has a high proportion of large-budded cells (Figure 3.7 B). I deleted *MAD3*, a critical downstream component of the SAC, in 22 GFP kinetochore strains and repeated the SPI assay with both wild-type and *mad3*Δ GFP strains. I predicted that if some of the Cdc14-kinetochore associations activate the checkpoint then *mad3*Δ would suppress those SPIs. However, the Cdc14 SPIs were not suppressed by *mad3*Δ, suggesting that the SAC is not necessary for the Cdc14-kinetochore SPI phenotype (Figure 3.12 A&B). Conversely, some of the Cdc14 SPIs produced even a stronger growth defect when *MAD3* was deleted (for example, Ame1, Cep3 and Nsl1), indicating that these SPIs might disrupt kinetochore function which is supressed by the SAC in wild-type cells. Next, I repeated the Cdc14 SPI screen with and without the microtubule poison benomyl, but this had no significant effect upon the SPI data (data not shown). Finally, I wanted to examine the large-budded phenotype more closely and assess if this was due to the phosphatase activity of Cdc14. I labelled chromosome V at the *URA3* locus using the TetO/TetR-RFP system in a Mtw1-YFP strain (GBP binds YFP equivalently to GFP) containing either the wild-type Cdc14-GBP and cdc14-pd-GBP (both without RFP) and quantified large-budded cells and compared cells that had segregated chromosomes in the two strains (see section 2.5.4 for details). However, there was no significant difference of metaphase-arrested cells

between expressing wild-type Cdc14-GBP and cdc14-pd-GBP (Figure 3.12 C). These data suggest that the Cdc14-kinetochore SPI phenotype is not a direct consequence of SAC activation, nor do they result in SAC deficiency.

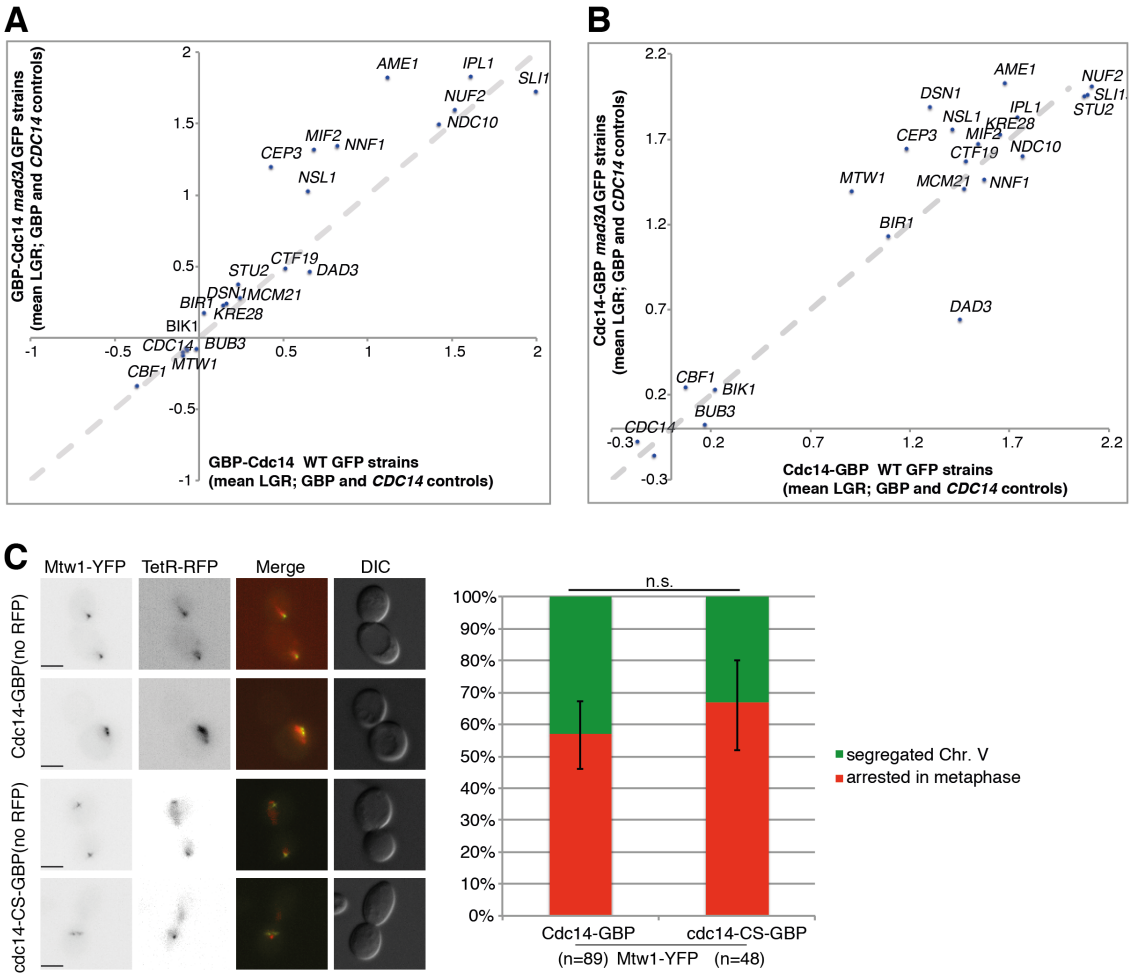

Figure 3.12 The SAC is not involved in the Cdc14-kinetochore SPI phenotype

A-B) The four plasmid constructs (GBP-Cdc14, Cdc14-GBP, Cdc14, and GBP) were introduced into 21 GFP-tagged strains detected as SPIs (including controls) with GBP-Cdc14 or Cdc14-GBP as before, but now in both wild-type and *mad3Δ* strains, and arrayed with 16 replicates. The average of the Cdc14 and GBP controls versus the GBP-Cdc14 (A) or Cdc14-GBP (B). The mean LGRs were calculated and plotted on a scatter-graph (wild-type on x axis and *mad3Δ* on y axis). Deletion of *MAD3* does not suppress any GBP-Cdc14 SPIs. However, several GBP-Cdc14 SPIs are stronger in *mad3Δ* strains (Cep3, Mif2, Nsl1, Nnf1, and Ame1) (A). Only one SPI with Cdc14-GBP, Dad3, is suppressed (B); however, the colony sizes of this comparison are very small and consequently their ratios are subject to larger errors. Several Cdc14-GBP SPIs increase the growth phenotype when *MAD3* is deleted (Mtw1, Cep3, Dsn1, Nsl1, and Ame1). The dotted diagonal line indicates the position expected if the LGRs are the same in both wild-type and *mad3Δ* strains; points below this line would be suppressed by the *mad3Δ* allele.
C) Examples of large-budded cells of a strain encoding a marked chromosome V locus (*ura3-1::3xURA3-tetOx112 TETR-RFP*) containing Mtw1-YFP and either Cdc14-GBP or cdc14-CS-GBP plasmids are shown both with separated chromosomes or

unsegregated chromosomes. Note that the GBP alleles in this case are not RFP-tagged and that GBP binds to YFP equivalently to GFP. The proportion of large-budded cells, arrested specifically in metaphase with unsegregated chromosomes, is quantified and does not differ in cells expressing Cdc14-GBP compared with cells expressing cdc14-pd-GBP. Error bars are 95% binomial confidence intervals. n.s., not statistically significant p-value > 0.05. (Scale bars, 5 μm).

3.2.5 Do Cdc14 SPIs misregulate the kinetochore?

The MIND complex stood out as the kinetochore subcomplex with the most and consistent SPIs with Cdc14 (Figure 3.10). I therefore investigated the Cdc14 SPIs with Mtw1, Nnf1, Nsl1 and Dsn1 in more detail. Dsn1 is the only MIND complex subunit that has known CDK phosphosites (Ubersax *et al.*, 2003; Holt *et al.*, 2009), and importantly a conserved phosphoserine on Dsn1 (S264) has been shown to be dephosphorylated in a Cdc14-dependent manner in metaphase prior to its bulk release by FEAR and MEN, implying there is a pool of active Cdc14 outside the nucleolus before anaphase (Akiyoshi & Biggins, 2010). However, when serine 264 is mutated to alanine cells are viable. Therefore, to ask whether Dsn1 was being constitutively dephosphorylated by the forced Cdc14 association with the MIND complex, I examined the phospho-status of Dsn1-3xHA using Western blot analysis (see section 2.6.2 for details). I found that phosphorylation of Dsn1 is reduced when Cdc14-GBP was expressed in Nnf1-GFP cells in contrast to expression of cdc14-pd-GBP (Figure 3.13 A). This implies that by forcing Cdc14 to one component of a subcomplex via the GBP-GFP interaction it can dephosphorylate another subunit of the same complex or even possibly surrounding substrates.

However, since dephosphorylation of the CDK phosphosite at Dsn1 does not inhibit growth, I cannot link the Cdc14 SPI phenotype with this particular dephosphorylation event. Dsn1 is phosphorylated by Aurora B/Ipl1 kinase, but the function of this modification is unclear. It has been suggested that Aurora B-dependent Dsn1 phosphorylation facilitates kinetochore assembly (Emanuele *et al.*, 2008; Yang *et al.*, 2008*b*; Dimitrova *et al.*, 2016), but it has also been argued that Dsn1 phosphorylation by Aurora B is involved in regulation of microtubule-kinetochore attachment (Welburn *et al.*, 2010). More recently, it was also shown that Ipl1-dependent phosphorylation of Dsn1, on serines 240 and 250, is required for its stabilisation and protection from Mub1-Ubr2-dependent degradation (Akiyoshi *et al.*, 2013*a*). Moreover, Dsn1 phosphorylation by Ipl1 is required for interactions of the inner kinetochore with the outer kinetochore and the dsn1-S240A-S250A mutant appears to be inviable.

Substitution of the CDK site S264 to alanine rescued the lethality caused by dsn1-S240-250A mutations (Akiyoshi *et al.*, 2013*a*). Taken together these data suggest that Cdc14-dependent dephosphorylation of Dsn1 can overwrite and protect Dsn1 that has previously been dephosphorylated at the Ipl1 phosphoserines (S240 and S250), presumably by another phosphatase such as PP1/Glc7, and thus marked for ubiquitin-mediated destruction by the proteasome. The timing of this seems logical since the Cdc14-dependent dephosphorylation of Dsn1 occurs during metaphase when it is crucial to stabilise the outer kinetochore and microtubule attachment in order to proceed into anaphase and promote faithful chromosome segregation.

Because, the prevention of Dsn1 serine 264 phosphorylation does not affect growth, I asked whether constitutive Cdc14 phosphatase activity at the MIND complex was able to dephosphorylate the other serines at 240 and 250, and thus promote Dsn1 ubiquitylation-dependent degradation by Mub1-Ubr2. I therefore, deleted the non-essential *UBR2* (which is sufficient to block Mub1-Ubr2 activity) in kinetochore-GFP strains (Nnf1, Nsl1 and Nuf2) and introduced the GBP-Cdc14 and control plasmids, and in addition I deleted *UBR2* in a Cdc14-GFP strain and introduced plasmids encoding Mtw1-GBP, Nuf2-GBP, Mif2-GBP and Ctf19-GBP and controls, and found that none of these SPIs were suppressed by deleting *UBR2* (Figure 3.13 B-D).

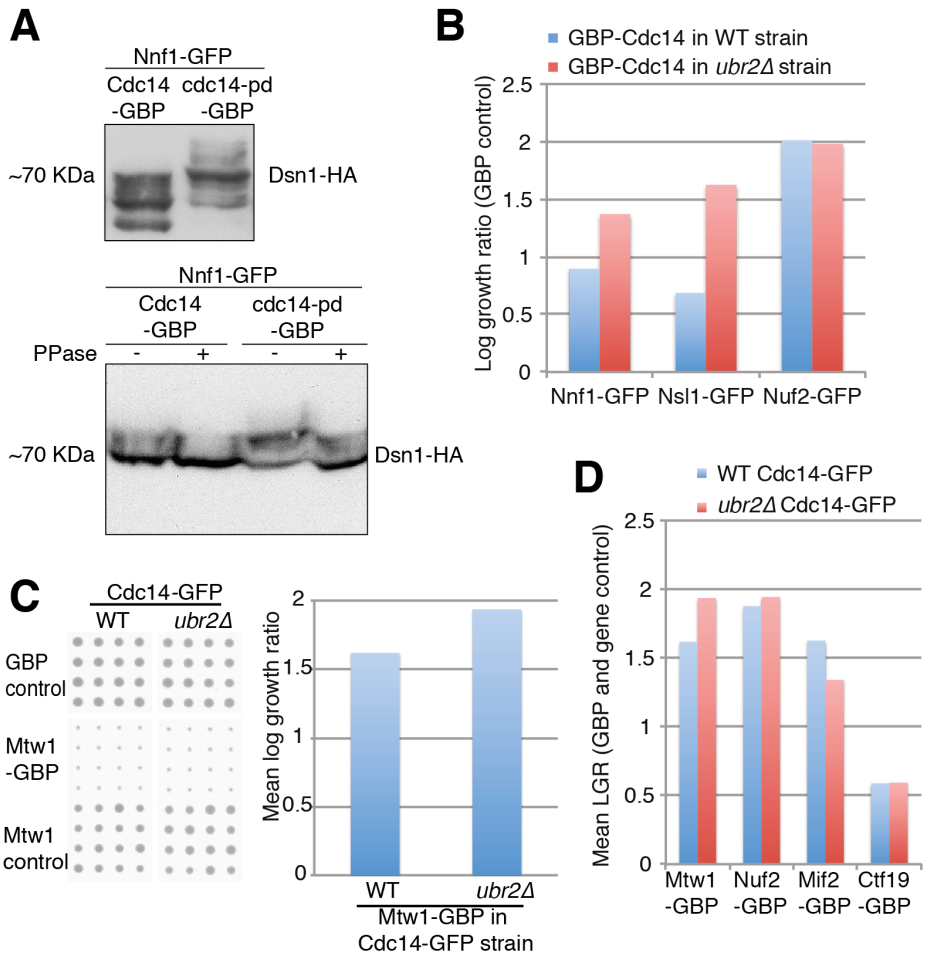

Figure 3.13 Cdc14-MIND complex SPI sufficiently dephosphorylates Dsn1, but it is independent of the growth phenotype

A) I extracted proteins from Nnf1-GFP cells encoding Dsn1-3xHA, which also contained either a wild-type Cdc14-GBP or cdc14-pd-GBP plasmid. I separated the proteins using SDS-PAGE gels containing Phos-Tag reagent to specifically separate phosphorylated proteins, and the resulting blot shows the effect of recruiting wild-type Cdc14 versus phosphatase-dead mutant (top). Protein extracts from the same strains with or without Lambda phosphatase treatment where also compared (bottom). I found significant protein degradation caused by the incubation at 30 °C, which is part of the phosphatase treatment. However, it is clear that the higher band, which is largely absent when wild-type Cdc14 is recruited, is depleted by phosphatase treatment.
B) Deletion of *UBR2* does not supress growth inhibition caused by expression of Cdc14-GBP in cells containing GFP-tagged Nnf1, Nsl1, and Nuf2.
C) Three plasmid constructs (Mtw1-GBP, Mtw1, and GBP) were introduced into wild-type and *ubr2Δ* strains containing Cdc14-GFP and arrayed with 16 replicates. The average of the Mtw1 and GBP controls versus the Mtw1-GBP experiment (mean LGR) were compared and show that the Cdc14-GFP *ubr2Δ* strain is also inhibited by Mtw1-GBP.
D) I also created additional plasmids encoding kinetochore-GBP fusions, including Nuf2-GBP and Ctf19-GBP (both of which were Cdc14 SPIs) and Mif2-GBP. None of these are suppressed by the *ubr2Δ* mutation.

Next, I decided to test whether Dsn1 degradation explained the SPI phenotype in another way, by designing and introducing additional plasmids containing phospho-mimetic mutants of Dsn1, into the GBP-Cdc14-containing GFP strains. I predicted that if the Cdc14-MIND complex SPI phenotype was a consequence of premature dephosphorylation of Dsn1 then expression of phospho-mimetic mutant Dsn1 should suppress the growth defect. I made a plasmid with the two serines 240 and 250 substituted to aspartic acids (dsn1-S240-250D), expression of which would create a pool of stabilised Dsn1 that cannot be degraded in a Ubr2-dependent manner (Akiyoshi *et al.*, 2013*b*). I then repeated the Cdc14 SPI assay with the GFP-kinetochore strains as before, but now also containing the Dsn1 mutant plasmid in addition to the GBP-Cdc14 fusion or control plasmids. However, the addition of stabilised Dsn1 (dsn1-S240-250D) was not sufficient to suppress the Cdc14 SPI phenotype with MIND complex subunits (Figure 3.14 and Table 3.3). Furthermore, I also performed the same experiment with other Dsn1 phospho-mimetic mutants, first with the conserved CDK site changed to aspartic acid (S264D), second with a mutant of two additional CDK sites (S69,170,264D), and third with all of these serines changed to aspartic acid (S69,170,240,250,264D). In no case did the mutations of *DSN1* suppress the SPI phenotype of recruiting Cdc14 to the MIND complex (Figure 3.14 and Table 3.3). Hence, I conclude that the SPI growth phenotype of forcing Cdc14 to the MIND complex is not likely caused by dephosphorylation of the CDK and Ipl1 phosphoserines within Dsn1. However, further experiments are required to confirm these results.

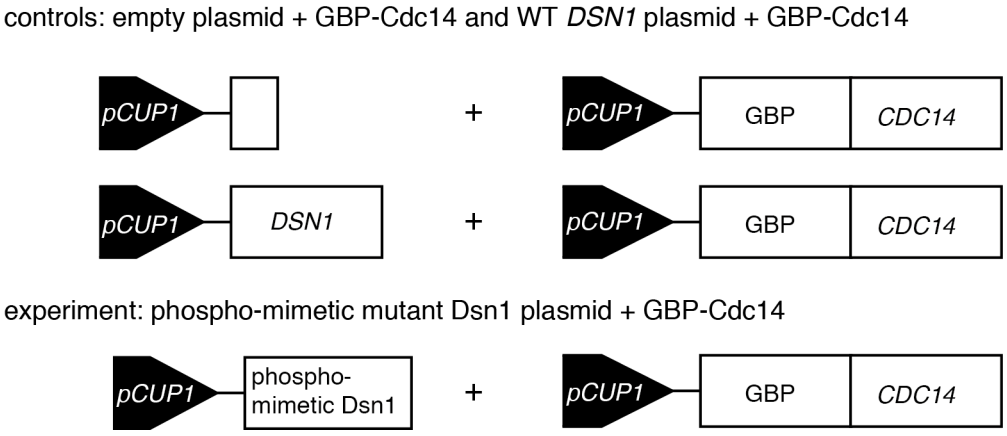

Figure 3.14 Plasmid constructs used in the Dsn1 phospho-mimetic suppression SPI screen

The GBP-Cdc14 plasmid construct was introduced into the GFP-tagged kinetochore strains as before, but now including a second plasmid construct encoding a phospho-mimetic mutant of Dsn1. Four mutants were generated: Serine 264 to aspartic acid

(dsn1-S264D), serines 240 and 250 to aspartic acid (dsn1-S240-250D), serines 69, 170, and 264 to aspartic acid (dsn1- S69D-S170D-S264D), and finally all five serines to aspartic acids (dsn1-5D). As controls, the GBP-Cdc14 construct was used along with either an empty construct or a wild-type Dsn1 construct.

Table 3.3 Phospho-mimetic Dsn1 mutants do not suppress the kinetochore-Cdc14 SPI phenotype.

		Mean log growth ratio (2 controls)			
gene name	systematic name	*dsn1-S264D*	*dsn1-S240-250D*	*dsn1-3D (S69D-S170D-S264D)*	*dsn1-5D*
NDC80	YIL144W	1.46	1.07	1.07	1.15
BIR1	YJR089W	0.71	0.73	0.48	0.96
NSL1	YPL233W	0.56	0.63	0.51	0.84
MTW1	YAL034W-A	0.37	0.61	0.43	0.81
SPC105	YGL093W	0.31	0.63	0.10	0.78
CDC20	YGL116W	0.74	0.81	0.55	0.78
KRE28	YDR532C	0.70	0.64	0.58	0.71
NNF1	YJR112W	0.65	0.66	0.53	0.67
HHT2	YNL031C	0.23	0.54	0.26	0.65
SPC25	YER018C	0.29	0.45	0.42	0.59
BIM1	YER016W	0.29	0.44	0.41	0.54
SPC97	YHR172W	0.39	0.34	0.23	0.53
TPD3	YAL016W	0.39	0.38	0.40	0.52
HTA1	YDR225W	0.07	0.47	0.48	0.43
SPC34	YKR037C	-0.09	0.46	0.50	0.42
KAR3	YPR141C	0.28	0.21	0.23	0.41
BUB3	YOR026W	0.17	0.35	0.26	0.41
DAD1	YDR016C	-0.04	0.24	0.21	0.40
STU2	YLR045C	0.47	0.17	0.38	0.34
DAD2	YKR083C	-0.08	0.25	0.15	0.34
KIP3	YGL216W	0.36	0.16	0.35	0.32
BUB1	YGR188C	0.25	0.48	0.14	0.32
SPC24	YMR117C	0.17	0.49	0.14	0.27
CTF19	YPL018W	-0.24	0.08	0.33	0.11
ULP2	YIL031W	0.04	-0.05	-0.12	0.04
MIF2	YKL089W	0.04	0.11	-0.18	-0.01
STU1	YBL034C	-0.08	-0.14	-0.07	-0.05
HHF1	YBR009C	-0.09	0.04	0.19	-0.06
DSN1	YIR010W	-0.02	0.00	-0.09	-0.08
SLK19	YOR195W	-0.14	-0.06	-0.19	-0.15
NUP170	YBL079W	-0.03	-0.09	0.01	-0.16
NUP157	YER105C	-0.09	-0.10	-0.01	-0.19
HHT1	YBR010W	-0.06	-0.05	-0.11	-0.22

+ve LGR (growth reduced compared to controls)
-ve LGR (growth enhanced compared to controls)
no growth difference

A selection of average LGRs of the two controls with each Dsn1 mutant plus GBP-Cdc14 are shown in the table. Positive LGRs correspond to an increased growth defect (yellow cells) and negative LGRs correspond to a suppressed growth defect (blue cells). Members of the MIND complex are highlighted in bold.

Finally, I wanted to examine if the kinetochore-associated protein and Cdc14 substrate, Fin1, had a role in producing the Cdc14-kinetchore SPI phenotype. Fin1 is phosphorylated by CDK (Ubersax *et al.*, 2003; Loog & Morgan, 2005), accumulates during S-phase, then localises to the nucleus at metaphase. In anaphase Fin1 becomes dephosphorylated by Cdc14, which results in its relocalisation to the spindle (Woodbury & Morgan, 2007). Expression of a phospho-deficient Fin1 mutant results in premature spindle recruitment, chromosomal instability and lethality (Woodbury & Morgan, 2007). Thus it has been suggested that Fin1 joins Sli15 (CPC) and Stu1 as spindle-stabilising components whose Cdc14-mediated dephosphorylation is required for their relocalisation to the anaphase spindle (Pereira & Schiebel, 2003; Higuchi & Uhlmann, 2005; Woodbury & Morgan, 2007). It was later discovered that Fin1 operates as a regulatory subunit of PP1/Glc7, and the Fin1 phospho-deficient mutant phenotype was caused by premature PP1/Glc1 recruitment to the kinetochore and spindle, thus prematurely silencing the checkpoint (Akiyoshi *et al.*, 2009). Fin1 interacts with many components of the outer kinetochore including Dsn1 (Akiyoshi *et al.*, 2009), and *fin1*Δ cells are viable. I therefore, asked whether the SPI growth phenotype caused by forced recruitment of Cdc14 to the MIND complex was due to misregulation of Fin1, and thus deleting *FIN1* might suppress the SPI phenotype. However, the *fin1*Δ kinetochore-GFP strains tested (Mtw1, Nnf1, Nuf2, Dad2, Ctf19 and Cep3) were equally effected by the expression of GBP-Cdc14 and Cdc14-GBP as wild-type GFP strains (Figure 3.15 A&B). It remains a possibility that another Cdc14 SPI, which was not tested, could be suppressed by *fin1*Δ, if that association placed Cdc14-GBP at the optimal location within the kinetochore to dephosphorylate Fin1. However, based on these data the Cdc14-kinetochore SPI growth phenotype is not a consequence of Fin1 misregulation.

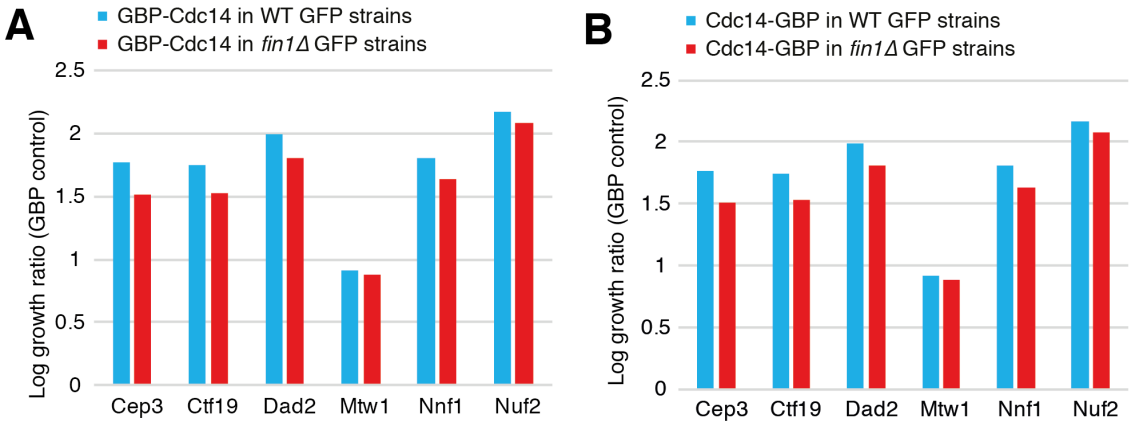

Figure 3.15 The kinetochore-Cdc14 SPI phenotype is not a consequence of Fin1 misregulation

A-B) I repeated the SPI analysis of six Cdc14 SPIs in both wild-type and *fin1*Δ strains. I expressed the GBP-Cdc14 and GBP-cdc14-pd-GBP control (A), and Cdc14-GBP and cdc14-pd-GBP control (B), but found no or negligible suppression by deleting *FIN1*.

While I cannot determine what the direct target of the forced Cdc14-kinatochore association is producing the SPI growth phenotype, together these results highlight the importance of CDK phosphorylation for kinetochore function and warrant a further investigation of the role of Cdc14 phosphatase at the kinetochore.

3.2.6 Extended studies to identify kinetochore regulators using a candidate SPI approach

In addition to the Mtw1 proteome-wide SPI screen and as part of another project in the lab we have performed two additional kinetochore proteome-wide SPI screens with a component of the NDC80 complex, Nuf2, and a DAM1/DASH complex subunit, Dad2 (Berry *et al.*, 2016). To extend my studies towards identifying candidates of kinetochore regulation, I assembled a collection of 439 GFP strains from the complete GFP library that include strains that produced SPIs in the Mtw1, Nuf2 and Dad2 SPI screens and additional proteins involved in kinetochore function and proteins that regulate post-translational modification, such as kinases and phosphatases. I next used the SPI system to associate each of these 439 proteins with 8 additional kinetochore proteins. These proteins were Skp1, Cbf1, Ctf3, Chl4, Ctf19, Mif2, Kre28 and Cnn1 at the inner and central kinetochore. I also retested the three kinetochore proteins previously assayed, the KMN network and outer kinetochore components Mtw1, Nuf2 and Dad2. These proteins were all tagged with GBP at the C termini, except Cbf1 which I tagged

at the N terminus and Cnn1, an elongated protein, which I tagged both at the C and N termini. All of these GBP-fusions were compared with the GBP and gene controls as before. The rationale behind this approach is to generate a higher quality map of kinetochore SPIs which could highlight potential candidates for further studies. I confirmed that in most cases the GBP-tagged kinetochore protein is sufficient to recruit a specific GFP-tagged protein to the kinetochore (Figure 3.16). Although, I cannot rule out that some growth defects may result from interactions away from the kinetochore. As previously, to minimise such effects of perturbing the GFP-tagged proteins I performed the SPI screen in both haploid cells (which contain a single allele of each GFP-tagged gene) and in heterozygous diploid cells (where the GFP allele is complemented with an untagged allele).

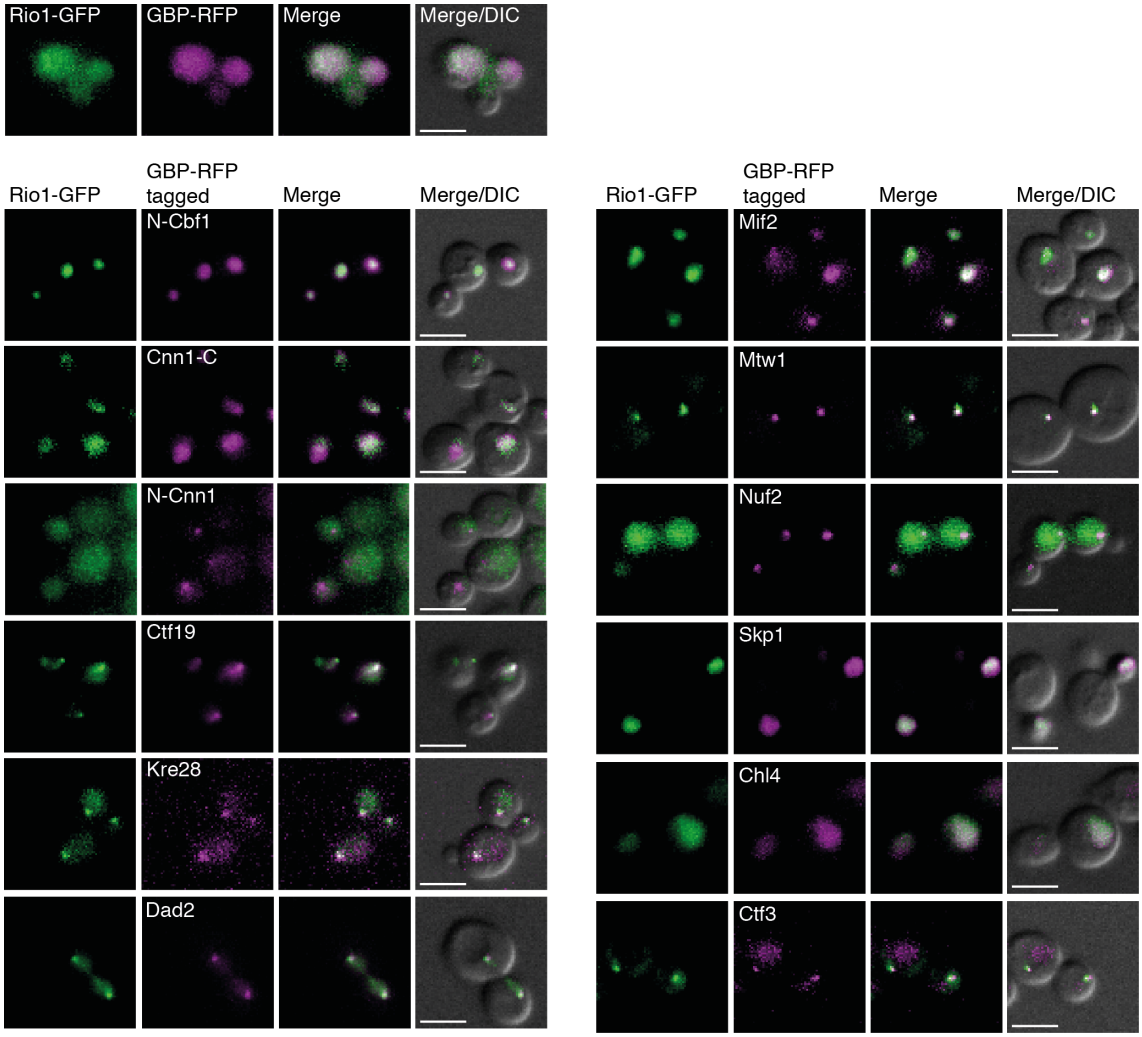

Figure 3.16 GBP-tagged kinetochore proteins can recruit GFP-tagged kinase to the kinetochore

A fluorescence microscopy imaging of a Rio1-GFP strain containing all the different kinetochore-GBP fusion plasmids. Rio1 is a kinase that localises diffusely throughout the cell. In most cases the Rio1-GFP signal colocalised with the kinetochore-GBP-RFP foci. I note that there are several exceptions, for example the Skp1-GBP-RFP and Chl1-GBP-RFP did not form kinetochore foci however they do colocalise with Rio1-GFP. Another exception is Nuf2-GBP-RFP, which did form kinetochore foci but the Rio1-GFP signal was still diffusely localised. All scale bars are 5μm.

When the resulting SPI data (over 10,000 binary interactions) are compared using a cluster analysis laid out in a heatmap of interactions (Figure 3.17) several groups of GFP proteins are seen to produce common growth defects or SPIs when associated with different kinetochore components, in other words, the analysis clusters together GFP strains that have a similar SPI profile across the different GBP-tagged kinetochore proteins. The first cluster group (blue box) is specific to haploids and are enriched for essential proteins; similarly as described previously (Berry *et al.*, 2016), the phenotype in these strains can be ascribed to compromising an essential protein by forcing association or mislocalisation. The second cluster group (red box) includes kinases such as casein kinase 2 (Cka1, Cka2 and Ckb1) and CDK/Cdc28, and PP2A phosphatase subunits (Tpd3 and Rts1), and components of the budding yeast 14-3-3 complex (Bmh1 and Bmh2). The third group (purple box) includes the mitotic phosphatase Cdc14, the Polo-like kinase Cdc5, and Mck1 kinase, together with multiple members of the cohesin and condensin complexes (Mcd1, Irr1, and Brn1 Ycg1, Smc4, respectively) and associated protein Pds5.

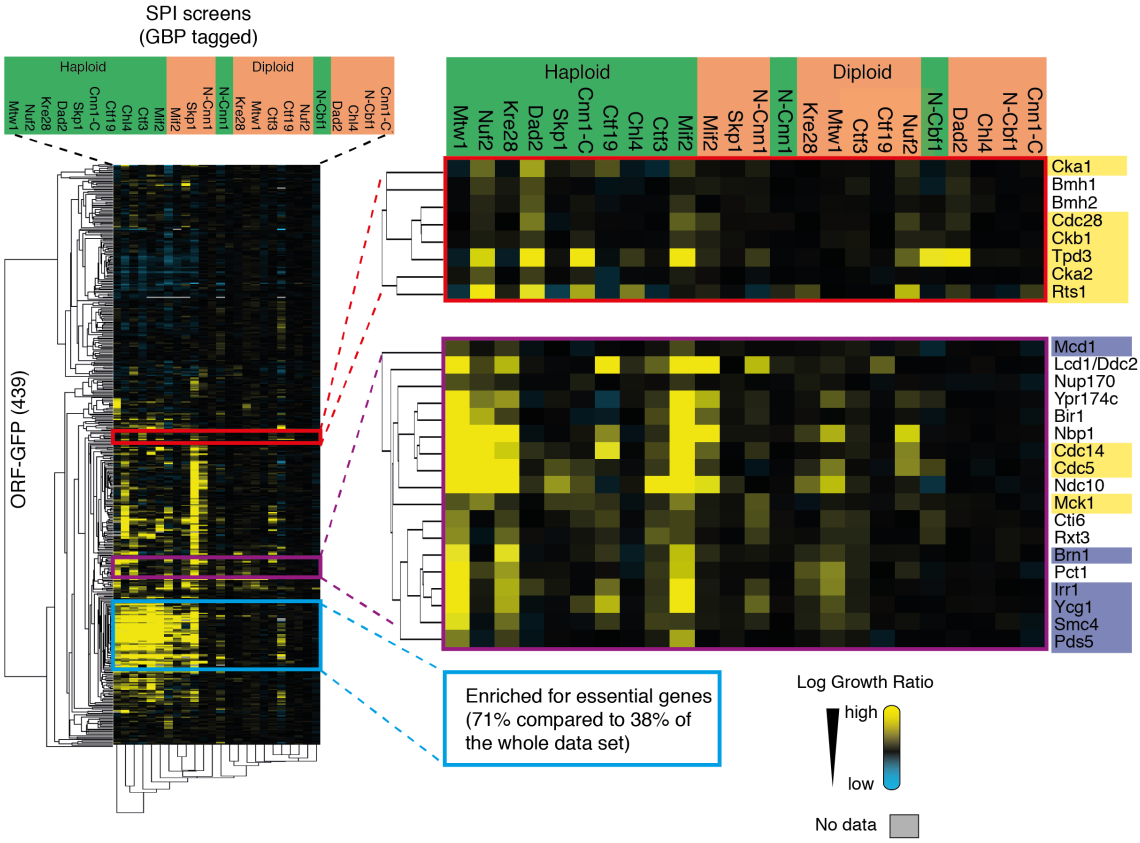

Figure 3.17 Cluster analysis of kinetochore SPIs

The haploid and diploid SPI data from the 12 kinetochore-GBP screens were analysed using Cluster 2.0 software and visualised the results using Java TreeView 1.1.6. The strength of the growth inhibition (log growth ratio) is shown using a yellow-blue colour scale where yellow is a strong SPI, black indicates no effect, and blue indicates growth enhancement. The clustering analysis distinctly clusters together the haploid SPI screens to the left (indicated in green) of the heatmap and diploid screens to the right (indicated in orange), with the exception of GBP-Cnn1 and GBP-Cbf1 screens. Furthermore, the cluster analysis clusters together GFP strains that are similarly affected by the GBP-tagged kinetochore proteins. For example, the cluster group in blue consists mostly of strains with essential GFP-tagged genes. The red cluster group consists of many proteins involved in phosphor-regulation (highlighted in yellow) and finally the purple group consists of many condensin/cohesin subunits (highlighted in violet) in addition to Cdc14 and Cdc5.

The most conservative cut-offs for SPIs in haploids (log growth ratio > 0.4) and diploids (log growth ratio > 0.2), produces a list of 123 GFP strains in total that were detected as SPIs with at least one of the 12 GBP-tagged kinetochore proteins (in both haploids and diploids). When I examined the mid- to outer kinetochore (Mtw1, Kre28, Nuf2 and Dad2) I found that these GBP-tagged kinetochore proteins produced a set of SPIs with 74 GFP strains and interestingly only few SPIs overlap between different GBP-tagged proteins (Figure 3.18). For example, Nbp1 perturbs growth when associated with Mtw1, Kre28 and Nuf2, and Ypr174c, a paralog of Nbp1, was detected as a SPI with Mtw1

and Nuf2. The Nuf2-GBP produced many SPIs that are specific to Nuf2, such as many kinases and two kinesin motor proteins, and similarly many histone deacetylase complex components and proteins involved in mitochondrial function are only found as SPIs with Mtw1-GBP. Intriguingly, Cdc14 phosphatase and Cdc5 Polo-like kinase, which clustered together, overlap with Mtw1 and Nuf2 SPIs and similarly CDK/Cdc28 and PP2A/Tpd3, which also clustered together, overlap with Dad2 and Nuf2 SPIs.

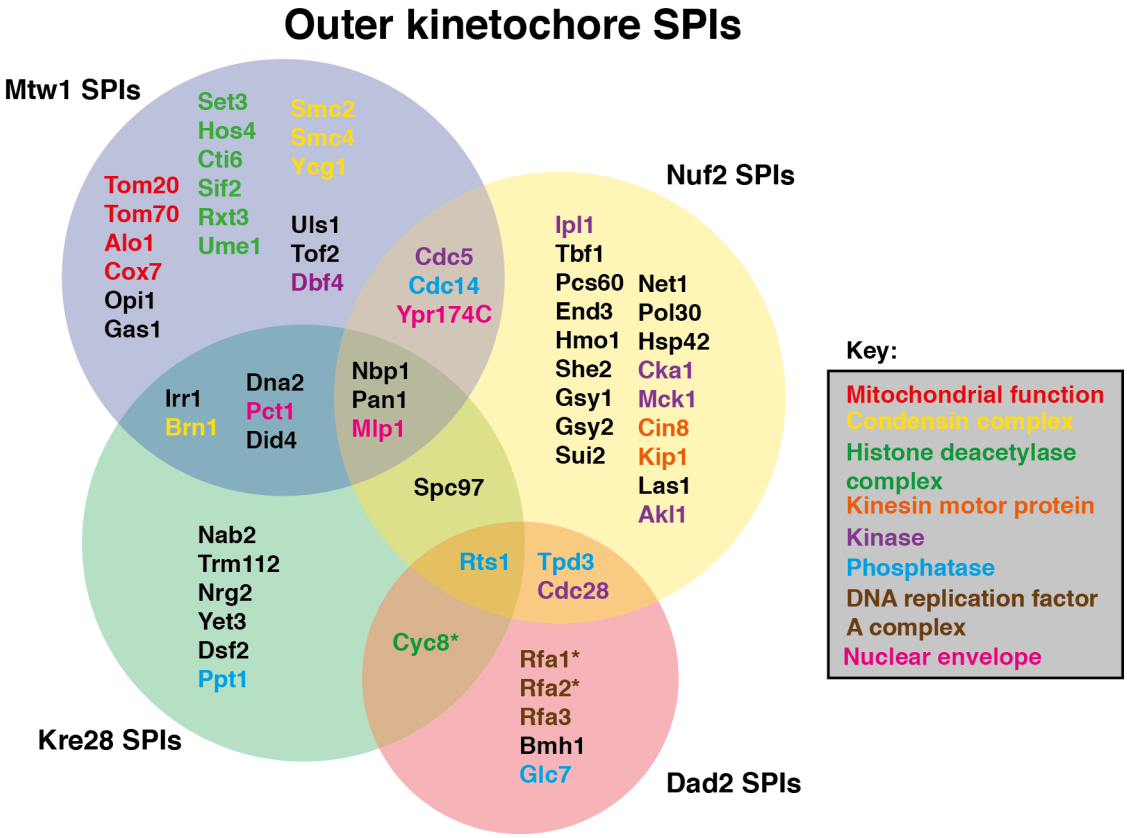

Figure 3.18 Overlap of outer kinetochore SPIs

A Venn diagram showing the conservative set of SPIs with GBP-tagged outer kinetochore components, Mtw1, Kre28, Nuf2 and Dad2. The whole outer kinetochore set contains 74 SPIs that were detected in both the haploid and diploid screens, but 12 structural kinetochore components are excluded from this diagram, since they are unlikely to be enzymatic kinetochore regulators. The forced kinetochore-kinetochore associations are explored in Figure 3.19. SPIs marked with asterix * (Cyc8, Rfa1 and Rfa2) were also SPIs with Mtw1. Some of these 74 SPIs were also detected in other kinetochore SPIs screens, but were not always repeated in heterozygous diploid GFP strains. For example, Uls1 was a haploid SPI with Mtw1, Ctf19, Ctf3, Mif2 and Cnn1, but a diploid SPI with Mtw1, Ctf3 and Mif2.

Finally, during the analysis of the extended set of 123 kinetochore SPIs, I noticed that many of them were kinetochore-GFP strains. I wanted to explore this in more detail and asked whether forced interactions between subunits within the same kinetochore

subcomplex were less likely to produce a SPI phenotype than between two subunits from different subcomplexes. I arranged the haploid SPI data from the 12 kinetochore-GBP screens and plotted them against the GFP kinetochore strains from the same subcomplexes as a heatmap (Figure 3.19 A). I found that forced interactions within the same subcomplex produced significantly fewer (4/36) and weaker (average log growth ratio of 0.13) SPIs than interactions between different subcomplexes, which produced more (111/393) and stronger (average log growth ratio of 0.36) SPIs (Figure 3.19 B&C). However, there are a few important exceptions, for example, the Nuf2-GBP association with Spc24-GFP and Spc25-GFP all within the NDC80 complex, give strong SPIs (log growth ratios of 2.4 and 1.8, respectively) and associations of Nuf2-GBP with itself, Nuf2-GFP and to Ndc80-GFP does not produce a SPI phenotype (log growth ratio of zero in both cases). It is known that Nuf2 and Ndc80 form a coiled-coil dimer and Spc24 and Spc25 dimerise as well (Wei *et al.*, 2006; Ciferri *et al.*, 2008; Valverde *et al.*, 2016). Most GBP tags and all the GFP tags are C-terminal and since the C termini of the Spc24-Spc25 dimer is important for NDC80 complex interaction with other subcomplexes, such as the MIND and SPC105 complexes, forced associations with it could interfere with these essential interactions; unless the forced associations are with MIND or SPC105 subunits. Indeed, when the interactions of both Spc24-GFP and Spc25-GFP are forced with Mtw1-GBP and Kre28-GBP (subunits of the MIND and SPC105 complexes, respectively) they do not produce a SPI phenotype. Furthermore, the N terminus of Cnn1 also interacts with the Spc24-Spc25 C termini (Malvezzi *et al.*, 2013) and in agreement, the SPI data shows that the N-terminal GBP-Cnn1 forced association with Spc24-GFP and Spc25-GFP does not produce a growth defect, and conversely forced associations of Spc24-GFP and Spc25-GFP with the C terminus of Cnn1, which binds to centromeric DNA, does generate a SPI phenotype. This suggests that there could be structural information gained from the SPI data as well as functional information.

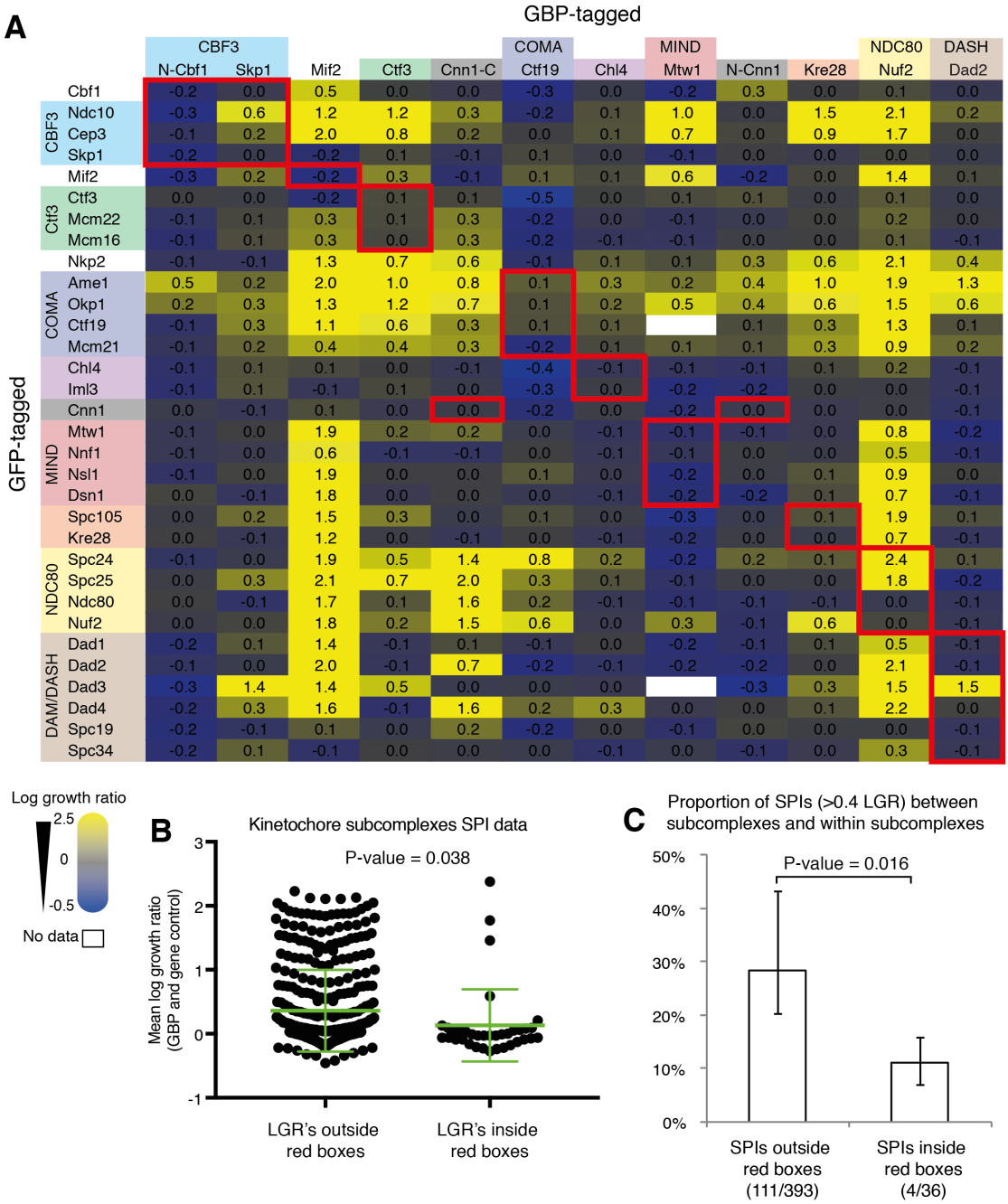

Figure 3.19 Forcing the associations of two kinetochore subunits

A) The extended haploid data of kinetochore SPIs is plotted as a heatmap of the mean log growth ratios (LGRs) using the GBP and gene controls. Yellow indicates a higher growth defect and grey/blue indicates no growth defect or enhancement compared to controls. Subunits of the same kinetochore subcomplex share the same colours on the x and y axis. Red boxes indicate the log growth ratios between subunits within the same subcomplex.
B) The LGRs of interactions (n = 36) within the same subcomplex (inside red boxes) are compared with LGRs of interactions (n = 393) between subunits of different subcomplexes (outside red boxes). All data points are indicated as black dots to show the spread of the data. The p-value was calculated using a two-tailed student's T-test.

The green horizontal lines indicate average LGR and error bars indicate SD of the mean.
C) The difference in proportion of SPIs (LGR > 0.4) between subunits of different subcomplexes (outside red boxes) and within the same subcomplex (inside red boxes) are compared. The p-value was calculated using Fisher's exact test and the error bars are 95% binomial confidence intervals.

3.3 Discussion

In this chapter, I described the proteome-wide SPI screen with the central kinetochore protein, Mtw1, where each member of the budding yeast proteome was individually associated with the kinetochore. Using the SPI methodology proved to be a valuable, novel approach to initially identify candidates of kinetochore regulation. The Mtw1 SPI screen, in addition to Nuf2 and Dad2 proteome-wide SPI screens, previously published (Berry *et al.*, 2016), identified a small subset of SPIs or forced interactions with the kinetochore that significantly affect growth. Among the Mtw1 SPIs are a number of proteins that associate with the inner kinetochore, including Rfa1, Brn1, Nmd5, and the polo-like kinase, Cdc5 (Ranjitkar *et al.*, 2010). In addition, I also detected Dbf4-dependent kinase (DDK), histone deacetylase complex components, and the SUMO-targeted ubiquitin ligase, Uls1. It is known that several kinetochore proteins are sumoylated (Montpetit *et al.*, 2006; Alonso *et al.*, 2012; Yong-Gonzales *et al.*, 2012; Ohkuni *et al.*, 2016). And intriguingly, it has been shown that STUbLs are involved in regulation of proteins at the kinetochore in budding yeast (Alonso *et al.*, 2012; Schweiggert *et al.*, 2016). Since kinetochore regulators are likely to be enzymes involved in post-translational modifications I focused on proteins such as kinases and phosphatases. Generally, phosphorylation plays an important role in kinetochore homeostasis and I found that one Mtw1 SPI was with Cdc14 phosphatase, which is activated at anaphase onset to reverse CDK activity. Among the targets of CDK are kinetochore proteins, however, the importance of these CDK phosphorylation/ dephosphorylation events is unclear. For example, Dsn1 is a member of the MIND complex, which is dephosphorylated before the bulk release of Cdc14 in anaphase (Akiyoshi & Biggins, 2010). However, *CDC14* conditional mutants only have a subtle defect in mitosis (D'Amours *et al.*, 2004). To map the effects of Cdc14 phosphatase activity, I used the SPI method to recruit both wild-type and inactive variants of Cdc14 to different kinetochore proteins. I found that a number of kinetochore complexes are sensitive to constitutive recruitment of the active phosphatase, including the MIND, the Cbf3, and the DAM1/DASH complexes, in addition the MAPs, Stu2 and Bik1. Although it is possible that the Mtw1-Cdc14 SPI phenotype is caused by partial relocation of

Mtw1 to another location (e.g., the nucleolus), this is unlikely for a number of reasons. First, the mutant Cdc14 binding causes equal kinetochore relocation as the wild-type (Figure 3.8), but does not give a SPI phenotype. Second, I did not identify other Cdc14-associated nucleolar proteins in the original Mtw1 SPI screen, despite screening most of the proteome. Third, not all kinetochore proteins produce a SPI phenotype with Cdc14. Fourth, the stoichiometry analysis did not support the notion of sequestration of low-abundance kinetochore proteins away from the kinetochore (Figure 3.11).

I showed that although phosphorylation of Dsn1 is inhibited by forced kinetochore recruitment of Cdc14, this dephosphorylation is unlikely to result in the Cdc14-Mtw1 SPI growth phenotype. Therefore, I speculate that either the Cdc14 forced kinetochore recruitment is removing other phosphates in neighbouring proteins; for example, CDK serine sites on Ask1 (Higuchi & Uhlmann, 2005), Cnn1 (Malvezzi *et al.*, 2013), Sli15 (Pereira & Schiebel, 2003), Bir1 (Widlund *et al.*, 2006), or even at non-CDK sites on other proteins. In any of these cases, the Cdc14 SPIs highlight the importance of phosphorylation of kinetochore proteins for mitosis and warrant further characterization of the role of phosphorylation in regulating kinetochore homeostasis. I explored the possibility of Fin1 being affected by the forced Cdc14 kinetochore localisation, but found that deletion of Fin1, a non-essential protein, did not suppress the Cdc14 SPIs (Figure 3.15).

Because Cdc14 normally functions as a dimer (Taylor *et al.*, 1997; Gray *et al.*, 2003; Kobayashi & Matsuura, 2017), the catalytically inactive mutants may be capable of recruiting the endogenous wild-type Cdc14 to the kinetochore in the mutant SPIs. This would produce false-negatives in the SPI screen; hence, it is possible that the kinetochore SPIs detected by the forced Cdc14 kinetochore recruitment is an under-representation of all of the critical CDK sites at the kinetochore.

Using a more extensive approach I identified a number of additional candidate kinetochore regulators, such as casein kinase 2 (CK2; Cka1/2 and Ckb1) and its opposing phosphatase Ppt1 (Cho *et al.*, 2014), and the Mck1 kinase (budding yeast GSK3). The highly conserved CK2 is involved in many processes such as cell-cycle regulation, transcription initiation, chromatin remodelling, Cse4 regulation (as described previously) and adaptation to the DNA damage checkpoint (Hanna *et al.*, 1995; Toczyski *et al.*, 1997; Ahmed *et al.*, 2002; Barz *et al.*, 2003; Tripodi *et al.*, 2013).

Importantly, CK2 has been shown to interact with Mif2 and phosphorylate both Mif2 and Ndc10 in vitro; and these events are suggested to antagonise Ipl1-dependent stabilisation of Mif2, but to control Ndc10 localisation synergistically along with Ipl1 kinase (Peng *et al.*, 2011). The Mck1 kinase has been reported to be involved in chromosome segregation (Shero & Hieter, 1991) and to also phosphorylate Ndc10 (Jiang *et al.*, 1995). In addition, Mck1 has been reported to control DNA replication by promoting Cdc6 degradation, and is implicated in a novel G1-phase checkpoint that is suggested to prevent DNA replication upon cell wall damage (Ikui *et al.*, 2012; Kono *et al.*, 2016). Moreover, overexpression of Mck1 rescued hydroxyurea (HU) lethality of cells with a mutation in *SPC24* (subunit of the NDC80 complex) (Ma *et al.*, 2007). Finally, using the data from the extended screening, I showed that the SPI data could be useful to probe the quaternary structure of multi-protein complexes such as the kinetochore (Figure 3.19). Similarly, we have showed, in another study, that the SPI data can provide information on quaternary structure of the nuclear pore, another large protein complex (Berry *et al.*, 2016).

The SPI screens described in this chapter failed to identify SAC components, a discrepancy from other reports, which will be explored in chapter 4. However, I did identify the phosphatases required for SAC silencing, PP1 (Glc7) and PP2A (Tpd3 and Rts1), which gave a SPI phenotype with Dad2 and Nuf2 (and Kre28) respectively (Figure 3.18). It has been reported that a forced recruitment of Glc7 to Spc105 did not prematurely silence the SAC, suggesting that PP1 is necessary but not sufficient for SAC silencing (Rosenberg *et al.*, 2011). Therefore, it would be interesting to explore the PP1 and PP2A kinetochore SPI phenotypes in more detail and examine if they are produced in a SAC silencing-independent manner.

Together, these results establish the SPI methodology as a useful tool to study protein-protein interactions and can complement other high-throughput screen data such as genetic and physical interactions. The investigation of the forced association of the CDK-counteracting phosphatase, Cdc14, to the kinetochore suggests that CDK phosphorylation of specific kinetochore subcomplexes is essential for normal mitotic progression in budding yeast. Moreover, using the SPI system in a proteome-wide manner has allowed me to both identify candidates of kinetochore regulation and later investigate their role in kinetochore function (for example Polo-like kinase, Cdc5, described in chapter 5).

Chapter 4. Results 2: Investigating the spindle assembly checkpoint using SPIs

4.1 Introduction

Defects during chromosome segregation can lead to aneuploidy – a situation where a cell inherits the abnormal number of chromosomes – which is a hallmark of cancer cells and specific birth defects such as Down syndrome. To help prevent this and ensure that all centromeres on every chromosome are correctly attached to the spindle in mitosis, the spindle assembly checkpoint (SAC) can block cells from progressing from metaphase to anaphase. When even a single kinetochore is unattached the SAC is activated to pause the cell in metaphase to allow time for recapturing microtubules. The SAC is also activated when kinetochores are incorrectly attached to the spindle and thus not under tension, for example, when microtubules from the same spindle pole are attached to each sister kinetochore (syntelic attachment) (Biggins & Murray, 2001; O'Connell *et al.*, 2008; Marston, 2014). When all kinetochores are correctly attached (bioriented) and under tension, the cell proceeds to anaphase and completes cell division (the SAC is described in detail in section 1.3.1. in the introduction).

Current understanding proposes that enrichment of checkpoint proteins at the kinetochore is necessary, and, in some cases, sufficient, for SAC activation. This proposal has been studied by artificially tethering individual checkpoint proteins to the kinetochore and associated proteins (Maldonado & Kapoor, 2011*a*; Ito *et al.*, 2012; Lau & Murray, 2012; Kuijt *et al.*, 2014; London & Biggins, 2014; Heinrich *et al.*, 2014; Kruse *et al.*, 2014; Ballister *et al.*, 2014; Aravamudhan *et al.*, 2015). Based on these findings, I was surprised not to have identified any GFP-tagged SAC components with the GBP-tagged kinetochore proteins in the kinetochore SPI screens described in chapter 3. The systematic recruitment of checkpoint proteins to each kinetochore protein has not been examined previously. It has also been suggested that the checkpoint can function separately from the kinetochore. Therefore, in this chapter I aim to study the SAC using the SPI methodology to both examine where a checkpoint component can act to activate the SAC, both in a kinetochore-dependent and -independent manner, and to map where at the kinetochore the checkpoint can be activated. Most of the data presented in this chapter has been published (Olafsson & Thorpe, 2016).

4.2 Results

4.2.1 Proteome-wide Mad2 SPI screen

It is thought that the SAC is primarily activated at the kinetochore, however there is evidence that it can be activated in a kinetochore-independent manner (Fraschini *et al.*, 2001; Poddar *et al.*, 2005; Kim & Burke, 2008; Rodriguez-Bravo *et al.*, 2014), and that SAC proteins can function in other cellular compartments (Iouk *et al.*, 2002; Wan *et al.*, 2014; Heasley *et al.*, 2017). Furthermore, it has been shown that the SAC can be activated through clustering of Aurora B independently of the kinetochore (Campbell & Desai, 2013).

Since it has been established that SAC activation occurs via sequential recruitment of SAC components to the kinetochore, I was surprised not to identify any SAC proteins in the kinetochore SPI screens described in chapter 3. To revaluate this result and to explore which non-kinetochore associations with a SAC protein could potentially arrest the cell cycle, I hypothesised that a proteome-wide SPI screen with the checkpoint protein Mad2 would identify novel targets for SAC activation and also confirm the known kinetochore targets. I created a plasmid encoding Mad2, a key SAC component, C-terminally fused to GBP (Mad2-GBP) and in addition to a control plasmid containing GBP alone, I created a plasmid expressing *MAD2* to control for its ectopic expression. Before performing the screen, I assessed the functionality of the Mad2-GBP fusion. I found that expression of the fusion protein could rescue benomyl sensitivity as effectively as expression of untagged *MAD2* in a *mad2*Δ non-GFP strain (Figure 4.1 A), suggesting it is able to activate the SAC. Since the GBP is tagged with RFP I used fluorescence microscopy to confirm that the Mad2-GBP colocalised with GFP-tagged proteins (Figure 4.1 B). Next, I transferred the Mad2-GBP and control plasmids into the whole GFP collection using the SPA method as before (see section 2.4.5 for details). The colonies on resulting agar plates with each GFP strain containing each of the three plasmids in quadruplicate were quantified and compared using the ScreenMill suite of software, as before (see section 2.4.6 for details). Since the readout of the SPI screens is cell growth and a constitutive SAC activation would block growth, the assay should be adequate to investigate forced protein-protein associations resulting in checkpoint activation in live cells. The colony sizes of GFP strains containing either of the two controls (GBP and Mad2 alone) were compared to colonies of strains expressing Mad2-GBP and gave similar results, hence I used the average growth score (z-score) (

Figure 4.2 A&B). I used the SPI method and retested the strongest 156 interactions with 16 replicates per strain (
Figure 4.2 C&E). Finally, I assessed the false discovery rate of this high-density retest (
Figure 4.2 F) and identified 37 GFP-tagged proteins that consistently produce a SPI phenotype with Mad2-GBP. A schematic of the Mad2 SPIs is shown in
Figure 4.2 D. Surprisingly, only few kinetochore components were identified as SPIs with Mad2, and they are either subunits of inner kinetochore subcomplexes or the chromosomal passenger complex (CPC). This result is consistent with the lack of SAC components detected in the kinetochore SPI screens described in chapter 3, but inconsistent with other studies using artificial tethering of SAC components to the KMN network at the kinetochore to activate SAC (for example: Maldonado & Kapoor, 2011*a*; London & Biggins, 2014; Aravamudhan *et al.*, 2015).

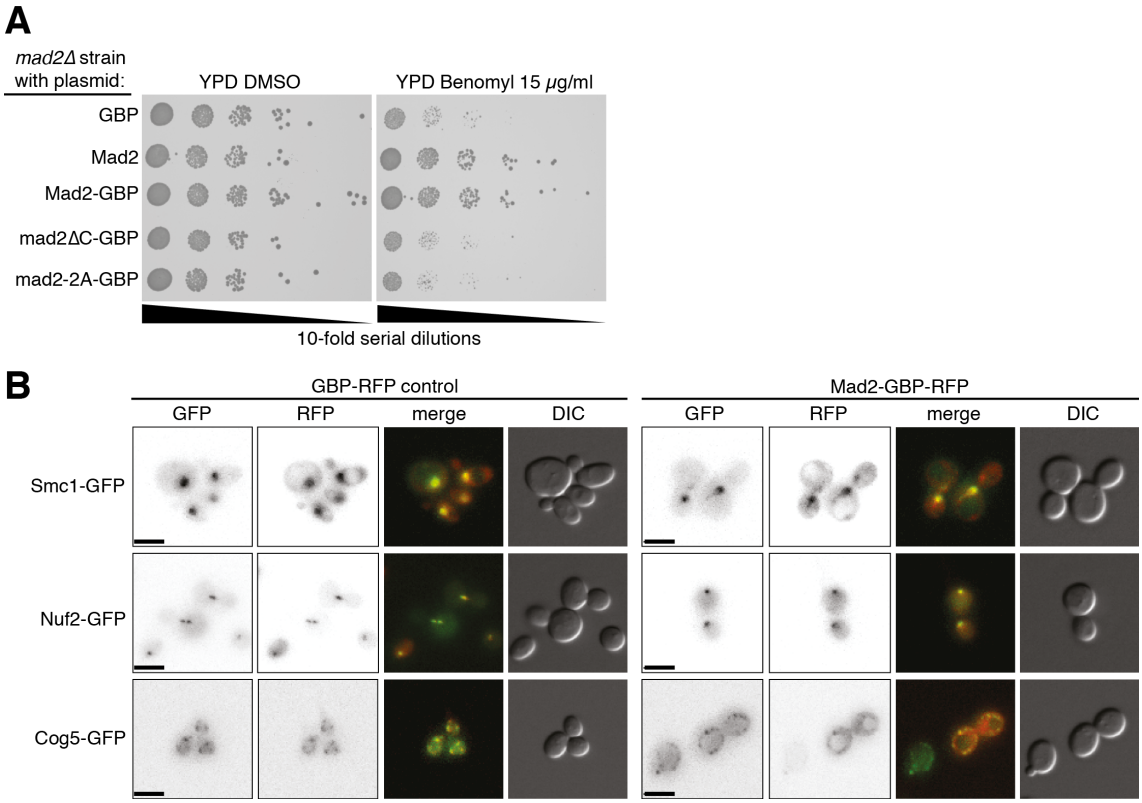

Figure 4.1 Mad2-GBP is functional and colocalises with GFP-tagged proteins

A) Serial dilutions of *mad2*Δ strain shows that cells with plasmids encoding Mad2 or Mad2-GBP rescue benomyl sensitivity of *mad2*Δ, but not plasmids encoding GBP, mad2ΔC-GBP or mad2-2A-GBP.
B) Fluorescence microscopy images of cells containing GFP-tagged cohesin (Smc1-GFP), kinetochore (Nuf2-GFP), and golgi complex (Cog5-GFP), expressing either GBP-RFP (left) or Mad2-GBP-RFP (right). All scale bars are 5μm.

Most of the 37 Mad2 SPIs are with nuclear proteins and many interact both genetically and physically with each other and with Mad2 and another SAC component Mad1 (Figure 4.2 G). For example, two Mad2 SPIs, Cdc20 and Nab2, are known to have direct physical and genetic interactions with Mad2 (Batisse *et al.*, 2009; Costanzo *et al.*, 2010; Barford, 2011). Additionally, three of the SPIs, Ame1, Cdc5 and Doa4 are encoded by genes with known genetic interactions with *MAD2* (Li *et al.*, 1997; Daniel *et al.*, 2006; Chiroli *et al.*, 2009). Gene ontology enrichment analysis (Eden *et al.*, 2009) of the Mad2 SPIs revealed that they are enriched for proteins that function in nuclear transport and the kinetochore (p-values 2×10^{-9} and 1×10^{-5}, respectively; Table 4.1). Phenotypic enrichment analysis (Thorpe *et al.*, 2012) of the Mad2 SPIs showed that mutants of genes that encode the SPIs are enriched for those affecting chromosomal instability (p-value 5×10^{-8}; Table 4.1). Therefore, the Mad2 proteome-wide SPI assay has identified proteins that specifically inhibit growth when forcibly associated with Mad2, are mostly involved in kinetochore function and chromosome segregation as well as proteins located at the nuclear periphery and are involved in nuclear transport. I note that many of the forced Mad2 interactions instead of inhibiting growth, seem to enhance growth compared to controls (negative z-scores at the lower right tail in Figure 4.2 B). I have not investigated these interactions further, however often when we have retested these positive interactions or “growth enhancing” interactions in other SPI screens they fail to replicate, suggesting they are often part of the noise and are frequently produced by comparison of small colonies of the GFP strains with the control plasmids. However, they warrant a further investigation and I note that the cohesin subunit Smc3 and the microtubule binding protein Stu1 are two of those proteins when associated with Mad2 enhanced growth relative to the controls.

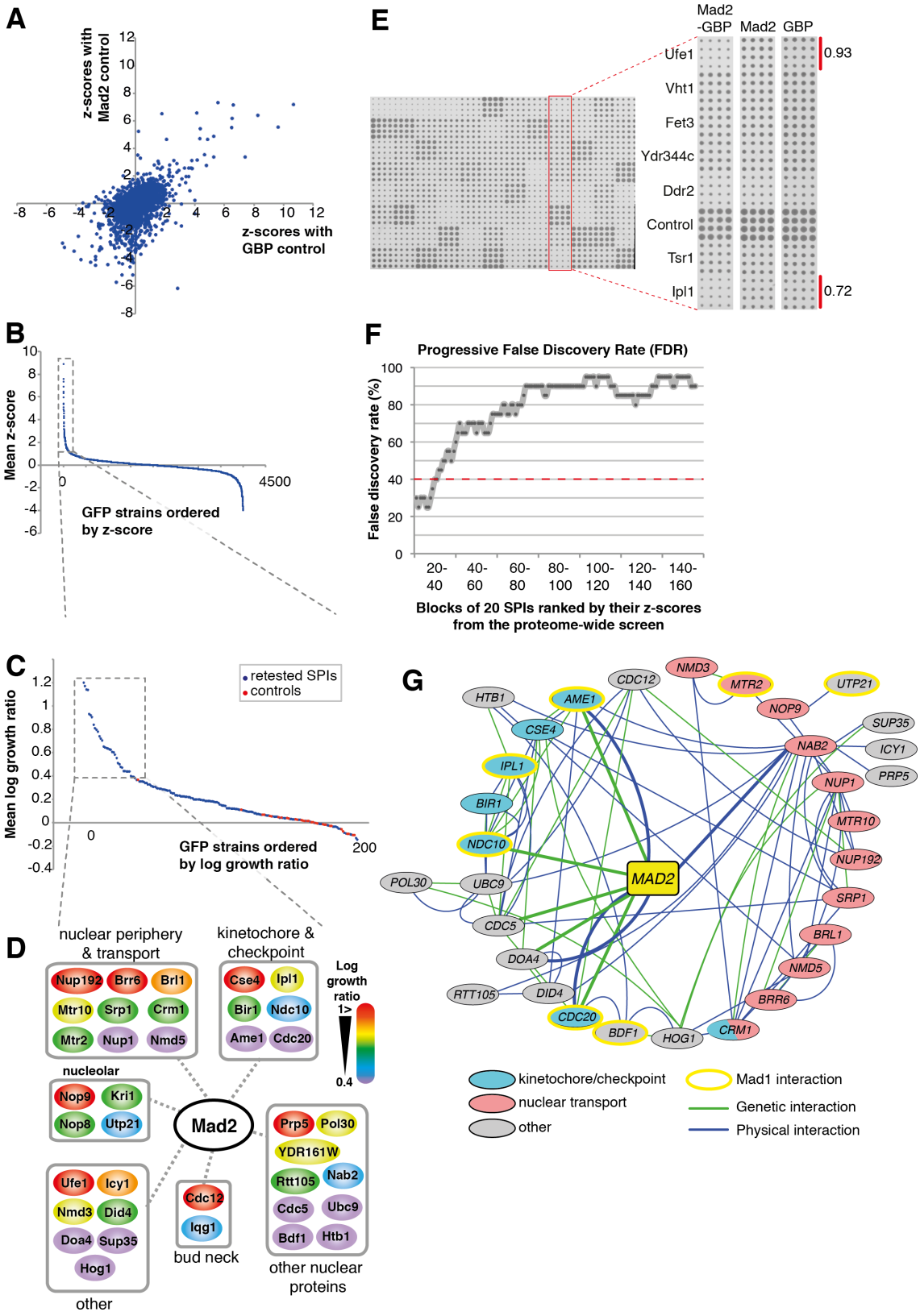

Figure 4.2 Proteome-wide Mad2 SPIs

A) The proteome-wide Mad2 SPI data (z-scores) comparing Mad2-GBP with the two controls, GBP and Mad2, are plotted on each axis in a scatter graph.
B) The average z-score for each interaction (in quadruplicate) is plotted in a descending order of the GFP strains. A z-score of 1 indicates ~1 standard deviation from the mean of the proteome-wide data. A positive z-score indicates growth inhibition caused by Mad2-GBP compared to controls. The grey box indicates z-scores > 1.5 which were retested and the resulting data is plotted in (C).
C) The strongest 156 SPIs (z-score > 1.5) from the proteome-wide assay were retested with 16 replicates to confirm the SPIs detected in the proteome-wide screen. In the retest the colony size differences between cells with the Mad2-GBP plasmid and control plasmids are measured using log growth ratios and red dots indicate control strains that do not contain a GFP-tagged protein. The grey box indicates the strongest growth defects (37 SPIs) which have log growth ratios higher than 0.4 and are above the most affected control.
D) A network showing the 37 Mad2 SPIs which are grouped by function or cellular compartment and colour-coded to indicate the strength of the SPI phenotype (high log growth ratios in red).
E) An example from the retest assay showing colonies of each GFP strain arrayed with 16 replicates. The red square indicates columns that were cropped from plate images showing colonies of GFP strains containing each of the three plasmids and the red bars highlight GFP strains (Ufe1-GFP and Ipl1-GFP) that were affected by expression of Mad2-GBP compared to controls (log growth ratios of 0.93 and 0.72 respectively).
F) The false discovery rate (FDR) was assessed and shows that the FDR increases as the strength of the SPI decreases. The first ~40 strongest SPIs have a FDR below 40%.
G) An interaction network of the Mad2 SPIs, showing genetic and physical interactions (green and blue lines respectively) between the genes/proteins which were detected as Mad2 SPIs. The colour-coding indicates the function of some of the SPIs; blue for kinetochore and spindle proteins and pink for proteins involved in nuclear transport. The Mad2 SPIs that have either a genetic or physical interaction with Mad1 are highlighted in yellow.

Table 4.1 Gene ontology and phenotypic enrichment analysis of Mad2 SPIs

Gene ontology enrichment	**Gene name**
Nuclear transport (2.00×10^{-9})	*BRL1, BRR6, CRM1, MTR2, MTR10, NAB2, NMD3, NOP9, NUP1, NUP192, NMD5, SRP1*
Kinetochore (1.04×10^{-5})	*AME1, NDC10, CRM1, BIR1, CSE4, IPL1*
Mutant phenotype enrichment	
Chromosomal instability (4.56×10^{-8})	*nop8, crm1, sup35, ubc9, cdc12, utp21, cse4, brl1, cdc20, ipl1, mtr10, cbf2, pol30, ame1*

GO enrichment analysis was performed using GOrilla online software, available on: http://cbl-gorilla.cs.technion.ac.il/ and phenotype enrichment analysis was performed using ScreenTroll, available on: http://www.rothsteinlab.com/tools/screenTroll.

4.2.2 Mad2 kinetochore SPIs

Forced kinetochore associations with SAC components has been shown to be sufficient for SAC activation, even when kinetochores are attached to microtubules

(Jelluma *et al.*, 2010; Maldonado & Kapoor, 2011*a*; Ito *et al.*, 2012; Ballister *et al.*, 2014; Aravamudhan *et al.*, 2015). However, it was striking that both the results from the kinetochore SPI screens in chapter 3 and the Mad2 SPI results in this chapter, show that most kinetochore-SAC associations do not produce any growth defect. I had expected a range of central and outer kinetochore proteins tagged with GBP to arrest growth in strains containing GFP-tagged SAC components, and similarly, I expected that Mad2-GBP would sufficiently activate the SAC in strains with GFP-tagged central and outer kinetochore components. However, since I was able to identify some kinetochore proteins in the proteome-wide Mad2 SPI screen, I wanted to both confirm the proteome-wide screen and explore this in more detail and ask which Mad2-kinetochore protein associations could activate the SAC. I therefore retested 88 GFP strains, each of which contains a different GFP-tagged kinetochore or kinetochore-related protein in a high-density format (16 replicates). This analysis reinforced the results from the proteome-wide assay; the only kinetochore protein to consistently produce a SPI phenotype with Mad2 is Cse4 (Figure 4.3 A). In addition, the CPC subunits, Ipl1 and Sli15, produce weak but consistent SPIs with Mad2. Two kinetochore proteins, Ame1 and Ndc10, that I had detected as weak SPIs in the proteome-wide screen, were below the threshold in this kinetochore-specific SPI screen (log growth ratio < 0.4).

It is possible that forcing proteins to the kinetochore could result in indirect SAC activation independently of the genuine SAC mechanism. In order to try to control for this and to detect more subtle effects I decided to make mutants of Mad2 as controls. I engineered additional plasmids containing two Mad2 mutants that are unable to function in the SAC. I initially created a Mad2 dimerization mutant (*mad2-R126A, Q127A;* referred to as *mad2-2A*) that binds normally to Mad1 but cannot form an active MCC as it fails to convert O-Mad2 to C-Mad2 (Nezi *et al.*, 2006). Secondly, I made a truncation mutant lacking the last 10 C-terminal amino acids (*mad2ΔC*); this mutant is both unable to bind Mad1 and form MCC (Nezi *et al.*, 2006). I fused both of these mutants to GBP (mad2-2A-GBP and mad2ΔC-GBP) and re-assayed the GFP kinetochore strains comparing wild-type Mad2-GBP with these mutants. These SPI screens using either the mad2-2A-GBP or the mad2ΔC-GBP as controls, produced essentially the same results as the screen with the standard controls (Figure 4.3 B&C). I did not detect any SPIs with central or outer kinetochore components, the SPI with Cse4 remained (Figure 4.3 E), and interactions with CPC subunits, produced weak

SPIs. The wild-type Mad2-Cdc20 SPI growth phenotype is striking when compared with the mutant mad2ΔC-GBP control, consistent with the inability of *mad2ΔC* to contribute to the MCC (Figure 4.3 C). It has been shown that artificial recruitment of active C-Mad2 to the kinetochore leads to metaphase arrest in human cells (Kruse *et al.*, 2014). Thus, I wanted to explore this in budding yeast and created a plasmid encoding mutant of Mad2 (*mad2-L7A*; referred to as C-Mad2) that is constitutively locked in the closed active conformation (Mapelli *et al.*, 2007; Yang *et al.*, 2008*a*), and fused it to GBP (C-Mad2-GBP). I performed another kinetochore SPI screen using this mutant, hoping it would efficiently activate the SAC when forced to the kinetochore. However, as seen before with wild-type Mad2-GBP, the C-Mad2-GBP produced SPIs only with Cse4, Cdc20, and to a lesser extent with Sli15 and Ipl1 (Figure 4.3 D). Moreover, I investigated another mutant of Mad2, mad2-T133A, V188N (referred to as O-mad2-GBP), which is constitutively in the open conformation (Mapelli *et al.*, 2007), and this did not change the results and the forced association of this mutant with either Cdc20 or Ipl1 did not produce SPI phenotype (Figure 4.3 F). In addition, I found that forced associations of wild-type Mad2-GBP, C-Mad2-GBP and dimerization-mutant Mad2 (mad2-2A-GBP) produced SPI growth phenotype with Cdc20, but the O-mad2-GBP and mad2ΔC-GBP did not (Figure 4.3 F). I confirmed that the GBP-tagged wild-type and mutant Mad2 were recruited to the kinetochore in cells containing GFP-tagged kinetochore proteins using fluorescence microscopy (Figure 4.3 G&H).

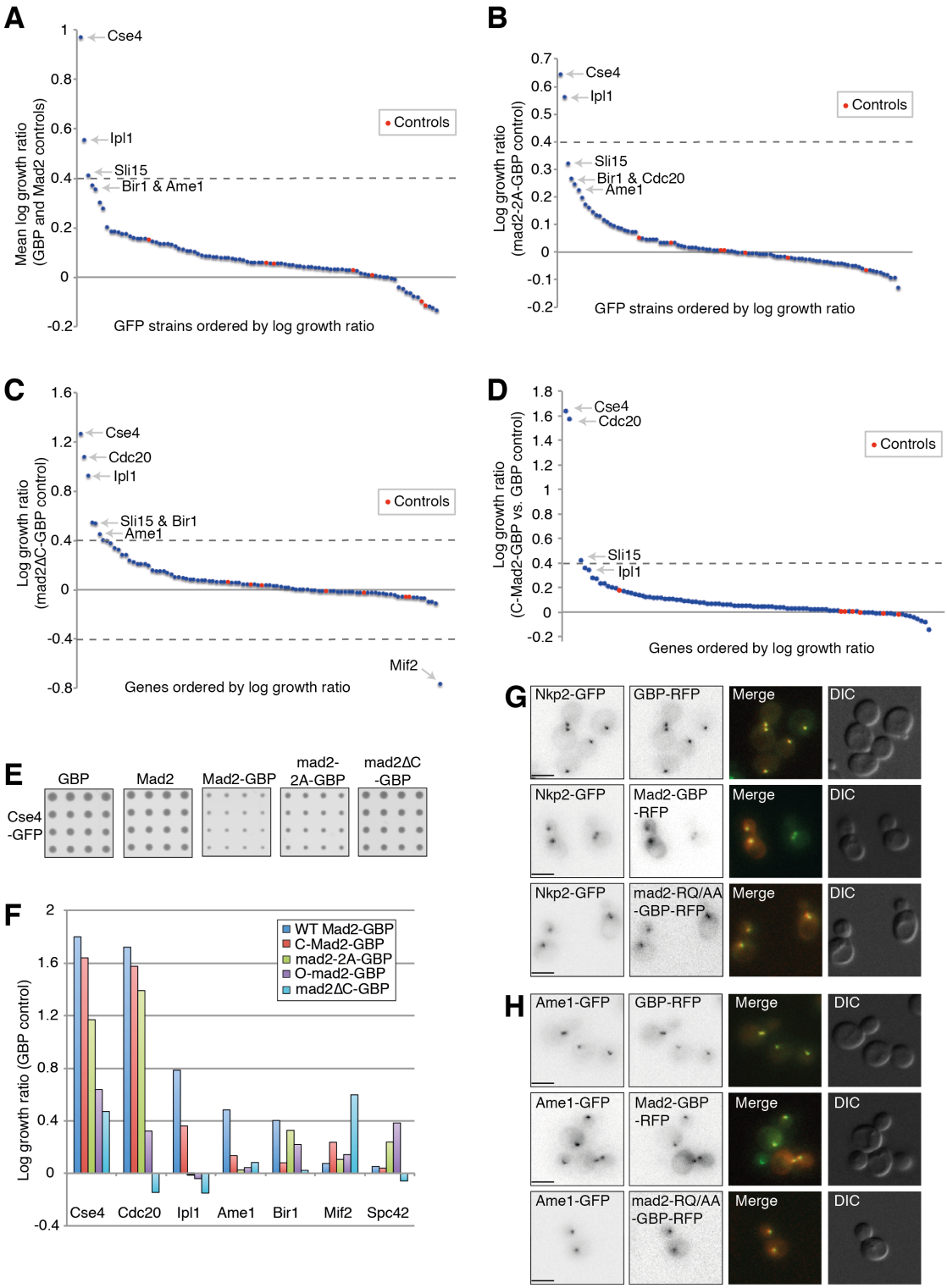

Figure 4.3 Mad2 kinetochore SPIs

A) The Mad2 SPI assay was repeated in 88 kinetochore and related GFP strains. The average log growth ratios using the two controls (GBP and Mad2) are plotted. Red dots indicate a non-GFP control strain.
B) A plot showing the Mad2 kinetochore SPI data using mad2-2A-GBP as a control.
C) A plot showing the Mad2 kinetochore SPI data using mad2ΔC-GBP as a control.

D) The SPI screen was repeated with the kinetochore-GFP strains containing the active C-Mad2-GBP and compared with GBP as a control.
E) An example of the raw SPI data showing the Cse4-GFP SPI with the Mad2-GBP and control plasmids.
F) A graph showing a selection of the Mad2 SPI data with all the Mad2-GBP fusion plasmids, including wild-type and mutants, compared with GBP control.
G-H) Fluorescence microscopy images of cells containing GFP-tagged kinetochore proteins, Nkp2-GFP in (G) and Ame1-GFP in (H), and
expressing either GBP-RFP, Mad2-GBP-RFP or mad2-2A-GBP-RFP. All scale bars are 5µm.

Next, to test whether the growth arrest caused by any of the Mad2 SPIs was functioning through the checkpoint, I investigated whether these SPIs could be suppressed by deleting *MAD3,* an essential component of the SAC. I repeated the Mad2 SPI screen with 21 GFP-tagged proteins in both wild-type and *mad3*Δ strains, and found that the SPIs with CPC subunits, Ipl1 and Sli15, were suppressed in *mad3*Δ strains (Figure 4.4 A&B). Cse4 was excluded in this assay, since the Cse4-GFP *mad3*Δ strain grew poorly, hence I will analyse this interaction using a different approach (see section 4.2.3 below). Using fluorescence microscopy, I confirmed that the Mad2-GBP-RFP signal (and mutant) cololocalised with Ipl1-GFP (Figure 4.4 C), and that forced association of another CPC subunit (Bir1-YFP) colocalised with Mad2-GBP-RFP at the kinetochore as seen in a strain containing Ask1-CFP (Figure 4.4 D).

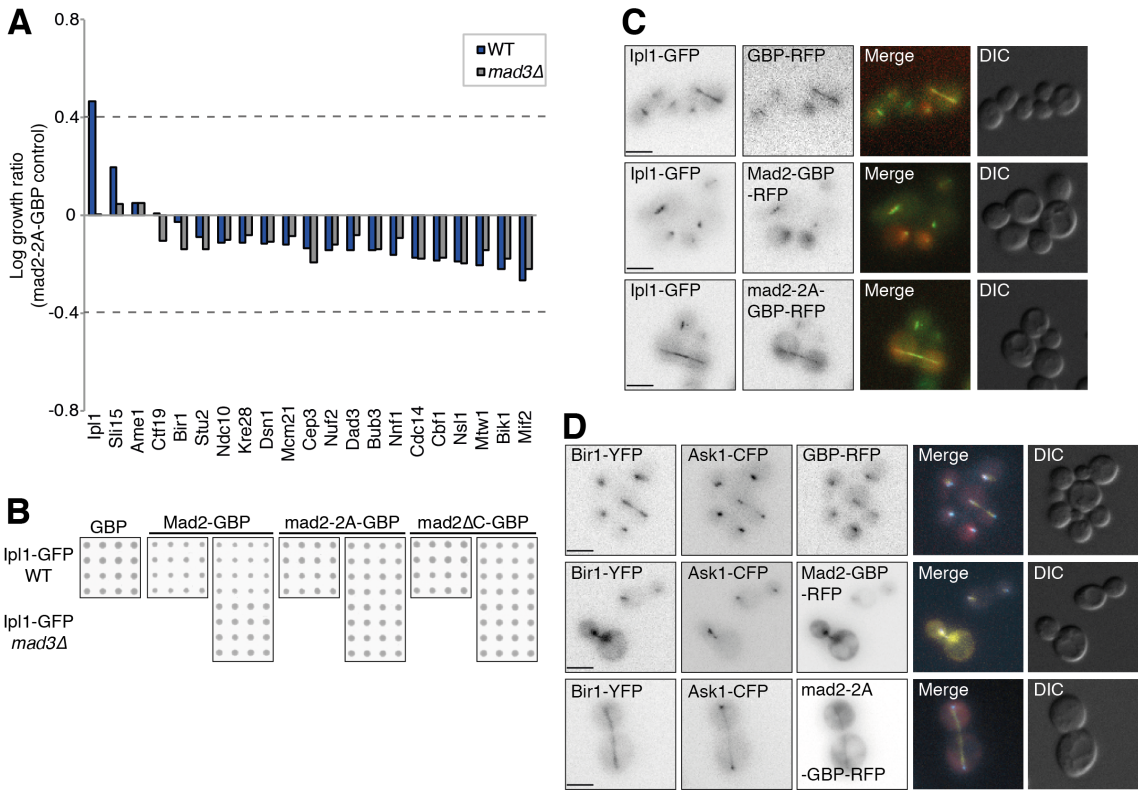

Figure 4.4 The Mad2-CPC SPI is SAC-dependent and localises to the kinetochore

A) The Mad2 SPI assay was repeated in 21 kinetochore GFP strains (x-axis), both wild-type and *mad3*Δ. The growth defect, log growth ratio, is calculated using mad2-2A-GBP as a control (y-axis).
B) Cropped images of the SPI screen plates show the Ipl1-GFP strain with the different Mad2 plasmids in both wild-type and *mad3*Δ strains.
C) Fluorescence microscopy of Ipl1-GFP cells containing GBP-RFP, Mad2-GBP-RFP and mad2-2A-GBP-RFP plasmids.
D) Fluorescence microscopy images of cells with Bir1-YFP and Ask1-CFP containing the GBP-RFP, Mad2-GBP-RFP and mad2-2A-GBP-RFP plasmids. Note that GBP binds to YFP but not CFP. All scale bars are 5μm.

Since, it is possible that a forced association of a kinetochore protein with other proteins can result in the mislocalisation of the kinetochore protein (Figure 3.6 D in section 3.2.3), I wanted to investigate in more detail whether the Mad2-GBP was indeed recruited correctly to the kinetochore. I introduced the Mad2-GBP plasmid (and mutant control) into Mtw1-YFP strains with either another kinetochore component tagged with CFP (Ask1-CFP) or a SPB subunit tagged with CFP (Spc110-CFP). If the Mad2-GBP failed to colocalise with the kinetochore in these strains it could explain why the forced Mad2-kinetochore interaction failed to activate the SAC and arrest growth, and thus not detected in the SPI screens. However, I confirmed that the Mad2-GBP-RFP and mutant control signal colocalised with Mtw1-YFP at the kinetochore (Figure 4.5 A), and between two SPB foci in mitotic cells (Figure 4.5 B).

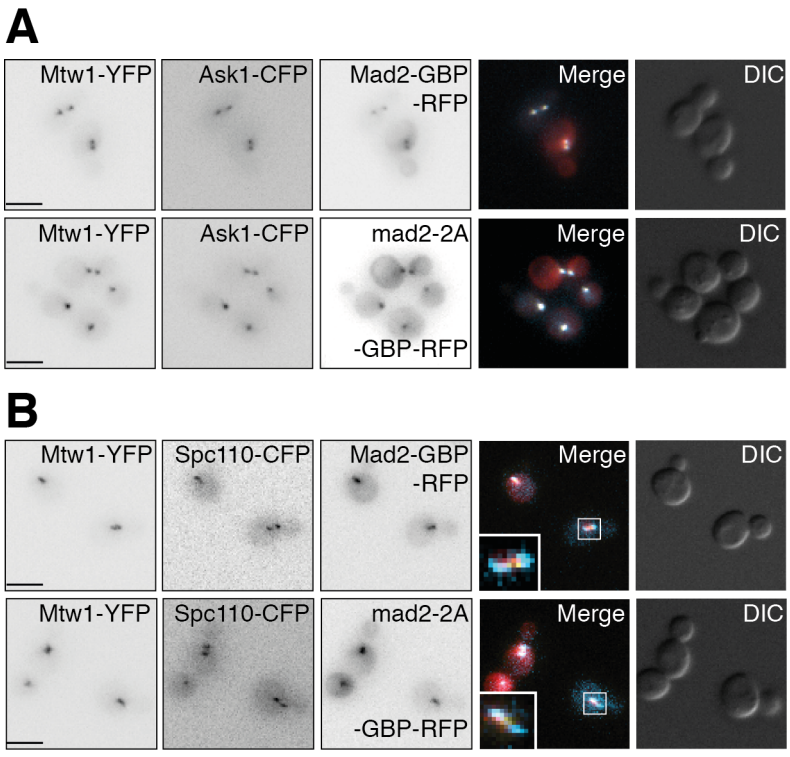

Figure 4.5 The Mad2-GBP and mutant colocalise with YFP-tagged kinetochore protein at the kinetochore

A) Fluorescence microscopy images of cells encoding Mtw1-YFP and Ask1-CFP from endogenous loci also containing Mad2-GBP-RFP (top) and mad2-2A-GBP-RFP (bottom) plasmids.
B) Fluorescence microscopy images of cells endogenously encoding Mtw1-YFP and Spc110-CFP also containing Mad2-GBP-RFP (top) and mad2-2A-GBP-RFP (bottom) plasmids. The inset shows a magnified view of the spindle. Note that GBP binds YFP but not CFP. All scale bars are 5μm.

In summary, although Mad2 was effectively recruited to the kinetochore using the SPI system, this was insufficient for SAC activation. However, forced association of wild-type or active Mad2 (C-Mad2), but not inactive Mad2 mutants, with components of the chromosomal passenger complex were able to produce a SAC-dependent growth phenotype, since these SPIs were suppressed by *mad3*Δ.

4.2.3 Further examination of forced Mad2-Cse4 interaction

The only kinetochore protein that consistently gave a SPI growth phenotype when associated with Mad2 was Cse4 (Figure 4.3 A-E). However, it is unlikely that Cse4 is a target for Mad2-dependent SAC activation. Cse4 is a centromere-specific histone variant which forms a specialised nucleosome required for kinetochore assembly (Stoler *et al.*, 1995; Collins *et al.*, 2005). As described previously, normal SAC activation occurs at the KMN network via Mad1-Mad2 interaction with Bub1-Bub3 bound to KNL1/Spc105. Therefore, I hypothesised that the forced Mad2 association with Cse4 was leading to a kinetochore defect, either directly causing a growth phenotype or indirectly activating the SAC. To discriminate between these two possibilities, I asked whether or not the growth defect could be suppressed by inactivating SAC by deleting checkpoint components. To achieve this, I created plasmids containing direct fusions of *MAD2* and *CSE4* under the control of a conditional promoter *pGAL1.* I fused Mad2 individually to both the C and N termini of Cse4 (*MAD2-CSE4* and *CSE4-MAD2*) and found that expression of both of these fusions inhibits growth (Figure 4.6 A&B). Interestingly, I found that deletion of *MAD1* or *MAD3* sufficiently rescued the growth defect of cells expressing the *MAD2-CSE4* fusion, but not the reverse *CSE4-MAD2* fusion (Figure 4.6 B). To confirm that the growth arrest was due to SAC activity, I introduced the *MAD2-CSE4* fusion plasmid (and control plasmids expressing *MAD2* or *CSE4* alone) into a strain with fluorescently tagged cohesin (Smc1-YFP) and histone (Hta1-CFP) and expressed the fusion for four

hours. I used fluorescence microscopy analysis to measure the stabilisation of cohesin (Smc1) (see section 2.3.2 for details), and consistent with SAC activation, I found that cells expressing the *MAD2-CSE4* fusion had increased Smc1-YFP intensity compared to cells ectopically expressing either of the single genes (Figure 4.6 C&D). Furthermore, I tested whether expression of the fusions would affect chromosomal instability and assessed plasmid and chromosome loss. I measured plasmid loss by introducing the fusion and control plasmids, which have the *LEU2* marker, into cells and additionally introduced another empty plasmid with a different selection marker (NAT) and plated the cells on –leu and –leu NAT media and assessed plasmid loss by counting the colonies (see section 2.5.1 for more details). I assessed chromosome loss using the established red-sectored colony assay (Spencer *et al.*, 1990)(see section 2.5.2 for details). Cells expressing the *MAD2-CSE4* fusion did not show an increased rate of plasmid or chromosome loss compared to cells expressing *MAD2* or *CSE4* alone (Figure 4.6 E&F respectively), whereas the reverse *CSE4-MAD2* fusion significantly increased chromosome loss compared to controls (Figure 4.6 F).

Cse4, a relatively small protein, is sensitive to fusions, which can result in abnormal kinetochore function (Wisniewski *et al.*, 2014). Additionally, changes to CENP-A homologs in other species disrupt its function (Ravi & Chan, 2010). Furthermore, it was shown that cells with C-terminally tagged Cse4 activate SAC at elevated temperature (Ho *et al.*, 2014). Fortunately, Cse4 tagged internally with GFP has been generated and appears to be functional (Chen *et al.*, 2000; Wisniewski *et al.*, 2014). I therefore repeated the SPI assay including a strain containing the internally tagged Cse4 (referred to here as Cs-GFP-e4 or Cse4-GFP^{int}), and found no growth inhibition with Mad2-GBP, despite effective colocalisation of Mad2-GBP-RFP and Cse4-GFP^{int} (data not shown and Figure 4.6 H). In addition, to confirm the SPI screen result, I created plasmids encoding GBP and Mad2-GBP under the control of *GAL1* promoter and found that expression of Mad2-GBP in a Cse4-GFP strain was lethal, whereas expression in a Cse4-GFP^{int} strain was not (Figure 4.6 G). Consistent with the notion of Cse4 sensitivity to C-terminal fusions overexpression of GBP alone was also lethal in Cse4-GFP strain, but not in Cse4-GFP^{int} strain.

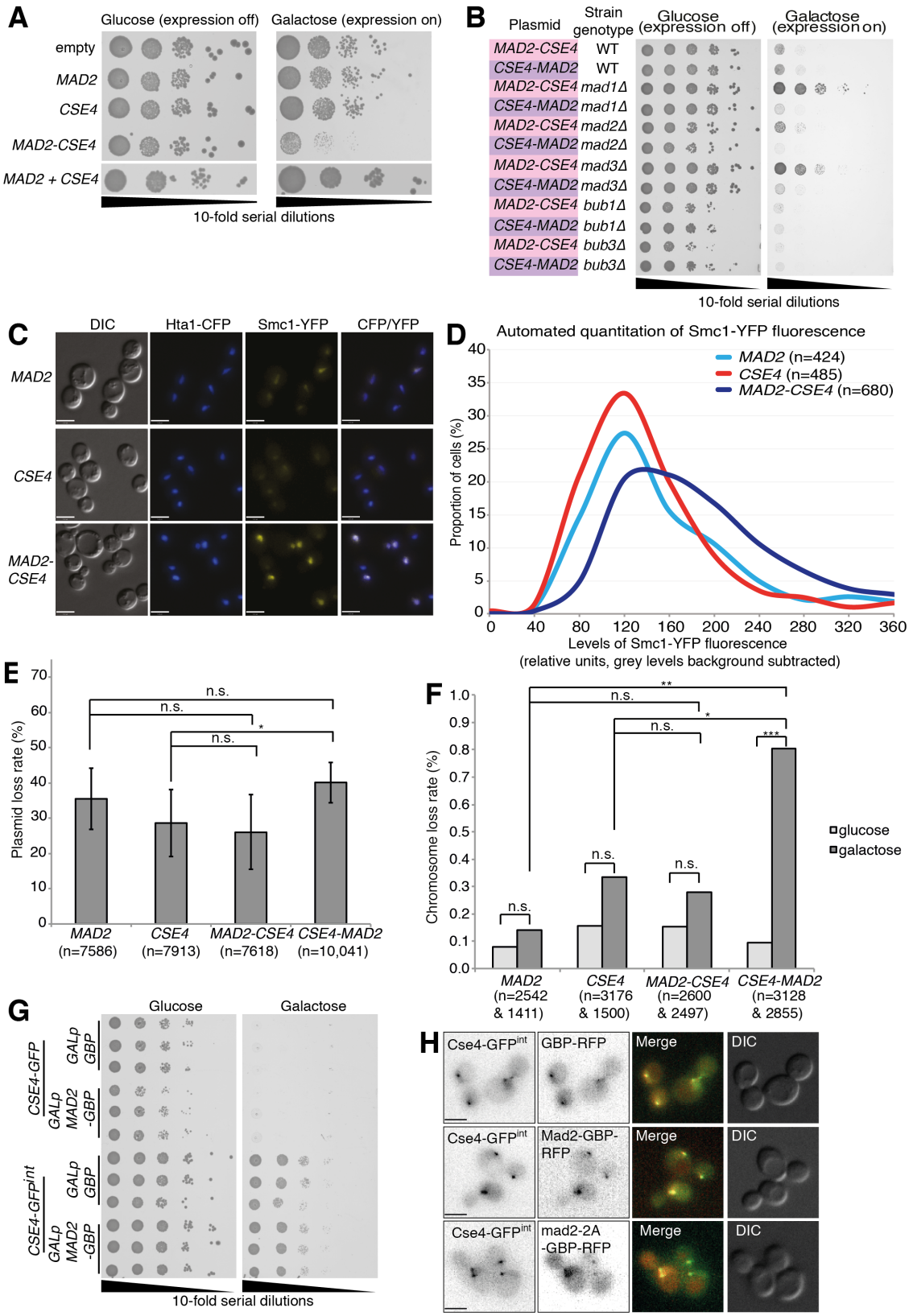

Figure 4.6 Analysis of forced Mad2-Cse4 association

A) Cells were transformed with plasmids expressing nothing (empty plasmid), *MAD2*, *CSE4* or a direct *MAD2-CSE4* fusion, as well as cells expressing both *MAD2* and

CSE4 together from separate plasmids, and 10-fold serial dilutions were spotted on glucose and galactose media. The latter condition drives expression of the transgene and only the *MAD2-CSE4* fusion restricts growth.
B) Six strains, wild-type (WT), *mad1*Δ, *mad2*Δ, *mad3*Δ, *bub1*Δ and *bub3*Δ, were transformed with either the *MAD2-CSE4* fusion, as in (A), or the reverse *CSE4-MAD2* fusion. A 10-fold serial-dilution assay shows both fusions inhibit growth when expressed (galactose), but only the *MAD2-CSE4* fusion is suppressed in *mad1*Δ and *mad3*Δ strains.
C) Expression of *MAD2-CSE4* stabilises cohesin as shown by fluorescence microscopy images of cells encoding tagged histone (Hta1-CFP) and cohesin (Smc1-YFP) expressing *MAD2*, *CSE4* or the *MAD2-CSE4* fusion.
D) An automated image analysis protocol was used to measure the Smc1-YFP fluorescence using the Hta1-CFP fluorescence as a guide for the nuclear volume. The *MAD2-CSE4* fusion elevates the levels of Smc1 fluorescence compared with controls.
E) A plasmid-loss assay was performed with *mad3*Δ strains containing the *MAD2*, *CSE4, MAD2-CSE4* and *CSE4-MAD2* plasmids along with an empty plasmid with a different selection marker (NAT). The expression of the *MAD2-CSE4* or *CSE4-MAD2* fusions did not significantly increase plasmid loss rate (of the empty NAT plasmid) compared to the expression of *MAD2* alone. There was a slight but statistically detectable increase in plasmid loss when expressing *CSE4-MAD2* fusion compared to *CSE4* alone (* = student's t-test p-value of 0.015), but no difference when the *MAD2-CSE4* fusion was expressed compared with *CSE4*. Error bars indicate standard deviation of the median and n.s. indicates no statistical difference (p-value > 0.05).
F) A chromosome-loss assay was performed with cells expressing *MAD2-CSE4* fusions. Expression of *MAD2-CSE4* did not increase chromosome loss compared to controls. In contrast, the expression of the reverse *CSE4-MAD2* fusion results in significantly increased chromosome-loss rate (*** = Fishers exact test p-value = 1.6 x 10-5, ** = p-value = 0.004, * = p-value = 0.04). n.s. indicates no statistical difference.
G) Cells encoding either C-terminal or internal GFP-tagged Cse4 were transformed with plasmids encoding GBP or Mad2-GBP and serial dilutions were plated on glucose and galactose. Expression of both GBP and Mad2-GBP arrested growth of cells encoding Cse4 with C-terminal GFP tag, but not internal GFP tag.
H) Images of cells encoding Cse4 with an internal GFP tag show that Mad2-GBP-RFP, and the mutant control, are colocalised with Cse4. All scale bars are 5μm.

Together these data are in agreement with the idea that forcing Mad2 to the C terminus of Cse4, either by direct fusion of the ORFs (Cse4-Mad2) or via the GBP-GFP association, disrupts kinetochore function and thus results in SAC-independent growth inhibition and chromosomal instability. In contrast, linking Mad2 to the N terminus of Cse4 (Mad2-Cse4) seems to result in artificial SAC activation, since the growth arrest is rescued by *mad1*Δ and *mad3*Δ. However, this phenotype cannot be recapitulated with an internally GFP-tagged Cse4, or by recruiting Mad2 locally to other proteins at the inner kinetochore. This suggests that the Mad2-Cse4-dependent SAC activation is not specifically a result of recruiting Mad2 to the centromeric nucleosome, but rather caused by interference with the N-terminal tail of Cse4 indirectly leading to SAC activation. Hence, after excluding Cse4, none of the forced Mad2 associations with kinetochore proteins produced a significant growth defect using the SPI methodology.

4.2.4 Mad1 kinetochore SPI screen

Since I failed to activate the SAC by forcing Mad2 to the kinetochore, I decided to test another SAC component, Mad1, which functions upstream of Mad2. Mad1 and Mad2 together catalyse the formation of C-Mad2, which along with the rest of MCC inhibit Cdc20. It has been shown that Mad1 activity at the kinetochore is required for proper SAC activity beyond recruiting Mad2 (London & Biggins, 2014; Heinrich *et al.*, 2014; Kruse *et al.*, 2014; Ballister *et al.*, 2014), and thus forcing Mad2 kinetochore recruitment, without Mad1 might not be sufficient for a SAC arrest. Therefore, I engineered a plasmid encoding Mad1-GBP in addition to control plasmids containing Mad1 alone, and three different mutants of Mad1. First, a Mad1 mutant with RLK residues at position 653-655 mutated to alanines (*mad1-RLK-AAA*), which lacks the ability to bind Bub1 (Brady & Hardwick, 2000), and thus is incapable of activating the SAC (Heinrich *et al.*, 2014; Ballister *et al.*, 2014). Second, a mutant with RIL residues at position 581-583 changed to alanines (*mad1-RIL-AAA*), which fails to bind Mad2 (Luo *et al.*, 2002), and consequently should not activate SAC. Finally, *mad1-A736T* (*mad1-2*), which acts as a *mad1*Δ mutant likely via its failure to bind or activate Mad2 (Chen *et al.*, 1999). Before performing the SPI assay with these plasmids, I investigated their functionality. I found that expression of Mad1-GBP rescued benomyl sensitivity in a *mad1*Δ strain as effectively as expression of untagged Mad1 (Figure 4.7 A), and as expected the mutants were unable to suppress benomyl-dependent growth inhibition of *mad1*Δ strain.

Next, I performed the kinetochore SPI screen with these plasmids as before and found that Cse4, Ndc10, Cep3, Spc42, Mif2, and Ipl1 all produced SPI phenotype with Mad1 using the standard controls (Mad1 and GBP alone) (Figure 4.7 B). However, analysing the data using any of three mutant controls did not produce any SPIs with significant growth defect (log growth ratio > 0.4) (Figure 4.7 C-E). I did detect a subtle growth inhibition with some inner kinetochore components such as Cep3 (Figure 4.7 F), and to test if they were SAC-dependent I repeated the SPI screen in 22 GFP strains, both wild-type and *mad3*Δ. The only weak Mad1 SPI to be suppressed by *mad3*Δ was Cdc20 (Figure 4.7 G). The subtle growth defect caused by forced Mad1 association with Cep3 was not suppressed by *mad3*Δ, suggesting that the phenotype of this association is independent of SAC activation.

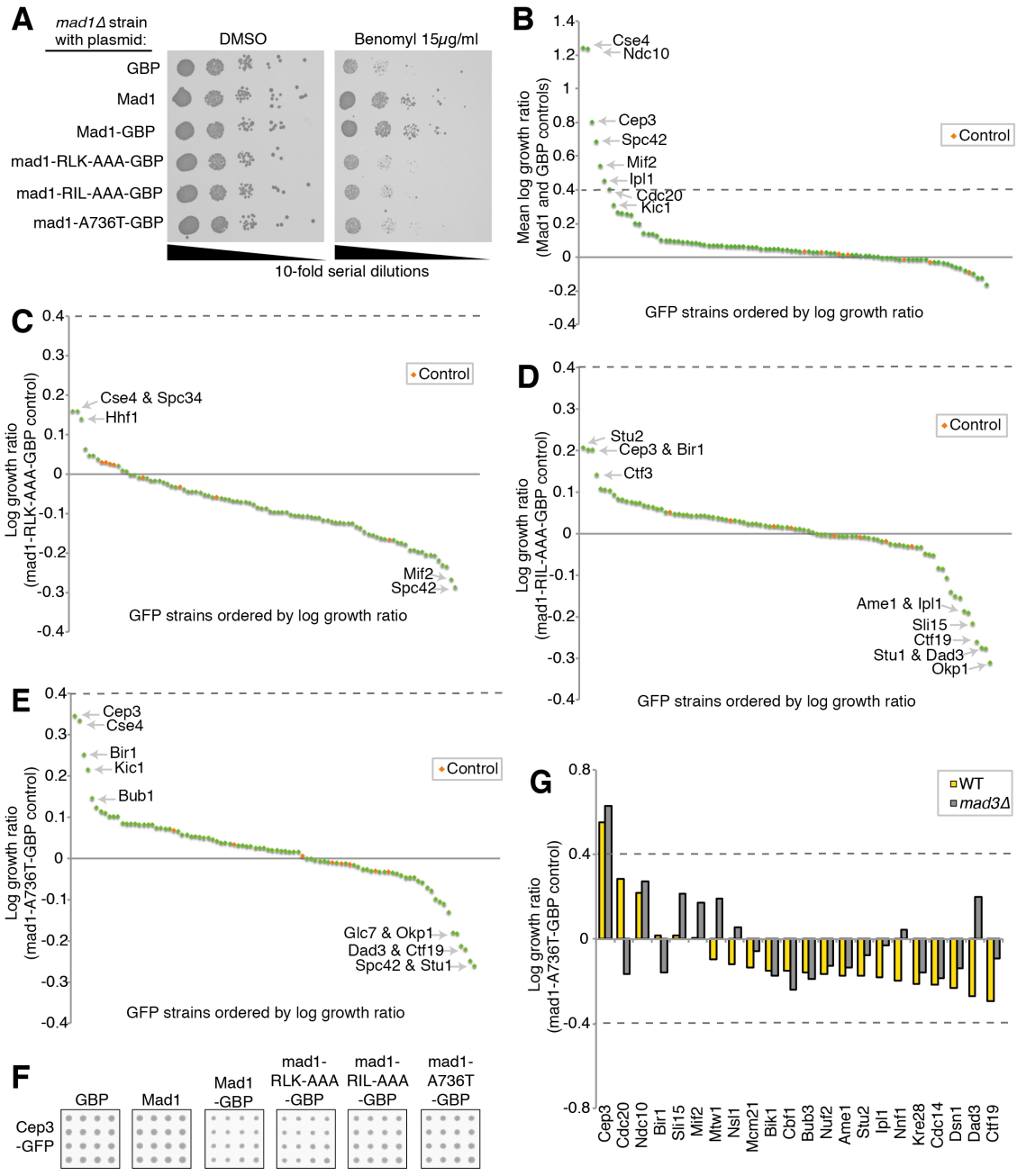

Figure 4.7 Mad1 kinetochore SPIs

A) A 10-fold serial dilution assay of *mad1*Δ strain shows that cells with plasmids encoding Mad1 or Mad1-GBP rescue benomyl sensitivity of *mad1*Δ, but not plasmids containing GBP, mad1-RLK-AAA-GBP, mad1-RIL-AAA-GBP or mad1-A736T-GBP.
B) A SPI screen with 88 kinetochore and related GFP strains was performed using Mad1-GBP plasmid and compared with control plasmids containing GBP and Mad1 alone. The average log growth ratios are plotted and orange dots indicate non-GFP control strains.
C) The Mad1 kinetochore SPI data are plotted as in (B) using mad1-RLK-AAA-GBP as a control.
D) The Mad1 kinetochore SPI data are plotted as in (B) using mad1-RIL-AAA-GBP as a control. I note that this comparison reveals many “growth enhancers”, which are

interactions in which cells are growing better with Mad1-GBP than the mutant; however, this effect is very subtle and within the threshold of LGR of -0.4.
E) The Mad1 kinetochore SPI data are plotted as in (B) using mad1-A736T-GBP as a control.
F) Cropped images of the SPI screen plates shows the growth of the Cep3-GFP strain with the different Mad1 plasmids.
G) The Mad1 SPI assay was repeated in 22 kinetochore GFP strains, both wild-type and *mad3*Δ. The colony sizes of the GFP strains containing the Mad1-GBP were compared with the GFP strains containing the mad1-A736T-GBP control plasmid. The Mad1-GBP was also compared with the standard Mad1 and GBP controls with essentially the same results (data not shown). The log growth ratio (y-axis) is plotted for each GFP strain (x-axis).

I used fluorescence microscopy to confirm that Mtw1-YFP cells expressing Mad1-GBP-RFP successfully recruited Mad1 to the kinetochore (Figure 4.8 A&B), although in many cells, a fraction of the Mad1-GBP-RFP and Mtw1-YFP is mislocalised from the kinetochore (red arrows in Figure 4.8 A&B); however, I note that this does not cause a detectable growth defect. Furthermore, I confirmed that the GBP-tagged Mad1 and a Mad1 mutant colocalise with GFP-tagged kinetochore proteins, Mif2-GFP and Cep3-GFP (Figure 4.8 C&D respectively).

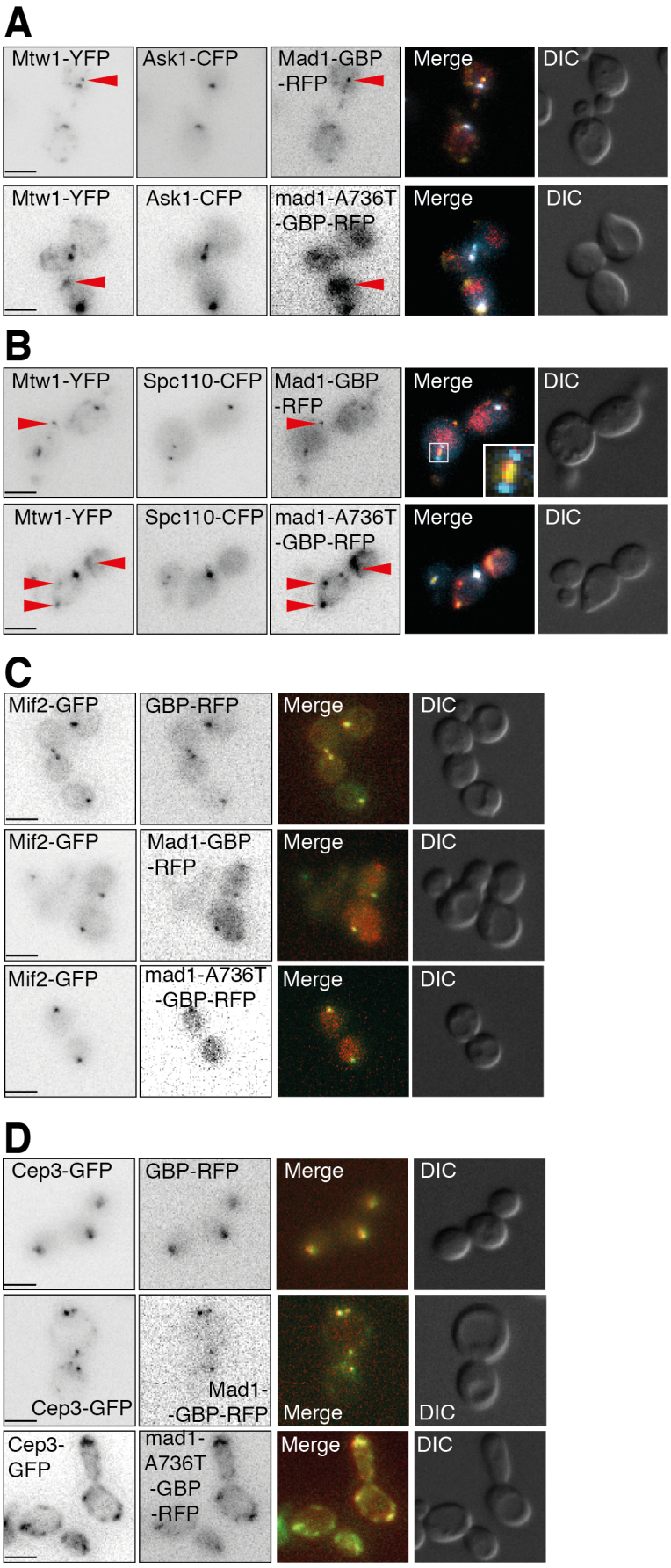
A
Mtw1-YFP
Ask1-CFP
Mad1-GBP -RFP
Merge
DIC
Mtw1-YFP
Ask1-CFP
mad1-A736T -GBP-RFP
Merge
DIC
B
Mtw1-YFP
Spc110-CFP
Mad1-GBP -RFP
Merge
DIC
Mtw1-YFP
Spc110-CFP
mad1-A736T -GBP-RFP
Merge
DIC
C
Mif2-GFP
GBP-RFP
Merge
DIC
Mif2-GFP
Mad1-GBP -RFP
Merge
DIC
Mif2-GFP
mad1-A736T -GBP-RFP
Merge
DIC
D
Cep3-GFP
GBP-RFP
Merge
DIC
Cep3-GFP
Mad1- -GBP-RFP
Merge
DIC
Cep3- GFP
mad1- A736T -GBP -RFP
Merge
DIC

Figure 4.8 Mad1-GBP localises to GFP-tagged kinetochores

A) Fluorescence microscopy images of cells endogenously encoding Mtw1-YFP and Ask1-CFP and also containing Mad1-GBP-RFP (top) and mad1-A736T-GBP-RFP (bottom) plasmids.
B) Fluorescence microscopy images of cells endogenously encoding Mtw1-YFP and Spc110-CFP and also containing Mad1-GBP-RFP (top) and mad1-A736T-GBP-RFP (bottom) plasmids. The inset shows a magnification of the spindle. Note that GBP binds YFP but not CFP. Red arrows indicate ectopic colocalisation of Mad1-GBP-RFP and Mtw1-YFP
C-D) Fluorescence microscopy images show that Mad1-GBP-RFP and mad1-A736T-GBP-RFP colocalise with both Mif2-GFP (C) and Cep3-GFP (D), the latter of which shows unusual localisation when associated with either Mad1 or its mutant version, similar to Mtw1-YFP in (A&B). All scale bars are 5μm.

Collectively, these data, together with those using Mad2, suggest that forcing Mad1 and Mad2 individually to the kinetochore is not sufficient to produce a SAC arrest, and is consistent with the notion that locally high concentrations of either Mad1 or Mad2 at the kinetochore is insufficient for activating the checkpoint. However, it is possible that the GFP-GBP association prevents SAC proteins from being in the precise location or orientation for efficient SAC response. I thus tested this notion by examining the effect of linker length between GBP and the tagged protein. The linker length I typically use is eight amino acids and is composed of glycines and serines, which forms a flexible linker (Reddy Chichili *et al.*, 2013). To test if linker length and composition made a difference, I created a plasmid containing Mad1 linked to GBP with a shorter four-alanine linker (Mad1-4Ala-GBP), to restrict Mad1 closer to the GFP-tagged protein. I repeated the kinetochore SPI assay using this construct and as well as the standard controls, I made a mutant mad1-A736T-4Ala-GBP control. However, the shorter linker had minimal effects on the Mad1 SPI results (Figure 4.9 A-C). I also repeated the Mad1 SPI screen in wild-type and *mad3*Δ GFP strains using the shorter linker, but this had no effect on the results (Figure 4.9 D).

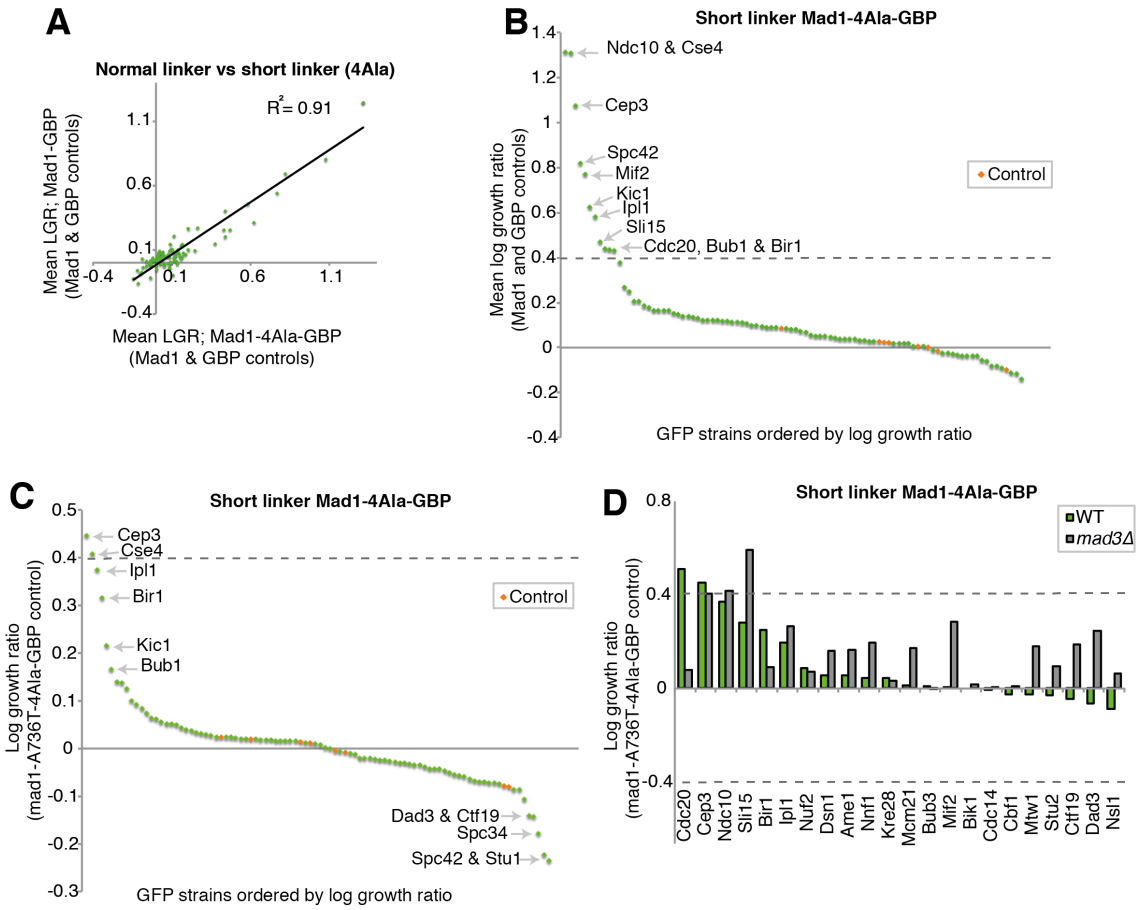

Figure 4.9 Changing the linker length between Mad1 and GBP does not affect the Mad1 SPI data

A-B) The same 88 GFP strains were screened with a variant of Mad1-GBP with a shorter linker (four alanine amino acids, Mad1-4Ala-GBP, instead of the normal eight glycines and serines). The mean log growth ratios were calculated using the GBP and Mad1 as controls. The Mad1-4Ala-GBP (x-axis) produced similar growth defect compared with the longer linker (y-axis) (Figure 4.7 B) (squared correlation coefficient, R^2=0.91).
C) The same GFP strains were screened with a version of Mad1-GBP with the shorter linker, Mad1-4Ala-GBP and compared with mad1-A736T-4Ala-GBP control. The log growth ratio data are plotted as in (B).
D) The *MAD3* gene was deleted from 22 GFP kinetochore strains and the wild-type and *mad3*Δ strains were retested for their sensitivity to Mad1-4Ala-GBP (mad1-A736-4Ala-GBP was used as control). Log growth ratios (y-axis) are plotted for each GFP strain (x-axis); green bars indicated a wild-type strain and grey bars a *mad3*Δ strain.

Next, I decided to utilise the mutant Mad1 (*mad1-RLK-AAA*) that is unable to bind Bub1 and thus is not recruited to the kinetochore (Brady & Hardwick, 2000) and investigate both whether the GBP-GFP interaction was preventing a SAC response, and where at the kinetochore this mutant could participate in SAC activation and thus rescue benomyl sensitivity through the GBP-GFP interaction. I hypothesised that if the *mad1-*

RLK-AAA was placed in the correct position at the kinetochore via the GBP-GFP association this would bypass the need for Bub1 interaction and rescue benomyl sensitivity. I performed a serial-dilution assay with *mad1*Δ strains either containing GFP-tagged kinetochore proteins or not, and as shown before, expression of mad1-RLK-AAA-GBP in a non-GFP strain does not rescue benomyl sensitivity in a *mad1*Δ strain, whereas ectopic expression of wild-type *MAD1* does (Figure 4.10). Interestingly, the forced associations of mad1-RLK-AAA-GBP with Bub1 and Spc105 (and other various kinetochore proteins) did not rescue benomyl sensitivity, however the associations with Cdc20, Ipl1 and Kre28, a subunit of the SPC105 complex, showed benomyl resistance (Figure 4.10). The phosphorylated MELT motifs that recruit Bub1-Bub3 and Mad1-Mad2 are located on the N terminus of Spc105, thus by associating mad1-RLK-AAA-GBP with C-terminally GFP-tagged Spc105 probably does not localise Mad1 correctly for SAC activation, whereas the binding partner of Spc105, Kre28, could be more suitable for placing Mad1 in the right place through the GBP-GFP interaction. It was previously suggested that the Mad1 RLK motif had a role in SAC activation beyond the kinetochore recruitment of Mad1 via the interaction with Bub1; my data suggest this is not true. The previous study used a direct fusion of mad1-RLK-AAA mutant with the C terminus of the Mtw1 homolog in fission yeast, Mis12 (Heinrich *et al.*, 2014), thus probably failing to place Mad1 in the correct position for SAC activation, similarly to the association of mad1-RLK-AAA-GBP with Mtw1-YFP shown in Figure 4.10. These data show that a tethered Mad1 protein with the kinetochore via the GBP-GFP association is able to participate in a SAC response, but the association has to be precisely localised. Recently, it was shown in human cells that the requirement of the Mad1-Bub1 interaction sites could indeed be bypassed by directly fusing Mad1 to the N terminus of Bub1 interaction mutant (Zhang *et al.*, 2017*a*).

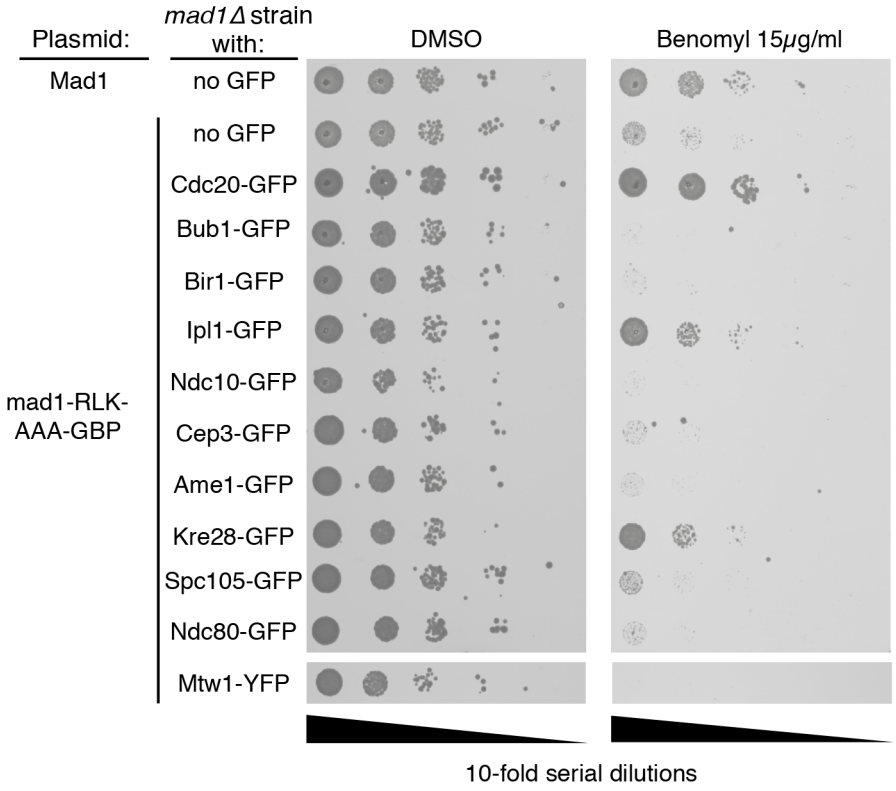

Figure 4.10 GBP-tagged mad1-RLK-AAA can participate in the checkpoint when forced to associate with the SPC105 complex

A 10-fold serial-dilution assay was performed with both *mad1*Δ non-GFP strain and *mad1*Δ strains containing different GFP-tagged kinetochore or SAC proteins. Non-GFP *mad1*Δ cells containing a plasmid encoding Mad1 were resistant to benomyl, in contrast non-GFP mad1Δ cells containing mad1-RLK-AAA-GBP were benomyl sensitive. Cells with *mad1*Δ and GFP-tagged Cdc20, Ipl1 and Kre28 (subunit of the SPC105 complex) became resistant to benomyl when expressing mad1-RLK-AAA-GBP.

It is noteworthy that the SPI screens failed to identify a growth defect when Mad1 (and Mad2) were forced to associate with any of the outer kinetochore components where these checkpoint proteins are normally recruited during SAC activation. Negative results are individually uninformative, since the precise spatial arrangement of Mad2 or Mad1 produced by the GBP-GFP interaction may not be appropriate for checkpoint activation. I therefore conclude based on these data that recruitment of Mad2 and Mad1 to the kinetochore, while necessary, is not sufficient for checkpoint activation.

4.2.5 Mps1 kinetochore SPI screen

Since neither the Mad1 and Mad2 forced associations with the kinetochore were able to activate the checkpoint, I asked whether the forced kinetochore recruitment of the checkpoint kinase Mps1 would be sufficient for SAC activation. I made a plasmid

encoding Mps1-GBP and in addition to the GBP and Mps1 controls, I created a kinase-dead mutant (Lauzé *et al.*, 1995; Araki *et al.*, 2010) version of Mps1-GBP (mps1-D580A-GBP; referred to as mps1-kd-GBP) to control for the kinase activity. I confirmed the GBP-tagged Mps1, which is essential, was functional by replacing *MPS1* endogenously with *MPS1-GBP* by genomic integration (data not shown). I performed the kinetochore SPI assay using these plasmid constructs and found, in contrast to the Mad1 and Mad2 SPI screens, that the expression of Mps1-GBP in cells endogenously encoding GFP-tagged KMN network members arrested growth. All ten of the KMN network GFP strains including Bub1, Bub3 and Mad1 produced a SPI growth phenotype compared to GBP and Mps1 controls (Figure 4.11 A). Using the mps1-kd-GBP as a control I detected most members of the KMN network, Ndc80, Nuf2, Dsn1, Nnf1, Mtw1, Nsl1, Kre28, and also Mad1 (Figure 4.11 B), consistent with the requirement of the kinase activity of Mps1 for SAC activation. To confirm that the growth defect caused by the forced Mps1 kinetochore association was due to SAC arrest, I repeated the assay in some of the Mps1 SPIs in both wild-type and *mad3*Δ GFP strains and found that *mad3*Δ suppressed all Mps1-KMN SPIs tested as well as Mps1-Bub1 SPI (Figure 4.11 C-E). In addition, deletion *MAD1* was also able to rescue the growth defect of Mps1 SPIs with Ndc80, Spc105, Kre28 and Bub1 (Figure 4.11 C, inset), in agreement with the idea that these Mps1 SPI growth phenotypes are caused by SAC activation.

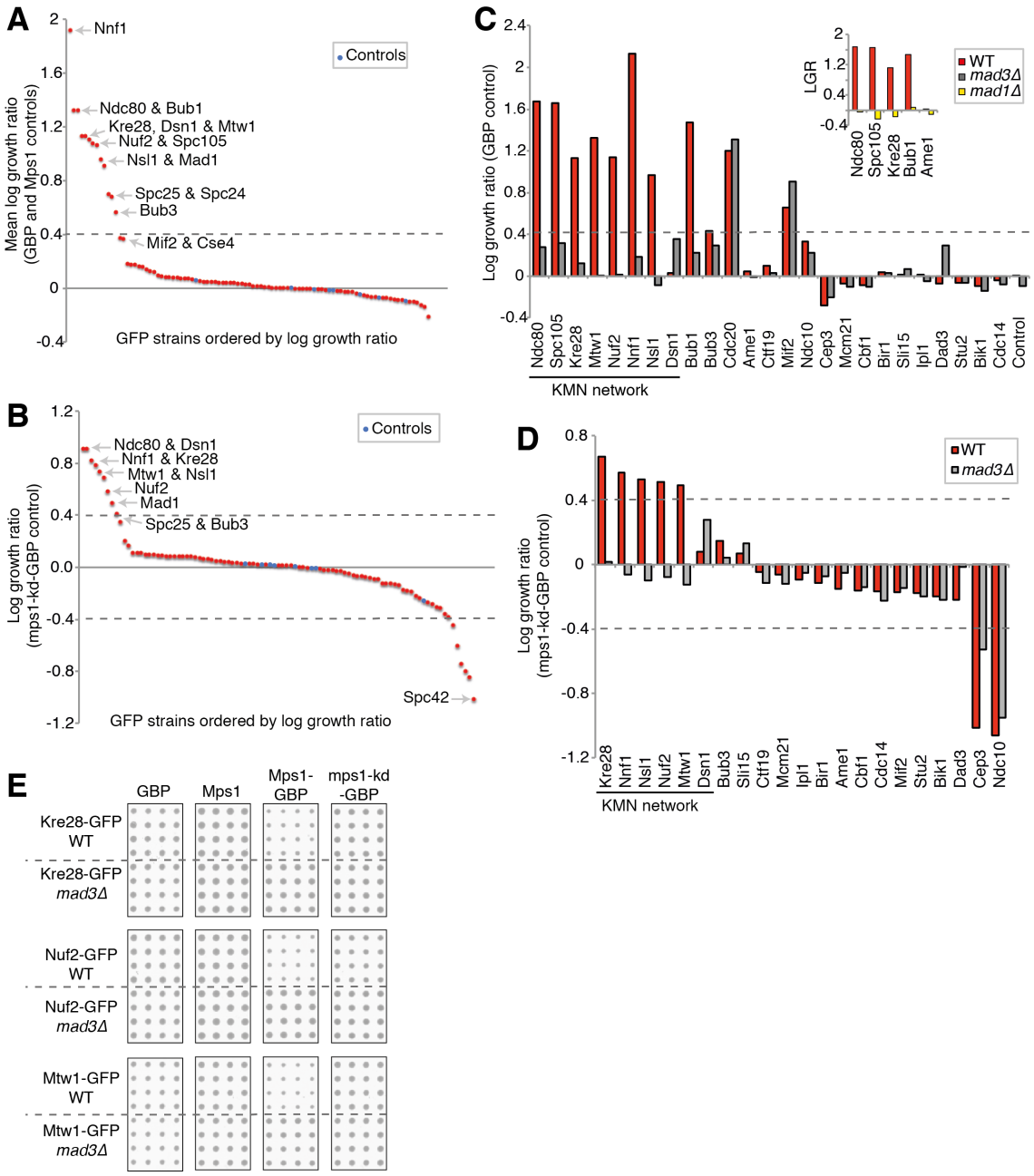

Figure 4.11 Mps1 kinetochore SPIs

A) The kinetochore SPI data with the average log growth ratios of Mps1-GBP compared to GBP and Mps1 controls plotted (y-axis) for each GFP strain (x-axis). Blue dots indicate non-GFP control strain.
B) The Mps1 kinetochore SPI data using mps1-kd-GBP as a control are plotted as in (A).
C) The Mps1 SPI screen was repeated in GFP strains, both wild-type (red) and *mad3*Δ (grey) using the GBP plasmid as control. Insert: five *mad1*Δ GFP strains (yellow bars) were also tested with Mps1-GBP. The log growth ratios (y-axis) are plotted for each GFP strain (x-axis).
D) The Mps1 SPI screen data with wild-type and *mad3*Δ GFP strains using the mps1-kd-GBP as control are plotted as in (C).

E) Cropped images of the Mps1 SPI screen shows colonies of wild-type and *mad3*Δ GFP strains with the different Mps1 plasmids.

I confirmed that the Mps1-GBP was recruited to GFP-tagged kinetochore proteins using fluorescence microscopy (Figure 4.12 A-D). Furthermore, I assessed the cell-cycle progression of five Mps1 SPIs: Nuf2, Nsl1, Mtw1, Kre28 and Bub1, by quantifying large-budded cells which are arrested in mitosis. I only quantified large-budded cells that had the two sister kinetochores in close proximity (i.e. arrested in metaphase) and only cells that had Mps1-GBP-RFP signal colocalised with the kinetochore-GFP signal, and found that all five GFP strains had increased frequency of large-budded cells when expressing Mps1-GBP compared to GBP alone (Figure 4.13 A). As expected and consistent with SAC activation, the large-budded cell phenotype was completely rescued by deleting *MAD3*.

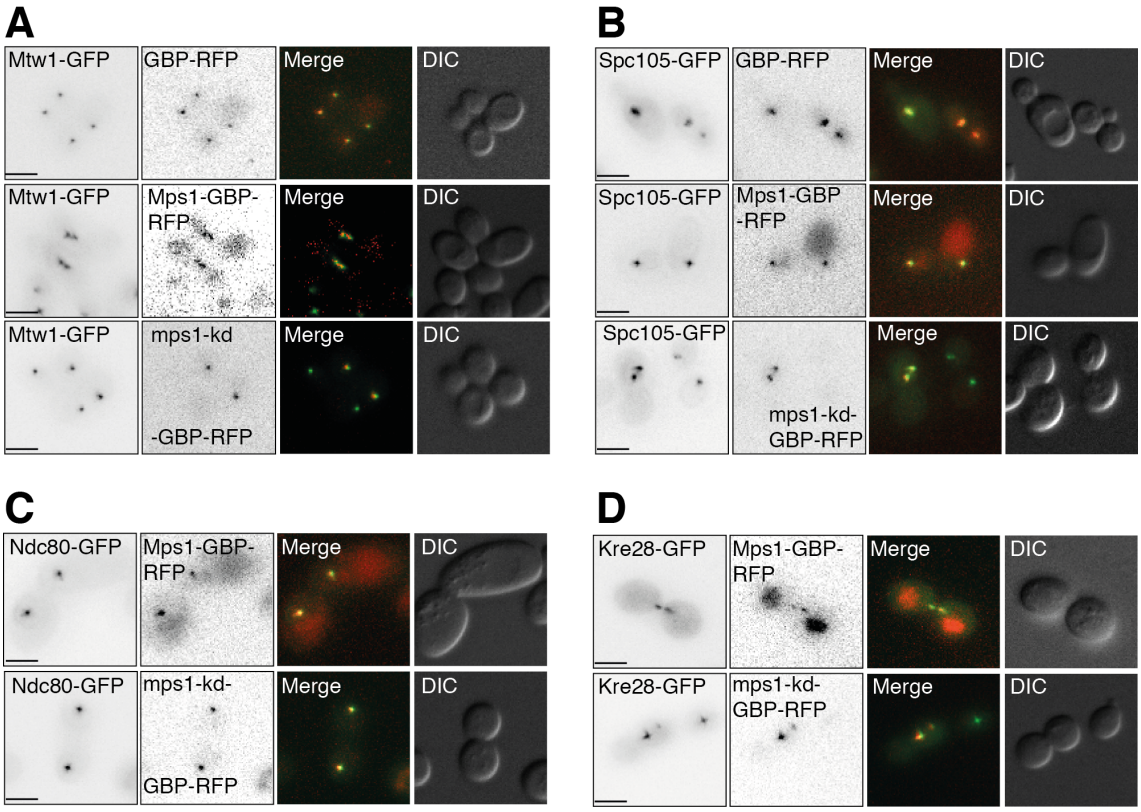

Figure 4.12 Mps1-GBP localises to GFP-tagged kinetochore proteins

A-D) Fluorescence microscopy images of cells with GFP-tagged kinetochore proteins, Mtw1 (A), Spc105 (B), Ndc80 (C), Kre28 (D), containing GBP-RFP, Mps1-GBP-RFP or mps1-kd-GBP-RFP plasmids. All scale bars are 5μm.

Next, I wanted to investigate if I could suppress the Mps1 kinetochore SPIs by increasing the expression of the counteracting phosphatase Glc7 (PP1), which is required for SAC silencing (Maldonado & Kapoor, 2011*b*; Rosenberg *et al.*, 2011). I

repeated the Mps1 SPI assay, but this time I included an additional plasmid in the same cells with the Mps1-GBP and control plasmids, by engineering a plasmid with a different selection marker and expressing *GLC7* under the control of *pCUP1,* and an empty plasmid as a control. Increasing the level of Glc7 did suppress some Mps1-kinetochore SPIs, specifically components of the KMN network, but to a small extent (Figure 4.13 B). In addition, I predicted that if the Mps1-KMN SPIs where activating the SAC through Mps1 phosphorylation of MELT motifs on Spc105 (which Glc7 dephosphorylates) I should be able to suppress the SPIs by expressing a phospho-deficient mutant of Spc105 (*spc105-6A*) that cannot be phosphorylated by Mps1 (London *et al.*, 2012; Primorac *et al.*, 2013). I thus repeated the Mps1 kinetochore SPI assay, including an additional plasmid, along with Mps1-GBP, expressing spc105-6A under the control of a weaker *GAL1* promoter (*pGALS-spc105-6A*). To control for the overexpression of *spc105-6A,* I also combined this plasmid in cells containing the GBP control plasmid. This screen revealed that out of the GFP strains containing Mps1-GBP and spc105-6A plasmids, all the KMN-GFP strains had a reduced growth defect compared to strains containing Mps1-GBP and empty control plasmids (Figure 4.13 B). However, the inclusion of *spc105-6A* did not completely rescue the growth phenotype, which can be partially explained by the fact that the strains do contain the endogenous wild-type *SPC105* allele, thus retrospectively, it would have been worth repeating this experiment in cells containing an endogenous *spc105-6A* allele. Interestingly, neither the Mps1 SPIs with Bub1 or Bub3 were suppressed by either of the plasmids (*pCUP1-GLC7* or *pGALS-spc105-6A*), despite being rescued by *mad3*Δ, suggesting that SAC activation by the forced Mps1 association with Bub1 (a Mps1 substrate) may act independently from the phosphorylated MELT repeats on Spc105.

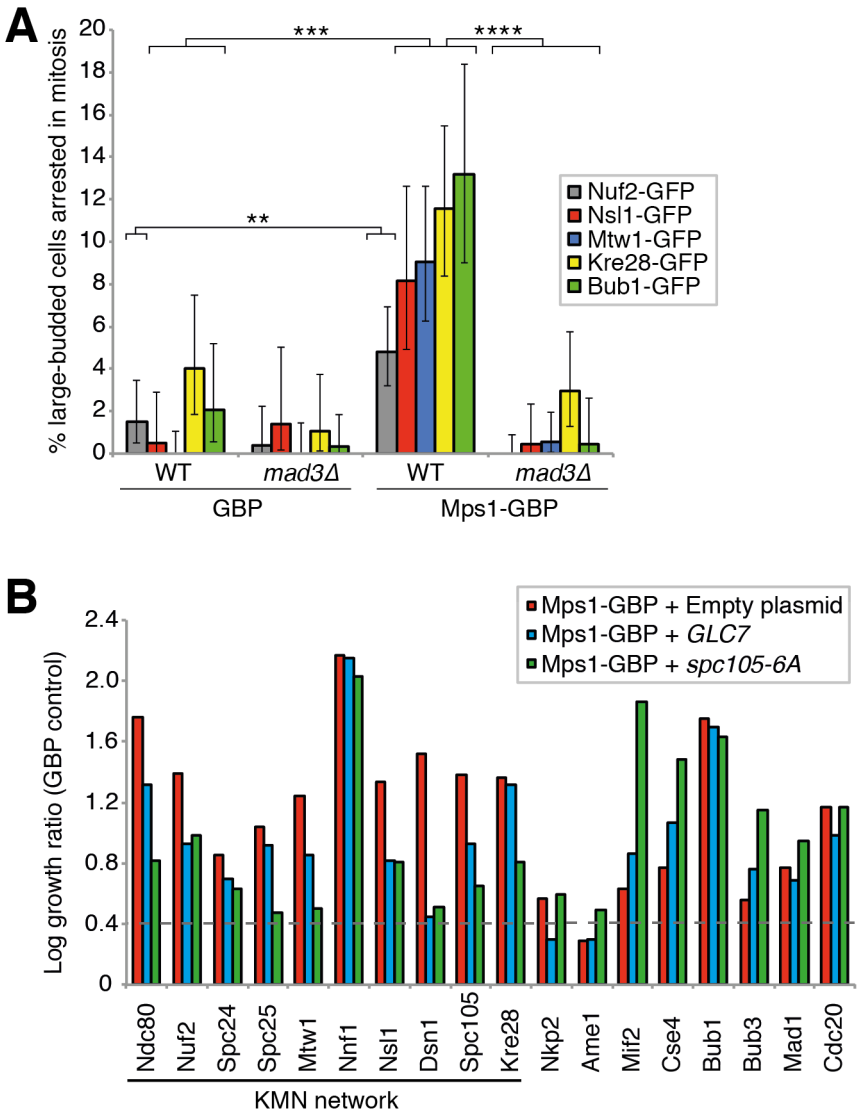

Figure 4.13 Forced Mps1 kinetochore association activates the SAC

A) Quantification of large-budded cells arrested in mitosis of GFP wild-type and *mad3*Δ strains containing the GBP or Mps1-GBP plasmids. Large-budded cells with separated kinetochore foci and/or without a GBP-RFP signal were discounted. Statistical analysis was done using Fishers exact test; **** = $p < 0.0001$. *** = $p < 0.001$, ** = $p < 0.01$. Error bars indicate 95% binomial confidence intervals.
B) The Mps1 kinetochore SPI screen was repeated with the 88 kinetchore GFP strains containing Mps1-GBP and compared to GBP control. In addition, three separate plasmids were also transferred simultaneously into these GFP strains, one empty, one with *pCUP1-GLC7*, and the third with *pGALS-spc105-6A*. A selection of the resulting data shows the log growth ratios (y-axis) plotted for each GFP strain (x-axis); these data show that both increased expression of *GLC7* (blue bars), and overexpression of *spc105-6A* (green bars), suppress the Mps1 SPI growth phenotype specifically at the KMN network compared to the empty plasmid (red bars).

These data are consistent with the notion that Mps1 kinase is the key driver of SAC activation, and that association of Mps1 with the kinetochore is sufficient and

necessary for a robust SAC response. To summarise my findings with Mps1, I mapped the Mps1 kinetochore SPIs onto a schematic of the kinetochore in Figure 4.14 to emphasise the result that forced Mps1 associations specifically with KMN network components results in a SAC-dependent growth arrest.

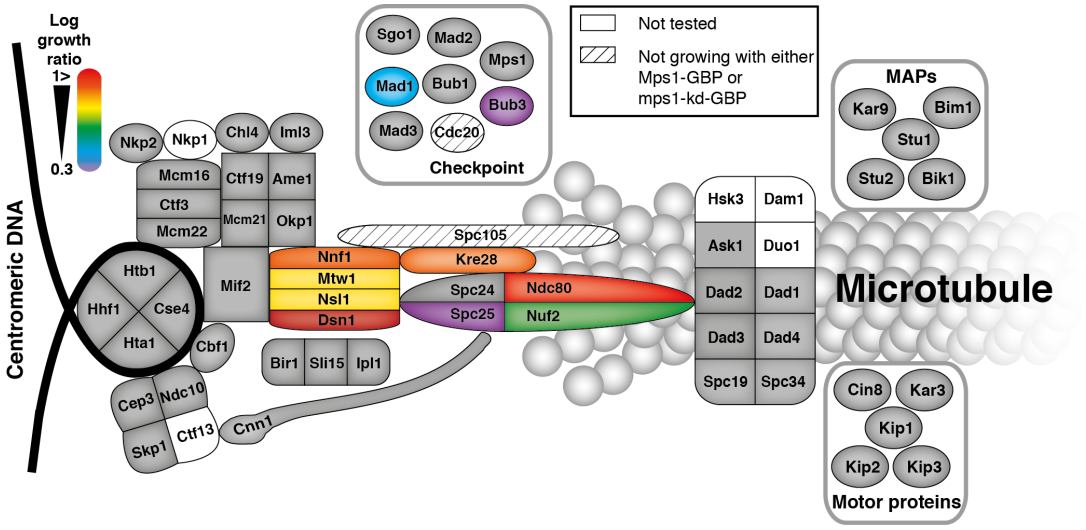

Figure 4.14 Mps1 kinetochore SPI map

The Mps1 kinetochore SPIs using the GBP-tagged kinase-dead Mps1 (mps1-kd-GBP) as a control are mapped onto a schematic of the kinetochore and are colour-coded according to the strength of the SPI phenotype (red indicates a high log growth ratio).

4.3 Discussion

In the previous chapter, to identify kinetochore regulators using SPIs, I was surprised not to detect any components of the SAC. I thus set out to test systematically where SAC protein localisation would be sufficient for SAC activation. In a proteome-wide Mad2 SPI screen I identified proteins related to kinetochore function and chromosome segregation, as well as proteins at the nuclear periphery, such as components of the nuclear pore complex which have been shown to recruit Mad1-Mad2 to generate a pre-mitotic SAC signal (Rodriguez-Bravo *et al.*, 2014). However, I failed to identify any kinetochore proteins except for Cse4. Cse4 is an improbable target for the SAC at the kinetochore and the C-terminal fusions to Cse4 likely disrupt the inner kinetochore structure. Therefore, I think the data gathered from analysing the forced Mad2 interaction with Cse4 raise an interesting dilemma for studying SAC activation in general, especially using artificial recruitment of proteins to the kinetochore, since

these interactions can lead to indirect SAC activation. For example, in the case of the Mad2-Cse4 interaction, the growth defect was rescued when the SAC was inactivated. Furthermore, when I forced mutants of Mad2 to Cse4 they did not produce, or gave a weaker, SPI growth phenotype compared to the wild-type or closed Mad2. It is possible that the wild-type Mad2, unlike the mutants, is able to interact with other proteins such as Mad1 and Cdc20 and thus co-recruiting them producing a stronger SPI phenotype; however this has to be tested experimentally. In recent studies, it was shown that the SAC can indeed be activated artificially and independently of the kinetochore and nuclear envelope (Yuan *et al.*, 2016; Chen *et al.*, 2017).

I was able to show that when a localisation-mutant of Mad1 (*mad1-RLK-AAA*) is forced to the SPC105 complex (specifically Kre28) via the GBP-GFP association it can participate in SAC activation by rescuing benomyl sensitivity in a *mad1*Δ strain, suggesting that the GBP fusion is not inhibiting the SAC response. However, when this mutant was untethered or forced to other kinetochore proteins, including Spc105 (C-terminal) and Bub1, it did not rescue benomyl sensitivity, highlighting the importance of accurate positioning of Mad1 at the kinetochore for effective SAC activation. Combined, these SPI data support a model in which the kinetochore recruitment of Mad1-Mad2, like Bub1-Bub3, while necessary, is not sufficient for robust SAC activation. Previous work in budding yeast has indirectly implied similar findings, for example, tethering the Mad1 binding domain of Bub1 to the N terminus of Spc105 increased recruitment of Mad1 to kinetochores but did not arrest growth, and was able to participate in the SAC, via suppression of benomyl sensitivity in cells containing a mutant Spc105 (*spc105-6A*) lacking phosphorylatable MELT motifs (London & Biggins, 2014). It is a possibility that some Mad1 or Mad2 kinetochore SPIs do activate the SAC, but that this activation is not maintained, since cells may adapt to a persistent checkpoint signal. This could result in a very subtle growth defect and the SPI system might not be sensitive enough to assay this, thus this may be better assayed using a conditional interaction system. However, artificial recruitment Mad1 to Mtw1 was shown to be insufficient to activate SAC using a conditional system (Aravamudhan *et al.*, 2015).

Conversely to the Mad1 and Mad2 SPI results, Mps1 produced a SAC-dependent growth defect when it was forcibly associated specifically with the KMN network of central and outer kinetochore components, consistent with other studies (Jelluma *et al.*,

2010; Ito *et al.*, 2012; Aravamudhan *et al.*, 2015; Dou *et al.*, 2015; Maciejowski *et al.*, 2017). Additionally, in agreement with the SPI between Mps1 and Mad1, overexpression of *MPS1* results in hyperphosphorylation of Mad1 and SAC activation (Hardwick *et al.*, 1996; Brady & Hardwick, 2000). Moreover, these data support the notion that Mps1 kinetochore activity is required for maintaining SAC activation by its involvement in catalysing the steps of the SAC cascade (Hewitt *et al.*, 2010; Maldonado & Kapoor, 2011*a*; Tipton *et al.*, 2013). In conclusion, the SPI data described here are consistent with the kinase activity of Mps1 being the critical regulator of the SAC, and unlike Mad1 and Mad2, is both necessary and sufficient for SAC activation when recruited to the KMN network.

Chapter 5. Results 3: Investigating the kinetochore function of the budding yeast Polo-like kinase, Cdc5

5.1 Introduction

Polo-like kinases (Plk1 in humans and Cdc5 in budding yeast, hereafter referred to as Polo kinases) are serine/threonine kinases, which are important for cell cycle progression in eukaryotes, and whose activity is tightly regulated during the cell cycle, both spatially and temporally. Polo kinases are highly conserved and the human Plk1 can complement the loss of Cdc5 activity in budding yeast (Lee & Erikson, 1997). Cdc5 is the only polo kinase in budding yeast and has multiple roles during the cell cycle, such as DNA damage checkpoint adaptation, cohesin regulation, SPB separation, mitotic entry and exit, cytokinesis, and meiosis (Toczyski *et al.*, 1997; Song & Lee, 2001; Bartholomew *et al.*, 2001; Hu *et al.*, 2001; Alexandru *et al.*, 2001; Clyne *et al.*, 2003; Geymonat *et al.*, 2003; Lee, 2003; Sakchaisri *et al.*, 2004; Crasta *et al.*, 2008; Vidanes *et al.*, 2010; Rock & Amon, 2011; Attner *et al.*, 2013; Ratsima *et al.*, 2016; Mishra *et al.*, 2016). The unique composition of polo kinases is characterised by a N-terminal catalytic kinase domain that is flexibly linked to a binding domain called Polo-box domain (PBD) whose key function is to target the kinase domain to its substrates by binding preferentially phosphosites that have previously been phosphorylated by another kinase, most commonly by cyclin-dependent kinase (CDK) or polo kinase itself (reviewed in: Park *et al.*, 2010) (Figure 5.1 A&B). The PBD preferentially binds phosphopeptides containing consensus sequence Ser-[pSer/pThr]-[Pro/X] (where X is any amino acid and p is phosphorylated residue) and the kinase domain has the preferred substrate consensus motif [Asp/Glu]-X-[Ser/Thr]-Φ (where Φ is a hydrophobic amino acid), although it has been proposed that it should be broadened to Leu-Φ-[Glu/Asn/Asp(Gln)]-X-[Ser/Thr]-Leu-Φ (Santamaria *et al.*, 2011).

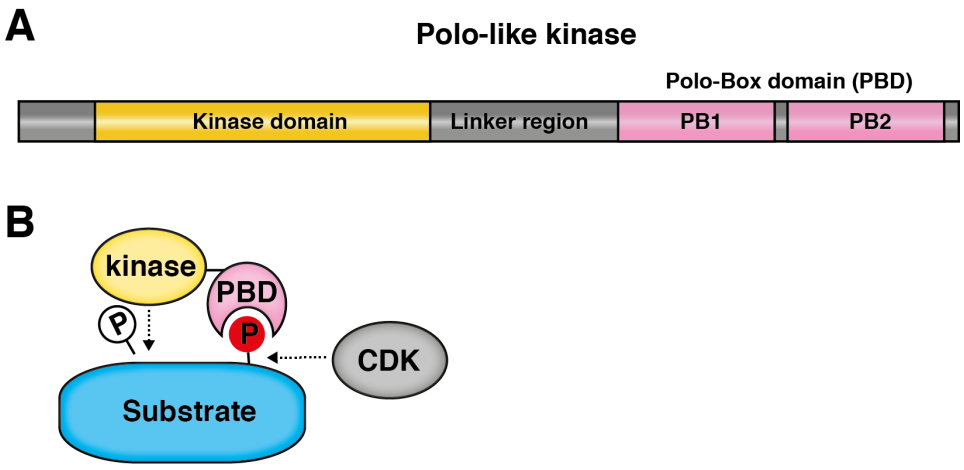

Figure 5.1 Polo-like kinase features.

A) The key domains of polo kinase are the N-terminal kinase domain and the C-terminal non-catalytic domain contains two polo-boxes (PB1 and PB2) called the polo-box domain (PBD) and a flexible linker region that joins the kinase domain and PBD. **B**) The PBD binds to previously phosphorylated sites (commonly by CDK) which targets the kinase domain of polo to its substrates and facilitates the phosphorylation at another site on the same substrate or at sites on surrounding substrates.

5.1.1 Polo kinase and cancer

Metazoans usually have multiple polo-like kinases, for example humans have five (Plk1-5) (reviewed in: De Cárcer *et al.*, 2011). Plk1 is most intensively studied in higher organisms and it is becoming increasingly clear that its functions are important for cancer development. Disruption of polo kinase activity generally results in misaligned pre-anaphase spindle and thus affects normal anaphase progression (Snead *et al.*, 2007). Plk1 is overexpressed in many cancer cells and is associated with poor prognosis and resistance against some anticancer treatments (reviewed in: Degenhardt & Lampkin, 2010; Strebhardt, 2010; Gutteridge *et al.*, 2016). Depletion of Plk1 has been shown to induce G2-M phase arrest and apoptosis in cancer cells (Liu & Erikson, 2003; Harris *et al.*, 2012; Amani *et al.*, 2016). Therefore, it is no surprise that both the catalytic domain and the PBD are proving to be important drug targets. Indeed, many Plk1 inhibitors are currently in clinical trials and some are showing real potential, either used alone or in combination with other therapies (Gjertsen & Schöffski, 2014; Park *et al.*, 2015*b*; Gutteridge *et al.*, 2016).

5.1.2 Polo kinase kinetochore function

Insights into polo kinase's role in kinetochore regulation has been accumulating in recent years. In mammalian cells, it has been shown that initial kinetochore recruitment of Plk1 requires CENP-U-Q complex (CENP-U, also known as PBIP1, and CENP-Q, are orthologs of yeast Ame1 and Okp1, respectively) and it is proposed that Plk1 phosphorylation of CENP-U-Q self-regulates the interaction between Plk1 and CENP-U-Q and then later in mitosis results in CENP-U-Q removal from the kinetochore, allowing Plk1 to interact with other kinetochore targets (Kang *et al.*, 2006, 2011; Lee *et al.*, 2008; Park *et al.*, 2015*a*). Furthermore, the localisation of both NudC (a dynein-associated protein) and CENP-F (a kinesin-7 motor protein) to the outer kinetochore in early mitosis is dependent on Plk1 activity in human cells (Nishino *et al.*, 2006; Santamaria *et al.*, 2011). Plk1 then directs NudC and CENP-F to relocalise to the spindle midzone in anaphase and to the midbody in telophase (Aumais *et al.*, 2003; Zhou *et al.*, 2003; Ma *et al.*, 2006).

The precise mechanisms behind these processes remain unclear, but it is thought that Plk1 activity at the outer kinetochore is involved in regulating microtubule attachment. Correct kinetochore-microtubule attachment is controlled by a complex network of kinases and phosphatases during mitosis to promote faithful chromosome segregation. Additionally, Plk1 has been shown to phosphorylate residues on several microtubule-associated proteins, such as plus-end microtubule protein CLASP2 (homolog of yeast Stu1), and the kinesin-13 proteins Kif2b and Kif2c (also known as MCAK) (Zhang *et al.*, 2011; Maia *et al.*, 2012; Hood *et al.*, 2012). CLASP2 is phosphorylated by CDK, thus priming Plk1 recruitment which phosphorylates CLASP2 at another site resulting in stabilisation of kinetochore-microtubule attachments and satisfaction of the spindle assembly checkpoint (SAC; discussed further below in section 5.1.3.) (Maia *et al.*, 2012). In contrast, Plk1 phosphorylation at C-terminal residues of MCAK promotes its microtubule depolymerising activity and thus increases microtubule dynamics and improves correction of erroneous kinetochore-microtubule attachments (Zhang *et al.*, 2011). However, it has also been shown that Plk1 phosphorylates another residue at MCAK resulting in its degradation by APC/C-Cdc20 (Sanhaji *et al.*, 2014).

After completion of mitosis, Plk1 has been observed to localise to centromeres in G1 phase to signal CENP-A deposition through phosphorylation of Mis18 complex in a process necessary to ensure genomic integrity (McKinley & Cheeseman, 2014). In

budding yeast, Cdc5 was identified to interact with the yeast CENP-A homolog Cse4 in vivo (Snead *et al.*, 2007). Although the purpose for this interaction has not been revealed, it has been shown that the centromeric localisation of Cdc5 enables the removal of cohesin from the pericentromere during mitosis (Mishra *et al.*, 2016).

These studies point to different roles for polo kinase, spanning the entire length of the kinetochore. Recently, it was suggested that Plk1 functions in different pools at the centromere-kinetochore axis in human cells (Lera *et al.*, 2016). In this study, using direct genetic fusion constructs of tethered Plk1 with inner centromere and outer kinetochore genes, the authors showed that the fusions produced different functional and phosphoproteomic signatures. Furthermore, in order to assess where Plk1 operates functionally they tested these different fusions of Plk1 lacking PBD (Plk1ΔC) with different centromeric/kinetochore components for complementation. They found that a Plk1ΔC-Kif2c fusion, which localises Plk1 to both inner centromere and outer kinetochore, rescued accurate chromosome alignment and segregation in cells with compromised Plk1 activity. However, Plk1ΔC fusions with histone H2B, and outer kinetochore components Dsn1 and Ndc80, and SAC components Bub1 and BubR1 all failed to rescue chromosome segregation and alignment, except Plk1ΔC-H2B which did rescue chromosome alignment (Lera *et al.*, 2016).

Finally, it is interesting to note that in distantly related kinetoplastids, which lack most of the conventional kinetochore proteins, the PBD of polo has evolved into several structural kinetochore components, suggesting a role for polo at the kinetochore early in eukaryotic evolution (Akiyoshi & Gull, 2014; Nerusheva & Akiyoshi, 2016). Indeed, based on evolutionary studies of the kinetochore the polo kinase is inferred of being present in the last eukaryotic common ancestor (LECA) (Hooff *et al.*, 2017).

5.1.3 Polo kinase and the spindle assembly checkpoint

In many metazoans, polo kinase is involved in SAC activation and/or maintenance. However, there is conflicting evidence that also point to polo kinase involvement in both stabilising microtubule-kinetochore attachment and SAC silencing. One key kinetochore target of Plk1 is the SAC component BubR1 (human homolog of yeast Mad3). However, it was thought that Plk1 phosphorylation of BubR1 in prometaphase was not directly required for checkpoint function in human cells, but instead was critical for stabilising microtubule-kinetochore attachment and chromosome alignment on the

mitotic spindle (Elowe *et al.*, 2007; Matsumura *et al.*, 2007; Foley *et al.*, 2011). Phosphorylation of the BubR1 KARD motif by Plk1 facilitates direct binding of BubR1 with the PP2A-B56α phosphatase which in turn dephosphorylates Aurora B targets at the kinetochore thus counteracting the microtubule destabilising effects of Aurora B (Suijkerbuijk *et al.*, 2012). More recently it was shown that the kinetochore phosphatase activity of PP2A is directly involved in SAC silencing (Nijenhuis *et al.*, 2014; Espert *et al.*, 2014). This, therefore, indicates an indirect, Plk1-dependent role of SAC silencing, since the Aurora B antagonising activity of PP2A at the kinetochore depends on Plk1 phosphorylation of BubR1 (Figure 5.2).

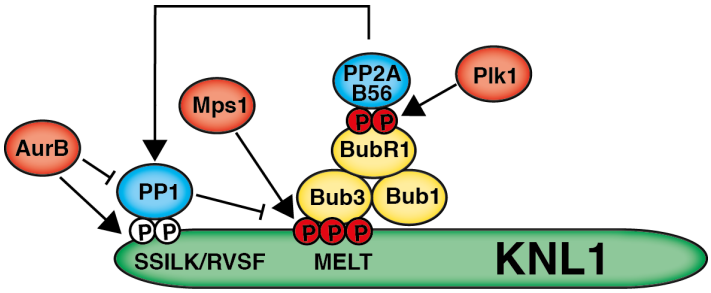

Figure 5.2 Schematic describing the role of Plk1 in SAC silencing.

When kinetochores have achieved correct microtubule attachment Plk1 phosphorylates BubR1 (P-labelled red dots) which recruits PP2A to kinetochores. PP2A dephosphorylates N-terminal Aurora B sites on KNL1(P-labelled white dots) resulting in PP1 recruitment. PP1 in turn dephosphorylates KNL1 MELT motifs leading to decoupling of SAC components and ultimately checkpoint silencing.

However, this is in direct contrast to many other metazoans, in which polo-like kinase directly activates the SAC. For example, *Xenopus lævis*, in which polo kinase Plx1 phosphorylates BubR1 to generate a SAC signal (Wong & Fang, 2007). And in *Cænorhabditis elegans*, which lacks Mps1, PLK-1 instead phosphorylates KNL-1 to activate the SAC (Espeut *et al.*, 2015). Indeed, in human cells it was recently argued that Plk1 supports Mps1 activation and KNL1 MELT motif phosphorylation (von Schubert *et al.*, 2015). Similarly, in *Drosophila melanogaster,* Polo kinase is required to recruit Mps1 to unattached kinetochores and generate the SAC signal (Donaldson *et al.*, 2001; Conde *et al.*, 2013). Moreover, it was recently shown that Plk1 activity was required for maintaining Aurora B localisation at kinetochores and a robust SAC response (O'Connor *et al.*, 2015). Further, in support of the SAC role of polo kinase, its removal from kinetochores seems to be critical for SAC silencing. The Lampson laboratory has shown that cells with persistent Plk1 activity at the kinetochore fail to silence the SAC, suppress microtubule dynamics, and accumulate attachment errors (Liu *et al.*, 2012). Conversely though, they also report that Plk1 kinetochore localisation

is required for the stabilisation of initial kinetochore-microtubule attachments in early mitosis and interestingly, that the prevention of Plk1 kinetochore activity results in SAC activation. Finally, recent evidence suggests another role for Plk1 in SAC activation, through Plk1 interacting with Bub1 and BubR1 at the kinetochore to phosphorylate Cdc20 and thereby directly inactivating APC/C independently of the mitotic checkpoint complex (MCC) (Jia *et al.*, 2016).

5.1.4 Polo-like kinase regulation in yeast mitosis

All of these studies highlight the importance of polo kinase's cell cycle-dependent function for accurate chromosome segregation, mitotic progression, and to facilitate and/or silence the SAC in metazoan cells. However, its precise role remains elusive. Moreover, it is even less clear how polo kinase functions at the kinetochore, or if it even has a SAC role, in yeast cells. As noted above, polo kinase has many important functions in fission and budding yeast. Descriptions of these functions are beyond the scope of this work and here I will mostly focus on its mitotic roles.

Cdc5 activity peaks during mitosis and is triggered by Cdc28 phosphorylation of an evolutionary conserved residue, threonine 242. A mutation of this residue (T242A) prevents cell growth (Mortensen *et al.*, 2005; Rodriguez-Rodriguez *et al.*, 2016). Interestingly, phosphorylation of Plk1 by Aurora A and B kinases at the equivalent threonine (T210) in human cells is required for Plk1 activation (Macůrek *et al.*, 2008; Seki *et al.*, 2008; Carmena *et al.*, 2012*a*; Shao *et al.*, 2015). Furthermore, Cdc28-dependent phosphorylation of a N-terminal threonine (T70) is important for Cdc5 activity in the mitotic exit network (MEN) (Rodriguez-Rodriguez *et al.*, 2016).

As highlighted above, Cdc5 localisation is controlled by the PBD. The spatial distribution of Cdc5 is tightly regulated and is crucial for its different functions during the cell cycle. Cdc5 localises to the nucleus and SPBs during mitosis, and to the bud neck in later stages of the cell cycle, and mutants that disrupt PBD function result in mislocalisation of Cdc5 (Song *et al.*, 2000; Ratsima *et al.*, 2011). In late anaphase, Cdc5 is released from the nucleus in a Cdc14-dependent manner, and blocking this release leads to mitotic exit defects (Botchkarev *et al.*, 2014). Indeed, it was recently shown that to deactivate the MEN inhibitor, Bfa1, Cdc5 has to translocate from the nuclear site of the daughter SPB to the cytoplasmic site of the daughter SPB, where Bfa1 is located (Botchkarev *et al.*, 2017). Moreover, overexpression of PBD (*cdc5ΔN*)

prevents bud neck localisation of endogenous Cdc5 and inhibits cytokinesis (Song & Lee, 2001).

Among the vital roles of Cdc5 during mitosis is the phosphorylation of the CDK inhibitor Swe1 which results in its degradation and promotion of mitotic entry (Bartholomew *et al.*, 2001; Park *et al.*, 2004*b*; Asano *et al.*, 2005). During metaphase, sister chromatid separation is regulated by Cdc5 through phosphorylation of the cohesin subunit Scc1/Mcd1 which leads to cohesin cleavage by separase Esp1 (Uhlmann *et al.*, 1999; Alexandru *et al.*, 2001; Hornig & Uhlmann, 2004). Furthermore, Cdc5 is involved in the early anaphase release of Cdc14 (FEAR network) by phosphorylating both Cdc14 and Net1/Cfi1, a component of the RENT complex, whose role is to sequester Cdc14 in the nucleolus (Shou *et al.*, 2002; Visintin *et al.*, 2003; Rahal & Amon, 2008). The released Cdc14 phosphatase subsequently reverses CDK activity, activates APC/C-Cdh1, and stabilises the anaphase spindle by dephosphorylating Sli15, a subunit of the CPC, which results in CPC relocalisation from kinetochores to the spindle midzone (Pereira & Schiebel, 2003; Mirchenko & Uhlmann, 2010). The Cdc5-dependent release of Cdc14 is crucial for the mitotic exit network (MEN) in which Cdc5 plays additional roles through signalling at spindle poles, such as phosphorylating and inhibiting a MEN inhibitor Bfa1 and activating a MEN promoter Cdc15 (Hu *et al.*, 2001; Geymonat *et al.*, 2003; Rock & Amon, 2011). Taken together, these Cdc5 functions highlight the importance of Cdc5 activity to drive cell cycle progression.

The level of Cdc5 protein is also tightly regulated during the cell cycle. Degradation of Cdc5 at G1 phase is controlled by the ubiquitin ligase APC/C-Cdh1 pathway which recognises degron motifs at the N terminus of Cdc5 (Shirayama *et al.*, 1998; Arnold *et al.*, 2015). In turn though, Cdh1 is inhibited by Cdc5 (and Cdc28) phosphorylation in a process important for SPB separation (Crasta *et al.*, 2008). Cdc5 is also controlled by an APC/C-Cdh1-independent mechanism which requires phosphorylation of N-terminal residues on Cdc5 for its degradation, possibly by Pkc1 kinase (Simpson-Lavy *et al.*, 2015), and in addition, by Cdc28 to maintain Cdc5 levels during G2-phase (Simpson-Lavy & Brandeis, 2011). Ultimately, the degradation of Cdc5 is critical for the return of Cdc14 phosphatase to the nucleolus and subsequently silencing both FEAR and MEN (Visintin *et al.*, 2008). To sum up, Cdc5 is responsible for its own destruction by releasing Cdc14, which in turn activates APC/C-Cdh1, resulting in ubiquitylation of Cdc5 and eventually destruction by the proteasome.

In fission yeast, the polo kinase orthologue, Plo1, was reported to support biorientation of chromosomes during metaphase by phosphorylating Dam1, an member of the DAM1/DASH complex (Buttrick *et al.*, 2012). Cdc5 in budding yeast is required for proper microtubule dynamics and growth, and has been reported to phosphorylate Stu2 and Slk19, microtubule-associated proteins (MAPs) that are involved in mitotic spindle and kinetochore function (Park *et al.*, 2008). Interestingly, Plo1 phosphorylation the Alp7-Alp14 complex (fission yeast orthologue of human TACC-TOG and budding yeast Stu2) promotes its meiosis-specific association with the Ndc80 complex at unattached kinetochores, and thus facilitates microtubule attachment (Kakui *et al.*, 2013).

Additionally, during SAC activation, Mad3 (the yeast ortholog of BubR1) is phosphorylated in a Cdc5-dependent manner (and to a lesser extent Ipl1) (Rancati *et al.*, 2005). Although, it has not been proven in budding yeast whether or not this occurs at the kinetochore and if indeed whether this leads to PP2A recruitment as previously described for human cells. Finally, as stated before, Cdc5 localises to centromeres during mitosis to facilitate the removal of cohesin (Mishra *et al.*, 2016) and physically interacts with kinetochore components, Cse4 and Ndc80 in vivo (Snead *et al.*, 2007).

Although, the roles of these interactions with kinetochore components remain elusive, collectively these data as well as the results described in chapter 3 (forced Cdc5 kinetochore association caused a growth defect, and in one case, chromosomal instability), show that Cdc5 likely plays complex roles at the kinetochore in regulating different aspects of mitosis. To address the question of how this single kinase can act on multiple kinetochore substrates, I aimed to use the SPI methodology to separate some of these functions spatially.

5.2 Results and discussion

5.2.1 Proteome-wide Cdc5 SPI screen

Using the SPI methodology to identify kinetochore regulators, the polo kinase, Cdc5, stood out as a mitotic kinase that has established links to kinetochore function (See Figure 3.4 and Figure 3.18 in chapter 3). To initially ask which proteins are most sensitive to Cdc5 localisation, I fused Cdc5 to GBP and transferred this to the whole

GFP collection as before. This proteome-wide approach allows me to examine the growth defects caused by interaction with the kinetochore in the context of all other forced interactions throughout the cell.

I created a plasmid encoding Cdc5-GBP and a number of control plasmids including: untagged Cdc5 to control for ectopic expression of Cdc5, a kinase-deficient version of Cdc5 (cdc5-K110A) (Charles *et al.*, 1998) to investigate the catalytic activity of Cdc5, and a kinase-deficient version that also lacks the PBD phospho-binding activity (cdc5-K110A, W517F, H641A, K643M; cdc5-KA-FAM) to control for the PBD function of Cdc5 (Elia *et al.*, 2003; Snead *et al.*, 2007; Chen & Weinreich, 2010) (Figure 5.3 A&B).

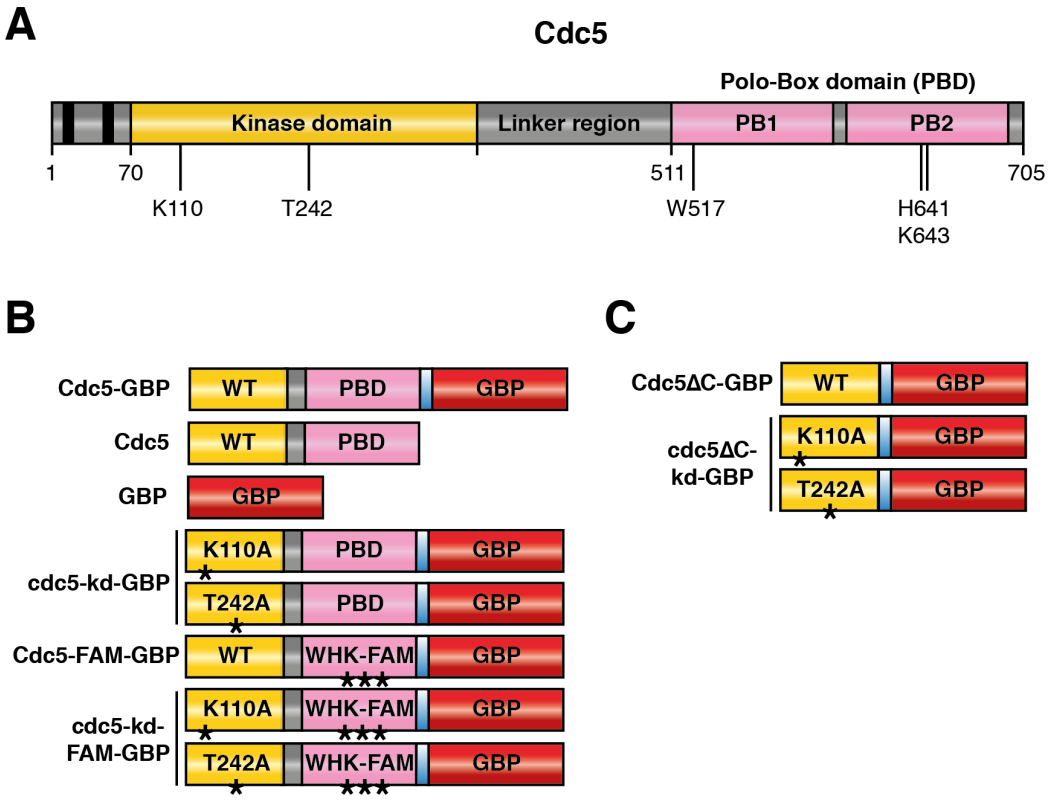

Figure 5.3 Cdc5-GBP constructs and controls for the Cdc5 SPI assay.

A) Sites on Cdc5 that are crucial for its kinase activity and PBD function. See detailed description in the text. Briefly, mutations of K110 and S242 to alanines disable catalytic activity of Cdc5. Mutations of W517, H641 and K643 to F, A, M, respectively to inhibit PBD binding to substrates (the two black bars at the N terminus represent the D-boxes).
B) The Cdc5-GBP constructs and controls used in the SPI assays. Expression of all constructs are controlled by *CUP1* promoter. The blue regions between PBD and GBP represent flexible eight amino acid linkers.
C) Additional Cdc5 constructs; lacking the C-terminal PBD. See text in section 5.2.6 for details.

I combined each of these Cdc5 plasmids separately with the members of the GFP collection and scored the resulting strains for growth as previously described. I find that approximately 100 GFP strains show growth defects when comparing the active kinase with any of the controls (Figure 5.4 A). What was striking from these data was the number of kinetochore proteins represented in this set of Cdc5 SPIs (GO enrichment p value = 3×10^{-15}; Table 5.1). I used fluorescence microscopy and imaged a selection of these strains to demonstrate that Cdc5 was indeed constitutively recruited to many different cellular locations, including the kinetochore (Figure 5.4 B).

Table 5.1 Gene Ontology analysis of Cdc5 SPIs

Process	Gene name
Chromosome segregation (2.4×10^{-10})	*DSN1, MTW1, NSL1, NDC80, NUF2, SPC24, SPC25, MCM21, NKP2, MIF2, DAD1, DAD2, DAD3, SLI15, SMC2*
Function	
Microtubule binding (8.01×10^{-6})	*BIM1, SPC97, SPC98, DAD1, DAD2, DAD3, SPC105*
Component	
Kinetochore (3.35×10^{-15})	*DSN1, MTW1, NSL1, NDC80, NUF2, SPC24, SPC25, KRE28, SPC105, MCM21, NKP2, AME1 MIF2, DAD1, DAD2, DAD3, SLI15, MAD1*
RNA polymerase II transcription factor complex (2.66×10^{-6})	*TFB2, MED4, SRB7, ROX3, RGR1, SIN4, TFG1, SPT15, TAF6, TAF12*
SAGA complex (8.84×10^{-5})	*SGF73, SPT20, SGF11, TAF6, TAF12*

GO enrichment analysis was performed using GOrilla online software available on: http://cbl-gorilla.cs.technion.ac.il/

Furthermore, gene ontology enrichment analysis of the Cdc5 SPI data, shows that components of the histone acetyltransferase SAGA complex are sensitive to constitutive Cdc5 association as well as RNA polymerase II transcription factor complex. Interestingly, it has been reported that the catalytic subunit of the SAGA complex, Gcn5, associates with the centromere in budding yeast and is important for chromosome segregation fidelity (Vernarecci *et al.*, 2008). Moreover, the ubiquitylation status of Cse4 is directly influenced by the SAGA complex through its deubiquitylation (DUB) module, suggesting a role for the SAGA complex in regulating Cse4 nucleosome homeostasis (Canzonetta *et al.*, 2015).

These data from the Cdc5 proteome-wide SPI screen are consistent with the data from other kinetochore SPI screens described in chapter 3 that identified Cdc5-GFP as SPIs in four out of 12 SPI screens: Mif2-GBP, Mtw1-GBP, Nuf2-GBP and Kre28-GBP. Most of these SPIs were reproduced in heterozygous diploid screens: Nuf2-GBP, Mtw1-GBP

and Kre28-GBP, but not Mif2-GBP. Collectively these data show that constitutive Cdc5 kinetochore localisation is detrimental for cell growth.

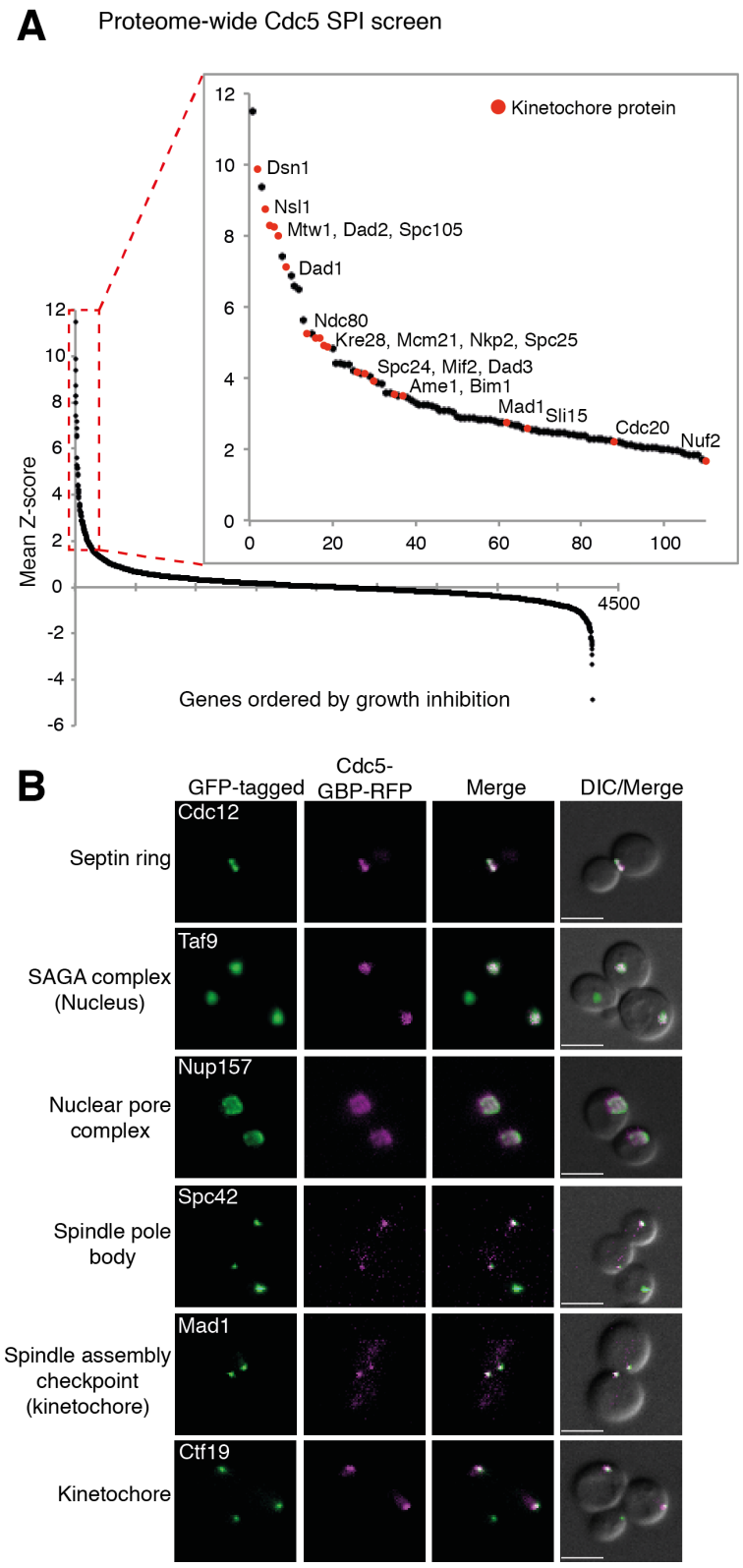

Figure 5.4 Proteome-wide Cdc5 SPI screen

A) The Cdc5 SPI screen identifies ~100 GFP-tagged proteins that produce a growth defect when combined with Cdc5-GBP versus controls (Z-score > 2). Inset: Kinetochore proteins are enriched in the 100 strongest SPIs.
B) Cdc5-GBP is recruited to many different subcellular locations when introduced into GFP strains. All scale bars are 5μm.

5.2.2 Kinetochore specific Cdc5 SPI screen

Since, Cdc5 produces a growth defect when associated with a number of different kinetochore proteins, I decided to rescreen Cdc5 to ask where within the kinetochore a constitutive Cdc5 localisation can produce a growth defect and dissect which subunits are specifically sensitive to constitutive Cdc5 kinase activity. In addition to the Cdc5-GBP, Cdc5 alone, cdc5-KA-GBP and cdc5-KA-FAM-GBP plasmids, I created an additional kinase-dead mutant cdc5-T242A-GBP. Threonine 242 is a CDK phosphosite which has been reported to inactivate Cdc5 when mutated to alanine (Mortensen *et al.*, 2005) (Figure 5.3 A&B). I combined each of these plasmids separately with a subset of the GFP strain collection containing 88 kinetochore and related GFP-tagged proteins and scored the resulting strains for growth as before, but at a higher density of 16 colonies per strain. The Cdc5 kinetochore SPIs I identify using GBP as a control are: all the members of the COMA, MIND and Ndc80 complexes, members of the CCAN; Nkp2 and Ndc10, members of the DAM1/DASH complex; Dad1,2,3,4, members of the chromosomal passenger complex; Ipl1 and Sli15, the microtubule-associated protein Bim1, and checkpoint proteins; Mad1 and Cdc20, and finally Cse4 (Figure 5.5). Using Cdc5 alone or kinase-dead Cdc5 (cdc5-kd; both K110A and T242A mutants) as controls identifies similar kinetochore SPIs, except for Ctf19 and Mcm21; members of the COMA complex, Ndc10, Mtw1, Ipl1 and Sli15. These data show that the MIND, NDC80, COMA and DAM1/DASH subcomplexes are all sensitive to constitutive Cdc5 kinase activity.

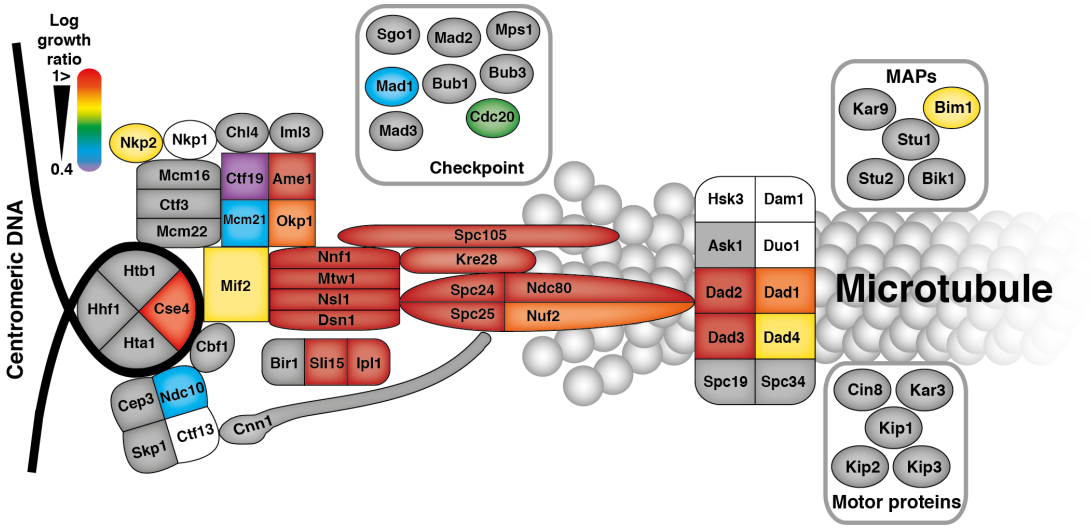

Figure 5.5 Cdc5 kinetochore SPI map.

A colour-coded heat-map depicting the kinetochore subunits that are sensitive to Cdc5 association compared to GBP control. Strong SPIs (log growth ratio > 1) are labelled red and weaker SPIs are purple. Grey-labelled subunits did not show any growth defect compared to GBP control. White label refers to subunits that were not tested. Note that the C terminus of Cse4 is sensitive to manipulation as described in section 4.2.3 in chapter 4, for this reason this SPI was examined using the internally GFP-tagged Cse4 and described later in section 5.2.7.

5.2.3 Kinase-dead Cdc5 kinetochore SPIs

Surprisingly, I find that many kinase-dead Cdc5 (cdc5-kd) kinetochore associations also produce a growth defect compared with the GBP control. However, it is a weaker effect than kinase-active Cdc5 and also with a smaller group of kinetochore proteins. These cdc5-kd SPIs include the KMN network: Mtw1, Dsn1, Spc105, Spc24, Spc25, Ndc80 and also Ame1, Cse4, Ipl1 and Sli15. The DAM1/DASH complex was also affected by constitutive cdc5-kd localization, but to a much lesser extent (Figure 5.6 A). Since both K110A and T242A kinase-dead mutants produce similar effects I will refer to both of them as cdc5-kd. Figure 5.6 B shows a kinetochore SPI map with the overlap of the kinase-active and kinase-dead Cdc5 kinetochore interactions. Consensus Cdc5 sites (phosphosites and PBD binding sites; black and white dots) are also overlaid on this map.

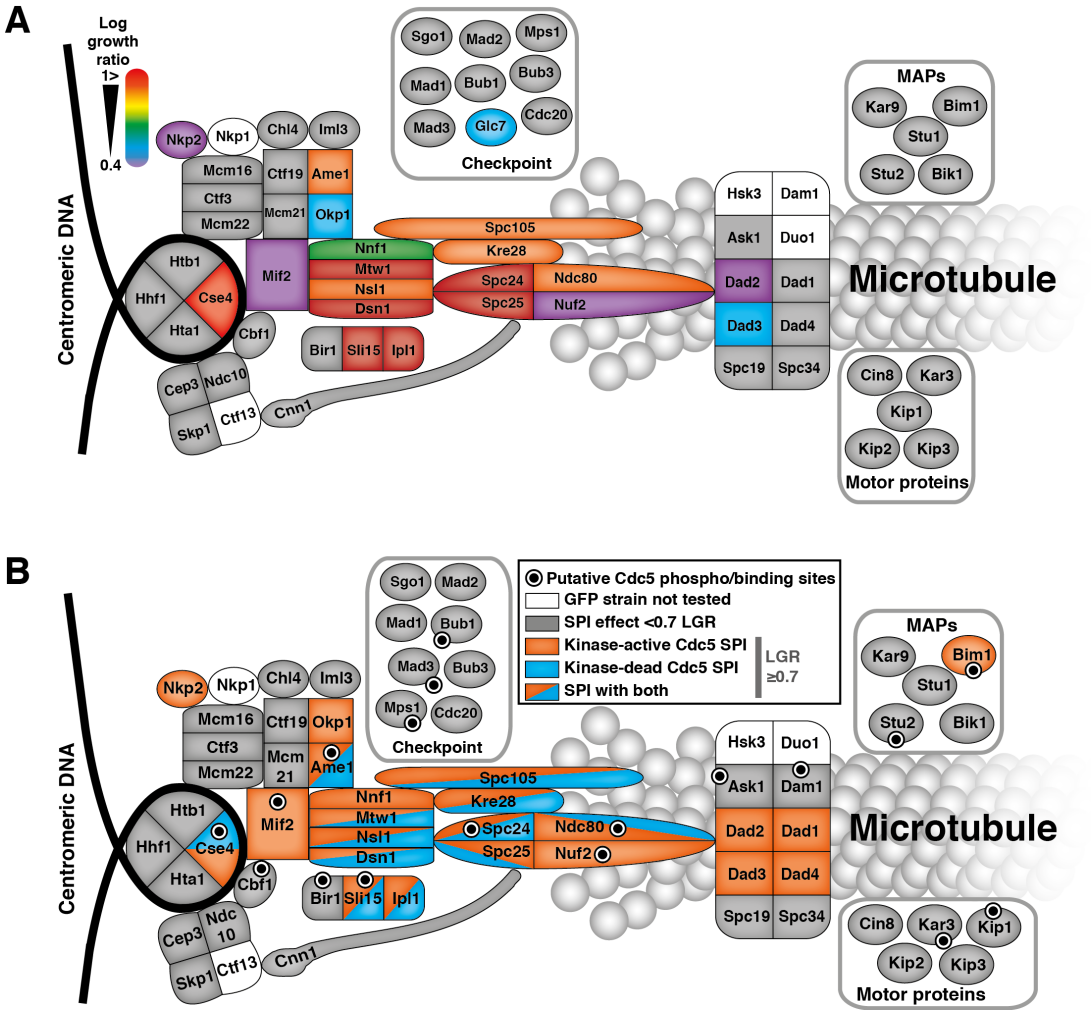

Figure 5.6 Kinase-dead Cdc5 kinetochore SPI map.

A) A colour-coded heat-map depicting the kinetochore subunits that are sensitive to kinase-dead Cdc5 association compared to GBP control (mean of cdc5-KA-GBP and cdc5-TA-GBP SPI data). Strong SPIs (log growth ratio > 1) are labelled red and weaker SPIs are purple. Subunits with a grey background did not show any growth defect compared to GBP control. Subunits with a white background were not tested.
B) A Cdc5 kinetochore map showing the strongest SPIs (log growth ratio > 0.7) of kinase-active Cdc5 SPIs in orange and kinase-dead Cdc5 SPIs in blue. Black/white dots show consensus sites for Cdc5 phosphorylation or PBD binding based on information from BioGRID; http://www.thebiogrid.org (Oughtred *et al.*, 2016).

5.2.4 Kinetochore protein tagged with GFP successfully recruits Cdc5-GBP

Before assessing the Cdc5 kinetochore SPIs in more detail, I first used fluorescence microscopy to confirm that both Cdc5-GBP-RFP and cdc5-kd-GBP-RFP were colocalised with a GFP-tagged kinetochore. It is formally possible that an association of a GBP-tagged protein with GFP-tagged kinetochore would mislocalise the kinetochore GFP-protein away from its normal location. Since Cdc5-Ctf19 SPI did not produce a growth phenotype and Ctf19 is a non-essential protein, I generated a strain with Ctf19

tagged to YFP, which associates with GBP, and Mtw1-CFP which does not bind to GBP. I then introduced the Cdc5-GBP and cdc5-kd-GBP plasmids into this strain and imaged the resulting cells with fluorescence microscopy. In all stages of the cell cycle Cdc5-GBP-RFP and cdc5-kd-GBP-RFP foci colocalises with Ctf19-YFP and Mtw1-CFP foci suggesting the Cdc5-GBP is not mislocalising Ctf19-YFP away from the CFP-tagged kinetochore (Figure 5.7 A). Additionally, I confirmed colocalisations of Cdc5-GBP-RFP and cdc5-kd-GBP-RFP with other GFP-tagged kinetochore proteins (for example, Spc105, Nnf1, Cep3 and Okp1) and in all cases the RFP and GFP signals are colocalised at the kinetochore foci (Figure 5.7 B).

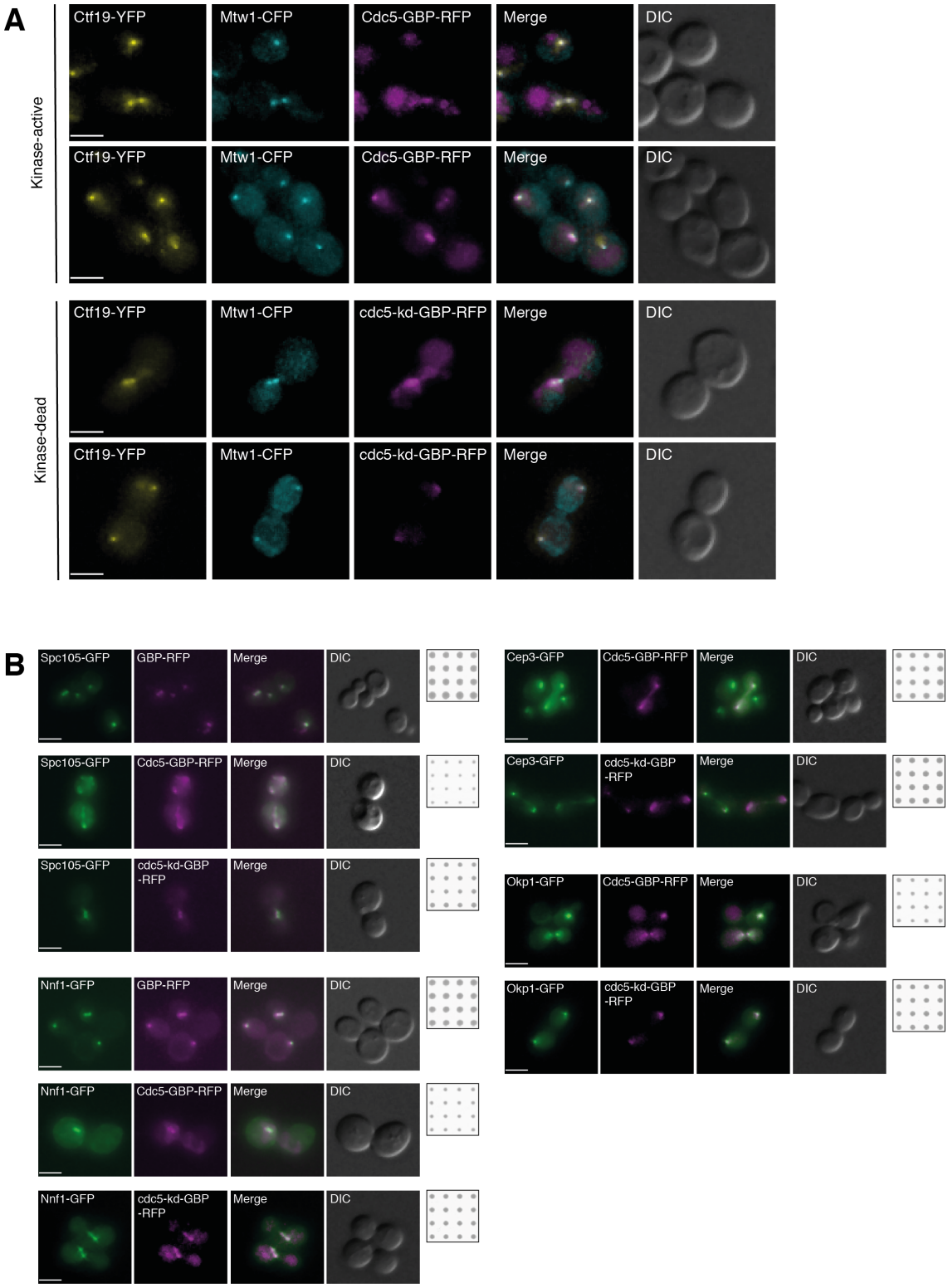

Figure 5.7 Cdc5-GBP-RFP colocalises with GFP-tagged kinetochore proteins at the kinetochore foci.

A) Fluorescence microscopy showing cells containing Ctf19-YFP and Mtw1-CFP and expressing either the Cdc5-GBP-RFP or cdc5-kd-GBP-RFP construct indicates that the

YFP, CFP and RFP signal is colocalised at different cell-cycle stages (Note that GBP does bind YFP, but does not bind CFP).
B) Fluorescence microscopy showing cells containing GFP-tagged kinetochore subunits Spc105, Nnf1, Cep3 and Okp1 and expressing either Cdc5-GBP-RFP or cdc5-kd-GBP-RFP constructs indicates colocalisation of GFP and RFP in all cases. Insets: Crops of the colonies from the SPI screen for each corresponding GFP strain is shown for reference. All scale bars are 5µm.

5.2.5 SAC dependency of Cdc5 kinetochore SPIs

Next, I asked if the growth defect caused by the constitutive Cdc5 kinetochore localisation was able to arrest growth in a SAC-dependent manner as has been reported in many higher eukaryotes (see section 5.2.3 above). I therefore repeated the Cdc5 kinetochore screen in *mad3*Δ GFP strains. However, the growth defect of Cdc5 kinetochore SPIs is not suppressed in *mad3*Δ cells, suggesting a SAC-independent growth arrest (Figure 5.8 A). I cannot rule out that the kinase-active Cdc5 is able to activate the SAC, but the growth defect could be a consequence of another SAC-independent activity, which is beyond *mad3*Δ-dependent suppression. Strikingly, and to my surprise, many of the cdc5-kd kinetochore SPIs are suppressed by *mad3*Δ and specifically SPIs at the KMN network, the key region where SAC signalling is initiated (Figure 5.8 B). The fact that the cdc5-kd-KMN SPIs are suppressed by *mad3*Δ supports the idea that this association is causing a SAC-dependent arrest, but I cannot exclude the possibility that these SPIs are activating the SAC indirectly, perhaps through a mild disruption of the kinetochore.

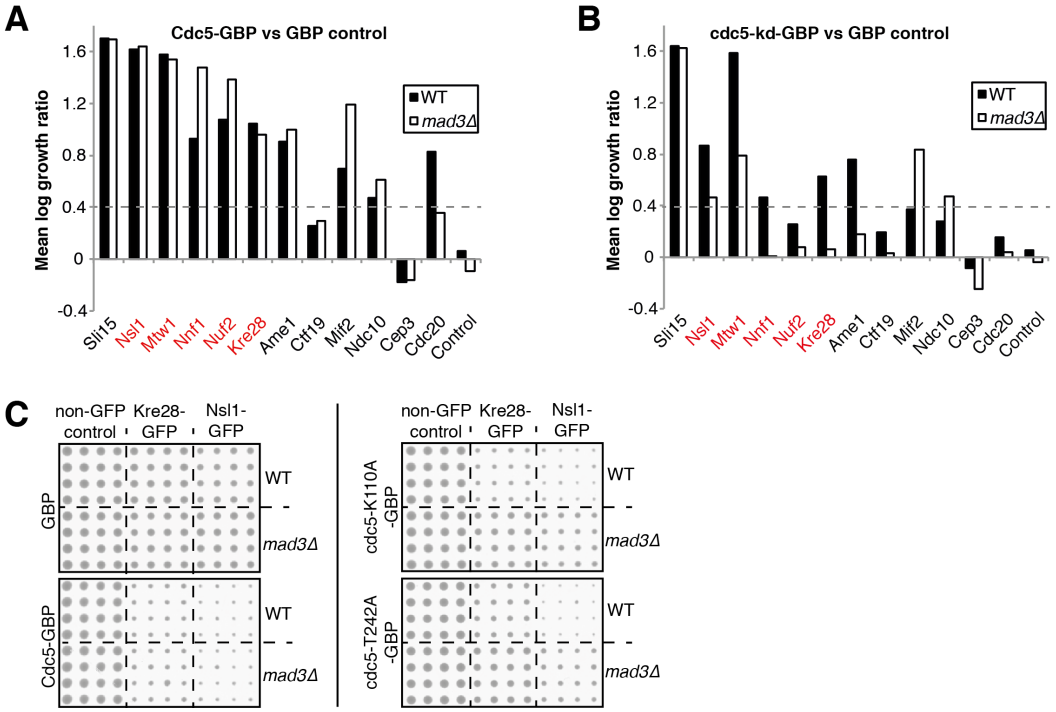

Figure 5.8 Deletion of *MAD3* does suppress kinase-dead Cdc5 kinetochore SPIs, not kinase-active SPIs.

A) A graph showing a selection of Cdc5 kinetochore SPI data indicating that deletion of the down-stream SAC component *MAD3,* does not suppress the growth defect of many kinetochore GFP strains. Control is a wild-type non-GFP strain and KMN network subunits are shown in red.
B) In contrast, a graph showing a selection of cdc5-kd kinetochore SPI data, indicates the growth defect caused by cdc5-kd-GBP is suppressed by *mad3*Δ specifically at the KMN network.
C) Cropped images from the SPI assay showing colonies (16 replicates) of wild-type and *mad3*Δ strains with GFP-tagged Kre28 and Nsl1, both components of the KMN network, containing either GBP alone, Cdc5-GBP or cdc5-kd-GBP (both K110A and T242A mutants) plasmids.

5.2.6 Polo-box domain mutants

Following up these surprising cdc5-kd results, I asked if the growth defect caused by the cdc5-kd-KMN SPIs was due to the Polo-box domain (PBD), which could still bind its phosphorylated substrates when forced to the kinetochore through the GFP-GBP association and possibly inhibit endogenous Cdc5 kinetochore activity (Figure 5.9 A). To test this notion, in addition to the PBD point mutations, I created truncation mutants lacking the C-terminal PBD of Cdc5 and cdc5-kd (both K110A and T242A) fused to GBP (Cdc5ΔC-GBP and cdc5ΔC-kd-GBP) (Figure 5.3 B&C in section 5.2.1 above). The reason for testing both PBD deletion (Cdc5ΔC) and the point mutants (Cdc5-FAM) is that they can give different phenotypes. Specifically, the Cdc5ΔC truncation mutant can rescue lethality of *cdc5*Δ only when directly fused to SPB and septin components (Park *et al.*, 2004*b*, 2004*a*), suggesting that it can function when recruited to cellular locations important for its activity. Conversely, a cdc5-WHK-FAM PBD point mutant, which cannot bind its substrates, is able to rescue growth when endogenous Cdc5 is deleted or activity is compromised (Chen & Weinreich, 2010; Ratsima *et al.*, 2011). This could either suggest that the WHK-FAM mutant is either still able to bind its targets to a small degree or that the PBD might have an essential function beyond targeting Cdc5 to its substrates. Previously, another PBD point mutant (cdc5-W517F, V518A, L530A) was shown to fail to complement a loss of Cdc5 activity (Song *et al.*, 2000). However, it was proposed that the temperature-sensitive mutant (*cdc5-1*) used in that study was acting in a dominant-negative manner at high temperature (Ratsima *et al.*, 2011).

I repeated the kinetochore specific SPI screens with the Cdc5ΔC truncation and WHK-FAM PBD point mutants fused to GBP. Both of the kinase-active PBD mutants

produced very similar results, equivalent to those of the wild-type Cdc5, suggesting that the PBD becomes irrelevant when Cdc5 kinase domain is forcibly targeted to the kinetochore through the GFP-GBP association (Figure 5.9 B&C). In contrast, the cdc5-kd PBD mutants (both ΔC and WHK-FAM) completely suppressed the growth defect in kinetochore GFP strains and were indistinguishable from GBP alone (Figure 5.9 C). These results show that the SAC-dependent growth arrest of cdc5-kd associations with the KMN network depends on the polo-box domain. To verify this, I deleted both *MAD1* and *MAD3* in GFP-tagged Spc105 strain since this the key platform for SAC signalling at the kinetochore. I find that that these SAC deletions also suppress the growth defect of kinase-dead Cdc5 association with Spc105 (Figure 5.9 D). The forced association of kinase-active Cdc5 with Spc105, by contrast, was not suppressed in either *mad1*Δ or *mad3*Δ strain. Moreover, mutating the PBD of the cdc5-kd does not produce any growth defect in an Spc105-GFP strain. It is worth noting that the Cdc5ΔC-GBP produced a much weaker growth phenotype with Spc105-GFP compared with the full length wild-type Cdc5-GBP, suggesting perhaps that the catalytic activity is being compromised by the ΔC truncation. Alternatively, the shorter form of the ΔC mutant fused to GBP (Cdc5ΔC-GBP) might not be able to place the kinase-domain to a suitable location at the KMN network to phosphorylate the same targets as the full-length protein (Cdc5-GBP or Cdc5-FAM-GBP).

Taken together, these results are in agreement with the working model depicted in Figure 5.9 A, and demonstrate that the forced associations of kinase-dead Cdc5 with KMN network components arrests growth in a SAC-dependent manner and this arrest is rescued by inhibiting PBD binding. Conversely, kinase-active Cdc5 SPIs with KMN and DAM1/DASH are both SAC- and PBD-independent. However, further experiments directly showing that endogenous Cdc5 kinetochore activity is being prevented by forced kinase-dead Cdc5 kinetochore recruitment are needed.

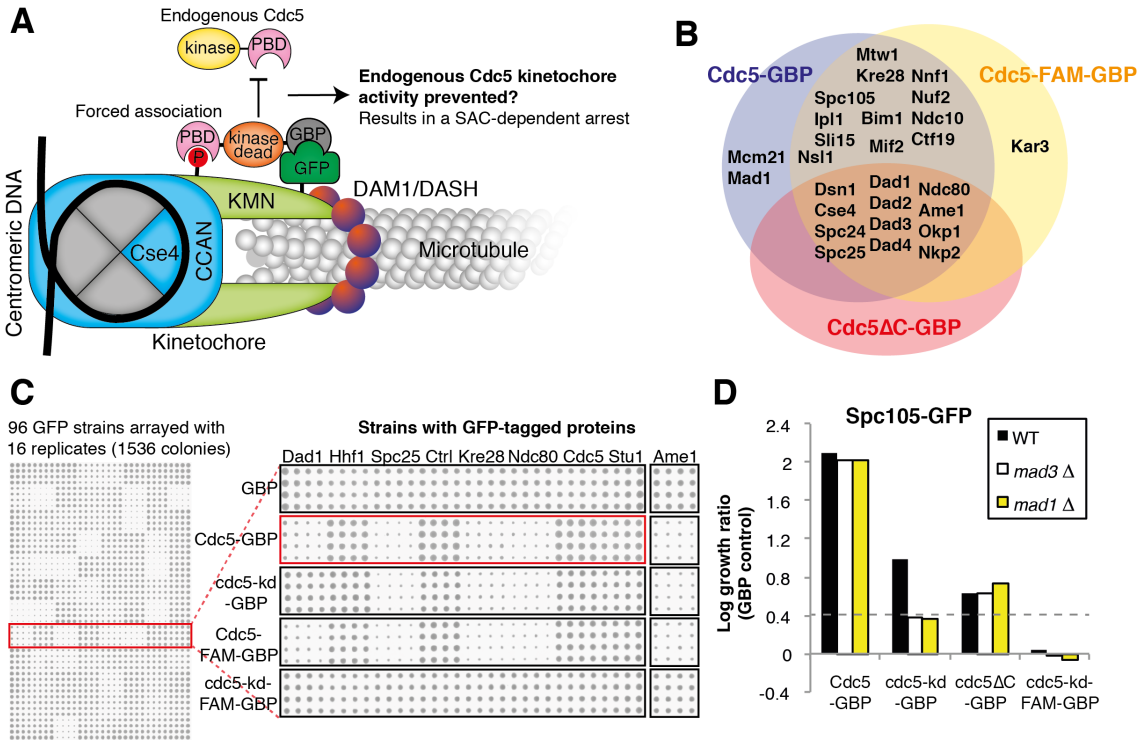

Figure 5.9 The SAC-dependent growth arrest caused by forced kinase-dead Cdc5 KMN association depends on the PBD.

A) A working model of the SAC-dependent cdc5-kd KMN SPI phenotype. By forcing a kinase-dead Cdc5 to the KMN network the endogenous Cdc5 KMN activity might be prevented through the PBD which could bind to phosphorylated docking sites required for Cdc5 KMN localisation.
B) The overlap of Cdc5 kinetochore SPI data comparing Cdc5-GBP, Cdc5-FAM-GBP or Cdc5ΔC-GBP with GBP control shows that the kinase-active Cdc5 SPIs are mostly PBD-independent, while Cdc5ΔC-GBP produces fewer (and weaker) SPIs.
C) An example of the Cdc5 SPI data and cropped images from the Cdc5 SPI screens showing 16 colonies of each GFP strain containing plasmids expressing GBP alone, Cdc5-GBP, cdc5-kd-GBP, Cdc5-FAM-GBP or cdc5-kd-FAM-GBP. GFP-tagged Spc25, Kre28, Ndc80 and Ame1 are sensitive to kinase-active and inactive Cdc5, whereas Dad1-GFP is only sensitive to active Cdc5. The growth phenotype of kinase-dead Cdc5-KMN SPIs is rescued by PBD mutation, in contrast the kinase-active Cdc5 kinetochore SPIs are not.
D) A graph showing the Cdc5 SPI effect upon Spc105, the key platform protein for SAC signalling, in a wild-type strain and both *mad1*Δ and *mad3*Δ *strains*. The SPI phenotype is not suppressed by *MAD1* or *MAD3* deletions with Cdc5-GBP or Cdc5ΔC-GBP, conversely the growth defect caused by cdc5-kd-GBP is suppressed by both deletions and by mutating PBD.

5.2.7 Internally GFP-tagged Cse4 produces a growth defect with Cdc5-GBP

Polo kinase has been reported to have a function in CENP-A regulation in human cells (see section 5.1.2). I therefore wanted to explore this in budding yeast. However, as described in chapter 4 (section 4.2.3), the C-terminal GFP tag on Cse4 compromises

its function, especially when additionally bound to GBP or GBP-tagged protein, making it difficult to interpret any SPI data with Cse4-GFP. Hence, I used the stable internally tagged Cse4 (Cs-GFP-e4) and repeated the SPI assay to ask if this GFP strain was sensitive to constitutive recruitment of Cdc5. I found that kinase-active Cdc5 with or without functional PBD caused a growth defect when forcibly recruited to Cse4 (Figure 5.10 A&B). This version of Cse4 was not sensitive to GBP alone or kinase-dead Cdc5 (K110A or T242A). For comparison and as shown previously Mif2-GFP is sensitive to both Cdc5-GBP and cdc5-kd-GBP, while Cep3-GFP is sensitive to neither. I used fluorescence microscopy to confirm that Cdc5-GBP-RFP is being recruited to the kinetochore. Surprisingly the Cdc5-GBP expressed in the Cs-GFP-e4 strain produced a striking phenotype showing a complete disruption of the kinetochore GFP foci with multiple GFP aggregates (Figure 5.10 C (white arrows in panel 2)) in majority of the cells with minimal colocalisation of GFP and RFP signal. However, some cells have normal kinetochore GFP foci with colocalised RFP signal, suggesting that the Cdc5-GBP is able to associate with Cs-GFP-e4 (Figure 5.10 C (yellow arrow in panel 2). Intriguingly, the kinase-dead Cdc5 also disrupts the GFP kinetochore foci, but without causing any growth defect. This suggests that the kinetochore itself is not being mislocalised by these Cs-GFP-e4 aggregates. Noticeably, the GFP and RFP signal is colocalised in these aggregates in cells with cdc5-kd-GBP (Figure 5.10 C (red arrows in panels 3 and 4)) compared to wild-type Cdc5-GBP where the GFP aggregates do not colocalise with RFP (Figure 5.10 C (black arrow in panel 2)). Furthermore, although I was only able to obtain very few cells containing Cs-GFP-e4 and Cdc5-GBP, since these cells are very sick, I note that many of them are unbudded and contain these abnormal Cs-GFP-e4 aggregates (Figure 5.10 C (panel 5)).

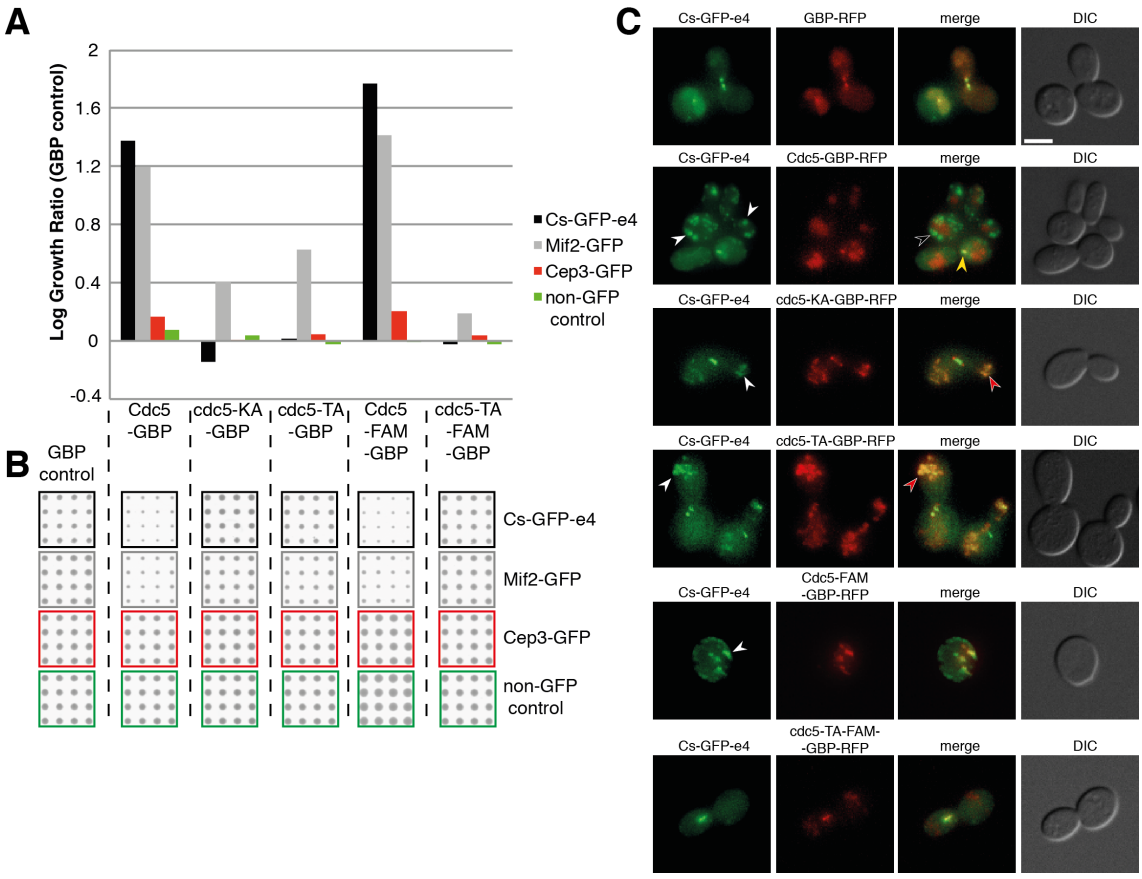

Figure 5.10 Forced association of kinase-active Cdc5 with Cse4 produces a growth defect and disrupts Cse4 kinetochore localisation.

A) A graph showing a selection of the data of GFP strains in the repeated SPI screen with a strain containing an internally GFP-tagged Cse4 (Cs-GFP-e4). See detailed description in the text.
B) Cropped images showing the colonies of the corresponding log growth ratios in (A).
C) Fluorescence microscopy of the Cdc5-Cse4 SPIs (see details in the text). White arrows show disrupted Cs-GFP-e4 foci. Black arrow shows GFP aggregates that do not colocalise with RFP. Yellow arrow shows normal Cs-GFP-e4 kinetochore foci with RFP colocalisation. Red arrows show Cs-GFP-e4 aggregates that colocalise with RFP. Scale bar is 5μm.

5.2.8 Kinase-dead Cdc5 kinetochore SPI arrests cells in mitosis

Next, I wanted to examine if constitutive Cdc5 and cdc5-kd kinetochore localisation caused cells to arrest at a specific stage of the cell-cycle. Since, the growth phenotype of cdc5-kd-kinetochore SPIs suggests a SAC activation, I decided to use fluorescence microscopy to quantify large-budded cells that have separated the two sister kinetochores but not undergone anaphase (i.e. arrested in metaphase). However, since the Cdc5-GBP and cdc5-kd GBP are constitutively expressed with the *CUP1* promoter and the forced Cdc5 or cdc5-kd kinetochore localisation causes a strong

growth defect in many cases, it is difficult to acquire sufficient live cells for imaging. With this in mind, I selected a relatively weak, but reproducible, kinetochore SPI with both Cdc5-GBP and cdc5-kd-GBP, Ame1-GFP. I grew up a culture of this strain with the Cdc5 plasmids and imaged the following day. I find that even with this weak SPI, compared to GBP alone, cdc5-kd-GBP has significantly higher proportion of large-budded cells, which is dependent on both *MAD3* and the PBD (Figure 5.11 A&B). This supports the notion that forced kinetochore recruitment of kinase-dead Cdc5 activates the SAC in a PBD-dependent manner.

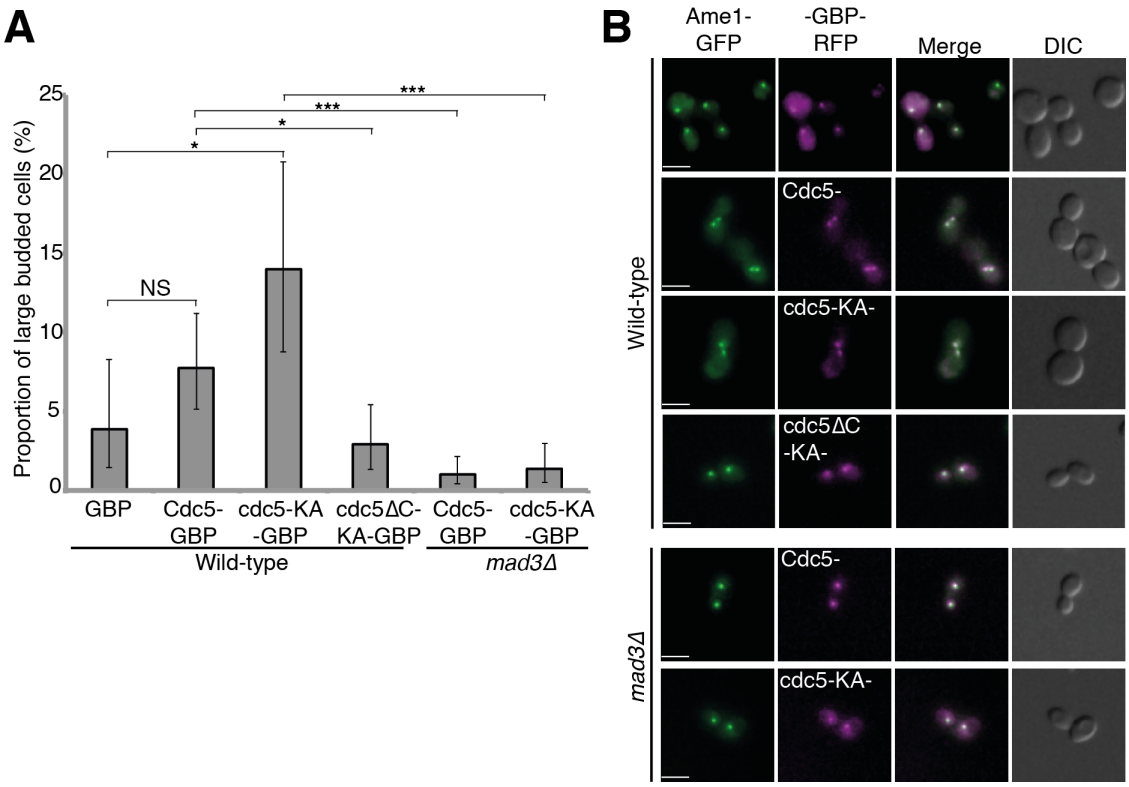

Figure 5.11 Forced kinetochore recruitment of kinase-dead Cdc5 increases large-budded cells arrested in mitosis.

A) Quantification of large-budded cells of Cdc5-Ame1 SPIs in wild-type and *mad3*Δ strains. See text for detailed description. Cells that did not have GBP-RFP signal colocalised with Ame1-GFP and large-budded cells with well separated kinetochore foci (i.e. anaphase-telophase cells) were excluded from this analysis. Statistical analysis was done using Fishers exact test; p-values * = $p < 0.05$, *** = $p < 1x10^{-6}$. Error bars indicate 95% binomial C.I.
B) Fluorescence microscopy images representative of the data in (A). All images show cells expressing GBP-RFP either unfused (first panel) or C-terminally fused to Cdc5 variants (wild-type or mutants). All scale bars are 5μm.

5.2.9 Forcing PBD to the kinetochore

In human cells, it has been shown that overexpression of PBD competes with endogenous Plk1 for kinetochore localisation resulting in SAC activation (Seong *et al.*, 2002; Hanisch *et al.*, 2006; Liu *et al.*, 2012). This is in agreement with the idea that forced cdc5-kd kinetochore recruitment could be inhibiting endogenous Cdc5 kinetochore localisation (see working model in Figure 5.9 A). Hence, I investigated this further by forcing PBD (Cdc5 N-terminal deletion mutant fused to GBP; PBD-GBP) to kinetochore proteins and hypothesised that this would recapitulate the cdc5-kd SPI results. In addition to PBD-GBP, I also created a mutant PBD-WHK-FAM-GBP plasmid to control for the PBD binding (Figure 5.12 A). I repeated the kinetochore SPI screen with these plasmids, but this screen produced only a few SPIs with kinetochore proteins and was not consistent with the cdc5-kd SPI results. Nevertheless, I found that Cse4 (internally tagged), Cdc20, Ndc10 and Mif2 produced smaller colonies with both PBD-GBP and PBD-WHK-FAM-GBP compared to the GBP control, but only Cdc20 and Cse4 SPI growth phenotype was suppressed with the PBD mutant (PBD-WHK-FAM-GBP) compared to PBD-GBP (Figure 5.12 B). In case the lack of SPI detection in this screen was due to PBD-GBP not associating with GFP-tagged kinetochores, I examined the cells with fluorescence microscopy. The imaging reveals that both the PBD- and PBD-FAM-GBP-RFP colocalise effectively with Ctf3-, Ctf19- and Mtw1-GFP foci. It is possible that a PBD alone without its N-terminal domain combined with a C-terminal fusion to GBP could compromise its function, thus a N-terminal fusion (GBP-PBD) might work better for future studies. Alternative interpretation of these data is that blocking the CDK sites at the kinetochore, by recruiting the PBD, is not sufficient to recapitulate the SAC activation seen by the cdc5-kd forced kinetochore recruitment.

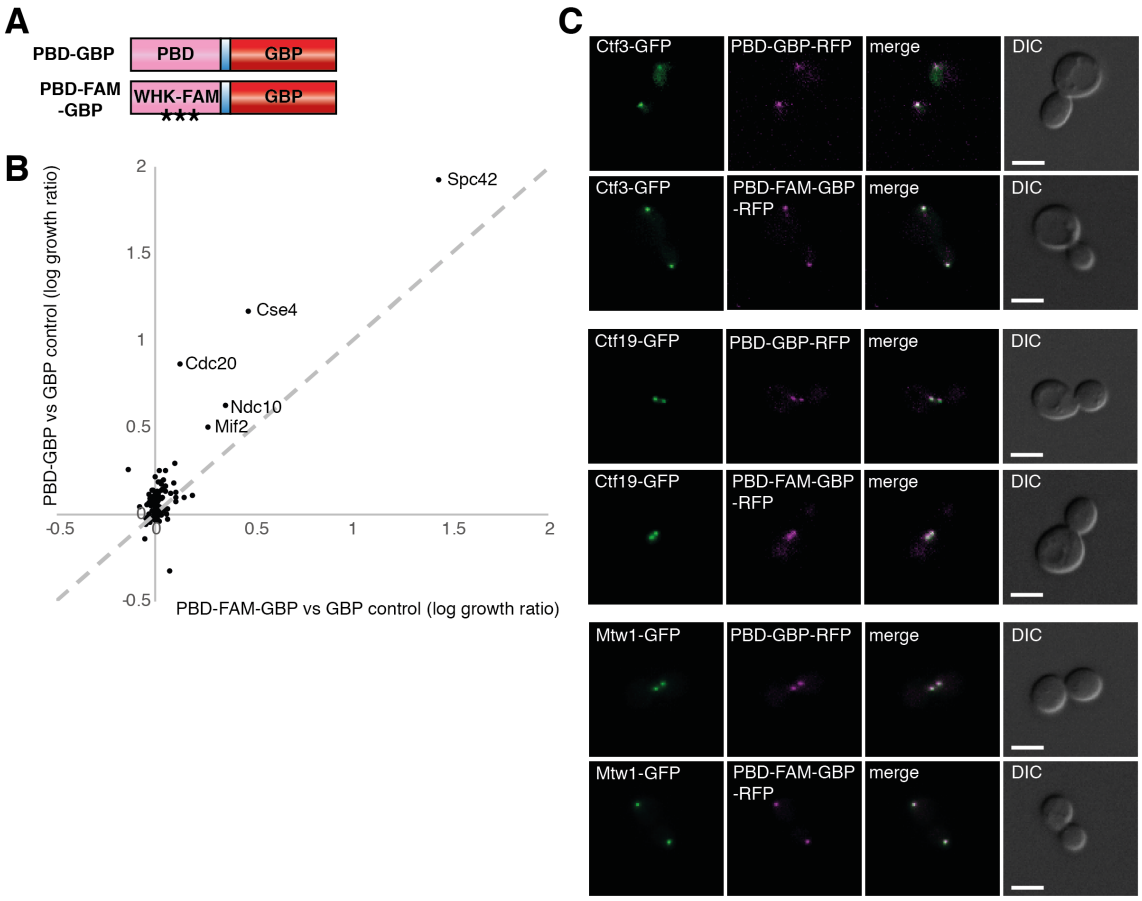

Figure 5.12 PBD kinetochore SPI screen.

A) Constructs used in the PBD kinetochore SPI screen (GBP control not shown).
B) The PBD and PBD-FAM SPI screen data are plotted against each other to show any SPIs which are suppressed by PBD point mutations. Cdc20-GFP and Cse4-GFP are less affected by PBD-FAM-GBP than PBD-GBP.
C) Fluorescence microscopy images of GFP-tagged GFP strains expressing either PBD-GBP-RFP or PBD-FAM-GBP-RFP. All scale bars are 5μm.

5.2.10 Experiments using an analog-sensitive Cdc5 mutant

The GBP-fusion constructs used in the SPI assays are expressed constitutively, but at low levels using the *CUP1* promoter without adding copper to the media. The disadvantage of this system is the fact that the GBP-tagged target protein and the endogenously GFP-tagged query protein are constitutively bound. If this results in a growth defect it makes it difficult to examine the SPI phenotype in more detail. Therefore, I also explored the use of an analog-sensitive mutant of Cdc5 (cdc5-as1; L158G) which becomes catalytically inactive when a specific inhibitor of cdc5-as1, CMK, is added to the media (Snead *et al.*, 2007). This approach thus allows me to temporally control the kinase activity of cdc5-as1-GBP leaving the endogenous Cdc5

unaffected. I repeated the kinetochore SPI assay, using cdc5-as1-GBP, on media with either CMK or DMSO control (Figure 5.13 A&B). Strikingly, instead of the expected outcome of weaker SPIs with the addition of CMK compared to DMSO, I noticed the opposite. Many of the kinetochore SPIs, especially the KMN network, were stronger when CMK was included in the media. Although, few SPIs were suppressed with CMK compared with DMSO. This suppression was subtle, but interestingly affected components of the COMA and DAM1/DASH complexes, and Bim1. In some way, this result supplements the previous results with the kinase-dead Cdc5-KMN SPIs (see section 5.2.3). However, this also implies that the kinase-activity of the analog-sensitive Cdc5 is possibly compromised even without the addition of the inhibitor, CMK. To test this idea, I repeated the cdc5-as1-GBP SPI screen with wild-type and *mad3*Δ GFP strains. I found that the growth defect was suppressed by *mad3*Δ in many GFP-tagged KMN network strains, even in the assay without CMK (Figure 5.13 C). Consistently, the suppression was even greater in the assay with CMK (Figure 5.13 D). This suggests that the forced cdc5-as1 kinetochore recruitment, without CMK, causes an intermediate SPI phenotype, between kinase-active and kinase-dead, while the addition of CMK phenocopies the kinase-dead Cdc5 SPIs. To test this idea further, I removed the PBD from cdc5-as1-GBP and hypothesised that this would not cause a strong growth phenotype similar to that seen with cdc5ΔC-kd-GBP when forced to the kinetochore (see Figure 5.9 C). Indeed, when the SPI screen was repeated with cdc5ΔC-as1-GBP it did not produce any growth defect in GFP-tagged kinetochore strains (Figure 5.13 E). These data suggest that I cannot use the cdc5ΔC-as1-GBP as a conditional system to induce Cdc5 kinase activity as the cdc5-as1-GBP produces a phenotype consistent with an inhibited Cdc5 kinase. It is not unusual for the so-called gatekeeper mutation of kinases to disrupt their activity (Zhang *et al.*, 2005; Snead *et al.*, 2007). It is also possible that the tethering of GBP to cdc5-as1 further compromises its activity. Alternatively, the Cdc5 kinetochore SPIs identified may rely upon a high level of kinase activity, only present in the wild-type Cdc5.

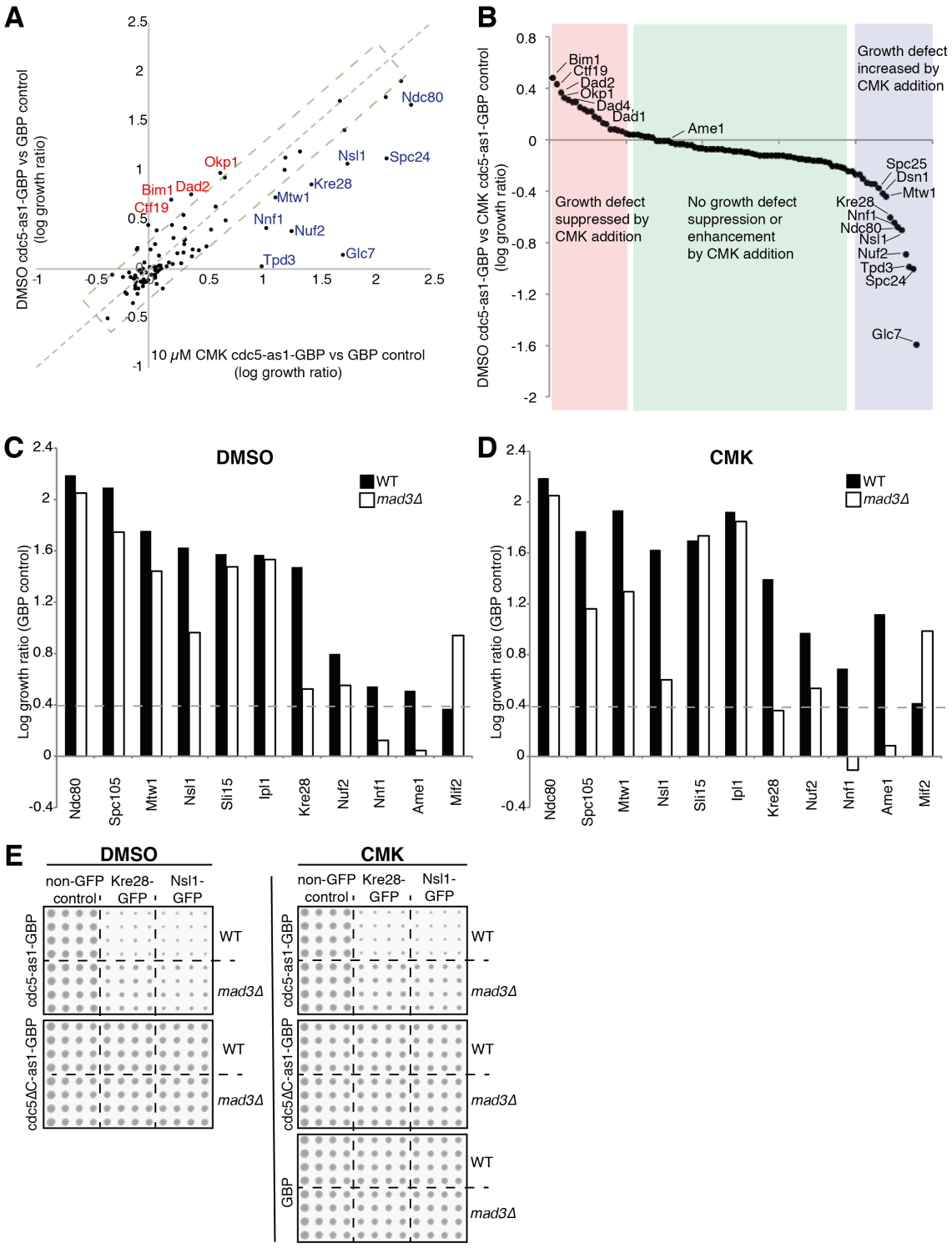

Figure 5.13 Analog-sensitive Cdc5 kinetochore SPI screen.

A) The cdc5-as1-GBP SPI data using GBP control with and without CMK are plotted against each other. SPIs in red are growing better in media with 10μM CMK, while SPIs in blue are growing worse. GFP strains in the green dotted box are not affected either way by CMK.
B) The cdc5-as1 SPI data was re-analysed comparing colonies of GFP strains containing cdc5-as1-GBP with DMSO versus cdc5-as1-GBP with CMK as the control

instead of GBP. GFP strains in the red region are more sensitive to 'active' cdc5-as-1 than 'inactive' cdc5-as1. Strains in the green region are equally or not sensitive to 'active' or 'inactive' cdc5-as1. Finally, GFP strains in the blue region are more sensitive to 'inactive' cdc5-as1.
C-D) A graph showing a selection of the data from the cdc5-as1 SPI screen repeated with wild-type and *mad3*Δ strains in media with either DMSO or CMK.
E) Cropped images from the cdc5-as1 SPI screen showing colonies (16 replicates) of wild-type and *mad3*Δ strains with GFP-tagged Kre28 and Nsl1, both components of the KMN network, containing cdc5-as1-GBP plasmid in media with either DMSO or CMK.

In order to conditionally and temporally control the GBP-GFP association, I also sought to tackle this problem using the auxin-inducible degradation (AID) system (Nishimura *et al.*, 2009; Nishimura & Kanemaki, 2014). Briefly, I designed a new plasmid expressing GBP fused to the AID degron motif and the E3 ubiquitin ligase, Afb2, that recognises it. In the presence of auxin, the Afb2 is able to ubiquitylate the AID-tagged protein resulting in its degradation by the proteasome. This approach worked well to degrade the GBP-RFP as seen by fluorescence microscopy (Appendix figure 1 A&C in chapter 7). However, when I re-engineered the Cdc5ΔC-GBP plasmid with the degron and introduced it into GFP-kinetochore strains in the presence of auxin it was still able to produce the SPI growth phenotype (data not shown), suggesting there was still enough un-degraded Cdc5ΔC-GBP-AID-RFP in the cells, but as seen by fluorescence microscopy the Cdc5ΔC-GBP-AID-RFP signal was significantly reduced in a couple of cases (Appendix figure 1 B&C in chapter 7). It is possible that additional AID motifs could result in a more efficient degradation of the Cdc5-GBP, thus future experiments with that in mind could be constructive.

5.2.11 Direct fusions of *CDC5* with kinetochore genes

Since, using both the auxin-inducible-degradation (AID) and the analog-sensitive systems were not successful to conditionally control the Cdc5-kinetochore interaction, I sought to approach this problem differently. The direct fusion of open reading frames of two genes has been used successfully to study protein-protein interactions (for example: Coudreuse & Nurse, 2010; Lau & Murray, 2012; Gurden *et al.*, 2016). I therefore, engineered plasmids with direct genetic fusions of Cdc5 and cdc5-kd with kinetochore components under the control of *GAL1* promoter, thus the fusion is only expressed on galactose containing medium. I fused Cdc5 and cdc5-kd to the C termini of Mtw1, Dad2, Bim1 and Ame1. Wild-type strains containing these fusion plasmids were then serially diluted and spotted on glucose and galactose containing media.

Overexpression of Cdc5 alone inhibits growth, but cdc5-kd does not (Figure 5.14 A). Surprisingly, expression of a direct fusion of Mtw1-Cdc5 (and Mtw1-cdc5-kd) did not inhibit growth, whereas, both expression of Ame1-Cdc5 (and Ame1-cdc5-kd) and Bim1-Cdc5 (and Bim1-cdc5-kd) blocked growth and expression of Dad2-Cdc5 (and Dad2-cdc5-kd) reduced growth, but to a lesser extent.

I chose the Ame1-Cdc5 fusion as a candidate for the forced Cdc5 kinetochore recruitment for further analysis, for several reasons: First, Ame1 was consistently identified in the Cdc5 and cdc5-kd SPI screens. Second, the forced Ame1-GFP association with cdc5-kd-GBP clearly arrested cells in a SAC-dependent manner. Third, it has been reported that the human Ame1 homolog CENP-U (also known as PBIP1) recruits Plk1 to kinetochores (Kang *et al.*, 2006). And finally, the Ame1 protein contains six N-terminal phosphoserines (Albuquerque *et al.*, 2008; Holt *et al.*, 2009; Gnad *et al.*, 2009; Breitkreutz *et al.*, 2010), many of which are CDK and Cdc5 consensus sites. Consequently, in addition to the C-terminal Ame1-Cdc5 fusions, I created plasmids with Cdc5 fused to the N terminus of Ame1 (Figure 5.14 B). After performing spot assays with cells containing these fusions including wild-type, kinase-dead and PBD mutants of Cdc5 with Ame1 in both wild-type and *mad3*Δ strains, I found that only the N-terminal Ame1 fusions were phenocopying the Cdc5 (and cdc5-kd) KMN SPIs (Figure 5.14 B&C). Peculiarly, the wild-type Cdc5-Ame1 C-terminal fusion did not block growth while removal of the PBD made it lethal (compare *CDC5-AME1* and *CDC5*Δ*C-AME1* in Figure 5.14 B). This could be explained by the shorter form of the Cdc5Δ, thus bringing the N-terminal kinase-domain closer to Ame1 or surrounding proteins. The differences between the C- and N-terminal Ame1 fusions could be explained by the fact that Ame1 is an elongated protein with its C terminus at the inner kinetochore while its N terminus extends towards the outer kinetochore and interacts with the MIND complex (Hornung *et al.*, 2014; Dimitrova *et al.*, 2016). Hence, the two fusions differ spatially for Cdc5 kinetochore localisation, resulting in different phenotypes.

Finally, I examined the tolerance of cells expressing these fusions for the microtubule poison benomyl. I performed a spot assay as before and compared on media with and without benomyl at two different concentrations (Figure 5.14 D). Cells expressing the Cdc5-Ame1 fusion were tolerant to low or high doses of benomyl (7.5 or 15µg/ml), but

cells expressing cdc5-kd-Ame1 and cdc5ΔC-kd-AME1 were very sensitive to a higher dose of benomyl (15µg/ml).

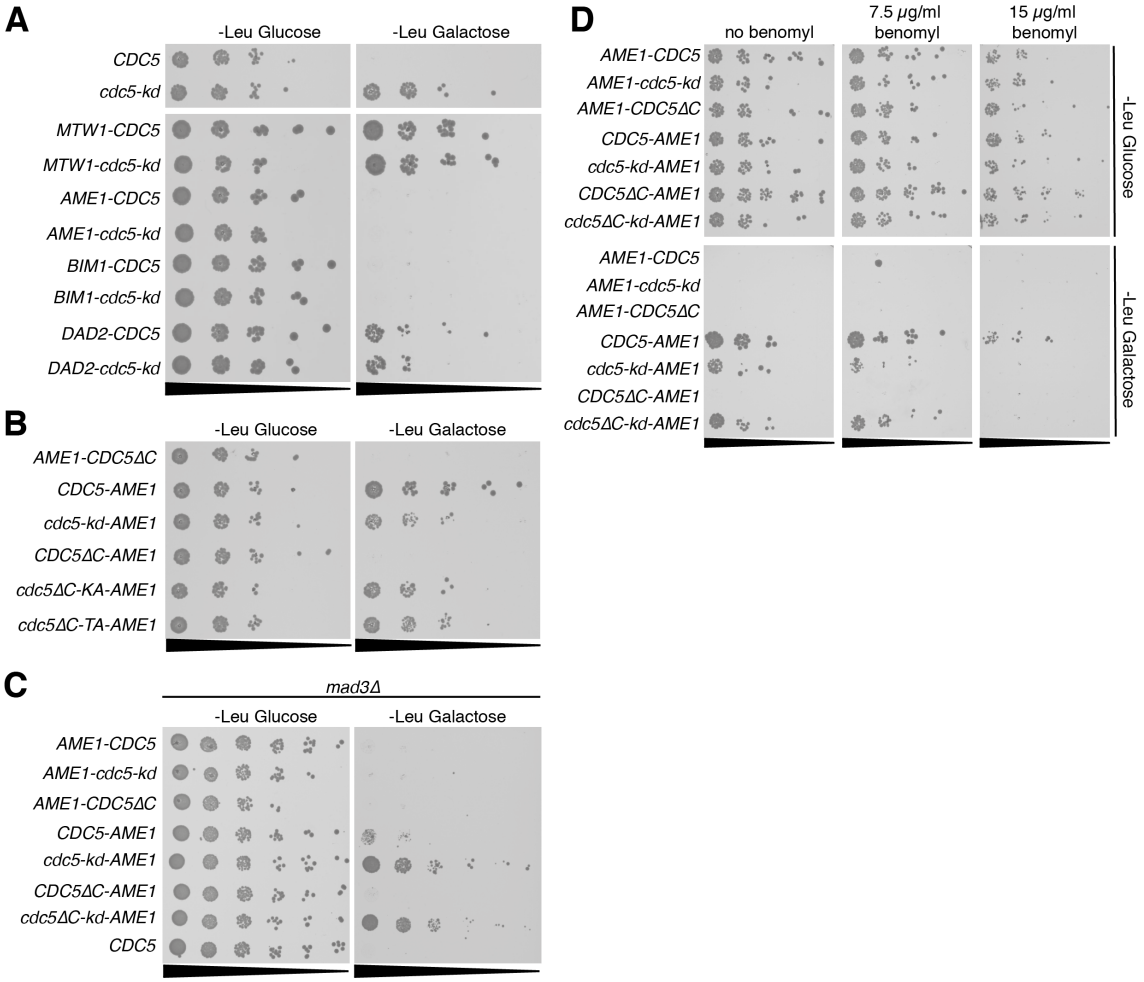

Figure 5.14 Direct genetic Cdc5-kinetochore fusions.

A-B) Spot assay of 10-fold serially-diluted wild-type strain containing plasmids with *pGAL1*-driven expression of Cdc5, cdc5-kd (K110A mutants) or fusions with kinetochore genes. Log-phase cultures were spotted on SC -leu media containing either glucose (expression off) or galactose (expression on).
C) The serial-dilutions spot assay was repeated with Ame1 fusions in *mad3*Δ strain.
D) The serial-dilutions spot assay of Ame1 fusions was repeated on media with or without the microtubule poison benomyl at two different concentrations (7.5 and 15 µg/ml).

5.2.12 Cell-cycle analysis of cells expressing direct Cdc5-Ame1 fusions

Next, I sought to assess the cell-cycle and spindle phenotypes of cells expressing these Ame1-Cdc5 fusions. I picked four Ame1 fusions with Cdc5 and cdc5-kd for this analysis, the two C-terminal fusions: Ame1-Cdc5Δ and Cdc5ΔC-Ame1, and the two N-terminal fusions: Ame1-cdc5-kd and cdc5-kd-Ame1. I chose the kinase-active Cdc5

without the PBD because I want to specifically examine kinase activity at the kinetochore, and the kinase-dead containing the PBD, since I want to explore the notion of the PBD of catalytically-inactive Cdc5 is preventing endogenous Cdc5 kinetochore activity when forced to the kinetochore.

I generated a strain with fluorescently tagged tubulin (mTurqoise2-Tub1), SPB (Spc42-RFP) and outer kinetochore (Dad4-YFP) to visualise the spindle in more detail and for easier determination of cell-cycle phases. This strain, containing the Ame1 fusion plasmids, was then cultured to log-phase in media supplemented with 2% raffinose and 0.1% glucose. The cultures where divided and resuspended in either the same media or media supplemented with 2% galactose for four hours before capturing images. Cell-cycle and spindle analysis of the four fusions is shown in Figure 5.15. Quantifying the cell-cycle stage, via both the morphology of the cells and the status of the fluorescent markers, revealed that the Ame1-Cdc5ΔC (Figure 5.15 B) and Ame1-cdc5-kd (Figure 5.15 A) fusions do not show a clear cell-cycle arrest phenotype, although both fusions result in decreased rate of cells in metaphase, and the Ame1-Cdc5ΔC fusion increases frequency of cells in G1-phase (Figure 5.15 B). Expression of Ame1-cdc5-kd fusion results in an increased proportion of cells with a prominent abnormal spindle phenotype and disrupted Dad4-YFP foci (Figure 5.15 A (insert) and Figure 5.15 E). The reverse fusions, both Cdc5ΔC-Ame1 and cdc5-kd-Ame1, show clearer phenotypes indicative of cell-cycle arrest. In accordance with a SAC arrest, the expression of cdc5-kd-Ame1 has increased number of metaphase cells and large-budded cells (Figure 5.15 C&F). Interestingly, expression of the Cdc5ΔC-Ame1 fusion has increased number of cells that seem to be arrested in G2-phase or early mitosis with small buds (Figure 5.15 D&G).

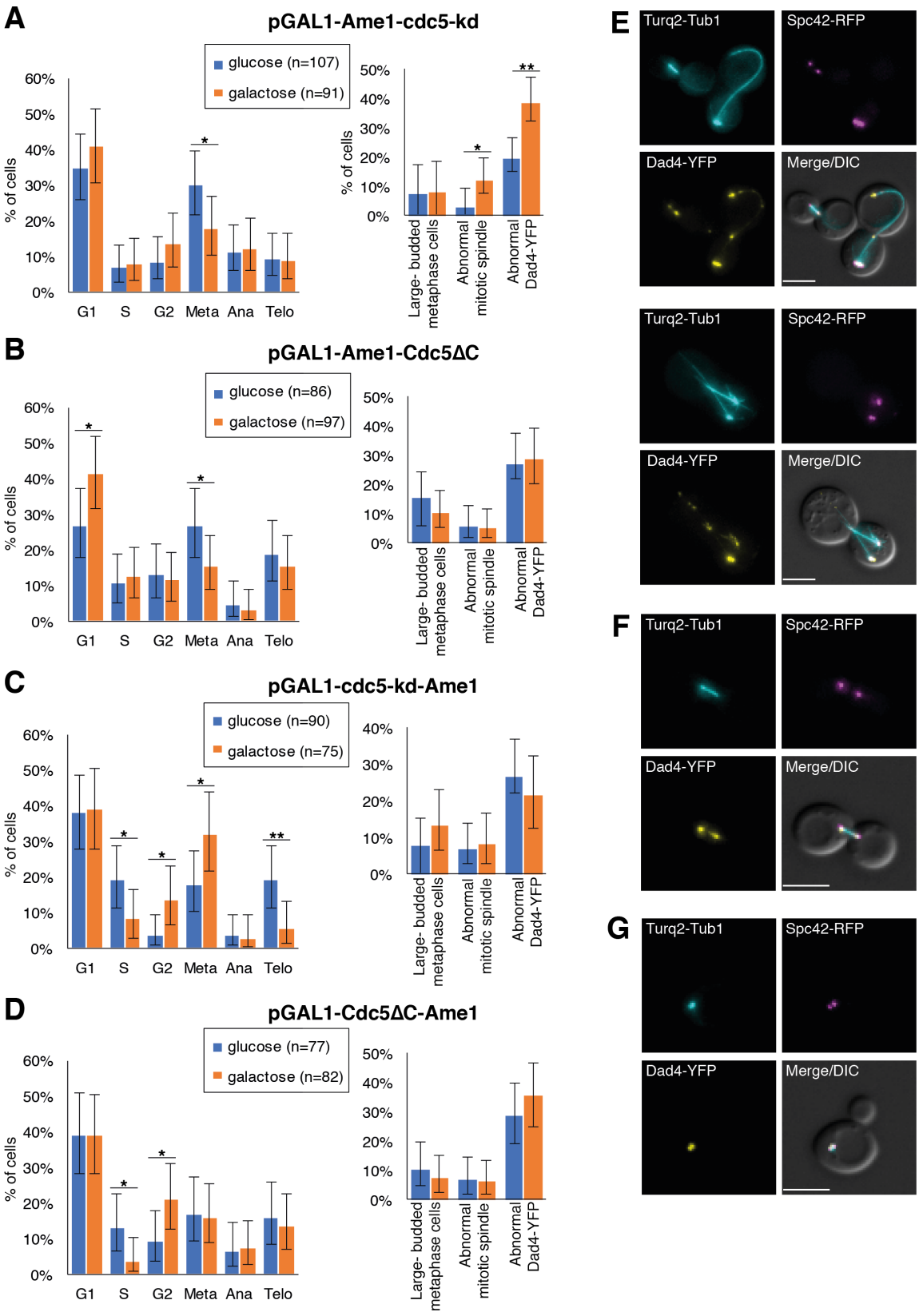

Figure 5.15 Cell-cycle analysis of Ame1-fusion expressing cells.

A-D) Cell-cycle analysis of cells containing the Ame1 fusions in asynchronous log-phase cultures after growing for four hours in raffinose/glucose or galactose SC -leu

media (see section 2.3.3 for detailed description). Insets are large-budded cell, spindle and Dad4-YFP analysis of same samples. Meta, Ana and Telo refer to metaphase, anaphase and telophase, respectively. Statistical analysis was done using Fishers exact test; p-values * = $p < 0.05$, ** = $p < 0.005$. No star indicates no significant difference. Error bars indicate 95% binomial C.I.
E) Fluorescence microscopy representative of cells in (A) with abnormal spindle and Dad4-YFP foci phenotypes (top and bottom panel).
F) Fluorescence microscopy representative of the large-budded cell phenotype in (C).
G) Fluorescence microscopy representative of small-budded G2 cell phenotype in (D).
All scale bars are 5µm.

To complement this fluorescence microscopy analysis, I also investigated the cell-cycle of the Cdc5-Ame1 fusion cells using flow cytometry. Log-phase cultures of wild-type cells with the same four Cdc5ΔC and cdc5-kd fusions to Ame1 (C and N termini) were grown for four hours in galactose containing media before fixing and DNA content was measured by flow cytometry (Figure 5.16) (see section 2.6.3 for details). Similar to the microscopy analysis the C-terminal Ame1 fusions to either Cdc5ΔC or cdc5-kd did not increase the quantity of cells in either G1- or G2-M phase compared to cells containing an empty plasmid. Interestingly, the cells expressing the Cdc5Δ-Ame1 fusion accumulate in G1, and show a second peak which is shifted to the left compared to the G2-M peak seen with the other fusions and empty plasmid. This could suggest that these cells are failing to finish DNA replication, and possibly arresting in S-phase. The relative increase of G1-phase cells with this Cdc5ΔC-Ame1 fusion appears to be in contrast to the microscopy analysis (Figure 5.15 D). It is a possibility that the cells I counted as G2-phase cells in the microscopy analysis were mischaracterised. As described in chapter 2 (section 2.3.3), I categorised cells with small- to medium-sized buds with a single kinetochore focus and two SPB foci in the mother as G2-phase cells. S-phase cells where categorised as small-budded cells with a single kinetochore and SPB focus. Another possibility is that cells expressing the Cdc5ΔC-Ame1 fusion have a morphologically similar G2-phase phenotype without completing significant DNA replication, conceivably attempting to enter mitosis prematurely before starting or completing S-phase. It is notoriously difficult to assess the short G2-phase in budding yeast, and it has even been proposed that budding yeast does not have any clear G2-phase (Kitamura *et al.*, 2007).

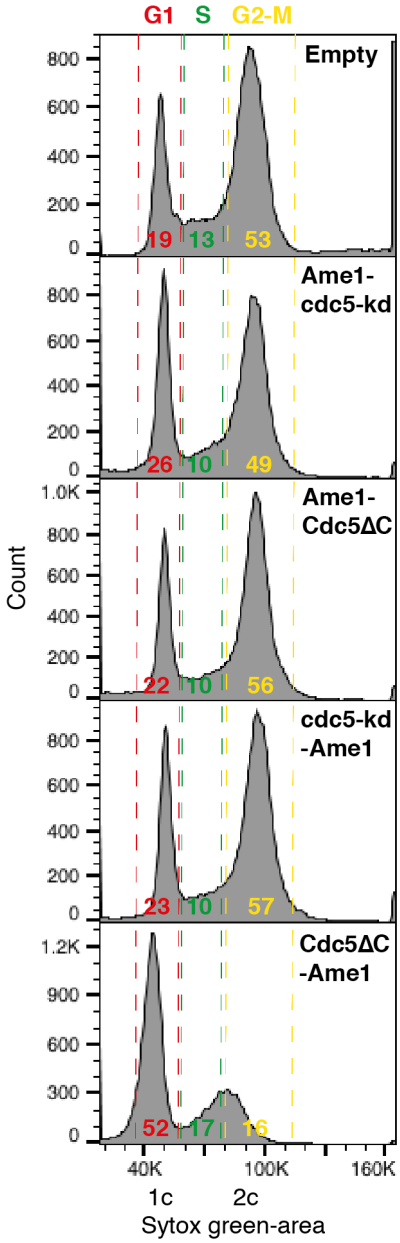

Figure 5.16 Cell-cycle analysis by flow cytometry of cells expressing Ame1 fusions.

Asynchronous log-phase cell cultures were grown in galactose for four hours before cell fixing and DNA staining with Sytox green and then measured with flow cytometry. The same G1 (red), S (green) and G2-M (yellow) gates were used for all samples. The coloured numbers indicate the percentages of cells in each cell-cycle stage. This experiment was done in duplicate with the same results (data not shown).

As stated above, the contrasting results between the C- and N-terminal fusions of either Cdc5ΔC or cdc5-kd with Ame1 are noteworthy. The N terminus of Ame1 has been shown to extend towards the outer kinetochore and directly interacts with Mtw1 subunit of the MIND complex. The C terminus of Ame1 faces the inner kinetochore and

interacts with Okp1, also an essential subunit of the COMA complex. Hence fusions to the C-terminal end of Ame1 could be disrupting the interaction to its binding partner, thus resulting in similar phenotypes regardless of kinase activity.

Taken together, these results suggest that a kinase-active Cdc5ΔC linked to the N terminus of Ame1 arrests cells early in the cell-cycle, without completing DNA replication, but perhaps with 'G2-phase-like' features like small buds and in some cases separated SPBs. The kinase-dead Cdc5 N-terminal Ame1 fusion activates the SAC and arrests cells in metaphase. Whereas, the C-terminal Ame1 fusions (both Cdc5ΔC and cdc5-kd) more likely cause disruptions in assembly of inner kinetochore subcomplex components. Although, I cannot rule out that Cdc5 might also have a different role around the C terminus of Ame1 at the inner kinetochore.

5.2.13 Conditional Cdc5-kinetochore SPI

Since the cell-cycle analysis of cells with either the kinase-active or kinase-dead N-terminal Ame1 fusions, revealed distinct phenotypes, and since Ame1 N terminus interacts with the MIND complex as part of the KMN network at the outer kinetochore, I sought to investigate the Cdc5 association with the MIND complex in more detail. Although, instead of using direct fusions, I exploited the fact that in contrast to the lethality caused by Cdc5 overexpression (Figure 5.14 A and Charles *et al.*, 1998), Cdc5ΔC overexpression is not, presumably because it is unable to bind its substrates (Figure 5.17 A). However, Cdc5ΔC-GBP becomes lethal when expressed in GFP-tagged kinetochore strains (Mtw1-GFP and Ndc80-GFP). Therefore, this allows me to switch on and off the Cdc5-kinetochore association by changing the carbon source of the media between glucose/raffinose (expression off) and galactose (expression on). Moreover, this could potentially be useful for dissecting the kinetochore specific function of Cdc5 since Cdc5ΔC should not have the same global effects as an overexpression of wild-type Cdc5 has on other cellular processes.

First, using fluorescence microscopy, I wanted to confirm that the *pGAL1*-controlled expression of Cdc5ΔC-GBP and cdc5ΔC-kd-GBP are successfully localised to YFP-tagged kinetochore protein, Mtw1-YFP, in a strain that also has a CFP-tagged SPB component Spc110-CFP, which does not bind GBP. Both the Cdc5ΔC-GBP-RFP and cdc5ΔC-kd-GBP-RFP signals colocalise with the Mtw1-YFP foci between the separated Spc110-CFP foci in mitotic cells (Figure 5.17 B). Next, I introduced these

plasmids into a strain containing Mtw1-YFP and mTurqoise2-Tub1 and examined the cell-cycle and spindle phenotype. After growing the cultures for four hours in galactose containing media, I captured images via fluorescence microscopy. Since, the GBP is tagged with RFP I can visualise cells that have the Cdc5-Mtw1 association, thus I only analysed cells that had colocalised signal of YFP and RFP foci. This analysis revealed that the forced Cdc5ΔC-GBP recruitment to Mtw1-YFP caused accumulation of cells in S/G2-phase of the cell cycle, in agreement with the previous analysis of cells expressing the Cdc5ΔC-Ame1 fusion (Figure 5.17 C&D). In contrast, and analogous to the cdc5-kd-Ame1 fusion, Mtw1-YFP cells expressing cdc5Δc-kd-GBP accumulate in metaphase (Figure 5.17 C&D). It should be noted however, that this kinase-dead Cdc5 does not contain the PBD, and thus according to the working model (see Figure 5.9 A) should not be interfering with endogenous Cdc5 kinetochore activity resulting in SAC activation. It is a possibility that the cdc5ΔC-kd-GBP overexpression using the *GAL1* promoter (compared to the mild expression with *CUP1* promoter) in this construct is problematic for kinetochore function, thus increasing the length of the metaphase-anaphase transition. Indeed, overexpressing GBP alone in cells containing Mtw1-YFP also accumulates cells in metaphase, although to a lesser extent (Figure 5.17 E).

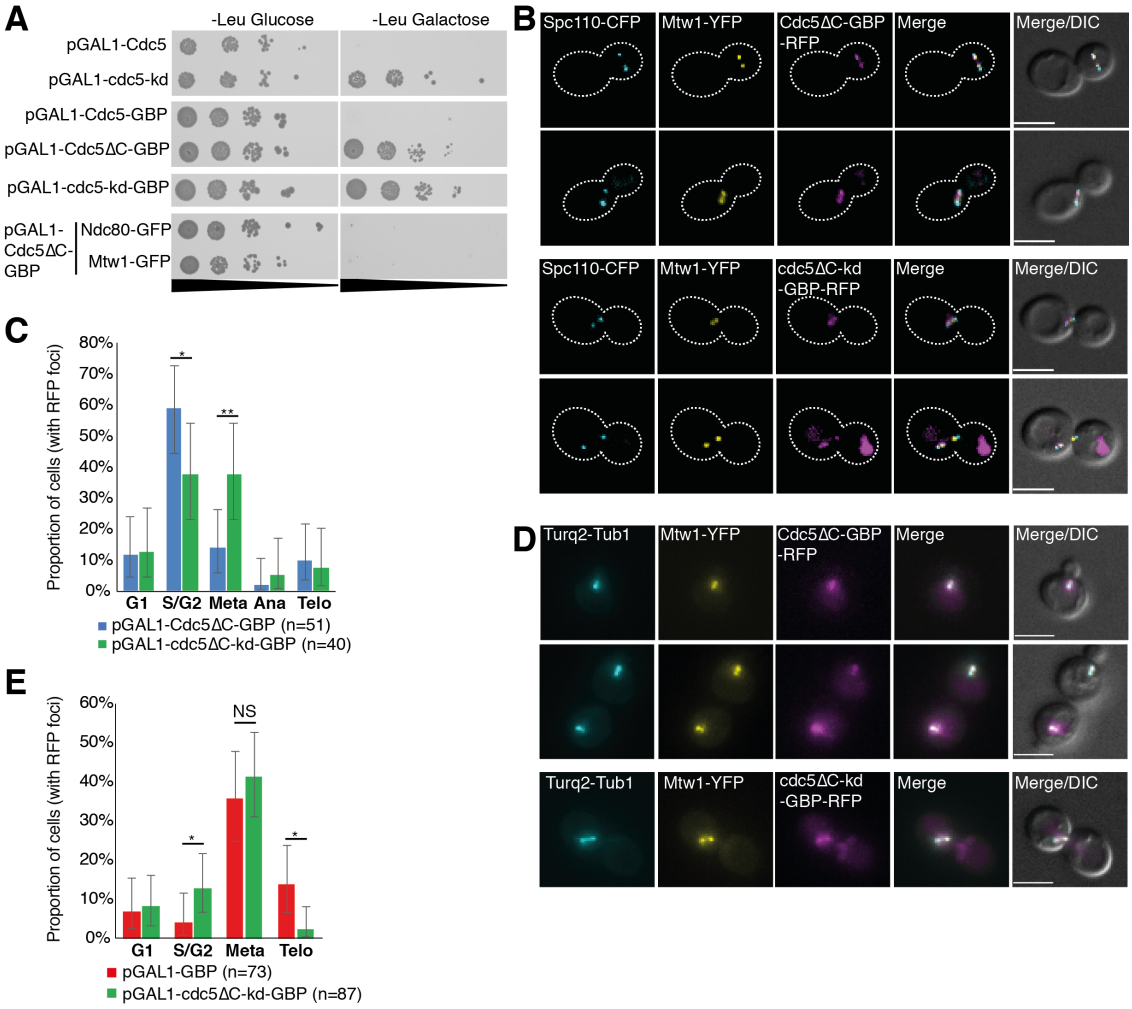

Figure 5.17 Forced central-kinetochore recruitment of Cdc5 arrests cells early in the cell cycle.

A) Spot assay of 10-fold serially-diluted wild-type strain (rows 1-5) containing plasmids with *pGAL1*-driven expression of Cdc5 alone, cdc5-kd alone, Cdc5-GBP, Cdc5ΔC-GBP or cdc5ΔC-kd-GBP or GFP-tagged kinetochore strains (rows 6 and 7) containing *pGAL1*-Cdc5ΔC-GBP plasmid.
B) Fluorescence microscopy images of cells containing Spc110-CFP and Mtw1-YFP and expressing either Cdc5Δ-GBP-RFP or cdc5ΔC-kd-GBP-RFP.
C) Cell-cycle analysis of Mtw1-YFP cells expressing either Cdc5ΔC-GBP or cdc5ΔC-kd-GBP after growing for four hours in galactose media. Cells without GBP-RFP signal were excluded from this analysis. Meta, Ana and Telo refers to metaphase, anaphase and telophase, respectively. Statistical analysis was done using Fishers exact test; p-values * = $p < 0.05$, ** = $p < 0.005$. No star or NS indicates no significant difference. Error bars indicate 95% binomial C.I.
D) Fluorescence microscopy representative of cells in (C) containing Mtw1-YFP and mTurquoise2-Tub1 and expressing either Cdc5ΔC-GBP-RFP or cdc5ΔC-kd-GBP-RFP. All scale bars are 5μm.
E) The experiment in (C) was repeated with cells expressing either GBP alone or cdc5ΔC-kd-GBP and the cell-cycle analysed.

During the cell-cycle analysis, I noticed that the mitotic spindles of Mtw1-YFP cells expressing the Cdc5ΔC-GBP were considerably shorter than spindles of Mtw1-YFP cells expressing cdc5ΔC-kd-GBP. To investigate this further, I engineered a Mtw1-YFP strain containing *CDC20* under the control of the repressible *MET3* promoter. Since the *MET3* promoter is turned off by the addition of methionine, cells can be arrested in metaphase by adding methionine to the media to deplete Cdc20 (Yeong *et al.*, 2000; Makrantoni & Stark, 2009). Using this strain, I can examine the specific effects on the mitotic spindle caused by the Cdc5 kinetochore association in a controlled manner. I arrested the cells by growing them for two hours in media containing methionine, after which about 70% of cells were in metaphase (Figure 5.18 A). Then, I expressed either Cdc5ΔC-GBP or cdc5ΔC-kd-GBP by galactose addition and captured images after 2 hours. I measured the sister kinetochore distance using a semi-automated quantification protocol (see section 2.3.3). Interestingly, the metaphase sister-kinetochore distance was significantly reduced in Mtw1-YFP cells containing Cdc5ΔC-GBP (mean value of 0.62μm) compared to cells expressing cdc5ΔC-kd (mean value of 0.89μm) (Figure 5.18 B&C). Furthermore, I asked if these cells would continue the cell cycle into telophase after releasing them from metaphase arrest by turning on Cdc20 expression by removing methionine, but keeping them on galactose. After growing for additional two hours in media containing galactose and lacking methionine, Mtw1-YFP cells expressing Cdc5ΔC-GBP successfully continued the cell cycle through anaphase and telophase, although at slightly lower frequency than cells expressing cdc5ΔC-kd (Figure 5.18 D). This is consistent with reported centromeric localisation of Cdc5 during metaphase-anaphase transition, and thus a forced Cdc5 activity at the kinetochore specifically during this period was not necessarily anticipated to cause problems. In addition, I measured the distance between kinetochore and SPB foci and found no difference between cells expressing Cdc5ΔC-GBP and cdc5ΔC-kd-GBP (Figure 5.18 E).

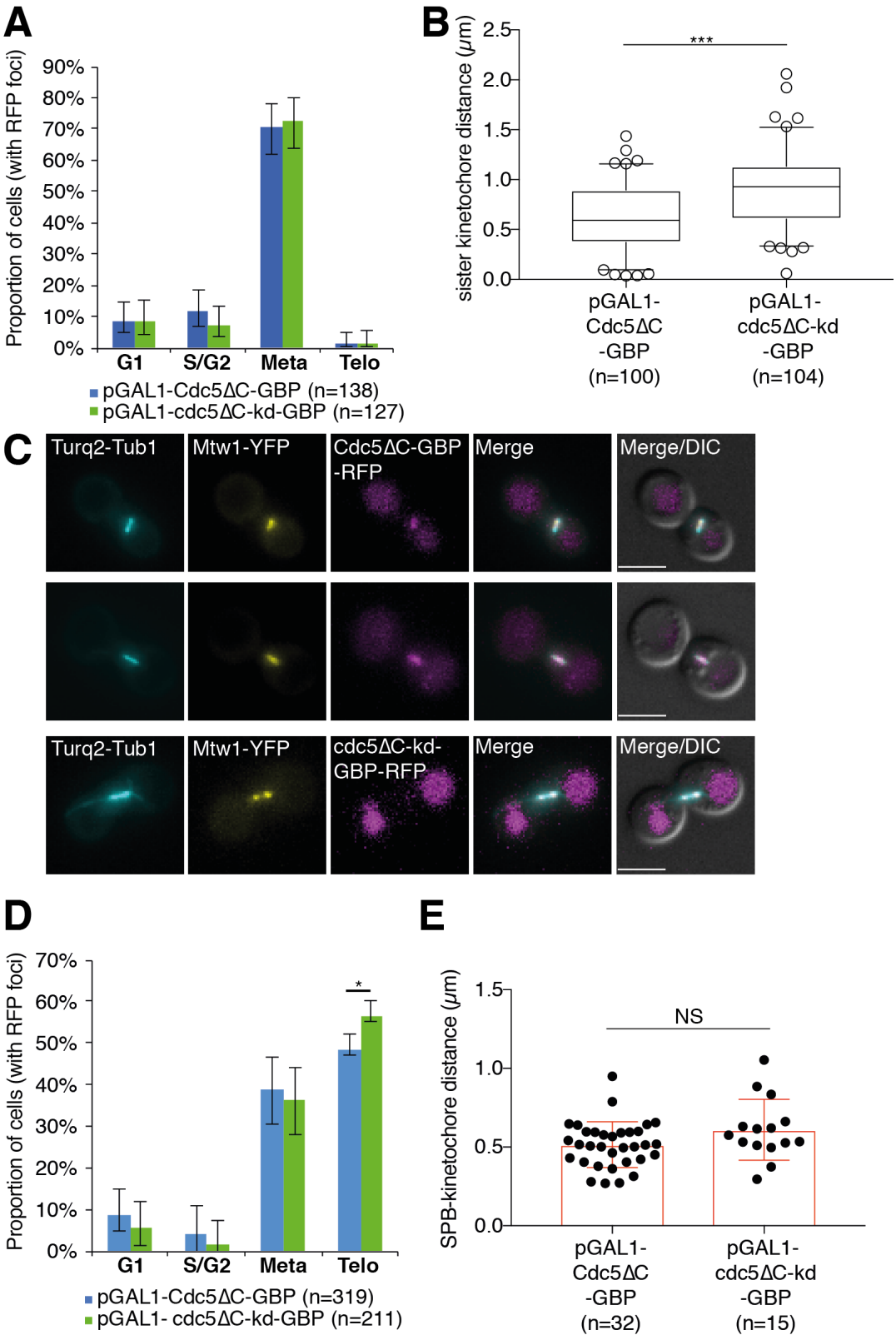

Figure 5.18 Forced kinetochore recruitment of Cdc5 reduces mitotic spindle length.

A) A quantification of the cell-cycle stage of the Mtw1-YFP strain containing *cdc20Δ::pMET3-CDC20* and either the pGAL1-Cdc5ΔC-GBP or cdc5ΔC-kd-GBP plasmids, which was arrested in metaphase by Cdc20 depletion for two hours in media containing raffinose and methionine. Meta and Telo refers to metaphase and telophase, respectively. Error bars indicate 95% binomial C.I.
B) The cell cultures in (A) were treated with galactose for two hours to express either Cdc5ΔC-GBP or cdc5ΔC-kd-GBP. The sister kinetochore distance was measured using a semi-automated foci quantification ImageJ script (see section 2.3.2 for details). The box and whiskers plot indicates the mean sister kinetochore distance and standard deviation of the variance (line and box, respectively). The whiskers indicate the 95 percentile and outliers are indicated as circles. Statistical analysis was done using two-tailed student's t-test; p-value *** = 5.4×10^{-8}.
C) Fluorescence microscopy representative of cells in (B), showing reduced mitotic spindle length of Mtw1-YFP cells expressing Cdc5ΔC-GBP compared with cells expressing cdc5ΔC-kd-GBP. All scale bars are 5μm.
D) The cells in (B) were released from Cdc20 depletion by resuspending and growing the cultures for two hours in galactose media lacking methionine and cell cycle analysed. Statistical analysis was done using Fishers exact test; p-values * = $p < 0.05$. Error bars indicate 95% binomial C.I.
E) A *cdc20Δ::pMET3-CDC20* strain containing Mtw1-YFP and Spc110-CFP and expressing either Cdc5ΔC-GBP or cdc5ΔC-kd-GBP was treated exactly the same as in (A), but the distance between SPB (Spc110-CFP) and kinetochore (Mtw1-YFP) foci was measured instead using an adapted version of the semi-automated foci quantification script. The bar graph shows the mean SPB-kinetochore distance and error bars indicate standard deviation of the variance. The data points (black dots) are overlaid on the graph to show the spread of the data.

Finally, I examined the cell-cycle phenotype of the forced Cdc5 recruitment to the DAM1/DASH complex. I introduced the pGAL1-Cdc5ΔC-GBP, pGAL1-cdc5ΔC-kd-GBP and pGAL1-GBP plasmids into a strain containing Dad4-YFP and mTurqoise2-Tub1 and assessed the cell-cycle stages after growing the cells for four hours in galactose medium. Surprisingly, and in contrast to the forced Cdc5ΔC association with Mtw1, which resulted in early cell-cycle arrest, the forced Cdc5 association with Dad4 accumulates cells late in the cell cycle, possibly in late anaphase or telophase (Figure 5.19 A&C). Furthermore, expression of Cdc5ΔC-GBP in Dad4-YFP cells disrupts the Dad4-YFP foci and the spindle (Figure 5.19 B&D).

In conclusion, these results imply that the short spindle phenotype caused by the forced Cdc5 association with Mtw1 during metaphase is not catastrophic for anaphase progression, and the kinetochores are able to attach to microtubules and presumably regain tension and continue the cell cycle. In contrast, the forced Cdc5-Dad4 association seems to disrupt the anaphase spindle and/or telophase-G1-phase transition. Consequently, based on these combined results, I conclude that the growth phenotype caused by forced Cdc5 localisation to the MIND complex (Mtw1) is not a

consequence of post-metaphase defects (anaphase onwards), rather it is more likely caused by pre-mitotic disruptions, most likely in S-phase. The growth phenotype caused by forced Cdc5 recruitment to the DAM1/DASH complex (Dad4) is possibly a result of spindle disruption during anaphase, although further experiments are needed to gain more understanding of these forced Cdc5-kinetochore interactions.

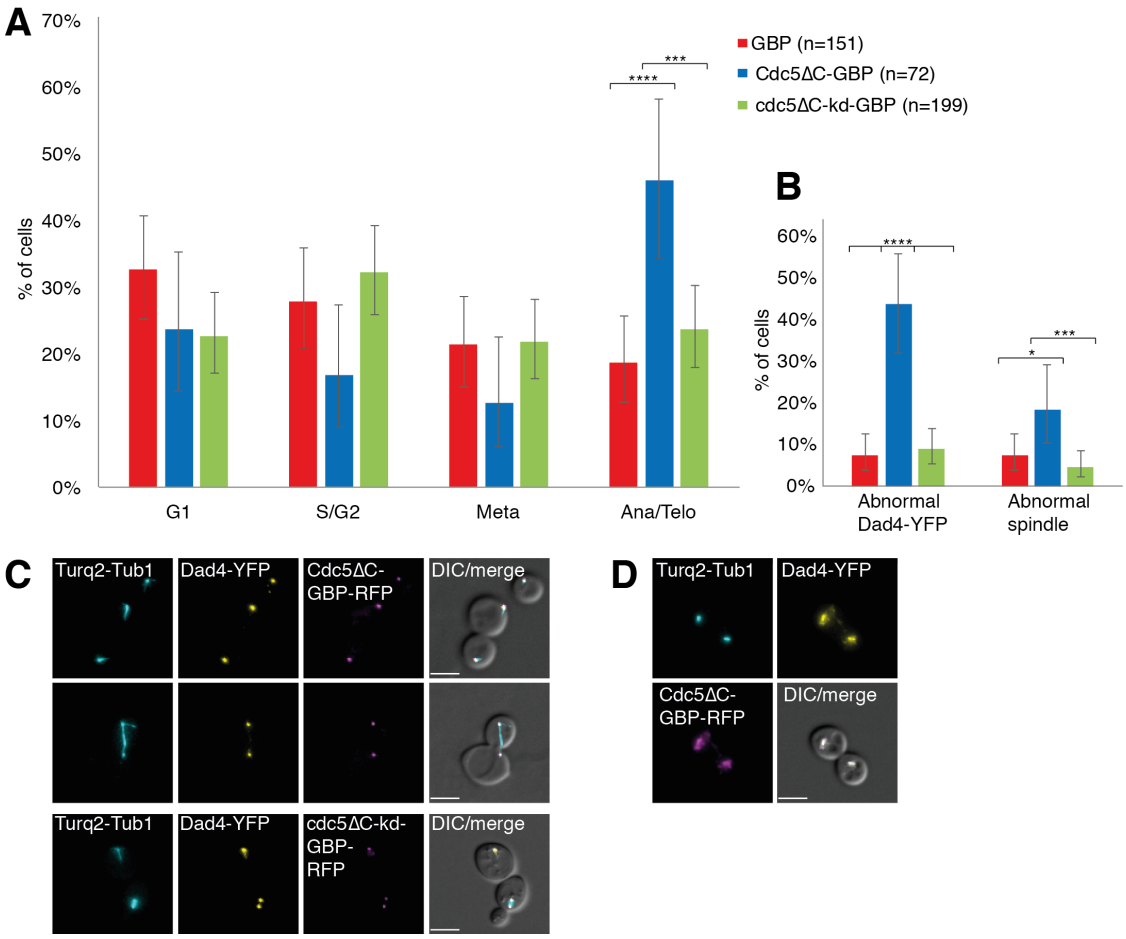

Figure 5.19 Forced Cdc5 recruitment to the DAM1/DASH complex accumulates cells late in the cell cycle.

A) A graph showing the cell-cycle analysis of Dad4-YFP cells expressing Cdc5ΔC-GBP, cdc5ΔC-kd-GBP or GBP alone, all under the control of *GAL1* promoter. Meta, Ana and Telo refers to metaphase, anaphase and telophase, respectively.
B) The Dad4-YFP signal and the spindle phenotype of the cells in (A) were analysed. Statistical analysis was done using Fishers exact test; p-values * = $p < 0.05$, *** = $p < 1x10^{-3}$, **** = $p < 1x10^{-4}$. Error bars indicate 95% binomial confidence intervals.
C) Fluorescence microscopy representative of cells in (A), showing Dad4-YFP cells expressing Cdc5ΔC-GBP in telophase (upper panel) and anaphase (middle panel) and cells expressing cdc5ΔC-kd-GBP (lower panel).
D) Fluorescence microscopy representative of cells in (B) with abnormal Dad4-YFP signal caused by Cdc5ΔC-GBP expression. All scale bars are 5µm.

5.2.14 Experiments to suppress the Cdc5-kinetochore growth phenotype

The potential kinetochore targets that get phosphorylated by tethered Cdc5 are numerous. However, I suspect that for any given SPI only one, or a small number, of phosphorylated residues lead to the cell-cycle phenotype. Identifying these residues is the next key step in this work.

I performed experiments in an attempt to suppress the growth defects causing the Cdc5-kinetochore SPIs. First, I overexpressed the PP1 phosphatase (Glc7), however, this failed to suppress any of Cdc5 kinetochore SPIs, if anything it enhanced the growth defect of many of them (Figure 5.20 A). For example, Bim1, Spc24, Nkp2, Mif2, Kar3, Sgo1 and Bub1 all had an increased growth defect when Glc7 was overexpressed compared to an empty plasmid. In contrast, the cdc5-kd kinetochore SPIs where not affected, enhanced nor suppressed, by Glc7 overexpression (Figure 5.20 B). I also repeated the Cdc5 SPI assay with Ipl1 overexpression plasmid (pGAL1-Ipl1) to ask if it could suppress any Cdc5 kinetochore SPIs. However, overexpression of Ipl1 did not affect Cdc5 (or cdc5-kd) SPIs compared with an empty plasmid (Figure 5.20 C&D).

Furthermore, I also sought to identify specific critical Cdc5 phosphosites by creating mutants of kinetochore subunits that cannot be phosphorylated. In the case of Mps1 kinetochore SPIs, for example, I was able to suppress the Mps1-KMN SPIs by expressing a mutant of Spc105 that has the MELT motifs modified so that they cannot be phosphorylated (spc105-6A) (see section 4.2.5 in chapter 4). Since, the DAM1/DASH complex was specifically sensitive to kinase-active Cdc5, but not cdc5-kd, I decided to make phospho-mutants of its subunits in order to prevent phosphorylation. I chose Dam1 and Ask1, which are both well characterised phosphoproteins. It has been reported that Ask1 is phosphorylated by CDK/Cdc28 and Ipl1 kinases (Cheeseman *et al.*, 2002; Li & Elledge, 2003). CDK has been shown to phosphorylate Ask1 on two serine residues at position 216 and 250 (Li & Elledge, 2003; Higuchi & Uhlmann, 2005). Although, these sites have not been reported to be phosphorylated by Cdc5, serine 250 is a polo kinase consensus phosphosite. I created two plasmids one containing wild-type Ask1 and another containing a mutant with both serines mutated to alanines (S216A and S250A) under the control of *GALS* promoter (pGALS-Ask1 and pGALS-ask1-2A, respectively), which is a weaker version of the *GAL1* promoter (Mumberg *et al.*, 1994). However, addition of ask1-2A mutant in the

SPI screen did not suppress any of the Cdc5 kinetochore SPIs compared with overexpression of wild-type Ask1 (Figure 5.20 E).

Another important kinetochore phosphoprotein and also a component of the DAM1/DASH complex, Dam1, is phosphorylated by Ipl1 at many sites to regulate kinetochore-microtubule attachment in budding yeast (Cheeseman *et al.*, 2002). The Dam1 phosphosite (S143) in *S. pombe* matches completely polo-kinase consensus sequence, but the equivalent site in *S. cerevisiae* (S221) has been shown to be phosphorylated by Mps1 in vitro (Shimogawa *et al.*, 2006; Buttrick & Millar, 2011). However, Cdc5 might phosphorylate this site in budding yeast in vivo (Buttrick & Millar, 2011). Also, Mps1 phosphorylation at serines 218 and 221 of Dam1 in budding yeast is thought to stabilise microtubule binding, thus counteracting the destabilising activity of Ipl1 phosphorylation at the other sites on Dam1 (Shimogawa *et al.*, 2006). I examined the possibility that the forced Cdc5 kinetochore recruitment could phosphorylate these sites by repeating the Cdc5 kinetochore SPI screen and co-expressing a Dam1 mutant with these two sites (S218 and S221) changed to alanines from a plasmid and test if it would suppress the SPI phenotype compared to a plasmid with a wild-type Dam1 (pGALS-dam1-2A and pGALS-Dam1, respectively). However, the Cdc5-DAM1/DASH SPIs where not suppressed by overexpressing dam1-2A compared to wild-type Dam1 nor any other kinetochore SPIs, suggesting that other phosphorylation events might be important for the SPI growth phenotype (Figure 5.20 F).

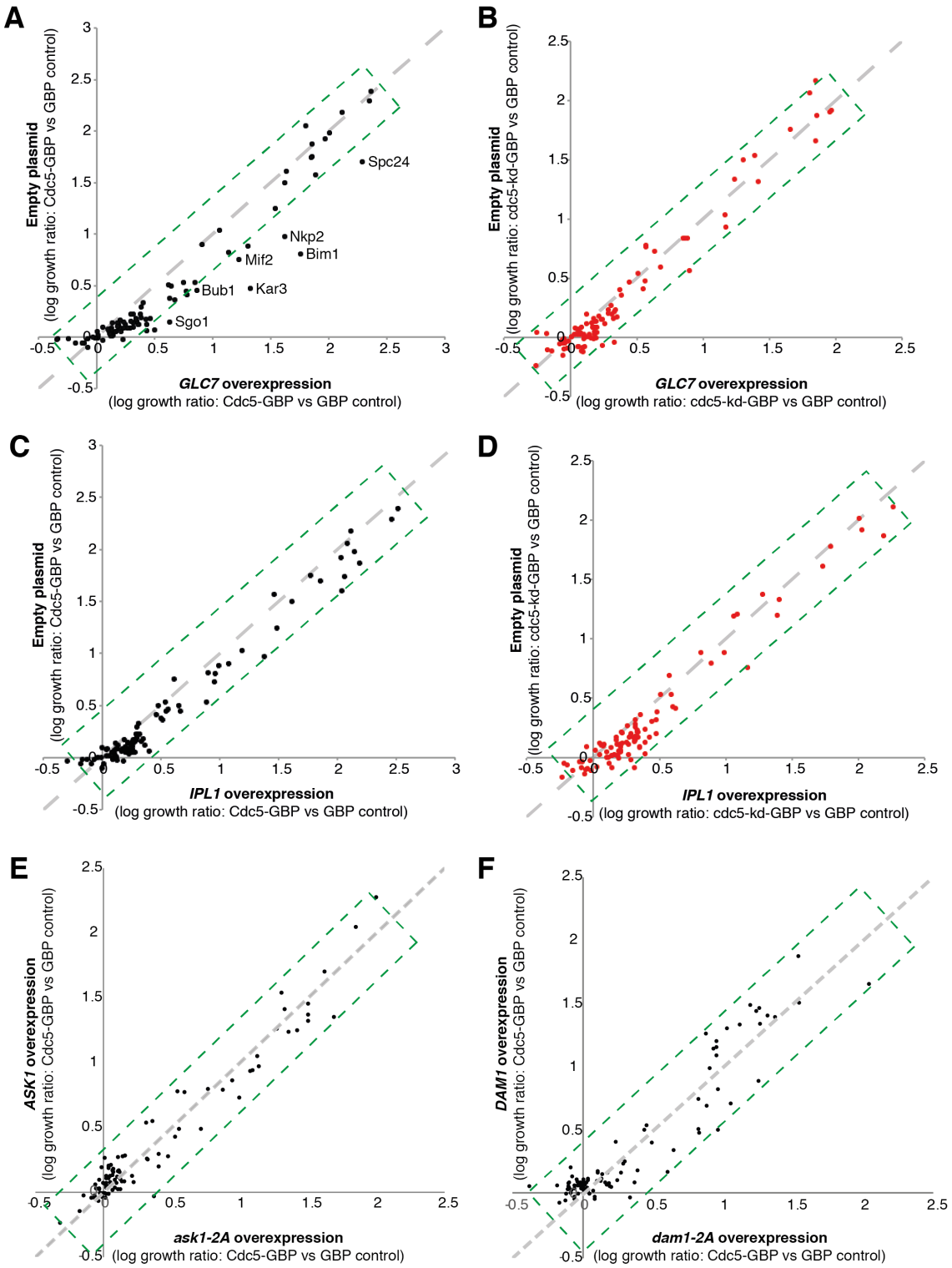

Figure 5.20 Suppression of the Cdc5-kinetochore SPIs.

A-B) The Cdc5 kinetochore SPI assay was repeated with both an empty plasmid and a Glc7-overexpression plasmid in addition to the Cdc5-GBP (A) and cdc5-kd-GBP (B) plasmids and the GBP control and the resulting data was plotted as shown with empty plasmid on the y-axis and *GLC7* on the x-axis.
C-D) The Cdc5 kinetochore SPI assay was repeated with both an empty plasmid and an Ipl1-overexpression plasmid in addition to the Cdc5-GBP (C) and cdc5-kd-GBP (D)

plasmids and the GBP control and the resulting data was plotted as shown with the empty plasmid on the y-axis and *IPL1* on the x-axis.
E) The Cdc5 kinetochore SPI assay was repeated with both a plasmid containing wild-type Ask1 and a plasmid containing a ask1-2A mutant under the control of a GALS promoter in addition to the Cdc5-GBP (C) and cdc5-kd-GBP (D) plasmids and the GBP control and resulting data was plotted as shown with wild-type Ask1 on the y-axis and ask1-2A on the x-axis.
F) The Cdc5 kinetochore SPI assay was repeated with both a plasmid containing wild-type Dam1 and a plasmid containing a dam1-2A mutant under the control of a GALS promoter in addition to the Cdc5-GBP (C) and cdc5-kd-GBP (D) plasmids and the GBP control and the resulting data plotted as shown with wild-type Dam1 on the y-axis and dam1-2A on the x-axis. In all cases the green square regions indicate interactions that were not affected by the additional plasmid.

Collectively, these attempts to suppress the growth phenotype caused by forcing Cdc5 kinetochore recruitment have so far been unsuccessful. I still cannot rule out the possibility that the phosphosites on Ask1 and Dam1 are being constitutively phosphorylated by some Cdc5 kinetochore SPIs, but the growth defect is caused by simultaneous phosphorylation of two (or more) residues, consequently the phenotype is not suppressed by any single mutant. However, it can still be speculated that a single site on a single substrate is being hit in any one Cdc5 SPI, therefore in theory it should be possible to rescue a growth phenotype by preventing the phosphorylation of that single site. Yet, it would be an immense and time-consuming endeavour to attempt to make single site mutations of every possible phosphosite at the kinetochore with the hope that one might suppress a Cdc5 SPI. Therefore, I sought to narrow down the possible phosphosites affected by the forced Cdc5 kinetochore recruitment using a different approach.

5.2.15 Quantitative phosphoproteomics analysis of Cdc5 kinetochore SPI

In order to investigate which phosphosites are being affected by the forced Cdc5 kinetochore localisation I decided to use stable isotope labelling with amino acids in cell culture (SILAC) methodology (Jiang & English, 2002; Ong, 2002) (see section 2.6.4 for details of sample preparation for SILAC analysis). First, I asked which kinetochore phosphosites are being inhibited by the forced kinase-dead Cdc5 kinetochore recruitment. According to the working model forcing cdc5-kd to kinetochore subunits of the KMN network prevents the endogenous Cdc5 activity through the binding of PBD to its substrates at this region and results in SAC activation (Figure 5.9 A). Therefore, I hypothesised that heavy/light ratios for Cdc5 consensus phosphosites within kinetochore components in vicinity of a GFP-tagged kinetochore protein will be

quantitatively downregulated by the expression of cdc5-kd-GBP. I modified a budding yeast strain that has been designed for SILAC treatment (Gruhler *et al.*, 2005; Godfrey *et al.*, 2017) (see T619 in Table 2.1 in section 2.1.1). I transformed *MTW1-YFP::HIS3MX* into this strain as well as *mad1Δ::NATMX,* since a constitutive expression of cdc5-kd-GBP would arrest growth in a Mtw1-YFP wild-type *MAD1* strain. I made cultures of this strain containing either the pCUP1-cdc5-kd-GBP plasmid or the pCUP1-cdc5-kd-FAM-GBP plasmid lacking functional PBD, to control for its activity, since the variable under investigation is the PBD. Next, I mixed equal amounts of 'heavy' culture containing cdc5-kd-GBP with a 'light' culture containing cdc5-kd-FAM-GBP and the reverse. As additional controls, I also prepared two samples of heavy/light mixtures each containing the same plasmid, thus these samples should not have large differences (H/L ratios) in phosphopeptide abundance. Hence, total of four lysate samples were prepared for further treatment before mass spectrometry (see section 2.6.4 for details).

These experiments are still ongoing but preliminary data show a number of candidate phosphosites (Appendix figure 2). These include downregulated phosphosites caused by the forced Mtw1-association with cdc5-kd compared to cdc5-kd-FAM. These phosphosites are, among others, on the microtubule-associated proteins (MAPs) Bim1 and Bik1, the kinetochore protein Spc105, and the APC/C inhibitor Acm1.

Importantly, the downregulated phosphosites identified on Bim1, threonine and serine at positions 175 and 176 respectively, are not consensus sites for Cdc5 phosphorylation, but Aurora B/Ipl1. It has been reported that the CPC phosphorylates multiple residues clustered at a flexible linker region connecting a N-terminal CH domain and a C-terminal EB1-like domain which are both highly conserved (Zimniak *et al.*, 2009). The downregulated phosphoserine 176 detected by the SILAC experiment is one of these sites. The study also showed that these sites are phosphorylated during anaphase and reduce the affinity of Bim1 for microtubules. Bim1 normally localises to microtubule plus ends and accumulates at the spindle midzone in anaphase. A phospho-deficient mutant of Bim1 (*bim1-6A*) is not removed from the spindle midzone and results in spindle disassembly defects and eventually spindle breakage, suggesting a crucial role for Ipl1 in regulating the stability of the overlapping microtubules at the midzone during anaphase, and for spindle disassembly in telophase (Zimniak *et al.*, 2009).

Another downregulated phosphosite identified by the SILAC experiment is serine 117 on Bik1. Bik1 (homolog of human CLIP-170), like Bim1 is also a plus-end tracking microtubule protein. Bim1 and Bik1 have been shown to form a complex and together regulate microtubule dynamics (Blake-Hodek *et al.*, 2010). As previously described (section 5.1.2), Plk1 regulates plus-end microtubule proteins in human cells, and additionally, both CLIP-170/Bik1 and EB1/Bim1 associate with CLASP1 and -2 (related to yeast Stu1), and this interaction has been reported to be important for microtubule plus-end dynamics (Mimori-Kiyosue *et al.*, 2005). Therefore, it is a possibility that similar regulation by Cdc5 exists in budding yeast.

Interestingly, two phosphoserines at kinetochore protein Spc105 were detected by the SILAC experiment, but one was upregulated (S380) and the other downregulated (S385). These sites have not been examined previously in detail, but the upregulated serine 380 is a minimal CDK consensus phosphosite, thus a possible PBD docking site, and both were detected in a global analysis of phosphosites that overlap with ubiquitylation sites (Swaney *et al.*, 2013), suggesting that this region might perhaps be regulated for Spc105 degradation, possibly by Cdc28 and Cdc5.

Finally, two phosphoserines belonging to Acm1 (S87 and S95) were also detected by the SILAC experiment as being strongly downregulated by the cdc5-kd forced kinetochore recruitment. Acm1, a pseudosubstrate inhibitor of APC/C-Cdh1, and together with Bmh1 and Bmh2 (members of the 14-3-3 complex in yeast) prevent Cdh1 from activating the APC/C (Martinez *et al.*, 2006; Ostapenko *et al.*, 2008). APC/C-Cdh1 is inactive in S-phase when Acm1 is predominantly expressed and remains until late mitosis. To inhibit Cdh1, Acm1 phosphorylation is required for the binding with Bmh1/2 and Cdh1, and deletion of *ACM1* results in accumulation of S-phase cells (Dial *et al.*, 2007). Acm1 is phosphorylated by Cdc28 at multiple sites which is critical for its stabilisation. The two Acm1 phosphoserines (S87 and S95) detected in the SILAC experiment do fit minimal Cdc5 consensus and both are uncharacterised, but they were also detected by the phosphosite-ubiquitylation site overlap study (Swaney *et al.*, 2013). Intriguingly, Plk1 regulates the APC/C-Cdh1 inhibitor, Emi1, in human cells (David V. Hansen *et al.*, 2004; Moshe *et al.*, 2004). Emi1 protein level accumulates in S-phase and is reduced early in mitosis through phosphorylation by Plk1 leading to ubiquitylation-dependent degradation, thus allowing the necessary APC/C activity in

late mitosis. Although, the yeast Acm1 and human Emi1 are not considered homologs they are functionally similar (Ostapenko *et al.*, 2008), and thus it would be exciting to investigate a possible role for Cdc5 in regulating Acm1 (and therefore APC/C activity) in the future and if kinetochore localisation is important for this process.

In summary, these preliminary SILAC data, suggest that phosphorylation status of several proteins is affected by the forced cdc5-kd kinetochore association. However, it is important to note that any of these phosphorylation changes could be a secondary consequence of the forced association. For example, the SAC activation caused by cdc5-kd kinetochore recruitment could initiate chain of events eventually affecting Acm1 phosphorylation status, even in a SAC-deficient *mad1*Δ strain, especially since the Cdc20 and Cdh1 co-activators of APC/C are separately regulated. In future SILAC experiments I will assess the phosphorylation changes caused by forced kinetochore recruitment of the kinase-active Cdc5, and it will be interesting to see if the same or novel phosphosites will be detected.

5.3 Summary

Throughout this chapter I have discussed the results individually, so here I will provide a summary of key findings. Initially, the proteome-wide Cdc5 SPI screen confirmed previous results showing that a forced Cdc5 kinetochore recruitment is detrimental for cell growth. In addition, the SAGA complex and the RNA polymerase II transcription factor complex are sensitive to constitutive Cdc5 association. A more detailed analysis of the Cdc5 kinetochore SPIs revealed that many central and outer kinetochore proteins were sensitive to constitutive Cdc5 association. The DAM1/DASH complex (and Cse4) was specifically sensitive to kinase-active Cdc5, but not to kinase-dead mutant. Conversely, the KMN network proteins and Ame1 were sensitive to both kinase-active and inactive Cdc5. I found that the kinase-dead Cdc5 forced association with these proteins arrested cells in mitosis in a SAC-dependent manner. This mitotic arrest was relieved when the PBD was either removed or mutated. While the kinase-active Cdc5 kinetochore SPIs were produced independently of the PBD. These results let to the hypothesis that the forced kinase-dead Cdc5 recruitment to the KMN network was preventing endogenous Cdc5 kinetochore activity which results in SAC activation through a currently unknown mechanism.

Further cell-cycle analysis of the forced kinase-active Cdc5 central kinetochore association suggests that the phenotype is a consequence of a pre-mitotic disruption of kinetochore function, possibly during S-phase. While the sister kinetochore distance was reduced by the forced Cdc5-kinetochore association in cells that were arrested in metaphase by Cdc20 depletion, the cell cycle continued after Cdc20 restoration and the cells progressed normally through anaphase. In contrast, the forced Cdc5 recruitment to the DAM1/DASH complex, seems to prolong anaphase and/or telophase.

Experiments designed to suppress the kinase-active Cdc5 kinetochore SPIs, by either co-expressing other kinetochore regulators or phospho-deficient mutants were unsuccessful. Nevertheless, the preliminary phosphoproteomics analysis revealed kinetochore or associated proteins whose phosphorylation status was changed by the forced kinetochore recruitment of kinase-dead Cdc5, thus providing additional candidates that might be important for the Cdc5 SPI phenotype. In conclusion, it is clear that constitutive Cdc5 (either active or inactive) localisation at the kinetochore disrupts the cell cycle in different ways, and at different times, depending on which subcomplex Cdc5 is associated with. Future experiments will continue to try to dissect these different Cdc5 kinetochore functions (discussed further in chapter 6).

Chapter 6. Discussion

6.1 The SPI methodology identifies candidates for kinetochore regulation

We have developed a method to systematically force the association of two proteins in vivo. We term this approach 'synthetic physical interactions' or SPIs and use it to force any protein of interest with most members of the budding yeast proteome. In order to identify kinetochore regulators, I performed a proteome-wide SPI screen with the central kinetochore protein Mtw1. I then followed this up with additional SPI screens with subunits representing the different kinetochore subcomplexes. This produced a list of candidate kinetochore regulators, some of which have known kinetochore functions, such as the Aurora B/Ipl1 kinase (Figure 3.18 in section 3.2.6). Others have less defined kinetochore roles, such as the Cdc14 phosphatase and the Cdc5 Polo-like kinase. Moreover, other post-translational modification proteins such as acetylases, deacetylases, methylases, SUMO ligases and deubiquitinases have only been relatively recently appreciated as important regulators of kinetochore function and mitosis. Among the kinetochore SPIs, I found several kinases and phosphatases, a SUMO-targeted ubiquitin ligase, together with subunits of the RPD3 and SET3 histone deacetylase complexes (HDAC).

A constitutive deacetylase activity at the kinetochore could have a negative impact on centromeric transcription which is thought to be important for centromere function, as well as kinetochore assembly and maintenance (Volpe *et al.*, 2002; Ohkuni & Kitagawa, 2011; Chan *et al.*, 2012*a*; Chan & Wong, 2012; Liu *et al.*, 2015; Blower, 2016; Molina *et al.*, 2016). Consistent with this, I also detected Opi1 and Cyc8 as kinetochore SPIs. Opi1 is a transcriptional repressor which has been shown to recruit Cyc8 (Kliewe *et al.*, 2017), a corepressor which in turn is involved in recruiting HDAC to repress transcription (Wu *et al.*, 2001; Fleming *et al.*, 2014). Interestingly though, the Hog1 MAP kinase (which was detected as a weak kinetochore SPI) is able to convert the Cyc8 repressor complex into a transcriptional activator by recruiting the SAGA and SWI/SNF complexes (Proft & Struhl, 2002).

Furthermore, I found that forced recruitment of Dbf4 (subunit of DDK) to the kinetochore gave a SPI phenotype. Recently, the molecular mechanism was described for DDK-dependent cohesin loading on centromeres (Hinshaw *et al.*, 2017 and references therein). DDK is recruited to the Ctf3 kinetochore subcomplex in late G1-phase and phosphorylates the N terminus of the Ctf19 protein (subunit of the COMA complex), which signals the recruitment of the cohesin loader Scc2/4. This ensures proper cohesin enrichment at centromeres and prepares it for early replication in S-phase. Indeed, it has been shown that DDK also facilitates the recruitment of replication initiation factors to the kinetochore (Natsume *et al.*, 2013). I also frequently detected both cohesin and condensin subunits as kinetochore SPIs. Hence, the constitutive DDK-kinetochore association I created could be "overloading" the centromere with cohesin or perhaps initiating DNA replication inappropriately. Whereas, the cohesin/condensin SPIs might be preventing removal of cohesin/condensin or sliding of cohesin to the pericentromere. In addition, there is some evidence which suggests that DDK might inhibit Cdc5 through a largely elusive mechanism (Miller *et al.*, 2009; Chen & Weinreich, 2010). This is could be an interesting possibility for future research, since Cdc5 is involved in removal of centromeric cohesin (discussed previously and further in section 6.3.2 below). Cohesion at the pericentromere is not only important for centromeric replication and for keeping the two sister chromatids together until anaphase, it has also been proposed to be required for establishing an appropriate geometry at the centromere necessary for biorientation (Ng *et al.*, 2009; Winey & Bloom, 2012; Lawrimore *et al.*, 2016; Salmon & Bloom, 2017).

Taken together, it remains to be seen how exactly these SPIs affect kinetochore function and if their phenotype is a consequence of misregulation of centromeric transcription, cohesin loading, replication, or by some other processes. In general, the SPI data serves as a good basis for further research and in many cases, supplements previous reports, thus future investigation of the kinetochore SPIs discussed here would be worthwhile.

6.1.1 What is the role of Cdc14 at the kinetochore?

Cdc14 phosphatase has important roles in ensuring mitotic progression and exit. First, it is released from the nucleolus in early anaphase through the FEAR mechanism, and later by the MEN pathway to reverse CDK activity and to initiate mitotic exit and

cytokinesis. The early release permits the Cdc14-dependent regulation of the 14-3-3 complex (Bmh1 and Bmh2 in budding yeast) which liberates Fin1-Glc7 and licences its relocation to the kinetochore to silence the SAC and to the spindle midzone to stabilise the anaphase spindle (Woodbury & Morgan, 2007; Akiyoshi *et al.*, 2009; Bokros *et al.*, 2016). Misregulated Fin1 is detrimental for successful mitosis, however I ruled out Fin1 as being responsible for the Cdc14 kinetochore SPI phenotype (Figure 3.15 in section 3.2.5). Cdc14 is also directly involved in dephosphorylating proteins at the centromere/kinetochore. Important for anaphase spindle elongation, Cdc14 dephosphorylation of CPC relocates it from the centromere to the spindle midzone (Pereira & Schiebel, 2003; Mirchenko & Uhlmann, 2010). Cdc14 also dephosphorylates a CDK site on Dsn1, prior to anaphase (Akiyoshi & Biggins, 2010). When Ipl1 phosphorylation of Dsn1 is prevented it becomes targeted for Mub1-Upr2-mediated degredation, however the additional Cdc14 dephosphorylation can overwrite this (Akiyoshi *et al.*, 2013*b*). I found that the constitutive Cdc14 association with the MIND complex was able to reduce phosphorylation of Dsn1, however this was not sufficient to produce the SPI phenotype (Figure 3.13 A and
Table 3.3 in section 3.2.5). Furthermore, the Cdc14 SPI phenotype did not involve the ubiquitin ligase, Ubr2 (Figure 3.13 B-D). Another Cd14 substrate, Ask1, a component of the DAM1/DASH complex is dephosphorylated by Cdc14 which is thought to silence microtubule dynamics at the kinetochore and promote successful anaphase (Higuchi & Uhlmann, 2005). However, the precise mechanism behind these dephosporylation events is still unclear. I found that several subcomplexes were sensitive to constitutive Cdc14 localisation in a SAC-independent manner, including the DAM1/DASH and MIND complexes, as well as components of the CEP3 and COMA complexes and the MAPs, Stu2 and Bik1 (Figure 3.10). Many of these proteins contain CDK consensus phosphosites. However, it remains a question which CDK phosphosites are affected by the forced Cdc14 recruitment to different kinetochore subcomplexes. Nevertheless, these data highlight the importance of CDK phosphorylations for kinetochore homeostasis. In the future, it would be interesting to examine the involvement of the other known Cdc14 substrates, Ask1 and the CPC in producing the Cdc14 kinetochore SPIs, as well as exploring the potential roles of the COMA and CEP3 complexes and the MAPs with Cdc14.

Future experiments such as quantitative phosphoproteomics could also narrow down the possible kinetochore substrates of Cdc14. In addition, cell-cycle analysis using

fluorescence microscopy and flow cytometry of these Cdc14 SPIs are required to further characterise the role of Cdc14 at the kinetochore. There were some limitations with the Cdc14 kinetochore SPIs that prevented me from studying their phenotype further. Even though I am confident that the partial mislocalisation of the GFP-tagged kinetochore (Mtw1-GFP) to the nucleolus in cells expressing Cdc14-GBP was not causing the phenotype (since the mislocalisation persisted with the mutant Cdc14-GBP without causing a growth phenotype), it creates issues for using fluorescence microscopy in examining, for example, the mitotic spindle status of cells, since additional kinetochore signals could be misinterpreted. Furthermore, Cdc14 dimerises and, in some SPIs, there wasn't much difference in growth when recruiting either the phosphatase-active or phosphatase-dead versions of Cdc14. I attributed this to the possibility that the mutant Cdc14 was able to dimerise with the endogenous wild-type Cdc14 and thus producing similar effects as forcibly recruiting the wild-type Cdc14. However, this could also point to an equivalent notion that I later ascribed to the forced recruitment of kinase-dead Cdc5 to the kinetochore; that is to say, the phosphatase-dead Cdc14 recruitment to kinetochore proteins could be preventing dephosphorylation by the endogenous wild-type Cdc14, thus resulting in hyper-phosphorylation of some kinetochore proteins which could be damaging for proper kinetochore function.

6.2 Investigating the mitotic checkpoint with SPIs

The proteome-wide Mad2 SPI screen identified many proteins which when were forced into contact with Mad2 inhibited cell growth. These Mad2 SPIs were enriched for nuclear envelope and transport proteins in agreement with the notion that the SAC proteins have a role at nuclear pores (Iouk *et al.*, 2002; Rodriguez-Bravo *et al.*, 2014). I also found some kinetochore proteins as Mad2 SPIs, but after further examination of these SPIs I found that the growth inhibition was either SAC independent or indirectly resulting in SAC activation, as was seen by the direct genetic fusion of Cse4 and Mad2 (Figure 4.6 in section 4.2.3). As discussed, this creates an important problem for creating artificial associations with kinetochore proteins in general, which could disrupt their function, thus causing SAC activation independently of the actual SAC pathway. This idea though cannot rule out a possible role for Mad2 at the inner kinetochore, since cells expressing the Cse4-Mad2 fusion were viable in a *mad3*Δ strain (Figure 4.6 B in section 4.2.3).

6.2.1 Kinetochore enrichment of Mad1 and Mad2 is not sufficient for SAC activation in budding yeast.

As discussed previously, forcing Mad1 and Mad2 to kinetochore proteins was insufficient to activate the SAC. I found that the SPI system was not preventing SAC activation by the GBP-GFP interaction, since the forced recruitment of a localisation-mutant Mad1 to the SPC105 complex was able to rescue benomyl sensitivity of a *mad1*Δ strain (Figure 4.10 in section 4.2.4). The discrepancy of other data from metazoans and the data presented in this work in budding yeast, could be partly explained by the importance for SAC silencing through the removal of Mad1 and Mad2 from metazoan kinetochores by dynein and Spindly (Howell *et al.*, 2001; Wojcik *et al.*, 2001; Barisic *et al.*, 2010; Gassmann *et al.*, 2010), a mechanism which budding yeast lacks. Furthermore, the SAC can be reactivated in human cells even after initial silencing by forcing Mad1 recruitment to the kinetochore (Kuijt *et al.*, 2014). Based on my data this does not seem to occur in budding yeast, suggesting that at least for SAC silencing, the mechanisms are different between the two species.

In contrast, I showed that Mps1 kinase specifically arrested growth in a SAC-dependent manner when I forced it to the KMN network of the kinetochore. This supports previous reports and confirms that Mps1 kinase is the key driver of SAC activation.

6.2.2 Do SAC proteins have a role at the inner kinetochore?

As discussed, the forced Mad2 association with Cse4 does disrupt growth in a SAC-dependent manner; although it is unlikely a direct target for SAC activation. Interestingly, I did find subtle effects of forced associations of Mad1 with inner kinetochore proteins (Ndc10, Cep3 and Mif2) although these effects disappeared when the data was analysed with mutants of Mad1 as controls (Figure 4.7 in section 4.2.4). However, it is unlikely that these Mad1-inner kinetochore SPIs are simply a consequence of forcing any protein association with these inner kinetochore proteins since they are not detected in many SPI screens. Furthermore, in both Mad1 and Mad2 SPI screens I observed a weak SPI phenotype (log growth ratio between 0.2 and 0.4) with subunits of the COMA complex. COMA is a subcomplex of the Ctf19 complex or CCAN of inner and central kinetochore proteins. Interestingly, both the CBF3 and COMA complexes have been shown to be required for SAC activity (Gardner *et al.*,

2001; Pot *et al.*, 2005). The COMA complex was also shown to be required, in a separate pathway to the KMN network, to recruit Mad1 and Mad2 (Matson *et al.*, 2012). Additionally, the Ctf3 and Chl4 (subunits of CCAN) were shown to be required for SAC activity (Matson *et al.*, 2012). Moreover, the SAC component Bub1 and the inner kinetochore subunit Skp1 have been shown to interact and this interaction was proposed to be important to transmit a signal to the checkpoint in case of low kinetochore tension (Kitagawa *et al.*, 2003). Therefore, it remains possible that Mad1 and Mad2 may have a function at the inner kinetochore.

Interestingly, forced Mad2 and Mad1 associations with CPC subunits, did arrest growth and in some cases in a SAC-dependent manner. The interplay between the SAC pathway and the CPC is well defined, however as far as I know, Ipl1 and Mad2 have not been reported to interact directly to activate the SAC. Hence it would be interesting to characterise this SAC-CPC SPI phenotype further in the future.

6.3 Does Cdc5 have functionally separate roles at the kinetochore?

The proteome-wide Cdc5 SPI screen detected around 100 SPIs, almost half of which were kinetochore or associated proteins (Figure 5.4 in section 5.2.1). In addition, the screen detected many subunits of the SAGA complex and the RNA polymerase II transcription factor complex as Cdc5 SPIs; which is interesting with regard to transcription at the kinetochore. In terms of the kinetochore SPIs though, we have never seen such enrichment of a single cellular component in any of our screens. However, the question is whether Cdc5 has a single effect upon being forced to kinetochore proteins or are the kinetochore Cdc5 SPIs functionally different? In human cells, it has been shown that Plk1 has multiple independent roles depending on its location at the centromere-kinetochore axis (described in sections 5.1.2 and 5.1.3).

6.3.1 Does constitutive kinase-dead Cdc5 kinetochore localisation inhibit endogenous Cdc5 kinetochore activity?

In my working model, proposed in Figure 5.9 A (section 5.2.3), I hypothesised that the forced recruitment of the kinase-dead Cdc5 to the kinetochore might by preventing endogenous Cdc5 from binding to CDK substrates at the kinetochore via the polo-box domain (PBD). This idea was supported by my observation that mutation of PBD was

sufficient to completely rescue the kinase-dead Cdc5 kinetochore SPIs. This is also in agreement with overexpression of PBD preventing Plk1 kinetochore activity in human cells. Interestingly, I found that the kinase-dead Cdc5 kinetochore SPIs with the KMN network were also suppressed when I deleted SAC proteins required for checkpoint activation. This is also in agreement with the study in human cells which showed that PBD overexpression let to SAC activation (Liu *et al.*, 2012). However, I cannot rule out the possibility that the SAC is not the sole reason for the kinase-dead Cdc5 SPIs, since SAC deletion did not rescue all kinetochore SPIs, and a couple where only partially suppressed (Figure 5.8 B); suggesting there could be additional SAC-independent effects by preventing endogenous Cdc5 kinetochore activity. However, I haven't shown directly whether wild-type Cdc5 kinetochore activity is compromised in these cells. We have attempted to tackle this problem by performing the phosphoproteomics analysis, but not many kinetochore phosphosites were identified in the preliminary experiments, thus further work is required to show definitively whether this idea is true. In addition, the model is limited by the fact that cells lacking Cdc5, but containing Cdc5ΔC fused to the SPB are viable (Park *et al.*, 2004*b*); thus these cells should not have Cdc5 at the kinetochore. It is possible that these cells were able to adapt to loss of Cdc5 from kinetochores or that sufficient amount of Cdc5ΔC-SPB fusion protein was produced so that some was able to reach kinetochores during mitosis when Cdc5 is normally at the centromere. I note that the rescue by the Cdc5ΔC-SPB fusion in *cdc5Δ* cells is not complete (Park *et al.*, 2004*b*).

6.3.2 Does constitutive Cdc5 kinetochore localisation affect centromeric cohesion?

Since Cdc5 has a well-documented role in cohesin regulation at centromeres, future experiments need to address the possibility that the constitutive Cdc5 kinetochore localisation is affecting centromeric cohesin. However, I speculate that this is unlikely causing the SPI phenotype, at least with Mtw1. For example, if cohesin is being destabilised prematurely this would have created an "artificial anaphase" onset in the Cdc20-depleted cell experiment described in section 5.2.13 (Figure 5.18), where the kinetochore-Cdc5 association was induced specifically during metaphase. It has been shown previously that Cdc20-depleted cells in which cohesin cleavage was induced conditionally, either by an artificially cleavable site (the TEV-protease system) on Scc1 (Uhlmann *et al.*, 2000), or when Esp1 (separase) is overexpressed (Lu & Cross, 2009), that these cells undergo anaphase and mitotic exit. However, in my experiment I found

that the cells remained in metaphase, but with reduced sister-kinetochore distance compared to control cells (Figure 5.18 B&C). These cells were nevertheless able to continue mitotic exit after reintroduction of Cdc20, even in the presence of the Cdc5-kinetochore association (Figure 5.18 D). Furthermore, I did not find that forced kinetochore recruitment of Esp1 produced a SPI phenotype. Although, individual negative results can be uninformative, this suggests that perhaps the Cdc5-kinetochore SPI result could be involved in cohesin misregulation or disruption. For example, the constitutive Cdc5 activity at the centromere/kinetochore could be interfering with the biorientation role of the centromeric cohesin. However, further experiments such as fluorescence microscopy of cells with a labelled cohesin complex and expressing the Cdc5-kinetochore association are required to asses this question.

6.3.3 Does constitutive Cdc5 kinetochore localisation affect microtubule attachment?

The interplay between Polo kinase and Aurora B kinase in regulating microtubule-attachment remains enigmatic. Aurora B/Ipl1 (which activates Plk1 in humans) is known to destabilise attachment when kinetochores are not under tension. In contrast, there is evidence that point to a microtubule-stabilising role for Polo kinase/Cdc5. Furthermore, Polo kinase is known to regulate MAPs that are involved in microtubule dynamics and either stabilising or destabilising microtubule attachments. Hence, I speculate that it is possible that Cdc5 could have direct or indirect roles in controlling attachment at the kinetochore; either stabilising correct attachments when kinetochores are under tension or destabilise erroneous attachments, perhaps depending on its localisation at the kinetochore. Hence, this control would need to be tightly spatiotemporally regulated to specifically stabilise correct attachments. Accordingly, the Cdc5 kinetochore SPIs could be a consequence of disruption of microtubule attachments or inappropriate stabilisation of incorrect attachments, or both, depending on the kinetochore sub-localisation or the timing of the SPI. The MAP, Stu2, is a known substrate of Cdc5, and it was shown that Stu2 can both stabilise and destabilise kinetochore-microtubule attachment depending on the tension-state of the kinetochore (Park *et al.*, 2008; Miller *et al.*, 2016). It is not known however, if phosphorylation by Cdc5 or other kinases, plays a role in this tension-sensing function of Stu2. I did not detect Stu2 as a Cdc5 SPI in my screen, however I found that another MAP, Bim1 was specifically sensitive to kinase-active Cdc5. Furthermore, it has been shown that the MAPs, Bim1, Bik1 and Stu2 interact in a complex network to control microtubule

dynamics (Wolyniak *et al.*, 2006; Blake-Hodek *et al.*, 2010), and similarly, Dis1/Stu2 and Mal3/Bim1 interact in fission yeast to promote faithful chromosome segregation (Matsuo *et al.*, 2016). Moreover, Stu2 localises to the overlapping coiled-coiled region of the Ndc80-Nuf2 dimer and the Spc24-Spc25 dimer, thus forcing Cdc5 to this region could target Stu2. I note that they were all detected as strong Cdc5 SPIs (Figure 5.5 in section 5.2.2). Interestingly, I found that Bik1 and Stu2 were Cdc14 SPIs, and the preliminary phosphoproteomics analysis suggests that both Bik1 and Bim1 are affected by the forced kinase-dead Cdc5 association with the kinetochore. In addition, Cdc14 was shown to control the localisation of Stu1 during anaphase (Higuchi & Uhlmann, 2005). Thus, there might exist a complex interaction network between these MAPs and their possible regulators, Cdc5 kinase and Cdc14 phosphatase, which merits future research.

Finally, it is known that Cdc5 activity is required for controlling Cdc14 localisation by aiding its release from the nucleolus (Visintin *et al.*, 2003), and more recently it was reported that Cdc14 was necessary for relocalising Cdc5 from the nucleus in late anaphase, and from the nuclear plaque of the SPB to the cytoplasmic plaque (Botchkarev *et al.*, 2014, 2017). This opens up an intriguing possibility that Cdc14 could also regulate Cdc5 localisation at kinetochores.

6.3.4 Other possible roles for Cdc5 at the kinetochore

My data show that cells with induced Cdc5-kinetochore association accumulate in S-G2-phase, as seen by fluorescence microscopy (Figure 5.15 D&G in section 5.2.12 and Figure 5.17 C&D in section 5.2.13), or even as early as late G1 or early S-phase, as seen by flow cytometry (Figure 5.16 in section 5.2.12). This combined with the result that when the association is induced during metaphase arrest, the cells progress relatively normally through mitotic exit when they are released (Figure 5.18 in section 5.2.13), suggests that the growth phenotype is a consequence of pre-mitotic kinetochore disruption or misregulation by the forced Cdc5 recruitment. As discussed above, a disruption of centromeric DNA replication, could be one reason for this phenotype. In case of DNA replication stress during S-phase and DNA damage, the cell-cycle checkpoints ensure that mitotic entry is delayed until replication is completed and damage repaired (for example: Pardo *et al.*, 2017 and references therein). However, during prolonged cell-cycle arrest the cells respond by adapting to the checkpoint and continue proliferation in the presence of damage (for example: Serrano

& D'Amours, 2014 and references therein). In multicellular organisms, these cells would decide to induce cell death by apoptosis via the p53 pathway, however, cancer cells or single-cell organisms like budding yeast, often continue proliferation. It has been shown in most eukaryotes that the adaptation to DNA damage response depends on Polo-like kinases ((Serrano & D'Amours, 2014 and references therein). Mutations in Cdc5 prevents the adaptation response in budding yeast (Toczyski *et al.*, 1997). However, the precise mechanism of how Polo kinase promotes adaptation is currently unknown. Recently, it was found that full kinase activity of Cdc5 through phosphorylation of an additional threonine 238 was important for adaptation (Rawal *et al.*, 2016). And furthermore, the PBD-dependent localisation of Cdc5 to SPBs as well as its interaction with the RSC chromatin remodelling complex was needed for this process (Ratsima *et al.*, 2016).

Given these data, as well as the involvement of polo kinase in recruiting PP2A to the kinetochore, it is tempting to speculate that Cdc5 could be involved in silencing the spindle assembly checkpoint (SAC). It has been shown that there is cross-talk between the SAC and the DNA damage checkpoint (Kim & Burke, 2008; Dotiwala *et al.*, 2010; Eliezer *et al.*, 2014). The localisation of Cdc5 to centromeres is tightly regulated and constrained to mitosis; in terms of my data and the phenotypes associated with the forced Cdc5 recruitment to Mtw1 or Ame1, it could be speculated that forced Cdc5 centromeric localisation could result in premature mitotic entry or even anaphase onset, thus be devastating for S-phase cells that would be undergoing DNA replication, producing the observed phenotype. Speculation aside, further experiments are required to dissect which processes are activated or misregulated by the forced early recruitment of Cdc5 to kinetochores.

The phenotype I observed with Cdc5 forced recruitment to the DAM1/DASH complex, resulting in accumulation of late anaphase cells (Figure 5.19 in section 5.2.13), suggests a completely different role for Cdc5 at the outer kinetochore, possibly in stabilising the anaphase spindle, hence this SPI might be preventing spindle disassembly in telophase or disrupting mitotic exit in another way. Indeed, it has been shown, that inhibition of Cdc14-dependent translocation of Cdc5 from the nucleus, in late anaphase, disrupts mitotic exit (Botchkarev *et al.*, 2014). More work is needed to fully understand this phenotype, but it supports the notion of differential functions for Cdc5 at the kinetochore.

The importance of kinetochore regulation by interplay between Polo kinase and sumoylation has been realised in recent years (Mukhopadhyay & Dasso, 2010; Yong-Gonzales *et al.*, 2012; Sridharan & Azuma, 2016). Furtermore, Cdc5 was shown to regulate the SUMO pathway by opposing the desumoylation enzyme Ulp2 (Baldwin *et al.*, 2009). In addition, the same study suggested that Ulp2 maintains centromeric cohesion by antagonising Cdc5 activity in regulating centromeric cohesion.

For any of these hypotheses, the phosphotarget(s) being affected has to be identified. Further experiments such as phosphoproteomics using the kinase-active Cdc5 need to be performed in order to narrow down the possible phosphosites that were misregulated by the forced recruitment of Cdc5 to the kinetochore. It remains a possibility that multiple sites are affected by any single Cdc5 SPI, thus mutations on individual proteins to suppress the growth defect could be challenging.

6.4 Limitations of the SPI methodology

6.4.1 The GBP-GFP interaction

The GBP-GFP association is constitutive. The GBP-tagged protein is modestly expressed and driven by the *CUP1* promoter without addition of copper from a single-copy CEN plasmid. However, the expression is constant and since the affinity of GBP to GFP is strong the forced interaction between the two tagged proteins is constitutive, as was seen by fluorescence microscopy. This creates problems for examining SPI phenotypes which results in lethality. In cases where the SPIs create a slow growth phenotype, any living cells might have either lost the GBP-fusion plasmid or adapted to the forced interaction, thus resulting in a “survivor phenotype” which could be independent of the phenotype caused by the SPI.

Using a conditional promoter such as *pGAL1* could overcome this issue in some cases, but this would result in a high overexpression of the GBP-tagged protein, which could lead to toxicity independent of the SPI phenotype. I tackled this problem by designing an auxin-inducible degradation (AID) version of the GBP plasmid. This worked well to reduce the GBP-RFP protein as seen by microscopy, but this worked less sufficiently to prevent the SPI phenotype, i.e. the level of the GBP-AID-tagged protein was still

sufficient to create a SPI phenotype. Future work will assess if the GBP could be sufficiently degraded by using additional AID motifs.

In addition, I attempted to control the kinetochore SPIs by using an analog-sensitive mutant (cdc5-as1-GBP), however this of course does not prevent the GBP-GFP interaction and as I discovered, the SPIs with catalytic-inactive mutants also create a phenotype, thus making the approach impractical as a conditional system. However, analog-sensitive mutants could be used in certain cases.

Ultimately, I was able to conditionally control the induction the of Cdc5-kinetochore association by replacing the PBD with GBP. Although the Cdc5ΔC-GBP expression was driven by *pGAL1* this didn't cause toxicity in a non-GFP strain, however when expressed in strains containing GFP-tagged kinetochore proteins, I was able to investigate in detail the SPI phenotype soon after the forced association was induced. However, this approach was unique to Cdc5ΔC and might be difficult to repeat with other regulators. In the lab, we are continuing to develop a temporal control of the SPIs, such as a temperature-sensitive version of the GBP, which would not bind GFP at a specific temperature.

The direction of association – when the GBP- and GFP-tagged proteins interact, how can we know which protein recruits which to its location? Does the GFP-tagged protein recruit the GBP-tagged protein or vice versa? This is a caveat of most artificial recruitment approaches. Fortunately, the GBP is tagged with RFP so we can visualise the GBP-GFP interaction using fluorescence microscopy. In theory, the direction of association could be equal between the GFP- and GBP-tagged proteins, in practice however, we find that irrelevant of the tag, if a structural or membrane-bound proteins are associated with a "free-floating" enzyme or a small complex the latter will be mislocalised to the cellular location of the former (Berry *et al.*, 2016). However, if the two tagged proteins are similar in terms of structure or function the direction of localisation is more specific to individual associations. In principle, even in the same cell, the GBP-tagged protein could be mislocalised to the GFP-tagged protein and vice versa. Another possibility is mislocalisation of both tagged proteins to a different cellular location ectopic to both. For example, when I forced the Mad1-GBP association with Mtw1-YFP, I noticed that many cells had additional, abnormal RFP and YFP signals which were mislocalised away from the kinetochore, although without causing a

growth defect (Figure 4.8 in section 4.2.4). Therefore, for each SPI under investigation it is crucial to examine how the two proteins behave when they are forced to interact. In most cases when candidates of kinetochore regulation where forced to interact with a kinetochore protein they colocalised at the kinetochore.

Another caveat shared by artificial tethering systems is the hypothetical, but likely, situation of affecting surrounding proteins by the forced association, be it through the GBP-GFP interaction, fusing two proteins, or by any other artificial interaction approach. As pointed out in chapter 2 (Figure 2.2 in section 2.4.2), the theoretical reach of the GBP-tagged protein when bound to GFP is about 10nm in radius due to the flexible amino acid linkers on both tags. I showed for example, that by forcing Cdc14 to associate with Nnf1, it was sufficient to change the phosphorylation status of another protein, Dsn1, in the same complex (the MIND complex) (Figure 3.13 in section 3.2.5).

The budding yeast GFP strain collection is a great resource for the yeast research community. However, since every gene in the collection is C-terminally tagged with GFP it limits the variety of SPIs. I have designed plasmids with the GBP tagged to the N termini of some proteins, but it would be interesting to investigate more N-terminal GFP-tagged kinetochore proteins in the future, since this could, for example, place the GBP-tagged regulatory protein in a more appropriate position to reach its potential substrates. The benefit of the SPI methodology is that since it uses a high-throughput screening approach with most members of the proteome, it creates numerous possible associations of the GBP-tagged protein with N termini of other surrounding proteins, although in an indirect manner. In addition, by using this approach, for each SPI we frequently find that the GFP query protein's binding partners or subunits of the same complex are also SPIs with the same GBP-tagged target protein.

6.4.2 The selective-ploidy ablation (SPA) method

Although the SPI screens are relatively quick to perform using the SPA mating and selection method, as soon as the cells are mated in theory the GBP- and the GFP-tagged proteins start to associate. These cells are then allowed to grow and are selected by two subsequent pinning steps and are grown for two days on the last selection plate (see Figure 2.3 in section 2.4.5). Thus instead of measuring growth rate of colonies over time the colony sizes are assessed after a number of days of growth,

which could miss subtle growth inhibition effects caused by the SPIs. Individual colonies are then picked into liquid culture and grown overnight for further analysis; this, as discussed above, creates issues in assessing very toxic SPIs. Furthermore, since the SPA method uses the universal donor strain that contains conditional centromeres, with *pGAL1-CEN* on all its chromosomes in order to eliminate them from the final haploid product; this creates a striking situation for the temporary diploid cells when half their genome becomes highly unstable once they are growing on galactose media by the continuous transcription through the centromere. The effect of the 16 conditional centromeres in the universal donor strain remains elusive, however it is inviable on galactose. In case the conditional chromosomes are inherited by the next generation those cells are counter-selected against by the *URA3* loci close to each conditional centromere, which results in conversion of 5-FOA added to the growth media into lethal 5-fluorouracil. Thus, these cells undergo a fairly harsh treatment before being assessed. Nevertheless, most of the strains at the end of every screen survive and grow well. Interestingly, a strain with a single conditional centromere on chromosome 3 (*pGAL1-CEN3*), is viable on galactose, but a deletion of *MCM21*, which diminishes cohesin at centromeres, reduces viability in these cells (Tsabar *et al.*, 2016); in addition, increasing cohesin at centromeres in these mutants by deleting *SIR2*, which redistributes cohesin from the nucleolus to centromeres, increases cell viability and restores Mif2 level at the kinetochore. In the SPI screens, as pointed out above, when the cells become heterozygoes diploids is also the point the GBP- and GFP-tagged protein can begin to interact. Thus it can be speculated that in some cases the SPIs could select against diploid formation and inadvertently select for haploid cells, which would not survive without the plasmid in following steps. The negative effects of the SPA method are averted by repeating the SPI assays by growing the cells on media lacking galactose (instead containing glucose) and 5-FOA in order to keep the cells as heterozygoes diploids whose growth inhibition would only be subject to the GBP-GFP association, additionally these cells also contain alleles with the non-GFP gene, thus controlling for the effects disrupting the function of the GFP-tagged protein.

Despite these limitations, I conclude that the objective to use the SPI system to identify kinetochore regulators was met. Although understanding of the roles of most of these SPIs in kinetochore function remains largely elusive, progress was made in individual cases and the further characterisation of these regulators is still ongoing.

Chapter 7. Appendix

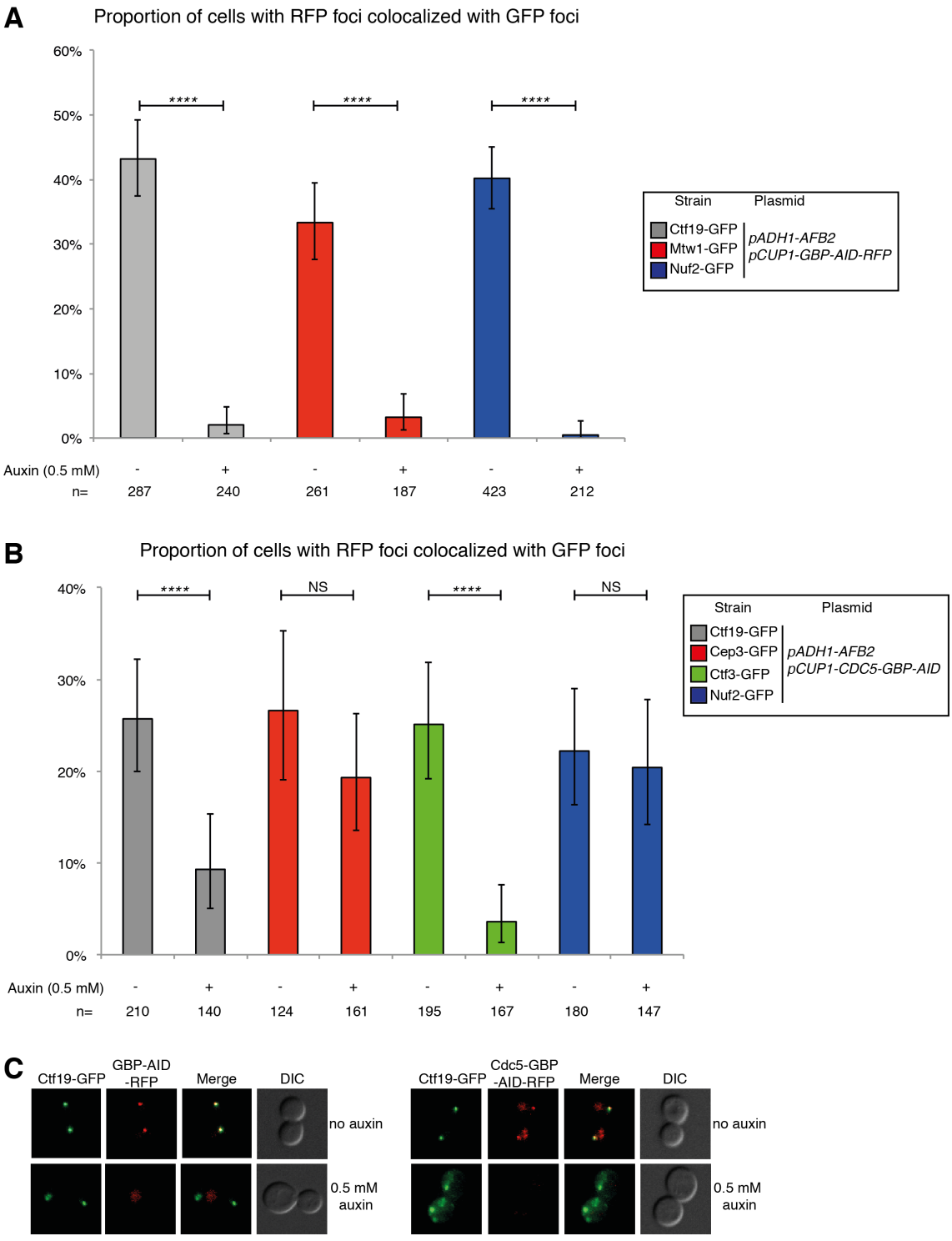

Appendix figure 1. SPIs using the auxin-inducible degradation system

(**A**) A graph showing the quantification of kinetochore-GFP cells containing GBP-AID-RFP signal with or without the addition of 0.5mM auxin (see text in section 5.2.10 for details). Statistical analysis was done using Fishers exact test; p-values **** = p < $1x10^{-4}$. Error bars indicate 95% binomial C.I.
(**B**) A graph showing the quantification of kinetochore-GFP cells containing Cdc5-GBP-AID-RFP signal, with same treatment as in (A).
(**C**) Fluorescence microscopy of Ctf19-GFP cells in (A&B), showing the GFP and RFP signal in the absence or presence of auxin. I note that the Ctf19-GFP foci is disrupted in the presence of Cdc5-GBP-AID-RFP and auxin.

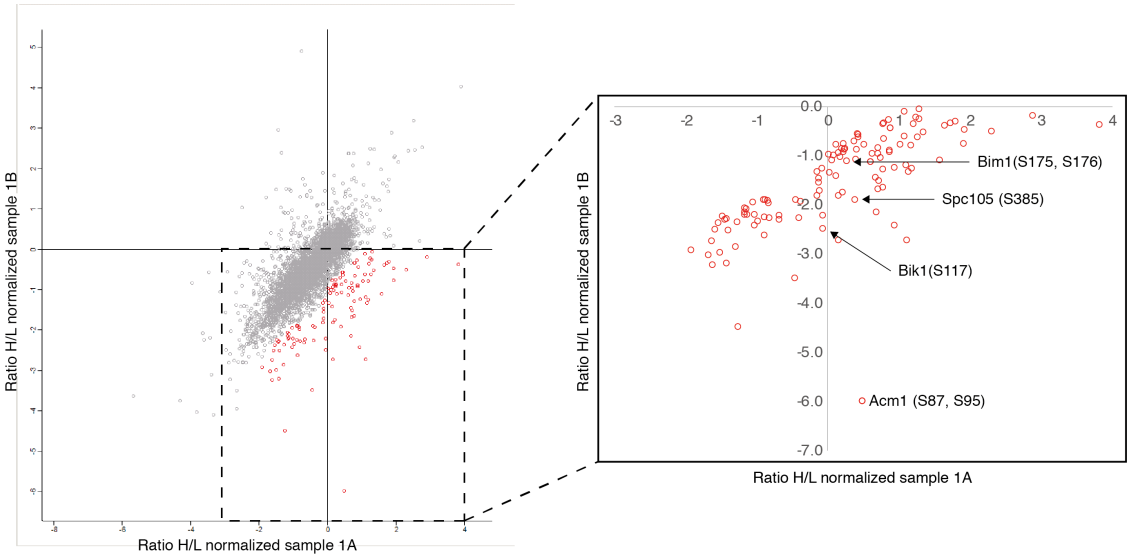

Appendix figure 2. Preliminary data from phosphoproteomics analysis of cdc5-kd kinetochore SPI.

The quantified phosphopeptides were compared by plotting the “heavy” and “light” peptide ratios as shown with sample 1A (see table 2.3 in section 2.6.4) on the x-axis and sample 1B in the y-axis. Therefore, downregulated phosphopeptides would be on the bottom-right site of the plot, i.e. phosphosites that were negatively affected by forced cdc5-kd association with Mtw1 compared to cdc5-kd-FAM. Upregulated phosphosites would be on the top-left site of the plot. A common issue with the SILAC technique is the metabolic conversion of the isotope-labelled arginine to proline, which leads to underestimation of the abundance of peptides containing proline in the experiments. Thus, many peptides may have shifted to the left on the plot. In this experiment, the conversion issue was tackled by supplementing the growth media with additional proline, which improved the conversion issue, but did not prevent it.

Reference List

Ahmed K, Gerber DA & Cochet C (2002). Joining the cell survival squad: an emerging role for protein kinase CK2. *Trends in Cell Biology* **12,** 226–230.

Akiyoshi B & Biggins S (2010). Cdc14-dependent dephosphorylation of a kinetochore protein prior to anaphase in Saccharomyces cerevisiae. *Genetics* **186,** 1487–1491.

Akiyoshi B & Gull K (2014). Discovery of unconventional kinetochores in kinetoplastids. *Cell* **156,** 1247–1258.

Akiyoshi B, Nelson CR & Biggins S (2013*a*). The Aurora B Kinase Promotes Inner and Outer Kinetochore Interactions in Budding Yeast. *Genetics* **194,** 785–789.

Akiyoshi B, Nelson CR, Duggan N, Ceto S, Ranish JA & Biggins S (2013*b*). The Mub1/Ubr2 ubiquitin ligase complex regulates the conserved Dsn1 kinetochore protein. *PLoS Genetics* **9,** e1003216.

Akiyoshi B, Nelson CRC, Ranish J a. & Biggins S (2009). Quantitative proteomic analysis of purified yeast kinetochores identifies a PP1 regulatory subunit. *Genes & development* **23,** 2887–2899.

Albuquerque CP, Smolka MB, Payne SH, Bafna V, Eng J & Zhou H (2008). A multidimensional chromatography technology for in-depth phosphoproteome analysis. *Molecular & cellular proteomics : MCP* **7,** 1389–1396.

Alexandru G, Uhlmann F, Mechtler K, Poupart MA & Nasmyth K (2001). Phosphorylation of the cohesin subunit Scc1 by Polo/Cdc5 kinase regulates sister chromatid separation in yeast. *Cell* **105,** 459–472.

Alonso A, D'Silva S, Rahman M, Meluh PB, Keeling J, Meednu N, Hoops HJ & Miller RK (2012). The yeast homologue of the microtubule-associated protein Lis1 interacts with the sumoylation machinery and a SUMO-targeted ubiquitin ligase. *Molecular biology of the cell* **23,** 4552–4566.

Alushin GM, Musinipally V, Matson D, Tooley J, Stukenberg PT & Nogales E (2012). Multimodal microtubule binding by the Ndc80 kinetochore complex. *Nature Structural & Molecular Biology* **19,** 1161–1167.

Amani V, Prince EW, Alimova I, Balakrishnan I, Birks D, Donson AM, Harris P, Levy JMM, Handler M, Foreman NK, Venkataraman S & Vibhakar R (2016). Polo-like Kinase 1 as a potential therapeutic target in Diffuse Intrinsic Pontine Glioma. *BMC cancer* **16,** 647.

De Antoni A, Pearson CG, Cimini D, Canman JC, Sala V, Nezi L, Mapelli M, Sironi L, Faretta M, Salmon ED & Musacchio A (2005). The Mad1/Mad2 complex as a template for Mad2 activation in the spindle assembly checkpoint. *Current biology : CB* **15,** 214–225.

Araki Y, Gornbos L, Migueleti SPS, Sivashanmugam L, Antony C & Schiebel E (2010). N-terminal regions of Mps 1 kinase determine functional bifurcation. *Journal of Cell Biology* **189,** 41–56.

Aravamudhan P, Goldfarb AA & Joglekar AP (2015). The kinetochore encodes a mechanical switch to disrupt spindle assembly checkpoint signalling. ; DOI: 10.1038/ncb3179.

Arnold L, Höckner S & Seufert W (2015). Insights into the cellular mechanism of the yeast ubiquitin ligase APC/C-Cdh1 from the analysis of in vivo degrons. *Molecular Biology of the Cell* **26,** 843–858.

Asano S, Park J-E, Sakchaisri K, Yu L-R, Song S, Supavilai P, Veenstra TD & Lee KS (2005). Concerted mechanism of Swe1/Wee1 regulation by multiple kinases in budding yeast. *The EMBO journal* **24,** 2194–2204.

Asbury CL, Gestaut DR, Powers AF, Franck AD & Davis TN (2006). The Dam1 kinetochore complex harnesses microtubule dynamics to produce force and movement. *Proceedings of the National Academy of Sciences* **103,** 9873–9878.

Attner MA, Miller MP, Ee L-S, Elkin SK & Amon A (2013). Polo kinase Cdc5 is a central regulator of meiosis I. *Proceedings of the National Academy of Sciences of the United States of America* **110,** 14278–14283.

Au W-C, Dawson AR, Rawson DW, Taylor SB, Baker RE & Basrai MA (2013). A novel role of the N terminus of budding yeast histone H3 variant Cse4 in ubiquitin-mediated proteolysis. *Genetics* **194,** 513–518.

Aumais JP, Williams SN, Luo W, Nishino M, Caldwell KA, Caldwell GA, Lin SH & Yu-Lee LY (2003). Role for NudC, a dynein-associated nuclear movement protein, in mitosis and cytokinesis. *J Cell Sci* **116,** 1991–2003.

Baldwin ML, Julius JA, Tang X, Wang Y & Bachant J (2009). The yeast SUMO isopeptidase Smt4/Ulp2 and the polo kinase Cdc5 act in an opposing fashion to regulate sumoylation in mitosis and cohesion at centromeres. *Cell Cycle* **8,** 3406–3419.

Ballister ER, Riegman M & Lampson M a. (2014). Recruitment of Mad1 to metaphase kinetochores is sufficient to reactivate the mitotic checkpoint. *The Journal of Cell Biology* **204,** 901–908.

Banaszynski LA, Chen L chun, Maynard-Smith LA, Ooi AGL & Wandless TJ (2006). A Rapid, Reversible, and Tunable Method to Regulate Protein Function in Living Cells Using Synthetic Small Molecules. *Cell* **126,** 995–1004.

Bansal PK, Abdulle R & Kitagawa K (2004). Sgt1 associates with Hsp90: an initial step of assembly of the core kinetochore complex. *Molecular and cellular biology* **24,** 8069–8079.

Barford D (2011). Structure, function and mechanism of the anaphase promoting complex (APC/C). *Q Rev Biophys* **44,** 153–190.

Barisic M, Sohm B, Mikolcevic P, Wandke C, Rauch V, Ringer T, Hess M, Bonn G & Geley S (2010). Spindly/CCDC99 Is Required for Efficient Chromosome Congression and Mitotic Checkpoint Regulation. *Molecular biology of the cell* **21,** 4042–4056.

Bartholomew CR, Woo SH, Chung YS, Jones C & Hardy CF (2001). Cdc5 interacts with the Wee1 kinase in budding yeast. *Mol Cell Biol* **21,** 4949–4959.

Baryshnikova A, Costanzo M, Kim Y, Ding H, Koh J, Toufighi K, Youn J-YY, Ou J, San Luis B-JJ, Bandyopadhyay S, Hibbs M, Hess D, Gingras A-CC, Bader GD, Troyanskaya OG, Brown GW, Andrews B, Boone C & Myers CL (2010). Quantitative analysis of fitness and genetic interactions in yeast on a genome scale. *Nature methods* **7,** 1017–1024.

Barz T, Ackermann K, Dubois G, Eils R & Pyerin W (2003). Genome-wide expression screens indicate a global role for protein kinase CK2 in chromatin remodeling. *Journal of cell science* **116,** 1563–1577.

Batisse J, Batisse C, Budd A, Böttcher B & Hurt E (2009). Purification of Nuclear Poly(A)-binding Protein Nab2 Reveals Association with the Yeast Transcriptome and a Messenger Ribonucleoprotein Core Structure. *Journal of Biological Chemistry* **284,** 34911–34917.

Beach D, Durkacz B & Nurse P (1982). Functionally homologous cell cycle control genes in budding and fission yeast. *Nature* **300,** 706–709.

Berry LK, Guðjon Olafsson, Ledesma-Fernandez E & Thorpe PH (2016). Synthetic protein interactions reveal a functional map of the cell. *eLife*; DOI: 10.7554/eLife.13053.

Bharadwaj R & Yu H (2004). The spindle checkpoint, aneuploidy, and cancer. *Oncogene* **23,** 2016–2027.

Biggins S (2013). The composition, functions, and regulation of the budding yeast kinetochore. *Genetics* **194,** 817–846.

Biggins S & Murray AW (2001). The budding yeast protein kinase Ipl1/Aurora allows the absence of tension to activate the spindle checkpoint. *Genes Dev* **15,** 3118–3129.

Blake-Hodek KA, Cassimeris L & Huffaker TC (2010). Regulation of Microtubule Dynamics by Bim1 and Bik1, the Budding Yeast Members of the EB1 and CLIP-170 Families of Plus-End Tracking Proteins. *Molecular biology of the cell* **21,** 2013–2023.

Bloom J, Cristea IM, Procko AL, Lubkov V, Chait BT, Snyder M & Cross FR (2011). Global analysis of Cdc14 phosphatase reveals diverse roles in mitotic processes. *The Journal of biological chemistry* **286,** 5434–5445.

Blower MD (2016). Centromeric Transcription Regulates Aurora-B Localization and Activation. *Cell reports* **15,** 1624–1633.

Bock LJ, Pagliuca C, Kobayashi N, Grove RA, Oku Y, Shrestha K, Alfieri C, Golfieri C, Oldani A, Dal Maschio M, Bermejo R, Hazbun TR, Tanaka TU & De Wulf P (2012). Cnn1 inhibits the interactions between the KMN complexes of the yeast kinetochore. *Nature cell biology* **14,** 614–624.

Boeckmann L et al. (2013). Phosphorylation of centromeric histone H3 variant regulates chromosome segregation in Saccharomyces cerevisiae. *Molecular biology of the cell* **24,** 2034–2044.

Bokros M, Gravenmier C, Jin F, Richmond D & Wang Y (2016). Fin1-PP1 Helps Clear Spindle Assembly Checkpoint Protein Bub1 from Kinetochores in Anaphase. *Cell Reports* **14,** 1074–1085.

Botchkarev V V., Garabedian M V., Lemos B, Paulissen E & Haber JE (2017). The budding yeast Polo-like kinase localizes to distinct populations at centrosomes during mitosis.

Molecular Biology of the Cell **28,** 1011–1020.
Botchkarev V V., Rossio V & Yoshida S (2014). The budding yeast Polo-like kinase Cdc5 is released from the nucleus during anaphase for timely mitotic exit. *Cell Cycle* **13,** 3260–3270.
Brachmann CB, Davies A, Cost GJ, Caputo E, Li J, Hieter P & Boeke JD (1998). Designer deletion strains derived from Saccharomyces cerevisiae S288C: A useful set of strains and plasmids for PCR-mediated gene disruption and other applications. *Yeast* **14,** 115–132.
Brady DM & Hardwick KG (2000). Complex formation between Mad1p, Bub1p and Bub3p is crucial for spindle checkpoint function. *Current biology : CB* **10,** 675–678.
Breitkreutz A et al. (2010). A global protein kinase and phosphatase interaction network in yeast. *Science (New York, NY)* **328,** 1043–1046.
Butt TR, Sternberg EJ, Gorman JA, Clark P, Hamer D, Rosenberg M & Crooke ST (1984). Copper metallothionein of yeast, structure of the gene, and regulation of expression. *Proceedings of the National Academy of Sciences of the United States of America* **81,** 3332–3336.
Buttrick GJ, Lancaster TC, Meadows JC & Millar JB a (2012). Plo1 phosphorylates Dam1 to promote chromosome bi-orientation in fission yeast. *Journal of cell science* **125,** 1645–1651.
Buttrick GJ & Millar JBA (2011). Ringing the changes: Emerging roles for DASH at the kinetochore-microtubule interface. *Chromosome Research* **19,** 393–407.
Camahort R, Li B, Florens L, Swanson SK, Washburn MP & Gerton JL (2007). Scm3 Is Essential to Recruit the Histone H3 Variant Cse4 to Centromeres and to Maintain a Functional Kinetochore. *Molecular Cell* **26,** 853–865.
Campbell CS & Desai A (2013). Tension sensing by Aurora B kinase is independent of survivin-based centromere localization. *Nature* **497,** 118–121.
Canzonetta C, Vernarecci S, Iuliani M, Marracino C, Belloni C, Ballario P & Filetici P (2015). SAGA DUB-Ubp8 Deubiquitylates Centromeric Histone Variant Cse4. *G3 (Bethesda, Md)* **6,** 287–298.
De Cárcer G, Manning G & Malumbres M (2011). From Plk1 to Plk5: Functional evolution of Polo-like kinases. *Cell Cycle* **10,** 2255–2262.
Carmena M, Pinson X, Platani M, Salloum Z, Xu Z, Clark A, MacIsaac F, Ogawa H, Eggert U, Glover DM, Archambault V & Earnshaw WC (2012*a*). The chromosomal passenger complex activates Polo kinase at centromeres. *PLoS Biology*; DOI: 10.1371/journal.pbio.1001250.
Carmena M, Wheelock M & Funabiki H (2012*b*). The Chromosomal Passenger Complex (CPC): From Easy Rider to the Godfather of Mitosis. *Nat Rev Mol Cell Biol* **13,** 789–803.
Chan FL, Marshall OJ, Saffery R, Kim BW, Earle E, Choo KHA & Wong LH (2012*a*). Active transcription and essential role of RNA polymerase II at the centromere during mitosis. *Proceedings of the National Academy of Sciences of the United States of America* **109,** 1979–1984.
Chan FL & Wong LH (2012). Transcription in the maintenance of centromere chromatin identity. *Nucleic Acids Research* **40,** 11178–11188.
Chan YW, Jeyaprakash a A, Nigg E a & Santamaria A (2012*b*). Aurora B controls kinetochore-microtubule attachments by inhibiting Ska complex-KMN network interaction. *The Journal of cell biology* **196,** 563–571.
Charles JF, Jaspersen SL, Tinker-Kulberg RL, Hwang L, Szidon A & Morgan DO (1998). The Polo-related kinase Cdc5 activates and is destroyed by the mitotic cyclin destruction machinery in S . cerevisiae. *Current Biology* **8,** 497–507.
Cheeseman IM, Anderson S, Jwa M, Green EM, Kang JS, Yates JR, Chan CSM, Drubin DG & Barnes G (2002). Phospho-regulation of kinetochore-microtubule attachments by the Aurora kinase Ipl1p. *Cell* **111,** 163–172.
Cheeseman IM, Chappie JS, Wilson-Kubalek EM & Desai A (2006). The conserved KMN network constitutes the core microtubule-binding site of the kinetochore. *Cell* **127,** 983–997.
Chen C, Whitney IP, Banerjee A, Sekhri P, Kern D, Fontan A, Tyson JJ, Cheeseman IM & Joglekar AP (2017). Ectopic activation of the Spindle Assembly Checkpoint reveals its biochemical design and physiological operation. *bioRxiv [preprint]*154054.

Chen R, Brady DM, Smith D, Murray AW & Hardwick KG (1999). The Spindle Checkpoint of Budding Yeast Depends on a Tight Complex between the Mad1 and Mad2 Proteins. **10,** 2607–2618.

Chen Y-C & Weinreich M (2010). Dbf4 regulates the Cdc5 Polo-like kinase through a distinct non-canonical binding interaction. *The Journal of biological chemistry* **285,** 41244–41254.

Chen Y, Baker RE, Keith KC, Harris K, Stoler S & Fitzgerald-Hayes M (2000). The N terminus of the centromere H3-like protein Cse4p performs an essential function distinct from that of the histone fold domain. *Molecular and cellular biology* **20,** 7037–7048.

Chiroli E, Rancati G, Catusi I, Lucchini G, Piatti S & Milano-bicocca S (2009). Cdc14 inhibition by the spindle assembly checkpoint prevents unscheduled centrosome separation in budding yeast. *Molecular biology of the cell* **20,** 2626–2637.

Cho B-R, Lee P & Hahn J-S (2014). CK2-dependent inhibitory phosphorylation is relieved by Ppt1 phosphatase for the ethanol stress-specific activation of Hsf1 in *S accharomyces cerevisiae*. *Molecular Microbiology* **93,** 306–316.

Choy JS, Acuña R, Au W-C & Basrai MA (2011). A role for histone H4K16 hypoacetylation in Saccharomyces cerevisiae kinetochore function. *Genetics* **189,** 11–21.

Ciferri C, Pasqualato S, Screpanti E, Varetti G, Santaguida S, Dos Reis G, Maiolica A, Polka J, De Luca JG, De Wulf P, Salek M, Rappsilber J, Moores CA, Salmon ED & Musacchio A (2008). Implications for Kinetochore-Microtubule Attachment from the Structure of an Engineered Ndc80 Complex. *Cell* **133,** 427–439.

Ciosk R, Zachariae W, Michaelis C, Shevchenko A, Mann M & Nasmyth K (1998). An ESP1/PDS1 complex regulates loss of sister chromatid cohesion at the metaphase to anaphase transition in yeast. *Cell* **93,** 1067–1076.

Clyne RK, Katis VL, Jessop L, Benjamin KR, Herskowitz I, Lichten M & Nasmyth K (2003). Polo-like kinase Cdc5 promotes chiasmata formation and cosegregation of sister centromeres at meiosis I. *Nature Cell Biology* **5,** 480–485.

Cohen RL, Espelin CW, Wulf P De, Sorger PK, Harrison SC & Simons KT (2008). Structural and Functional Dissection of Mif2p, a Conserved DNA-binding Kinetochore Protein. *Molecular biology of the cell* **19,** 4480–4491.

Collins KA, Castillo AR, Tatsutani SY & Biggins S (2005). De novo kinetochore assembly requires the centromeric histone H3 variant. *Mol Biol Cell* **16,** 5649–5660.

Collins SR, Schuldiner M, Krogan NJ & Weissman JS (2006). A strategy for extracting and analyzing large-scale quantitative epistatic interaction data. *Genome biology* **7,** R63.

Conde C, Osswald M, Barbosa J, Moutinho-Santos T, Pinheiro D, Guimarães S, Matos I, Maiato H & Sunkel CE (2013). Drosophila Polo regulates the spindle assembly checkpoint through Mps1-dependent BubR1 phosphorylation. *The EMBO Journal* **32,** 1761–1777.

Costanzo M et al. (2010). The genetic landscape of a cell. *Science (New York, NY)* **327,** 425–431.

Coudreuse D & Nurse P (2010). Driving the cell cycle with a minimal CDK control network. *Nature* **468,** 1074–1079.

Crasta K, Lim HH, Giddings TH, Winey M & Surana U (2008). Inactivation of Cdh1 by synergistic action of Cdk1 and polo kinase is necessary for proper assembly of the mitotic spindle. *Nature Cell Biology* **10,** 665–675.

D'Amours D, Stegmeier F & Amon A (2004). Cdc14 and condensin control the dissolution of cohesin-independent chromosome linkages at repeated DNA. *Cell* **117,** 455–469.

Daniel J a, Keyes BE, Ng YPY, Freeman CO & Burke DJ (2006). Diverse functions of spindle assembly checkpoint genes in Saccharomyces cerevisiae. *Genetics* **172,** 53–65.

David V. Hansen, Loktev A V., Ban KH & Jackson PK (2004). Plk1 Regulates Activation of the Anaphase Promoting Complex by Phosphorylating and Triggering SCF-TrCP-dependent Destruction of the APC Inhibitor Emi1. *Molecular biology of the cell* **15,** 5623–5634.

Degenhardt Y & Lampkin T (2010). Targeting polo-like kinase in cancer therapy. *Clinical Cancer Research* **16,** 384–389.

DeLuca JG, Howell BJ, Canman JC, Hickey JM, Fang G & Salmon ED (2003). Nuf2 and Hec1 Are Required for Retention of the Checkpoint Proteins Mad1 and Mad2 to Kinetochores. *Current Biology* **13,** 2103–2109.

Devit M, Cullen PPJ, Branson M, Sprague Jr. G, Fields S & Sprague GF (2005). Forcing interactions as a genetic screen to identify proteins that exert a defined activity. *Genome research* **15,** 560–565.

Deyter GMR & Biggins S (2014). The FACT complex interacts with the E3 ubiquitin ligase Psh1 to prevent ectopic localization of CENP-A. *Genes and Development* **28,** 1815–1826.

Dial JM, Petrotchenko E V. & Borchers CH (2007). Inhibition of APCCdh1 activity by Cdh1/Acm1/Bmh1 ternary complex formation. *Journal of Biological Chemistry* **282,** 5237–5248.

Dimitrova YN, Jenni S, Valverde R, Khin Y & Harrison SC (2016). Structure of the MIND Complex Defines a Regulatory Focus for Yeast Kinetochore Assembly. *Cell* **167,** 1014–1027.e12.

Dittmar JC, Pierce S, Rothstein R & Reid RJD (2013). Physical and genetic-interaction density reveals functional organization and informs significance cutoffs in genome-wide screens. *PNAS* **110,** 7389–7394.

Dittmar JC, Reid RJD & Rothstein R (2010). ScreenMill: a freely available software suite for growth measurement, analysis and visualization of high-throughput screen data. *BMC Bioinformatics* **11,** 353.

Donaldson MM, Tavares ÁAM, Ohkura H, Deak P & Glover DM (2001). Metaphase arrest with centromere separation in polo mutants of Drosophila. *Journal of Cell Biology* **153,** 663–675.

Dotiwala F, Harrison JC, Jain S, Sugawara N & Haber JE (2010). Mad2 prolongs DNA damage checkpoint arrest caused by a double-strand break via a centromere-dependent mechanism. *Current biology : CB* **20,** 328–332.

Dou Z, Liu X, Wang W, Zhu T, Wang X, Xu L, Abrieu A, Fu C, Hill DL & Yao X (2015). Dynamic localization of Mps1 kinase to kinetochores is essential for accurate spindle microtubule attachment. *Proceedings of the National Academy of Sciences* **112,** E4546–E4555.

Eden E, Navon R, Steinfeld I, Lipson D & Yakhini Z (2009). GOrilla: a tool for discovery and visualization of enriched GO terms in ranked gene lists. *BMC bioinformatics* **10,** 48.

Elia AEH, Rellos P, Haire LF, Chao JW, Ivins FJ, Hoepker K, Mohammad D, Cantley LC, Smerdon SJ & Yaffe MB (2003). The molecular basis for phosphodependent substrate targeting and regulation of Plks by the Polo-box domain. *Cell* **115,** 83–95.

Eliezer Y, Argaman L, Kornowski M, Roniger M & Goldberg M (2014). Interplay between the DNA damage proteins MDC1 and ATM in the regulation of the spindle assembly checkpoint. *Journal of Biological Chemistry* **289,** 8182–8193.

Elledge SJ (1996). Cell cycle checkpoints: preventing an identity crisis. *Science* **274,** 1664–1672.

Elowe S, Hümmer S, Uldschmid A, Li X & Nigg E a (2007). Tension-sensitive Plk1 phosphorylation on BubR1 regulates the stability of kinetochore–microtubule interactions. *Genes & Development* **21,** 2205–2219.

Emanuele MJ, Lan W, Jwa M, Miller S a, Chan CSM & Stukenberg PT (2008). Aurora B kinase and protein phosphatase 1 have opposing roles in modulating kinetochore assembly. *The Journal of cell biology* **181,** 241–254.

Espert A, Uluocak P, Bastos RN, Mangat D, Graab P & Gruneberg U (2014). PP2A-B56 opposes Mps1 phosphorylation of Knl1 and thereby promotes spindle assembly checkpoint silencing. *The Journal of cell biology* **206,** 833–842.

Espeut J, Cheerambathur DK, Krenning L, Oegema K & Desai A (2012). Microtubule binding by KNL-1 contributes to spindle checkpoint silencing at the kinetochore. *The Journal of cell biology* **196,** 469–482.

Espeut J, Lara-Gonzalez P, Sassine M, Shiau AKK, Desai A & Abrieu A (2015). Natural Loss of Mps1 Kinase in Nematodes Uncovers a Role for Polo-like Kinase 1 in Spindle Checkpoint Initiation. *Cell Reports* **12,** 58–65.

Fernius J, Nerusheva OO, Galander S, Alves FDL, Rappsilber J & Marston AL (2013). Cohesin-dependent association of Scc2/4 with the centromere initiates pericentromeric cohesion establishment. *Current Biology* **23,** 599–606.

Fisher TE, Marszalek PE, Oberhauser AF, Carrion-Vazquez M & Fernandez JM (1999). The micro-mechanics of single molecules studied with atomic force microscopy. *The Journal of physiology* **520 Pt 1,** 5–14.

Fleming AB, Beggs S, Church M, Tsukihashi Y & Pennings S (2014). Biochimica et Biophysica Acta The yeast Cyc8 – Tup1 complex cooperates with Hda1p and Rpd3p histone deacetylases to robustly repress transcription of the subtelomeric. *BBA - Gene Regulatory Mechanisms* **1839,** 1242–1255.

Foley EA, Maldonado M & Kapoor TM (2011). Formation of stable attachments between kinetochores and microtubules depends on the B56-PP2A phosphatase. *Nature cell biology* **13,** 1265–1271.

Fraschini R, Beretta A, Sironi L, Musacchio A, Lucchini G & Piatti S (2001). Bub3 interaction with Mad2, Mad3 and Cdc20 is mediated by WD40 repeats and does not require intact kinetochores. *EMBO J* **20,** 6648–6659.

Fridy PC, Li Y, Keegan S, Thompson MK, Nudelman I, Scheid JF, Oeffinger M, Nussenzweig MC, Fenyö D, Chait BT & Rout MP (2014). A robust pipeline for rapid production of versatile nanobody repertoires. *Nature methods* **11,** 1253–1260.

Funabiki H & Wynne DJ (2014). Making an effective switch at the kinetochore by phosphorylation and dephosphorylation. *Chromosoma* **122,** 135–158.

Funk C, Schmeiser V, Ortiz J & Lechner J (2014). A TOGL domain specifically targets yeast CLASP to kinetochores to stabilize kinetochore microtubules. *The Journal of Cell Biology* **205,** 555–571.

Gandhi SR, Gierliński M, Mino A, Tanaka K, Kitamura E, Clayton L & Tanaka TU (2011). Kinetochore-dependent microtubule rescue ensures their efficient and sustained interactions in early mitosis. *Developmental Cell* **21,** 920–933.

Gardner MK, Haase J, Mythreye K, Molk JN, Anderson M, Joglekar AP, Toole ETO, Winey M, Salmon ED, Odde DJ & Bloom K (2008). The microtubule-based motor Kar3 and plus end – binding protein Bim1 provide structural support for the anaphase spindle. *The Journal of cell biology* **180,** 91–100.

Gardner RD, Poddar A, Yellman C, Tavormina PA, Monteagudo MC & Burke DJ (2001). The spindle checkpoint of the yeast Saccharomyces cerevisiae requires kinetochore function and maps to the CBF3 domain. *Genetics* **157,** 1493–1502.

Gassmann R, Holland AJ, Varma D, Wan X, Filiz C, Oegema K, Salmon ED & Desai A (2010). controls spindle checkpoint silencing in human cells Removal of Spindly from microtubule-attached kinetochores controls spindle checkpoint silencing in human cells. *Genes & development* **24,** 957–971.

Gavin A-C et al. (2002). Functional organization of the yeast proteome by systematic analysis of protein complexes. *Nature* **415,** 141–147.

Geymonat M, Spanos A, Walker PA, Johnston LH & Sedgwick SG (2003). In vitro regulation of budding yeast Bfa1/Bub2 GAP activity by Cdc5. *Journal of Biological Chemistry* **278,** 14591–14594.

Gietz RD & Schiestl RH (2007). High-efficiency yeast transformation using the LiAc/SS carrier DNA/PEG method. *Nature protocols* **2,** 31–34.

Gjertsen BT & Schöffski P (2014). Discovery and development of the Polo-like kinase inhibitor volasertib in cancer therapy. *Leukemia*11–19.

Gkikopoulos T, Singh V, Tsui K, Awad S, Renshaw MJ, Scholfield P, Barton GJ, Nislow C, Tanaka TU & Owen-hughes T (2011). The SWI / SNF complex acts to constrain distribution of the centromeric histone variant Cse4 . *The EMBO journal* **30,** 1919–1927.

Gnad F, de Godoy LMF, Cox J, Neuhauser N, Ren S, Olsen J V & Mann M (2009). High-accuracy identification and bioinformatic analysis of in vivo protein phosphorylation sites in yeast. *Proteomics* **9,** 4642–4652.

Godfrey M, Touati SA, Kataria M, Jones A, Snijders AP & Uhlmann F (2017). PP2ACdc55 Phosphatase Imposes Ordered Cell-Cycle Phosphorylation by Opposing Threonine Phosphorylation. *Molecular Cell* **65,** 393–402.e3.

Gonen S, Iadanza MG, Biggins S, Duggan N, Gonen T, Akiyoshi B & Shi D (2012). The structure of purified kinetochores reveals multiple microtubule-attachment sites. *Nature Structural & Molecular Biology* **19,** 925–929.

Gray CH, Good VM, Tonks NK & Barford D (2003). The structure of the cell cycle protein Cdc14 reveals a proline-directed protein phosphatase. *The EMBO journal* **22,** 3524–3535.

Grishchuk EL, Spiridonov IS, Volkov V a, Efremov a, Westermann S, Drubin D, Barnes G, Ataullakhanov FI & McIntosh JR (2008). Different assemblies of the DAM1 complex follow shortening microtubules by distinct mechanisms. *Proceedings of the National Academy of Sciences of the United States of America* **105,** 6918–6923.

Gruhler A, Olsen J V, Mohammed S, Mortensen P, Faergeman NJ, Mann M & Jensen ON (2005). Quantitative Phosphoproteomics Applied to the Yeast Pheromone Signaling Pathway. *Mol Cell Proteomics* **4,** 310–327.

Gurden MD, Anderhub SJ, Faisal A & Linardopoulos S (2016). Aurora B prevents premature removal of spindle assembly checkpoint proteins from the kinetochore: A key role for Aurora B in mitosis. *Oncotarget*; DOI: 10.18632/oncotarget.10657.

Gutteridge REA et al. (2016). Plk1 Inhibitors in Cancer Therapy: From Laboratory to Clinics. *Molecular cancer therapeutics* **15,** 1427–1435.

Haase SB & Reed SI (2002). Improved flow cytometric analysis of the budding yeast cell cycle. *Cell cycle (Georgetown, Tex)* **1,** 132–136.

Hanisch A, Wehner A, Nigg EA & Sillje HHW (2006). Different Plk1 Functions Show Distinct Dependencies on Polo-Box Domain-mediated Targeting. *Molecular biology of the cell* **17,** 448–459.

Hanna DE, Rethinaswamy A & Glover C V (1995). Casein kinase II is required for cell cycle progression during G1 and G2/M in Saccharomyces cerevisiae. *The Journal of biological chemistry* **270,** 25905–25914.

Hardwick KG, Johnston RC, Smith DL & Murray AW (2000). MAD3 encodes a novel component of the spindle checkpoint which interacts with Bub3p, Cdc20p, and Mad2p. *Journal of Cell Biology* **148,** 871–882.

Hardwick KG, Weiss E, Luca FC, Winey M & Murray a W (1996). Activation of the budding yeast spindle assembly checkpoint without mitotic spindle disruption. *Science* **273,** 953–956.

Harris PS, Venkataraman S, Alimova I, Birks DK, Donson AM, Knipstein J, Dubuc A, Taylor MD, Handler MH, Foreman NK & Vibhakar R (2012). Polo-like kinase 1 (PLK1) inhibition suppresses cell growth and enhances radiation sensitivity in medulloblastoma cells. *BMC cancer* **12,** 80.

Hartwell L & Weinert T (1989). Checkpoints: controls that ensure the order of cell cycle events. *Science* **246,** 629–634.

Hartwell LH, Culotti J, Pringle JR & Reid BJ (1974). Genetic control of the cell division cycle in yeast. *Science (New York, NY)* **183,** 46–51.

Hartwell LH, Culotti J & Reid B (1970). Genetic Control of the Cell-Division Cycle in Yeast, I. Detection of Mutants. *Proceedings of the National Academy of Sciences* **66,** 352–359.

Haruki H, Nishikawa J & Laemmli UK (2008). The anchor-away technique: rapid, conditional establishment of yeast mutant phenotypes. *Molecular cell* **31,** 925–932.

Hassold T & Hunt P (2001). To err (meiotically) is human: the genesis of human aneuploidy. *Nat Rev Genet* **2,** 280–291.

Hatano Y, Naoki K, Suzuki A & Ushimaru T (2016). Positive feedback promotes mitotic exit via the APC/C-Cdh1-separase-Cdc14 axis in budding yeast. *Cellular Signalling* **28,** 1545–1554.

Heasley LR, Markus SM & DeLuca JG (2017). “Wait anaphase” signals are not confined to the mitotic spindle. *Molecular Biology of the Cell* **28,** 1186–1194.

Heinrich S, Sewart K, Windecker H, Langegger M, Schmidt N, Hustedt N & Hauf S (2014). Mad1 contribution to spindle assembly checkpoint signalling goes beyond presenting Mad2 at kinetochores. *EMBO reports* **15,** 291–298.

Herrero E & Thorpe PH (2016). Synergistic Control of Kinetochore Protein Levels by Psh1 and Ubr2. *PLoS Genetics* **12,** 1–23.

Herzog F, Primorac I, Dube P, Lenart P, Sander B, Mechtler K, Stark H & Peters JM (2009). Structure of the anaphase-promoting complex/cyclosome interacting with a mitotic checkpoint complex. *Science* **323,** 1477–1481.

Hewawasam G, Shivaraju M, Mattingly M, Venkatesh S, Martin-Brown S, Florens L, Workman JL & Gerton JL (2010). Psh1 Is an E3 Ubiquitin Ligase that Targets the Centromeric Histone Variant Cse4. *Molecular Cell* **40,** 444–454.

Hewawasam GS, Mattingly M, Venkatesh S, Zhang Y, Florens L, Workman JL & Gerton JL (2014). Phosphorylation by casein kinase 2 facilitates Psh1 proteinassisted degradation of Cse4 protein. *Journal of Biological Chemistry* **289,** 29297–29309.

Hewitt L, Tighe A, Santaguida S, White AM, Jones CD, Musacchio A, Green S & Taylor SS (2010). Sustained Mps1 activity is required in mitosis to recruit O-Mad2 to the Mad1-C-Mad2 core complex. *Journal of Cell Biology* **190,** 25–34.

Higuchi T & Uhlmann F (2005). Stabilization of microtubule dynamics at anaphase onset promotes chromosome segregation. *Nature* **433,** 171–176.

Hildebrand EM et al. (2016). Regulation of Budding Yeast CENP-A levels Prevents

Misincorporation at Promoter Nucleosomes and Transcriptional Defects ed. Sullivan BA. *PLOS Genetics* **12,** e1005930.
Hill A & Bloom K (1989). Acquisition and processing of a conditional dicentric chromosome in Saccharomyces cerevisiae. *Molecular and cellular biology* **9,** 1368–1370.
Hinshaw SM & Harrison SC (2013). An Iml3-Chl4 Heterodimer Links the Core Centromere to Factors Required for Accurate Chromosome Segregation. *Cell Reports* **5,** 29–36.
Hinshaw SM, Makrantoni V, Harrison SC & Marston AL (2017). The Kinetochore Receptor for the Cohesin Loading Complex. *Cell* **171,** 72–84.e13.
Hiruma Y, Sacristan C, Pachis ST, Adamopoulos A, Kuijt T, Ubbink M, von Castelmur E, Perrakis A, Kops GJPL & Yoshitaka Hiruma, Carlos Sacristan, Spyridon T. Pachis, Athanassios Adamopoulos, Timo Kuijt, Marcellus Ubbink, Eleonore von Castelmur, Anastassis Perrakis GJPLK (2015). Competition between MPS1 and microtubules at kinetochores regulates spindle checkpoint signaling. *Science* **348,** 1264–1267.
Ho K-H, Tsuchiya D, Oliger AC & Lacefield S (2014). Localization and Function of Budding Yeast CENP-A Depends upon Kinetochore Protein Interactions and Is Independent of Canonical Centromere Sequence. *Cell Reports* **9,** 2027–2033.
Hoffman CS & Winston F (1987). A ten-minute DNA preparation from yeast efficiently releases autonomous plasmids for transformation of Escherichia coli. *Gene* **57,** 267–272.
Holt L, Tuch B, Villén J & Johnson A (2009). Global analysis of Cdk1 substrate phosphorylation sites provides insights into evolution. *Science* **325,** 1–11.
Hood EA, Kettenbach AN, Gerber SA & Compton DA (2012). Plk1 regulates the kinesin-13 protein Kif2b to promote faithful chromosome segregation. *Molecular biology of the cell* **23,** 2264–2274.
Hooff JJE Van, Kops GJPL, Tromer E & Wijk LM Van (2017). Evolutionary dynamics of the kinetochore network in eukaryotes as revealed by comparative genomics. *EMBO reports*1–13.
van Hooff JJE, Snel B & Kops GJPL (2017). Unique Phylogenetic Distributions of the Ska and Dam1 Complexes Support Functional Analogy and Suggest Multiple Parallel Displacements of Ska by Dam1. *Genome biology and evolution* **9,** 1295–1303.
Hornig NCD & Uhlmann F (2004). Preferential cleavage of chromatin-bound cohesin after targeted phosphorylation by Polo-like kinase. *The EMBO journal* **23,** 3144–3153.
Hornung P, Troc P, Malvezzi F, Maier M, Demianova Z, Zimniak T, Litos G, Lampert F, Schleiffer A, Brunner M, Mechtler K, Herzog F, Marlovits TC & Westermann S (2014). A cooperative mechanism drives budding yeast kinetochore assembly downstream of CENP-A. *The Journal of cell biology* **206,** 509–524.
Howell AS & Lew DJ (2012). Morphogenesis and the cell cycle. *Genetics* **190,** 51–77.
Howell BJ, McEwen BF, Canman JC, Hoffman DB, Farrar EM, Rieder CL & Salmon ED (2001). Cytoplasmic dynein/dynactin drives kinetochore protein transport to the spindle poles and has a role in mitotic spindle checkpoint inactivation. *Journal of Cell Biology* **155,** 1159–1172.
Hoyt MA, Totis L & Roberts BT (1991). S. cerevisiae genes required for cell cycle arrest in response to loss of microtubule function. *Cell* **66,** 507–517.
Hu F, Wang Y, Liu D, Li Y, Qin J & Elledge SJ (2001). Regulation of the Bub2/Bfa1 GAP complex by Cdc5 and cell cycle checkpoints. *Cell* **107,** 655–665.
Hua S, Wang Z, Jiang K, Huang Y, Ward T, Zhao L, Dou Z & Yao X (2011). CENP-U cooperates with Hec1 to orchestrate kinetochore-microtubule attachment. *The Journal of biological chemistry* **286,** 1627–1638.
Huh W-KK, Falvo J V, Gerke LC, Carroll AS, Howson RW, Weissman JS & O'Shea EK (2003). Global analysis of protein localization in budding yeast. *Nature* **425,** 686–691.
Huis PJ, Jeganathan S, Petrovic A & John J (2016). Molecular basis of outer kinetochore assembly on CENP-T. ; DOI: 10.7554/eLife.21007.
Hyland KM, Kingsbury J, Koshland D & Hieter P (1999). Ctf19p: A novel kinetochore protein in Saccharomyces cerevisiae and a potential link between the kinetochore and mitotic spindle. *Journal of Cell Biology* **145,** 15–28.
Ibrahim B (2015). Toward a systems-level view of mitotic checkpoints. *Progress in Biophysics and Molecular Biology* **117,** 217–224.
Ikui AE, Rossio V, Schroeder L & Yoshida S (2012). A Yeast GSK-3 Kinase Mck1 Promotes Cdc6 Degradation to Inhibit DNA Re-Replication ed. Copenhaver GP. *PLoS Genetics* **8,**

e1003099.
Iouk T, Kerscher O, Scott RJ, Basrai MA & Wozniak RW (2002). The yeast nuclear pore complex functionally interacts with components of the spindle assembly checkpoint. *J Cell Biol* **159,** 807–819.
Ito D, Saito Y & Matsumoto T (2012). Centromere-tethered Mps1 pombe homolog (Mph1) kinase is a sufficient marker for recruitment of the spindle checkpoint protein Bub1, but not Mad1. *Proceedings of the National Academy of Sciences* **109,** 209–214.
Jaspersen SL, Charles JF & Morgan DO (1999). Inhibitory phosphorylation of the APC regulator Hct1 is controlled by the kinase Cdc28 and the phosphatase Cdc14. *Current Biology* **9,** 227–236.
Jelluma N, Dansen TB, Sliedrecht T, Kwiatkowski NP & Kops GJPL (2010). Release of Mps1 from kinetochores is crucial for timely anaphase onset. *Journal of Cell Biology* **191,** 281–290.
Ji Z, Gao H & Yu H (2015). Kinetochore attachment sensed by competitive Mps1 and microtubule binding to Ndc80C. *Science* **348,** 1260–1264.
Jia L, Li B & Yu H (2016). The Bub1-Plk1 kinase complex promotes spindle checkpoint signalling through Cdc20 phosphorylation. *Nature communications* **7,** 10818.
Jiang H & English a M (2002). Quantitative analysis of the yeast proteome by incorporation of isotopically labelled leucine. *Journal of Proteome Research* **1,** 345–350.
Jiang W, Lim MY, Yoon HJ, Thorner J, Martin GS & Carbon J (1995). Overexpression of the yeast MCK1 protein kinase suppresses conditional mutations in centromere-binding protein genes CBF2 and CBF5. *Molecular & general genetics : MGG* **246,** 360–366.
Joglekar A & P. A (2016). A Cell Biological Perspective on Past, Present and Future Investigations of the Spindle Assembly Checkpoint. *Biology* **5,** 44.
Joglekar AP & Aravamudhan P (2016). How the kinetochore switches off the spindle assembly checkpoint. *Cell Cycle* **15,** 7–8.
Joglekar AP, Bouck DC, Molk JN, Bloom KS & Salmon ED (2006). Molecular architecture of a kinetochore-microtubule attachment site. *Nature cell biology* **8,** 581–585.
Kakui Y, Sato M, Okada N, Toda T & Yamamoto M (2013). Microtubules and Alp7–Alp14 (TACC–TOG) reposition chromosomes before meiotic segregation. *Nature Cell Biology* **15,** 786–796.
Kang YH, Park CH, Kim TS, Soung NK, Bang JK, Kim BY, Park JE & Lee KS (2011). Mammalian polo-like kinase 1-dependent regulation of the PBIP1-CENP-Q complex at kinetochores. *Journal of Biological Chemistry* **286,** 19744–19757.
Kang YH, Park J, Yu L, Soung N, Yun S, Bang JK, Seong Y, Yu H, Garfield S, Veenstra TD & Lee KS (2006). Self-Regulated Plk1 Recruitment to Kinetochores by the Plk1-PBIP1 Interaction Is Critical for Proper Chromosome Segregation. *Molecular cell*409–422.
Keaton MA & Lew DJ (2006). Eavesdropping on the cytoskeleton: progress and controversy in the yeast morphogenesis checkpoint. *Current Opinion in Microbiology* **9,** 540–546.
Kennedy MJ, Hughes RM, Peteya LA, Schwartz JW, Ehlers MD & Tucker CL (2010). Rapid blue light induction of protein interaction in living cells. *Nature Methods* **7,** 973–975.
Keogh M-C, Kim J-A, Downey M, Fillingham J, Chowdhury D, Harrison JC, Onishi M, Datta N, Galicia S, Emili A, Lieberman J, Shen X, Buratowski S, Haber JE, Durocher D, Greenblatt JF & Krogan NJ (2006). A phosphatase complex that dephosphorylates gammaH2AX regulates DNA damage checkpoint recovery. *Nature* **439,** 497–501.
Kim EM & Burke DJ (2008). DNA damage activates the SAC in an ATM/ATR-dependent manner, independently of the kinetochore. *PLoS genetics* **4,** e1000015.
Kim J ook, Zelter A, Umbreit NT, Bollozos A, Riffle M, Johnson R, Maccoss MJ, Asbury CL & Davis TN (2017). The Ndc80 complex bridges two dam1 complex rings. *eLife* **6,** 1–22.
Kirchhofer A, Helma J, Schmidthals K, Frauer C, Cui S, Karcher A, Pellis M, Muyldermans S, Casas-Delucchi CS, Cardoso MC, Leonhardt H, Hopfner K-P & Rothbauer U (2010). Modulation of protein properties in living cells using nanobodies. *Nature structural & molecular biology* **17,** 133–138.
Kitada K, Johnson AL, Johnston LH & Sugino A (1993). A multicopy suppressor gene of the Saccharomyces cerevisiae G1 cell cycle mutant gene dbf4 encodes a protein kinase and is identified as CDC5. *Molecular and cellular biology* **13,** 4445–4457.
Kitagawa K, Abdulle R, Bansal PK, Cagney G, Fields S, Hieter P, Avenue W & Vz BC (2003). Requirement of Skp1-Bub1 Interaction for Kinetochore-Mediated Activation of the Spindle

Checkpoint. **11,** 1201–1213.
Kitagawa K, Skowyra D, Elledge SJ, Harper JW & Hieter P (1999). SGT1 encodes an essential component of the yeast kinetochore assembly pathway and a novel subunit of the SCF ubiquitin ligase complex. *Molecular cell* **4,** 21–33.
Kitamura E, Tanaka K, Kitamura Y & Tanaka TU (2007). Kinetochore microtubule interaction during S phase in Saccharomyces cerevisiae. *Genes & development* **21,** 3319–3330.
Kliewe F, Engelhardt M, Aref R & Schüller H-J (2017). Promoter recruitment of corepressors Sin3 and Cyc8 by activator proteins of the yeast Saccharomyces cerevisiae. *Current Genetics* **63,** 739–750.
Kobayashi J & Matsuura Y (2017). Structure and dimerization of the catalytic domain of the protein phosphatase Cdc14p, a key regulator of mitotic exit in *Saccharomyces cerevisiae*. *Protein Science* **26,** 2105–2112.
Kono K, Al-Zain A, Schroeder L, Nakanishi M & Ikui AE (2016). Plasma membrane/cell wall perturbation activates a novel cell cycle checkpoint during G1 in Saccharomyces cerevisiae. *Proceedings of the National Academy of Sciences* **113,** 201523824.
Kops GJPL, Weaver BAA & Cleveland DW (2005). On the road to cancer: aneuploidy and the mitotic checkpoint. *Nature Reviews Cancer* **5,** 773–785.
Kruse T, Larsen MSY, Sedgwick GG, Sigurdsson JO, Streicher W, Olsen J V & Nilsson J (2014). A direct role of Mad1 in the spindle assembly checkpoint beyond Mad2 kinetochore recruitment. *EMBO reports* **15,** 282–290.
Kuijt TEF, Omerzu M, Saurin AT & Kops GJPL (2014). Conditional targeting of MAD1 to kinetochores is sufficient to reactivate the spindle assembly checkpoint in metaphase. *Chromosoma* **123,** 471–480.
Lampson MA & Cheeseman IM (2011). Sensing centromere tension: Aurora B and the regulation of kinetochore function. *Trends in Cell Biology* **21,** 133–140.
Latham JA, Chosed RJ, Wang S & Dent SYR (2011). Chromatin signaling to kinetochores: transregulation of Dam1 methylation by histone H2B ubiquitination. *Cell* **146,** 709–719.
Lau DTC & Murray AW (2012). Mad2 and Mad3 cooperate to arrest budding yeast in mitosis. *Curr Biol* **22,** 180–190.
Lauzé E, Stoelcker B, Luca FC, Weiss E, Schutz a R & Winey M (1995). Yeast spindle pole body duplication gene MPS1 encodes an essential dual specificity protein kinase. *The EMBO journal* **14,** 1655–1663.
Lawrimore J, Aicher JK, Hahn P, Fulp A, Kompa B, Vicci L, Falvo M, Taylor RM & Bloom K (2016). ChromoShake: a chromosome dynamics simulator reveals that chromatin loops stiffen centromeric chromatin. *Molecular Biology of the Cell* **27,** 153–166.
Ledesma-Fernández E & Thorpe PH (2015). Fluorescent foci quantitation for high-throughput analysis. *Journal of biological methods* **2,** e22.
Lee BH (2003). Role of Polo-like Kinase CDC5 in Programming Meiosis I Chromosome Segregation. *Science* **300,** 482–486.
Lee KS & Erikson RL (1997). Plk is a functional homolog of Saccharomyces cerevisiae Cdc5, and elevated Plk activity induces multiple septation structures. *Mol Cell Biol* **17,** 3408–3417.
Lee KS, Oh D-Y, Kang YH & Park J (2008). Self-regulated mechanism of Plk1 localization to kinetochores: lessons from the Plk1-PBIP1 interaction. *Cell division* **3,** 4.
Lee MG & Nurse P (1987). Complementation used to clone a human homologue of the fission yeast cell cycle control gene cdc2. *Nature* **327,** 31–35.
Lera RF, Potts GK, Suzuki A, Johnson JM, Salmon ED, Coon JJ & Burkard ME (2016). Decoding Polo-like kinase 1 signaling along the kinetochore–centromere axis. *Nature Chemical Biology* **12,** 1–10.
Levskaya A, Weiner OD, Lim WA & Voigt CA (2009). Spatiotemporal control of cell signalling using a light-switchable protein interaction. *Nature* **461,** 997–1001.
Li R & Murray AW (1991). Feedback control of mitosis in budding yeast. *Cell* **66,** 519–531.
Li Y & Elledge SJ (2003). The DASH complex component Ask1 is a cell cycle-regulated Cdk substrate in Saccharomyces cerevisiae. *Cell cycle (Georgetown, Tex)* **2,** 143–148.
Li Y, Gorbea C, Mahaffey D, Rechsteiner M & Benezra R (1997). MAD2 associates with the cyclosome/anaphase-promoting complex and inhibits its activity. *Proceedings of the National Academy of Sciences of the United States of America* **94,** 12431–12436.
Li Y, Kao GD, Garcia BA, Shabanowitz J, Hunt DF, Qin J, Phelan C & Lazar MA (2006). A novel

histone deacetylase pathway regulates mitosis by modulating Aurora B kinase activity. 2566–2579.
Liu D, Davydenko O & Lampson MA (2012). Polo-like kinase-1 regulates kinetochore-microtubule dynamics and spindle checkpoint silencing. *The Journal of cell biology* **198,** 491–499.
Liu D, Vleugel M, Backer CB, Hori T, Fukagawa T, Cheeseman IM & Lampson M a. (2010). Regulated targeting of protein phosphatase 1 to the outer kinetochore by KNL1 opposes Aurora B kinase. *The Journal of cell biology* **188,** 809–820.
Liu H, Qu Q, Warrington R, Rice A, Cheng N & Yu H (2015). Mitotic Transcription Installs Sgo1 at Centromeres to Coordinate Chromosome Segregation. *Molecular cell* **59,** 426–436.
Liu X & Erikson RL (2003). Polo-like kinase (Plk)1 depletion induces apoptosis in cancer cells. *Proceedings of the National Academy of Sciences of the United States of America* **100,** 5789–5794.
London N & Biggins S (2014). Mad1 kinetochore recruitment by Mps1-mediated phosphorylation of Bub1 signals the spindle checkpoint. *Genes & development* **28,** 140–152.
London N, Ceto S, Ranish J a. & Biggins S (2012). Phosphoregulation of Spc105 by Mps1 and PP1 regulates Bub1 localization to kinetochores. *Current Biology* **22,** 900–906.
Loog M & Morgan DO (2005). Cyclin specificity in the phosphorylation of cyclin-dependent kinase substrates. *Nature* **434,** 104–108.
Lõoke M, Kristjuhan K & Kristjuhan A (2011). Extraction of genomic DNA from yeasts for PCR-based applications. *BioTechniques* **50,** 325–328.
Lu Y & Cross F (2009). Mitotic exit in the absence of separase activity. *Molecular biology of the cell* **20,** 1576–1591.
Luo X, Tang Z, Rizo J & Yu H (2002). The Mad2 Spindle Checkpoint Protein Undergoes Similar Major Conformational Changes Upon Binding to Either Mad1 or Cdc20. **9,** 59–71.
Ma L, McQueen J, Cuschieri L, Vogel J & Measday V (2007). Spc24 and Stu2 promote spindle integrity when DNA replication is stalled. *Molecular biology of the cell* **18,** 2805–2816.
Ma L, Zhao X & Zhu X (2006). Mitosin/CENP-F in mitosis, transcriptional control, and differentiation. *Journal of Biomedical Science* **13,** 205–213.
Maciejowski J, Drechsler H, Grundner-Culemann K, Ballister ER, Rodriguez-Rodriguez JA, Rodriguez-Bravo V, Jones MJK, Foley E, Lampson MA, Daub H, McAinsh AD & Jallepalli P V. (2017). Mps1 Regulates Kinetochore-Microtubule Attachment Stability via the Ska Complex to Ensure Error-Free Chromosome Segregation. *Developmental Cell* **41,** 143–156.e6.
Macůrek L, Lindqvist A, Lim D, Lampson M a, Klompmaker R, Freire R, Clouin C, Taylor SS, Yaffe MB & Medema RH (2008). Polo-like kinase-1 is activated by aurora A to promote checkpoint recovery. *Nature* **455,** 119–123.
Maia ARR, Garcia Z, Kabeche L, Barisic M, Maffini S, Macedo-Ribeiro S, Cheeseman IM, Compton DA, Kaverina I & Maiato H (2012). Cdk1 and Plk1 mediate a CLASP2 phospho-switch that stabilizes kinetochore-microtubule attachments. *Journal of Cell Biology* **199,** 285–301.
Maiato H, Gomes A, Sousa F & Barisic M (2017). Mechanisms of Chromosome Congression during Mitosis. *Biology* **6,** 13.
Maiolica A, Cittaro D, Borsotti D, Sennels L, Ciferri C, Tarricone C, Musacchio A & Rappsilber J (2007). Structural Analysis of Multiprotein Complexes by Cross-linking, Mass Spectrometry, and Database Searching. *Molecular & Cellular Proteomics* **6,** 2200–2211.
Makrantoni V & Stark MJR (2009). Efficient chromosome biorientation and the tension checkpoint in Saccharomyces cerevisiae both require Bir1. *Mol Cell Biol* **29,** 4552–4562.
Maldonado M & Kapoor TM (2011*a*). Constitutive Mad1 targeting to kinetochores uncouples checkpoint signalling from chromosome biorientation. *Nat Cell Biol* **13,** 475–482.
Maldonado M & Kapoor TM (2011*b*). Moving right along: how PP1 helps clear the checkpoint. *Developmental cell* **20,** 733–734.
Malvezzi F, Litos G, Schleiffer A, Heuck A, Mechtler K, Clausen T & Westermann S (2013). A structural basis for kinetochore recruitment of the Ndc80 complex via two distinct centromere receptors. *The EMBO journal* **32,** 409–423.
Mapelli M, Massimiliano L, Santaguida S & Musacchio A (2007). The Mad2 conformational dimer: structure and implications for the spindle assembly checkpoint. *Cell* **131,** 730–743.

Maresca TJ & Salmon ED (2010). Welcome to a new kind of tension: translating kinetochore mechanics into a wait-anaphase signal. *Journal of cell science* **123,** 825–835.
Marston AL (2014). Chromosome segregation in budding yeast: sister chromatid cohesion and related mechanisms. *Genetics* **196,** 31–63.
Martinez JS, Jeong D-E, Choi E, Billings BM & Hall MC (2006). Acm1 Is a Negative Regulator of the Cdh1-Dependent Anaphase-Promoting Complex/Cyclosome in Budding Yeast. *Molecular and Cellular Biology* **26,** 9162–9176.
Maskell DP, Hu XW & Singleton MR (2010). Molecular architecture and assembly of the yeast kinetochore MIND complex. *Journal of Cell Biology* **190,** 823–834.
Matson DR, Demirel PB, Stukenberg PT & Burke DJ (2012). A conserved role for COMA / CENP-H / I / N kinetochore proteins in the spindle checkpoint. *Genes & development*542–547.
Matsumura S, Toyoshima F & Nishida E (2007). Polo-like kinase 1 facilitates chromosome alignment during prometaphase through BubR1. *Journal of Biological Chemistry* **282,** 15217–15227.
Matsuo Y, Maurer SP, Yukawa M, Zakian S, Singleton MR, Surrey T & Toda T (2016). An unconventional interaction between Dis1/TOG and Mal3/EB1 promotes the fidelity of chromosome segregation. *Journal of Cell Science* **129,** jcs.197533.
Maure J-F, Komoto S, Oku Y, Mino A, Pasqualato S, Natsume K, Clayton L, Musacchio A & Tanaka TU (2011). The Ndc80 loop region facilitates formation of kinetochore attachment to the dynamic microtubule plus end. *Current biology : CB* **21,** 207–213.
McKinley KL & Cheeseman IM (2014). Polo-like kinase 1 licenses CENP-a deposition at centromeres. *Cell* **158,** 397–411.
Mechtler K, Westermann S, Lampert F, Schleiffer A, Hornung P, Maier M & Litos G (2012). CENP-T proteins are conserved centromere receptors of the Ndc80 complex. *Nat Cell Biol* **14,** 604–613.
Miller CT, Gabrielse C, Chen YC & Weinreich M (2009). Cdc7p-Dbf4p regulates mitotic exit by inhibiting polo kinase. *PLoS Genetics*; DOI: 10.1371/journal.pgen.1000498.
Miller MP, Asbury CL & Biggins S (2016). A TOG Protein Confers Tension Sensitivity to Kinetochore-Microtubule Attachments. *Cell* **165,** 1–12.
Mimori-Kiyosue Y, Grigoriev I, Lansbergen G, Sasaki H, Matsui C, Severin F, Galjart N, Grosveld F, Vorobjev I, Tsukita S & Akhmanova A (2005). CLASP1 and CLASP2 bind to EB1 and regulate microtubule plus-end dynamics at the cell cortex. *Journal of Cell Biology* **168,** 141–153.
Miranda JL, Wulf P De, Sorger PK & Harrison SC (2005). The yeast DASH complex forms closed rings on microtubules. *Nature Structural & Molecular Biology* **12,** 138–143.
Mirchenko L & Uhlmann F (2010). Sli15INCENP dephosphorylation prevents mitotic checkpoint reengagement due to loss of tension at anaphase onset. *Current Biology* **20,** 1396–1401.
Mishra PK, Ciftci-yilmaz S, Reynolds D, Au WW-C, Boeckmann L, Dittman LE, Jowhar Z, Pachpor T, Yeh E, Baker RE, Hoyt MA, DAmours D, Bloom K & Basrai MA (2016). Polo kinase Cdc5 associates with centromeres to facilitate the removal of centromeric cohesin. *Molecular Biology of the Cell* **27,** 1–56.
Mishra PK, Guo J, Dittman LE, Haase J, Yeh E, Bloom K & Basrai MA (2015). Pat1 protects centromere-specific histone H3 variant Cse4 from Psh1-mediated ubiquitination. *Molecular biology of the cell* **26,** 2067–2079.
Mishra PK, Ottmann AR & Basrai MA (2013). Structural integrity of centromeric chromatin and faithful chromosome segregation requires Pat1. *Genetics* **195,** 369–379.
Mizuguchi G, Xiao H, Wisniewski J, Smith MM & Wu C (2007). Nonhistone Scm3 and histones CenH3-H4 assemble the core of centromere-specific nucleosomes. *Cell* **129,** 1153–1164.
Molina O, Vargiu G, Abad MA, Zhiteneva A, Jeyaprakash AA, Masumoto H, Kouprina N, Larionov V & Earnshaw WC (2016). Epigenetic engineering reveals a balance between histone modifications and transcription in kinetochore maintenance. *Nature Communications* **7,** 13334.
Montpetit B, Hazbun TR, Fields S & Hieter P (2006). Sumoylation of the budding yeast kinetochore protein Ndc10 is required for Ndc10 spindle localization and regulation of anaphase spindle elongation. *The Journal of cell biology* **174,** 653–663.
Moorhead GBG, Trinkle-Mulcahy L & Ulke-Lemée A (2007). Emerging roles of nuclear protein phosphatases. *Nature reviews Molecular cell biology* **8,** 234–244.

Mortensen EM, Haas W, Gygi M, Gygi SP & Kellogg DR (2005). Cdc28-dependent regulation of the Cdc5/Polo kinase. *Current biology : CB* **15,** 2033–2037.

Moshe Y, Boulaire J, Pagano M & Hershko A (2004). Role of Polo-like kinase in the degradation of early mitotic inhibitor 1, a regulator of the anaphase promoting complex/cyclosome. *Proceedings of the National Academy of Sciences of the United States of America* **101,** 7937–7942.

Moyle MW, Kim T, Hattersley N, Espeut J, Cheerambathur DK, Oegema K & Desai a. (2014). A Bub1-Mad1 interaction targets the Mad1-Mad2 complex to unattached kinetochores to initiate the spindle checkpoint. *The Journal of Cell Biology*; DOI: 10.1083/jcb.201311015.

Mukhopadhyay D & Dasso M (2010). The fate of metaphase kinetochores is weighed in the balance of SUMOylation during S phase. *Cell Cycle* **9,** 3194–3201.

Mumberg D, Muller R & Funk M (1994). Regulatable promoters of saccharomyces cerevisiae: Comparison of transcriptional activity and their use for heterologous expression. *Nucleic Acids Research* **22,** 5767–5768.

Musacchio A & Salmon ED (2007). The spindle-assembly checkpoint in space and time. *Nat Rev Mol Cell Biol* **8,** 379–393.

Natsume T, Müller C a, Katou Y, Retkute R, Gierliński M, Araki H, Blow JJ, Shirahige K, Nieduszynski C a & Tanaka TU (2013). Kinetochores coordinate pericentromeric cohesion and early DNA replication by Cdc7-Dbf4 kinase recruitment. *Molecular cell* **50,** 661–674.

Nerusheva OO & Akiyoshi B (2016). Divergent polo box domains underpin the unique kinetoplastid kinetochore. *Open biology* **6,** 150206.

Nezi L, Rancati G, De Antoni A, Pasqualato S, Piatti S & Musacchio A (2006). Accumulation of Mad2-Cdc20 complex during spindle checkpoint activation requires binding of open and closed conformers of Mad2 in Saccharomyces cerevisiae. *The Journal of cell biology* **174,** 39–51.

Ng TM, Waples WG, Lavoie BD & Biggins S (2009). Pericentromeric sister chromatid cohesion promotes kinetochore biorientation. *Molecular biology of the cell* **20,** 3818–3827.

Nijenhuis W, Vallardi G, Teixeira A, Kops GJPL & Saurin AT (2014). Negative feedback at kinetochores underlies a responsive spindle checkpoint signal. *Nature Cell Biology* **16,** 1257–1264.

Nishimura K, Fukagawa T, Takisawa H, Kakimoto T & Kanemaki M (2009). An auxin-based degron system for the rapid depletion of proteins in nonplant cells. *Nature Methods* **6,** 917–922.

Nishimura K & Kanemaki MT (2014). Rapid depletion of budding yeast proteins via the fusion of an auxin-inducible degron (AID). *Current Protocols in Cell Biology* **2014,** 20.9.1-20.9.16.

Nishino M, Kurasawa Y, Evans R, Lin SH, Brinkley BR & Yu-Lee L yuan (2006). NudC Is Required for Plk1 Targeting to the Kinetochore and Chromosome Congression. *Current Biology* **16,** 1414–1421.

Novick P, Osmond BC & Botstein D (1989). Suppressors of yeast actin mutations. *Genetics* **121,** 659–674.

Nurse P (1975). Genetic control of cell size at cell division in yeast. *Nature* **256,** 547–551.

O'Connell CB, Loncarek J, Hergert P, Kourtidis A, Conklin DS & Khodjakov A (2008). The spindle assembly checkpoint is satisfied in the absence of interkinetochore tension during mitosis with unreplicated genomes. *J Cell Biol* **183,** 29–36.

O'Connor A, Maffini S, Rainey MD, Kaczmarczyk A, Gaboriau D, Musacchio A & Santocanale C (2015). Requirement for PLK1 kinase activity in the maintenance of a robust spindle assembly checkpoint. *Biology open* **5,** 11–19.

Ohkuni K & Kitagawa K (2011). Endogenous Transcription at the Centromere Facilitates Centromere Activity in Budding Yeast. *Current Biology* **21,** 1695–1703.

Ohkuni K, Takahashi Y, Fulp A, Lawrimore J, Au W-C, Pasupala N, Levy-Myers R, Warren J, Strunnikov A, Baker RE, Kerscher O, Bloom K & Basrai MA (2016). SUMO-Targeted Ubiquitin Ligase (STUbL) Slx5 regulates proteolysis of centromeric histone H3 variant Cse4 and prevents its mislocalization to euchromatin. *Molecular biology of the cell*mbc.E15-12-0827-.

Olafsson G & Thorpe PH (2015). Synthetic physical interactions map kinetochore regulators and regions sensitive to constitutive Cdc14 localization. *Proceedings of the National Academy of Sciences* **112,** 10413–10418.

Olafsson G & Thorpe PH (2016). Synthetic Physical Interactions Map Kinetochore-Checkpoint

Activation Regions. *G3 Genes|Genomes|Genetics* **6,** 2531–2542.
Olafsson G & Thorpe PH (2017). Rewiring the budding yeast proteome using Synthetic Physical Interactions (SPI). In *Genome Instability: Methods and Protocols*, ed. Muzi-Falconi M & Brown GW. Humana Press Inc.
Ong S-E (2002). Stable Isotope Labeling by Amino Acids in Cell Culture, SILAC, as a Simple and Accurate Approach to Expression Proteomics. *Molecular & Cellular Proteomics* **1,** 376–386.
Ortiz J, Stemmann O, Rank S & Lechner J (1999). A putative protein complex consisting of Ctf19, Mcm21, and Okp1 represents a missing link in the budding yeast kinetochore. *Genes and Development* **13,** 1140–1155.
Ostapenko D, Burton JL, Wang R & Solomon MJ (2008). Pseudosubstrate Inhibition of the Anaphase-Promoting Complex by Acm1: Regulation by Proteolysis and Cdc28 Phosphorylation. *Molecular and Cellular Biology* **28,** 4653–4664.
Oughtred R et al. (2016). BioGRID: A Resource for Studying Biological Interactions in Yeast: Table 1. *Cold Spring Harbor Protocols* **2016,** pdb.top080754.
Pagliuca C, Draviam VM, Marco E, Sorger PK & De Wulf P (2009). Roles for the conserved spc105p/kre28p complex in kinetochore-microtubule binding and the spindle assembly checkpoint. *PloS one* **4,** e7640.
Pardo B, Crabbé L & Pasero P (2017). Signaling pathways of replication stress in yeast. *FEMS Yeast Research* **17,** 1–11.
Park CH, Park JE, Kim TS, Kang YH, Soung NK, Zhou M, Kim NH, Bang JK & Lee KS (2015*a*). Mammalian polo-like Kinase 1 (Plk1) promotes proper chromosome segregation by phosphorylating and delocalizing the PBIP1??CENP-Q complex from kinetochores. *Journal of Biological Chemistry* **290,** 8569–8581.
Park CJ et al. (2008). Requirement for the budding yeast polo kinase Cdc5 in proper microtubule growth and dynamics. *Eukaryotic Cell* **7,** 444–453.
Park CJ, Song S, Giddings TH, Ro H-S, Sakchaisri K, Park J-E, Seong Y-S, Winey M, Lee KS & Lee KS (2004*a*). Requirement for Bbp1p in the proper mitotic functions of Cdc5p in Saccharomyces cerevisiae. *Molecular biology of the cell* **15,** 1711–1723.
Park J-E, Kim T-S, Meng L, Bang JK, Kim BY & Lee KS (2015*b*). Putting a bit into the polo-box domain of polo-like kinase 1. *Journal of analytical science and technology* **6,** 27.
Park J-E, Park CJ, Sakchaisri K, Karpova T, Asano S, McNally J, Sunwoo Y, Leem S-H & Lee KS (2004*b*). Novel functional dissection of the localization-specific roles of budding yeast polo kinase Cdc5p. *Molecular and cellular biology* **24,** 9873–9886.
Park JE, Soung NK, Johmura Y, Kang YH, Liao C, Lee KH, Park CH, Nicklaus MC & Lee KS (2010). Polo-box domain: a versatile mediator of polo-like kinase function. *Cellular and molecular life sciences : CMLS* **67,** 1957–1970.
Pekgöz Altunkaya G, Malvezzi F, Demianova Z, Zimniak T, Litos G, Weissmann F, Mechtler K, Herzog F & Westermann S (2016). CCAN Assembly Configures Composite Binding Interfaces to Promote Cross-Linking of Ndc80 Complexes at the Kinetochore. *Current Biology* **26,** 2370–2378.
Peng Y, Wong CCL, Nakajima Y, Tyers RG, Sarkeshik AS, Yates J, Drubin DG & Barnes G (2011). Overlapping kinetochore targets of CK2 and Aurora B kinases in mitotic regulation. *Molecular biology of the cell* **22,** 2680–2689.
Pereira G, Manson C, Grindlay J & Schiebel E (2002). Regulation of the Bfa1p-Bub2p complex at spindle pole bodies by the cell cycle phosphatase Cdc14p. *Journal of Cell Biology* **157,** 367–379.
Pereira G & Schiebel E (2003). Separase regulates INCENP-Aurora B anaphase spindle function through Cdc14. *Science (New York, NY)* **302,** 2120–2124.
Petrovic A, Keller J, Liu Y, Overlack K, John J, Dimitrova YN, Jenni S, van Gerwen S, Stege P, Wohlgemuth S, Rombaut P, Herzog F, Harrison SC, Vetter IR & Musacchio A (2016). Structure of the MIS12 Complex and Molecular Basis of Its Interaction with CENP-C at Human Kinetochores. *Cell* **167,** 1028–1040.e15.
Pfau SJ & Amon A (2012). Chromosomal instability and aneuploidy in cancer: from yeast to man. *EMBO reports* **13,** 515–527.
Piatti S, Venturetti M, Chiroli E & Fraschini R (2006). The spindle position checkpoint in budding yeast: the motherly care of MEN. *Cell Division* **1,** 2.
Pinsky B a, Kung C, Shokat KM & Biggins S (2006). The Ipl1-Aurora protein kinase activates

the spindle checkpoint by creating unattached kinetochores. *Nature cell biology* **8,** 78–83.
Pinsky BA, Nelson CR & Biggins S (2009). Protein Phosphatase I Regulates Exit from the Spindle Checkpoint in Budding Yeast. *Current Biology* **19,** 1182–1187.
Poddar A, Stukenberg PT & Burke DJ (2005). Two complexes of spindle checkpoint proteins containing Cdc20 and Mad2 assemble during mitosis independently of the kinetochore in Saccharomyces cerevisiae. *Eukaryot Cell* **4,** 867–878.
Pot I, Knockleby J, Aneliunas V, Nguyen T, Ah-Kye S, Liszt G, Snyder M, Hieter P & Vogel J (2005). Spindle checkpoint maintenance requires Ame1 and Okp1. *Cell Cycle* **4,** 1448–1456.
Pot I, Measday V, Snydsman B, Cagney G, Fields S, Davis TN, Muller EGD & Hieter P (2003). Chl4p and iml3p are two new members of the budding yeast outer kinetochore. *Molecular biology of the cell* **14,** 460–476.
Primorac I, Weir JR, Chiroli E, Gross F, Hoffmann I, van Gerwen S, Ciliberto A & Musacchio A (2013). Bub3 reads phosphorylated MELT repeats to promote spindle assembly checkpoint signaling. *eLife* **2013,** 2–4.
Proft M & Struhl K (2002). Hog1 kinase converts the Sko1-Cyc8-Tup1 repressor complex into an activator that recruits SAGA and SWI/SNF in response to osmotic stress. *Molecular cell* **9,** 1307–1317.
Rahal R & Amon A (2008). The polo-like kinase Cdc5 interacts with FEAR network components and Cdc14. *Cell Cycle* **7,** 3262–3272.
Rancati G, Crispo V, Lucchini G & Piatti S (2005). Mad3/BubR1 Phosphorylation during Spindle Checkpoint Activation Depends on both Polo and Aurora Kinases in Budding Yeast. *Cell Cycle*972–980.
Ranjitkar P, Press MO, Yi X, Baker R, MacCoss MJ & Biggins S (2010). An E3 ubiquitin ligase prevents ectopic localization of the centromeric histone H3 variant via the centromere targeting domain. *Mol Cell* **40,** 455–464.
Raspelli E, Cassani C, Chiroli E & Fraschini R (2015). Budding yeast Swe1 is involved in the control of mitotic spindle elongation and is regulated by Cdc14 phosphatase during mitosis. *Journal of Biological Chemistry* **290,** 1–12.
Ratsima H, Ladouceur A-MA-M, Pascariu M, Sauve V, Salloum Z, Maddox PS, D'Amours D, Sauvé V, Salloum Z, Maddox PS & D'Amours D (2011). Independent modulation of the kinase and polo-box activities of Cdc5 protein unravels unique roles in the maintenance of genome stability. *Proceedings of the National Academy of Sciences* **108,** E914–E923.
Ratsima H, Serrano D, Pascariu M & D'Amours D (2016). Centrosome-Dependent Bypass of the DNA Damage Checkpoint by the Polo Kinase Cdc5. *Cell Reports* **14,** 1422–1434.
Ravi M & Chan SWL (2010). Haploid plants produced by centromere-mediated genome elimination. *Nature* **464,** 615–618.
Rawal CC, Riccardo S, Pesenti C, Ferrari M, Marini F & Pellicioli A (2016). Reduced kinase activity of polo kinase Cdc5 affects chromosome stability and DNA damage response in S. cerevisiae. *Cell Cycle* **15,** 2906–2919.
Reber S & Hyman AA (2015). Emergent Properties of the Metaphase Spindle. *Cold Spring Harbor perspectives in biology* **7,** a015784.
Reddy Chichili VP, Kumar V & Sivaraman J (2013). Linkers in the structural biology of protein-protein interactions. *Protein Science* **22,** 153–167.
Reid RJD, Gonzalez-Barrera S, Sunjevaric I, Alvaro D, Ciccone S, Wagner M & Rothstein R (2011). Selective ploidy ablation, a high-throughput plasmid transfer protocol, identifies new genes affecting topoisomerase I-induced DNA damage. *Genome Res* **21,** 477–486.
Richmond D, Rizkallah R, Liang F, Hurt MM & Wang Y (2013). Slk19 clusters kinetochores and facilitates chromosome bipolar attachment. *Molecular Biology of the Cell* **24,** 566–577.
Rieder CL, Cole RW, Khodjakov A & Sluder G (1995). The checkpoint delaying anaphase in response to chromosome monoorientation is mediated by an inhibitory signal produced by unattached kinetochores. *Journal of Cell Biology* **130,** 941–948.
Rizk RS, Discipio K a, Proudfoot KG & Gupta ML (2014). The kinesin-8 Kip3 scales anaphase spindle length by suppression of midzone microtubule polymerization. *The Journal of cell biology* **204,** 965–975.
Rock JM & Amon A (2011). Cdc15 integrates Tem1 GTPase-mediated spatial signals with Polo kinase-mediated temporal cues to activate mitotic exit. *Genes and Development* **25,** 1943–1954.

Rodriguez-Bravo V, Maciejowski J, Corona J, Buch HK, Collin P, Kanemaki MT, Shah J V & Jallepalli P V (2014). Nuclear pores protect genome integrity by assembling a premitotic and Mad1-dependent anaphase inhibitor. *Cell* **156,** 1017–1031.

Rodriguez-Rodriguez J-A, Moyano Y, Játiva S & Queralt E (2016). Mitotic Exit Function of Polo-like Kinase Cdc5 Is Dependent on Sequential Activation by Cdk1. *Cell Reports*2050–2062.

Rosebrock AP (2017). Analysis of the Budding Yeast Cell Cycle by Flow Cytometry. *Cold Spring Harbor protocols* **2017,** pdb.prot088740.

Rosenberg JS, Cross FR & Funabiki H (2011). KNL1/Spc105 recruits PP1 to silence the spindle assembly checkpoint. *Current biology : CB* **21,** 942–947.

Rothbauer U, Zolghadr K, Muyldermans S, Schepers A, Cardoso MC & Leonhardt H (2008). A versatile nanotrap for biochemical and functional studies with fluorescent fusion proteins. *Mol Cell Proteomics* **7,** 282–289.

Rothbauer U, Zolghadr K, Tillib S, Nowak D, Schermelleh L, Gahl A, Backmann N, Conrath K, Muyldermans S, Cardoso MC & Leonhardt H (2006). Targeting and tracing antigens in live cells with fluorescent nanobodies. *Nature methods* **3,** 887–889.

Rothstein RJ (1983). One-step gene disruption in yeast. *Methods in enzymology* **101,** 202–211.

Ruchaud S, Carmena M & Earnshaw WC (2007). Chromosomal passengers: conducting cell division. *Nat Rev Mol Cell Biol* **8,** 798–812.

Russell P & Nurse P (1987). Negative regulation of mitosis by wee1+, a gene encoding a protein kinase homolog. *Cell* **49,** 559–567.

Sakchaisri K, Asano S, Yu L-R, Shulewitz MJ, Park CJ, Park J-E, Cho Y-W, Veenstra TD, Thorner J & Lee KS (2004). Coupling morphogenesis to mitotic entry. *Proceedings of the National Academy of Sciences of the United States of America* **101,** 4124–4129.

Salmon ED & Bloom K (2017). Tension sensors reveal how the kinetochore shares its load. *BioEssays* **39,** 1600216.

Samel A, Cuomo A, Bonaldi T & Ehrenhofer-Murray AE (2012). Methylation of CenH3 arginine 37 regulates kinetochore integrity and chromosome segregation. *Proceedings of the National Academy of Sciences of the United States of America* **109,** 9029–9034.

Sanchez-Diaz A, Nkosi PJ, Murray S & Labib K (2012). The Mitotic Exit Network and Cdc14 phosphatase initiate cytokinesis by counteracting CDK phosphorylations and blocking polarised growth. *The EMBO journal* **31,** 3620–3634.

Sanhaji M, Ritter A, Belsham HR, Friel CT, Roth S, Louwen F & Yuan J (2014). Polo-like kinase 1 regulates the stability of the mitotic centromere-associated kinesin in mitosis. *Oncotarget* **5,** 3130–3144.

Santamaria A, Wang B, Elowe S, Malik R, Zhang F, Bauer M, Schmidt A, Silljé HHW, Körner R & Nigg E a (2011). The Plk1-dependent phosphoproteome of the early mitotic spindle. *Molecular & cellular proteomics : MCP* **10,** M110.004457.

Saurin AT, van der Waal MS, Medema RH, Lens SM a & Kops GJPL (2011). Aurora B potentiates Mps1 activation to ensure rapid checkpoint establishment at the onset of mitosis. *Nature communications* **2,** 316.

von Schubert C, Cubizolles F, Bracher JM, Sliedrecht T, Kops GJPL & Nigg EA (2015). Plk1 and Mps1 Cooperatively Regulate the Spindle Assembly Checkpoint in Human Cells. *Cell Reports* **12,** 66–78.

Schweiggert J, Stevermann L, Panigada D, Kammerer D & Liakopoulos D (2016). Regulation of a Spindle Positioning Factor at Kinetochores by SUMO-Targeted Ubiquitin Ligases. *Developmental Cell* **36,** 415–427.

Seki A, Coppinger J a, Jang C-Y, Yates JR & Fang G (2008). Bora and the kinase Aurora a cooperatively activate the kinase Plk1 and control mitotic entry. *Science (New York, NY)* **320,** 1655–1658.

Seong YS, Kamijo K, Lee JS, Fernandez E, Kuriyama R, Miki T & Lee KS (2002). A spindle checkpoint arrest and a cytokinesis failure by the dominant-negative polo-box domain of Plk1 in U-2 OS cells. *Journal of Biological Chemistry* **277,** 32282–32293.

Serrano D & D'Amours D (2014). When genome integrity and cell cycle decisions collide: roles of polo kinases in cellular adaptation to DNA damage. *Systems and Synthetic Biology*195–203.

Shao H, Huang Y, Zhang L, Yuan K, Chu Y, Dou Z, Jin C, Garcia-Barrio M, Liu X & Yao X (2015). Spatiotemporal dynamics of Aurora B-PLK1-MCAK signaling axis orchestrates kinetochore bi-orientation and faithful chromosome segregation. *Scientific reports* **5,**

12204.
Sharma A, Antoku S, Fujiwara K & Mayer BJ (2003). Functional interaction trap: a strategy for validating the functional consequences of tyrosine phosphorylation of specific substrates in vivo. *Molecular & cellular proteomics : MCP* **2,** 1217–1224.
Shepperd LA, Meadows JC, Sochaj AM, Lancaster TC, Zou J, Buttrick GJ, Rappsilber J, Hardwick KG & Millar JBA (2012). Phosphodependent recruitment of Bub1 and Bub3 to Spc7/KNL1 by Mph1 kinase maintains the spindle checkpoint. *Current Biology* **22,** 891–899.
Shero JH & Hieter P (1991). A suppressor of a centromere DNA mutation encodes a putative protein kinase (MCK1). *Genes & development* **5,** 549–560.
Shimogawa MM, Graczyk B, Gardner MK, Francis SE, White EA, Ess M, Molk JN, Ruse C, Niessen S, Yates JR, Muller EGD, Bloom K, Odde DJ & Davis TN (2006). Mps1 Phosphorylation of Dam1 Couples Kinetochores to Microtubule Plus Ends at Metaphase. *Current Biology* **16,** 1489–1501.
Shirayama M, Zachariae W, Ciosk R & Nasmyth K (1998). The Polo-like kinase Cdc5p and the WD-repeat protein Cdc20p/fizzy are regulators and substrates of the anaphase promoting complex in Saccharomyces cerevisiae. *EMBO Journal* **17,** 1336–1349.
Shou W, Azzam R, Chen SL, Huddleston MJ, Baskerville C, Charbonneau H, Annan RS, Carr S a & Deshaies RJ (2002). Cdc5 influences phosphorylation of Net1 and disassembly of the RENT complex. *BMC molecular biology* **3,** 3.
Shrestha RL & Draviam VM (2013). Lateral to end-on conversion of chromosome-microtubule attachment requires kinesins CENP-E and MCAK. *Current biology : CB* **23,** 1514–1526.
Simpson-Lavy KJ & Brandeis M (2011). Phosphorylation of Cdc5 regulates its accumulation. *Cell Division* **6,** 23.
Simpson-Lavy KJ, Zenvirth D & Brandeis M (2015). Phosphorylation and dephosphorylation regulate APC/Ccdh1 substrate degradation. *Cell Cycle* **14,** 3138–3145.
Snead JL, Sullivan M, Lowery DM, Cohen MS, Zhang C, Randle DH, Taunton J, Yaffe MB, Morgan DO & Shokat KM (2007). A Coupled Chemical-Genetic and Bioinformatic Approach to Polo-like Kinase Pathway Exploration. *Chemistry and Biology* **14,** 1261–1272.
Song S, Grenfell TZ, Garfield S, Erikson RL & Lee KS (2000). Essential Function of the Polo Box of Cdc5 in Subcellular Localization and Induction of Cytokinetic Structures. **20,** 286–298.
Song S & Lee KS (2001). A novel function of Saccharomyces cerevisiae CDC5 in cytokinesis. *Journal of Cell Biology* **153,** 451–469.
Spencer F, Gerring SL, Connelly C & Hieter P (1990). Mitotic chromosome transmission fidelity mutants in Saccharomyces cerevisiae. *Genetics* **124,** 237–249.
Sridharan V & Azuma Y (2016). SUMO-interacting motifs (SIMs) in Polo-like kinase 1-interacting checkpoint helicase (PICH) ensure proper chromosome segregation during mitosis. *Cell Cycle* **15,** 2135–2144.
Stegmeier F, Visintin R & Amon A (2002). Separase , Polo Kinase , the Kinetochore Protein Slk19 , and Spo12 Function in a Network that Controls Cdc14 Localization during Early Anaphase. *Cell* **108,** 207–220.
Stemmann O, Neidig A, Köcher T, Wilm M & Lechner J (2002). Hsp90 enables Ctf13p/Skp1p to nucleate the budding yeast kinetochore. *Pnas* **99,** 8585–8590.
Stoler S, Keith KC, Curnick KE & Fitzgerald-Hayes M (1995). A mutation in CSE4, an essential gene encoding a novel chromatin-associated protein in yeast, causes chromosome nondisjunction and cell cycle arrest at mitosis. *Genes & development* **9,** 573–586.
Stoler S, Rogers K, Weitze S, Morey L, Fitzgerald-Hayes M & Baker RE (2007). Scm3, an essential Saccharomyces cerevisiae centromere protein required for G2/M progression and Cse4 localization. *Proceedings of the National Academy of Sciences* **104,** 10571–10576.
Strebhardt K (2010). Multifaceted polo-like kinases: drug targets and antitargets for cancer therapy. *Nat Rev Drug Discov* **9,** 643–660.
Sudakin V, Chan GK & Yen TJ (2001). Checkpoint inhibition of the APC/C in HeLa cells is mediated by a complex of BUBR1, BUB3, CDC20, and MAD2. *J Cell Biol* **154,** 925–936.
Suijkerbuijk SJE, Vleugel M, Teixeira A & Kops GJPL (2012). Integration of Kinase and Phosphatase Activities by BUBR1 Ensures Formation of Stable Kinetochore-Microtubule Attachments. *Developmental Cell* **23,** 745–755.

Swaney DL, Beltrao P, Starita L, Guo A, Rush J, Fields S, Krogan NJ & Villén J (2013). Global analysis of phosphorylation and ubiquitylation cross-talk in protein degradation. *Nature methods* **10,** 676–682.

Tanaka K, Kitamura E, Kitamura Y & Tanaka TU (2007). Molecular mechanisms of microtubule-dependent kinetochore transport toward spindle poles. *The Journal of cell biology* **178,** 269–281.

Tanaka TU, Rachidi N, Janke C, Pereira G, Galova M, Schiebel E, Stark MJR & Nasmyth K (2002). Evidence that the Ipl1-Sli15 (Aurora Kinase-INCENP) complex promotes chromosome bi-orientation by altering kinetochore-spindle pole connections. *Cell* **108,** 317–329.

Taylor GS, Liu Y, Baskerville C & Charbonneau H (1997). The activity of Cdc14p, an oligomeric dual specificity protein phosphatase from Saccharomyces cerevisiae, is required for cell cycle progression. *The Journal of biological chemistry* **272,** 24054–24063.

Thapa KS, Oldani a., Pagliuca C, De Wulf P & Hazbun TR (2015). The Mps1 Kinase Modulates the Recruitment and Activity of Cnn1CENP-T at Saccharomyces cerevisiae Kinetochores. *Genetics* **200,** 79–90.

Thorpe PH, Dittmar JC & Rothstein R (2012). ScreenTroll: a searchable database to compare genome-wide yeast screens. *Database (Oxford)* **2012,** bas022.

Tipton AR, Ji W, Sturt-Gillespie B, Bekier ME, Wang K, Taylor WR & Liu ST (2013). Monopolar spindle 1 (MPS1) kinase promotes production of closed MAD2 (C-MAD2) conformer and assembly of the mitotic checkpoint complex. *The Journal of biological chemistry* **288,** 35149–35158.

Toczyski DP, Galgoczy DJ, Hartwell LH, Cdc5 & Ckii (1997). CDC5 and CKII control adaptation to the yeast DNA damage checkpoint. *Cell* **90,** 1097–1106.

Trinkle-Mulcahy L & Lamond AI (2006). Mitotic phosphatases: no longer silent partners. *Current opinion in cell biology* **18,** 623–631.

Tripodi F, Nicastro R, Busnelli S, Cirulli C, Maffioli E, Tedeschi G, Alberghina L & Coccetti P (2013). Protein Kinase CK2 Holoenzyme Promotes Start-Specific Transcription in Saccharomyces cerevisiae. *Eukaryotic Cell* **12,** 1271–1280.

Tsabar M, Haase J, Harrison B, Snider CE, Eldridge B, Kaminsky L, Hine RM, Haber JE & Bloom K (2016). A Cohesin-Based Partitioning Mechanism Revealed upon Transcriptional Inactivation of Centromere. *PLoS Genetics* **12,** 1–25.

Tytell JD & Sorger PK (2006). Analysis of kinesin motor function at budding yeast kinetochores. *The Journal of cell biology* **172,** 861–874.

Ubersax JA, Woodbury EL, Quang PN, Paraz M, Blethrow JD, Shah K, Shokat KM & Morgan DO (2003). Targets of the cyclin-dependent kinase Cdk1. *Nature* **425,** 859–864.

Uhlmann F, Lottspeich F & Nasmyth K (1999). Sister-chromatid separation at anaphase onset is promoted by cleavage of the cohesin subunit Scc1. *Nature* **400,** 37–42.

Uhlmann F, Wernic D, Poupart M-A, Koonin E V & Nasmyth K (2000). Cleavage of Cohesin by the CD Clan Protease Separin Triggers Anaphase in Yeast. *Cell* **103,** 375–386.

Valverde R, Ingram J & Harrison SC (2016). Conserved Tetramer Junction in the Kinetochore Ndc80 Complex. *Cell Reports* **17,** 1915–1922.

Vernarecci S, Ornaghi P, Bâgu A, Cundari E, Ballario P & Filetici P (2008). Gcn5p plays an important role in centromere kinetochore function in budding yeast. *Molecular and cellular biology* **28,** 988–996.

Vidanes GM, Sweeney FD, Galicia S, Cheung S, Doyle JP, Durocher D & Toczyski DP (2010). CDC5 inhibits the hyperphosphorylation of the checkpoint kinase Rad53, leading to checkpoint adaptation. *PLoS biology* **8,** e1000286.

Visintin C, Tomson BN, Raha R, Paulson J, Cohen M, Taunton J, Amon A & Visintin R (2008). APC/C-Cdh1-mediated degradation of the Polo kinase Cdc5 promotes the return of Cdc14 into the nucleolus. *Genes and Development* **22,** 79–90.

Visintin R, Craig K, Hwang ES, Prinz S, Tyers M, Amon A & Irniger C (1998). The Phosphatase Cdc14 Triggers Mitotic Exit by Reversal of Cdk-Dependent Phosphorylation. *Molecular Cell* **2,** 709–718.

Visintin R, Stegmeier F & Amon A (2003). The Role of the Polo Kinase Cdc5 in Controlling Cdc14 Localization. *Molecular biology of the cell* **14,** 4486–4498.

Volpe TA, Kidner C, Hall IM, Teng G, Grewal SIS & Martienssen RA (2002). Regulation of Heterochromatic Silencing and Histone H3 Lysine-9 Methylation by RNAi. *Science* **297,**

1833–1837.
van der Waal MS, Hengeveld RCC, van der Horst A & Lens SM a (2012). Cell division control by the Chromosomal Passenger Complex. *Experimental cell research* **318,** 1407–1420.
Wan J, Zhu F, Zasadil LM, Yu J, Wang L, Johnson A, Berthier E, Beebe DJ, Audhya A & Weaver BA (2014). A Golgi-Localized Pool of the Mitotic Checkpoint Component Mad1 Controls Integrin Secretion and Cell Migration. *Current Biology* **24,** 2687–2692.
Wang H, Vilela M, Winkler A, Tarnawski M, Schlichting I, Yumerefendi H, Kuhlman B, Liu R, Danuser G & Hahn KM (2016). LOVTRAP: an optogenetic system for photoinduced protein dissociation. *Nature Methods* **13,** 755–758.
Wargacki MM, Tay JC, Muller EG, Asbury CL & Davis TN (2010). Kip3, the yeast kinesin-8, is required for clustering of kinetochores at metaphase. *Cell cycle (Georgetown, Tex)* **9,** 2581–2588.
Wei RR, Schnell JR, Larsen NA, Sorger PK, Chou JJ & Harrison SC (2006). Structure of a central component of the yeast kinetochore: the Spc24p/Spc25p globular domain. *Structure (London, England : 1993)* **14,** 1003–1009.
Welburn JPI, Grishchuk EL, Backer CB, Wilson- EM, Iii JRY & Cheeseman IM (2009). The human kinetochore Ska1 complex facilitates microtubule depolymerization-coupled motility. *Developmental cell* **16,** 374–385.
Welburn JPII, Vleugel M, Liu D, Yates JR, Lampson MA, Fukagawa T & Cheeseman IM (2010). Aurora B phosphorylates spatially distinct targets to differentially regulate the kinetochore-microtubule interface. *Molecular cell* **38,** 383–392.
Westermann S, Avila-Sakar A, Wang HW, Niederstrasser H, Wong J, Drubin DG, Nogales E & Barnes G (2005). Formation of a dynamic kinetochore-microtubule interface through assembly of the Dam1 ring complex. *Molecular Cell* **17,** 277–290.
Westermann S, Drubin DG & Barnes G (2007). Structures and Functions of Yeast Kinetochore Complexes. *Annual Review of Biochemistry* **76,** 563–591.
Westermann S, Wang H-W, Avila-Sakar A, Drubin DG, Nogales E & Barnes G (2006). The Dam1 kinetochore ring complex moves processively on depolymerizing microtubule ends. *Nature* **440,** 565–569.
Widlund PO, Lyssand JS, Anderson S, Niessen S, Yates JR & Davis TN (2006). Phosphorylation of the Chromosomal Passenger Protein Bir1 Is Required for Localization of Ndc10 to the Spindle during Anaphase and Full Spindle Elongation. **17,** 1065–1074.
Winey M & Bloom K (2012). Mitotic spindle form and function. *Genetics* **190,** 1197–1224.
Winzeler EA et al. (1999). Functional characterization of the S. cerevisiae genome by gene deletion and parallel analysis. *Science (New York, NY)* **285,** 901–906.
Wisniewski J, Hajj B, Chen J, Mizuguchi G, Xiao H, Wei D, Dahan M & Wu C (2014). Imaging the fate of histone Cse4 reveals de novo replacement in S phase and subsequent stable residence at centromeres. *eLife* **3,** e02203.
Wojcik E, Basto R, Serr M, Scaërou F, Karess R & Hays T (2001). Kinetochore dynein: its dynamics and role in the transport of the Rough deal checkpoint protein. *Nature Cell Biology* **3,** 1001–1007.
Wolyniak MJ, Blake-hodek K, Kosco K, Hwang E, You L & Huffaker TC (2006). The Regulation of Microtubule Dynamics in Saccharomyces cerevisiae by Three Interacting Plus-End Tracking Proteins. *Molecular biology of the cell* **17,** 2789–2798.
Wong OK & Fang G (2007). Cdk1 phosphorylation of BubR1 controls spindle checkpoint arrest and Plk1-mediated formation of the 3F3/2 epitope. *Journal of Cell Biology* **179,** 611–617.
Woodbury EL & Morgan DO (2007). Cdk and APC activities limit the spindle-stabilizing function of Fin1 to anaphase. *Nature cell biology* **9,** 106–112.
Wu J, Suka N, Carlson M & Grunstein M (2001). TUP1 utilizes histone H3/H2B-specific HDA1 deacetylase to repress gene activity in yeast. *Molecular cell* **7,** 117–126.
De Wulf P, McAinsh AD & Sorger PK (2003). Hierarchical assembly of the budding yeast kinetochore from multiple subcomplexes. *Genes Dev* **17,** 2902–2921.
De Wulf P, Montani F & Visintin R (2009). Protein phosphatases take the mitotic stage. *Current opinion in cell biology* **21,** 806–815.
Yang F, Moss LG & Phillips GN (1996). The molecular structure of green fluorescent protein. *Nature biotechnology* **14,** 1246–1251.
Yang M, Li B, Liu CJ, Tomchick DR, Machius M, Rizo J, Yu H & Luo X (2008*a*). Insights into Mad2 regulation in the spindle checkpoint revealed by the crystal structure of the

symmetric Mad2 dimer. *PLoS Biology* **6,** 0643–0655.
Yang X, Jost AP-T, Weiner OD & Tang C (2013). A light-inducible organelle-targeting system for dynamically activating and inactivating signaling in budding yeast. *Molecular Biology of the Cell* **24,** 2419–2430.
Yang Y, Wu F, Ward T, Yan F, Wu Q, Wang Z, McGlothen T, Peng W, You T, Sun M, Cui T, Hu R, Dou Z, Zhu J, Xie W, Rao Z, Ding X & Yao X (2008*b*). Phosphorylation of HsMis13 by Aurora B kinase is essential for assembly of functional kinetochore. *Journal of Biological Chemistry* **283,** 26726–26736.
Yeong FM, Lim HH, Padmashree CG & Surana U (2000). Exit from mitosis in budding yeast: biphasic inactivation of the Cdc28-Clb2 mitotic kinase and the role of Cdc20. *Molecular cell* **5,** 501–511.
Yong-Gonzales V, Hang LE, Castellucci F, Branzei D & Zhao X (2012). The Smc5-Smc6 complex regulates recombination at centromeric regions and affects kinetochore protein sumoylation during normal growth. *PloS one* **7,** e51540.
Yuan I, Leontiou I, Amin P, May KM, Soper Ní Chafraidh S, Zlámalová E & Hardwick KG (2016). Generation of a Spindle Checkpoint Arrest from Synthetic Signaling Assemblies. *Current Biology*137–143.
Yuen KWY, Montpetit B & Hieter P (2005). The kinetochore and cancer: what's the connection? *Current opinion in cell biology* **17,** 576–582.
Yuen KWY, Warren CD, Chen O, Kwok T, Hieter P & Spencer FA (2007). Systematic genome instability screens in yeast and their potential relevance to cancer. *Proceedings of the National Academy of Sciences of the United States of America* **104,** 3925–3930.
Zhang C, Kenski DM, Paulson JL, Bonshtien A, Sessa G, Cross J V, Templeton DJ & Shokat KM (2005). A second-site suppressor strategy for chemical genetic analysis of diverse protein kinases. *Nature methods* **2,** 435–441.
Zhang G, Kruse T, López-Méndez B, Sylvestersen KB, Garvanska DH, Schopper S, Nielsen ML & Nilsson J (2017*a*). Bub1 positions Mad1 close to KNL1 MELT repeats to promote checkpoint signalling. *Nature Communications* **8,** 15822.
Zhang G, Lischetti T & Nilsson J (2014). A minimal number of MELT repeats supports all the functions of KNL1 in chromosome segregation. *Journal of Cell Science* **127,** 871–884.
Zhang H, Aonbangkhen C, Tarasovetc E V, Ballister ER, Chenoweth DM & Lampson MA (2017*b*). Optogenetic control of kinetochore function. *Nature Chemical Biology* **13,** 1096–1101.
Zhang L, Shao H, Huang Y, Yan F, Chu Y, Hou H, Zhu M, Fu C, Aikhionbare F, Fang G, Ding X & Yao X (2011). PLK1 phosphorylates mitotic centromere-associated kinesin and promotes its depolymerase activity. *Journal of Biological Chemistry* **286,** 3033–3046.
Zhou T, Aumais JP, Liu X, Yu-Lee LY & Erikson RL (2003). A role for Plk1 phosphorylation of NudC in cytokinesis. *Developmental Cell* **5,** 127–138.
Zich J & Hardwick KG (2010). Getting down to the phosphorylated "nuts and bolts" of spindle checkpoint signalling. *Trends in biochemical sciences* **35,** 18–27.
Zimniak T, Stengl K, Mechtler K & Westermann S (2009). Phosphoregulation of the budding yeast EB1 homologue Bim1p by Aurora/Ipl1p. *Journal of Cell Biology* **186,** 379–391.
Zou H & Rothstein R (1997). Holliday junctions accumulate in replication mutants via a RecA homolog-independent mechanism. *Cell* **90,** 87–96.